SEISMIC WAVE SCATTERING AND THE SMALL SCALE INHOMOGENEITIES IN THE LITHOSPHERE

BY

WU, RU-SHAN

B.S. North-Western University, Sian, China (1962)

SUBMITTED TO THE DEPARTMENT IN PARTIAL FULFILLMENT OF THE REQUIREMENTS FOR THE DEGREE OF DOCTOR OF PHILOSOPHY

AT THE

MASSACHUSETTS INSTITUTE OF TECHNOLOGY

AUGUST 9, 1984

Signature of the author Wu Ru-Shan
Dept. of Earth, Atmosphere & Planetary Sciences

Certified by Keiiti Aki
Keiiti Aki
thesis supervisor

Accepted by Theodore R. Madden
Chairman, Departmental committee on Graduate Students

献给祖国

TO MY MOTHERLAND

母校

MY SCHOOLS

母亲

MY MOTHER

SEISMIC WAVE SCATTERING AND THE SMALL SCALE INHOMOGENEITIES IN THE LITHOSPHERE

Ru-Shan Wu

Submitted to the Department of Earth, Atmospheric and and Planetary Sciences on August 9, 1984, in partial fulfillment of the requirement for the degree of Doctor of Philosophy on Geophysics at the Massachusetts Institute of Technology

Abstract

Seismic wave scattering can be used to study the inhomogeneities in the lithosphere. In the past, the scalar wave single scattering theory has been widely used in the problems concerning seismic wave scattering. In this thesis, the scattering theory is advanced along two directions. One is to extend the scalar wave scattering theory to an elastic wave scattering theory. The other is to formulate the multiple scattering of seismic waves using the results of radiative transfer theory. The theory developed is then applied to the problems of small scale inhomogeneities in the lithosphere.

For deterministic problems, the formulas of elastic wave scattering for an arbitrary elastic heterogeneity were obtained using an equivalent source representation and the Born approximation. For Rayleigh scattering it is shown that the scattered fields of the density perturbation of the heterogeneity are like the radiation fields from a unidirectional point source. The perturbations in shear rigidity ($\delta\mu$) function like an in line couple point source for P wave incidence, and a double couple point source for S wave incidence. The perturbations in Lame constant λ behaves like an explosion point source. It is also shown that the perturbation of the medium parameters can be decomposed into an impedance term and a velocity term. The impedance term generates a main lobe of scattered field in the backward direction and no scattering in the exact forward direction. On the contrary, the velocity term generates a main lobe in the forward direction and no

scattering in the exact backward direction. For Mie scattering, i.e. when the wavelength is comparable to the size of the heterogeneity, the scattered field is a product of two factors: the elastic wave Rayleigh scattering and the "volume factor". As examples, the analytic results for a uniform sphere and a Gaussian heterogeneity have been derived.

The theory is applied to interpret the SH to SV cross-coupling due to scattering by a fracture zone in the experiments of differential vertical seismic profiling.

For random medium problems, the directional scattering coefficients for P and S wave incidences, and the total scattering coefficient for P wave incidence are derived. Comparisons between the scalar wave scattering and the elastic wave scattering show that there are some significant differences between them. It is also shown that, the scalar wave scattering approximation can be only used to forward scattering problems such as the phase and amplitude fluctuations, while the coda amplitude problem must be treated by elastic wave scattering theory.

Analysis of past observations using the theory shows that the lithosphere may have multi-scale inhomogeneities. In addition to the rather large scale (>10 km) velocity inhomogeneities, the lithosphere may be rich in small scale (<1 km) impedance inhomogeneities in tectonically active regions.

The results in radiative transfer theory are used to formulate the multiple scattering problems of seismic waves. The shape of the energy density distribution curve depends strongly on the values of medium seismic albedo ($B_o = \eta_s/(\eta_s+\eta_a)$, where η_s and η_a are the scattering coefficient and absorption coefficient of the medium respectively). Therefore the shape of

the curve can be used to separate absorption and scattering.

The theory is applied to the Hindu Kush earthquake data. The results suggest that in the frequency range 1.5-20 Hz, scattering is not the major factor of the apparent attenuation. The time domain analysis also supports this conclusion. The tectonic implication and the possible attenuation mechanism are also discussed.

The scattering attenuation problems are discussed in the appendices. The use of the mean field formalism to the problem of amplitude attenuation is critically reviewed. A simple renormalization procedure is used to formulate the scattering attenuation under the forward scattering approximation.

Thesis supervisor Keiiti Aki

Professor of Geophysics

When you leave home and go abroad to a very distant and completely unfamiliar place, you must take care of yourself. Don't worry about me at all. You must rely on good gentlemen and kind ladies. Make friends with them. Believe! everywhere in the world, there are always many good people.

my mother

Acknowledgement

I was an "exploration-geophysicist." I say this because I graduated from a physics department and worked in a research institute of mining-exploration geophysics with very little knowledge about geophysics. Fortunately I got the chance to visit MIT. I appreciated the opportunity so much that I started to plan rebuidling my background in Geophysics and enhancing my research capability, after having worked in industry for more than 16 years. I consulted with several old professors about this plan, and received much encouragement and praise. However, many of the talks ended up with a cautious and sympathetic remark: "Maybe it's a little too late!" Therefore I could not help wondering if it was too late, though I decided to push it through to the end without any hesitation. When I came to MIT and talked to Professor Keiiti Aki, my sponsor at that time and my advisor later on (well-known as Kei), about my plan, surprisingly he did not say any words like "it's a little late." His expression was so natural that it seemed that the question which bothered me should not even exist. I was so delighted at that time to be starting a new life in my career that I was almost as confident as he was.

"Everything is hard in the beginning," as the Chinese saying goes. I remember very clearly how I started my study and research. Once when we talked about my previous work in electromagnetic waves, he said that it would be easier for me to start my research with SH waves. I did not understand, and

asked him what SH waves were. He explained to me, and then the discussion went on. Everything was so natural. Nearly two years later, when I registered as a graduate student in this department and recalled the ground I had covered during that period, I was surprised by the fact that he had not been surprised by my SH question.

Every student is grateful to his or her advisor. So am I, and even more so because of my late start. I appreciate his enthusiasm and patience with me. I owe him a great deal for his time and effort. He taught, impressed and influenced me in many respects, from seismology, preparing talks, and writing papers to his attitude toward scientific research. I also remember so well how excited and impressed I was when I saw him writing in Chinese characters the quotation from a famous general and strategist of the Warring States period in China (475-221 B.C.), Sun Wu-Zi:

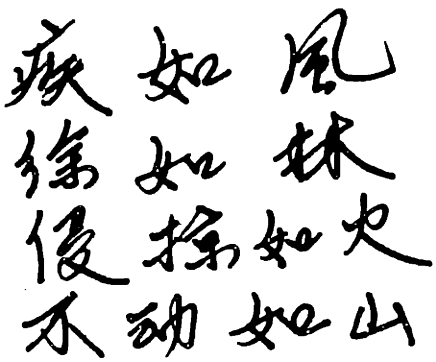

(Swift as wind)

(Silent as woods)

(Sweeping as blazes)

(Immobile as mountains)

I gratefully thank also the other faculty members who gave me encouragement, advice, help and support. Among them particularly Ted Madden and Nafi Toksoz are at the top of my list of gratitude. Ted is my academic advisor and has offered me help not only in academic matters but also in daily life during these years. After I moved my office to room 621, he brought me a porcelain tea cup which has been accompanying me until now. Nafi gave me a lot of advice, from research to my general exam and thesis defense. Among others, I would like to express my thanks to Professors Carl Wunsch and William Pinson for their help.

My particular gratitude should be given to Prof. Samuel C.C. Ting who introduced me to this department as a visiting scientist and offered me continuous encouragement and help during my Ph.D. study. I thank also Profs. C.C. Lin, Hung Cheng, J.A. Kong, and C.C. Mei for their help and advice.

Dr. Teng-fong Wong and Dr. Albert Hsui helped me to settle in cambridge and led me through that confusing period of culture change. Special thanks should be given to them.

After studying and working in the U.S. for more than five years, I have accumulated a long list of professors, research scientists, friends and colleagues, to whom I owe thanks. Some will be mentioned in the following (in a random series). If someone is forgotten, I hope it is forgivable. Dr. R. Turpening, Carol Blackway, Dr. S. Roecker, Dr. B. Chouet, Prof. A. Ben-Menahem, Dr. Fernand Baixas (CGG), Carol Monach (CGG), Dr. Vernon Cormier, Dr. Arthur Cheng, Dr. Barbara Romanowicz, and the visiting scholars from my country, Jin An-Shu, Qian Jia-Dong, Hu Dong-Xin, Gu Ji-Cheng, Wang Bi-Quan, Ye Hong, Zhang Jin-Zhong are among those people on my list of thanks.

I would like to extend my thanks and appreciation to the other side of the earth, Peking, China, to prof. Gu and Fu for their encouragement and help.

My fellow students also offered me tremendous help in both academic and social life. Dale Morgan, Earle Williams, Adolfo Figueroa-Vines, Gerry LaTorraca, Bob Nowack, Tien-Qing Cao, Paul Huang, Scott Phillips, Tim Keho, Wafik Beydoun, Steve Park, John Williams, Kiyoshi Yomogida, and Pei-Zhen Zhang are among them. I would like to thank them all.

Debby Roecker has helped me from the very beginning by leading me through the paper work as a visitor, later on passing through the registration procedure as a student, to the final stage of handing in my thesis. Sharon Feldstein, Donna Martel, Jan Nattier-Barbaro and Judy Roos also offered me much help in different respects.

Dorothy Frank helped me a great deal in typing my thesis and many of my papers. I would like to thank her for her patience with all those equations, which I am sure brought her a lot of headaches, and especially for her overtime work on the weekends.

During my stay in the United States, my cousin Yuk-Cheung Wu and her husband Shyur-jen Chien offered me enormous help and did their best to make my stay enjoyable. I express my heartfelt gratitude to them.

Finally, I thank my family, my wife, my daughter and my son, my brothers and sister for their patience and sacrifice. Also thanks should go to my institute and to my country for giving me such a good opportunity for study.

I express my deepest mourning to my mother, who died during my stay here. Her suffering and sacrifice and her lofty spirit of selflessness moved me deeply, and are engraved on my mind forever. I am sure that she would be very glad to see my thesis, so I will keep one copy for her, and it will surely be my most precious copy of all.

8.15, 1984
MIT, Cambridge, U.S.A.

SEISMIC WAVE SCATTERING AND THE SMALL SCALE INHOMOGENEITIES IN THE LITHOSPHERE

Table of Contents

Chapter 1

INTRODUCTION

Chapter 1

Singularity is almost invariably a clue.

- Sherlock Holmes, the Boscombe Valley Mystery

Sir Arthur Conan Doyle

The joy of being a seismologist comes to you, when you find something new about the earth's interior from the observation of seismic waves obtained on the surface, and realize that you did it without penetrating the earth or touching or examining it directly.

- Possibilities of Seismology in the 1980's

K. Aki, Presidential address at the Seattle Meeting of Seis. Soc. Amer.

INTRODUCTION

When the first earthquake seismogram was recorded in the early 1880's, seismologists were puzzled by the long duration of oscillations. Since then, the theory of elastic wave propagation has made significant progress. After the long period seismograph was invented by Hugo Benioff and others, seismologists were delighted by the agreement between the theory of elastic wave propagation using a layered earth model and the observed long period seismograms. Surface wave data have been used to infer the earth's structure and properties. People seemed to forget the complex appearance of the short period seismograms or just considered it as noise background. Until recently, only the earliest part of the waveform of short period seismograms was used in addition to the travel time data for gaining more information about the source or improving the resolution of the layered model of the earth. The rest of an earthquake seismogram may still be regarded as the "signal generated noise"

or "garbage". However, since Aki started the coda wave study in 1969, the "garbage" has become priceless "treasure'. People found that some very useful information about the medium properties which cannot be obtained from the main phases may be hidden in the coda waves. I believe that the heterogeneities of the lithosphere, even the mantle can be studied through the use of the whole seismogram including the coda waves. In fact, for the reflection seismic method in exploration geophysics, the only part of the seismogram which is used is the "coda wave" part.

The reason that the short period seismograms did not find widespread use is the lack of appropriate theory and modeling technique. In his 1969 paper which initialized the coda wave study, Aki wrote "One of the most urgent problems we are facing in present day seismology is the development of a practical analysis method for dealing with seismic waves in a laterally heterogeneous earth. ..... The need for such a method is desperate both for the source mechanism and for structure studies". Today, in 1980's, the need for such a method or methods is more urgent. The earth has been found to be laterally heterogeneous in every scale, and these different scale heterogeneities seem to situate at the most interesting places. The more heterogeneous, the more interesting the place is. For exploration geophysicists, heterogeneities mean a greater chance of finding oil and minerals. For geologists or tectonists, heterogeneities mean more geological or tectonic activities, such as the plate subduction, continent collision, ridge activity, boundary interaction, and mantle convection, etc. Seismic waves could be the most effective tools to explore and examine these heterogeneities. Therefore, wave propagation and scattering in laterally heterogeneous media has become a topic of current interest in both general and exploration geophysics. There are two approaches: deterministic and

statistic. When the heterogeneities or the local region of the heterogeneous medium are relatively simple, the problem is expected to be set up and solved deterministically. If the heterogeneous region we are interested in is so complicated, so that no practical deterministic method works, the only way to deal with the problem is to follow the statistical approach.

In the past two decades, the theory of propagation and scattering of scalar waves in inhomogeneous media has been widely used in both general seismology and seismic exploration. In the introduction of chapters 2 and 3, I reviewed briefly some applications of the scalar wave theory, its success and problems. In seismic wave explorations, the geophones are placed on the surface not far from the source. The earth model is a layered medium with smooth lateral variations. Therefore the small angle scattering approximation is used to the wave equation, that justifies the use of the scalar wave approximation to the problem of elastic wave propagation. However, since the introduction of shear wave source and three component geophones, the need for applying elastic wave theory to complex targets and structures become apparent and pressing, especially in the case of vertical seismic profiling, where the geophones are installed in the borehole and therefore are favorable for receiving wide-angle reflected or scattered waves.

In general seismology, the scalar wave theory for random media has been used to model the phase and amplitude fluctuations of P waves across a large seismic array (such as LASA or NORSAR). Therefrom the existence of velocity inhomogeneities with correlation length 10-20 km,and the r.m.s. velocity perturbation of 2-4% in the lithosphere has been inferred (see the introduction of Ch. 3). Another application of the scalar wave theory is to model the coda generation and envelope decay. Now the coda waves are believed to be scattered S waves from the small scale heterogeneities in the lithosphere. Aki and his coworkers proposed a single backscattering model

model to formulate the coda envelope decay. In the model the station is assumed at nearly the same point as the source and receives backscattered wave energy from randomly distributed scatterers in the lithosphere. This model can be used only for the coda waves with travel times greater than twice the direct wave travel time. Later, Sato developed a single isotropic scattering model, which can be used to the early part of coda waves. The coda measurement is easy and fast. From its envelope decay, the apparent attenuation can be derived. In fact, coda attenuations or their equivalent Q^{-1} values have been obtained for many regions over the world (see Appendix A). From the coda strength, in principle the strength of the local inhomogeneities could be estimated. However, there are two major problems concerning the coda measurement and interpretation. First is the cause of the apparent attenuation. What is the dominant factor, intrinsic absorption or scattering attenuation? How to separate them? Second is the inconsistency between measured coda strength and the inferred coda strength from the apparent attenuation. These problems could not be solved within the frame of scalar wave theory with single scattering approximation. We need the elastic wave theory and the multiple scattering theory. Dainty et al. have applied the diffusion approximation to the seismograms of moonquakes. This approximation is only valid for high Q and strong scattering media, which is probably hard to find in the earth. Gao et al. have derived an approximate multiple scattering formulae for the scalar wave isotropic scattering. However, in the formulation the station is put in the same place as the source. Therefore the early part of coda waves, which is more sensitive for the separation of absorption and scattering attenuation, is not consedered.

The purpose of this thesis is to advance the seismic wave scattering theory and apply the theory to the problems of small scale inhomogeneities in

the lithosphere. The theory is advanced along two directions. One is to develop the theory of elastic wave scattering and apply it to seismic wave problems along both the deterministic and statistical approaches. We find that there some significant differences in scattering characteristics between the elastic wave theory and the scalar wave theory. Second, we apply the radiative transfer theory developed in optics and neutron transport theory to seismic wave scattering problems and therefrom formulate the multiple scattering of seismic waves in frequency domain. From the solution of energy transfer equation we can obtain the energy density distribution in space for earthquakes. This solution has taken the multiple scattering and the intrinsic attenuation into consideration. The shape of the energy density distribution curve is dependent on the relative strengths of scattering and intrinsic absorption of the medium. Therefore the effects of scattering and absorption can be separated by the comparison between the observed and the theoretical energy density curves.

The elastic wave scattering theory developed here is applied to the fracture volume analysis in the vertical seismic profiling experiments in Michigan. The theory can explain the cross-coupling between the SH and SV waves due to scattering by the fracture zone. The statistical treatment of elastic wave scattering in random media is applied to the coda generation problem. We find that the lithosphere may have multi-scale inhomogeneities. Finally we apply the multiple scattering theory to the Hindu Kush data, and conclude that the intrinsic absorption is the major factor for the measured apparent S wave attenuations at frequencies from 1.5 Hz to 20 Hz. The tectonic implication of the results is discussed, some possible causes of the high intrinsic absorptions are spectulated.

In the following, I summarize the main work and contributions in each chapter.

In chapter 2 we derive the elastic wave scattering for an arbitrary elastic heterogeneity using the equivalent source method and Born approximation. For Rayleigh scattering, the equivalent source representation of the scattered fields gives a clear physical picture and a convenient computational tool. It is shown that the scattered fields of the density perturbation of the heterogeneity are like the radiation fields from a unidirectional point force, the perturbations in shear rigidity ($\delta\mu$) function like an in line couple point source for P wave incidence, and a double couple point source for S wave incidence. The perturbations in Lame constant $\delta\lambda$ behaves like an explosion point source. We believe that this equivalent source representation in terms of perturbations of density, shear rigidity and Lame constant is new. Knowing the equivalent source of the heterogeneity, composed of a single force and a force moment tensor, the scattered fields are easy to calculate. We also show that the scattered field can be decomposed into an "impedance type" and a "velocity type". The former has a main lobe in the backscattering direction and no scattering in the exact forward direction, while the latter to the contrary has a main lobe in the forward direction and no scattering in the exact backward direction. This decomposition is important for some applications.

For Mie scattering, i.e. when the wavelength is comparable to the size of the heterogeneity, we show that any scattered far-field is a product of two factors. One is that of the elastic wave Rayleigh scattering of a unit volume, the other is a scalar wave scattering factor for the parameter variation function of the heterogeneity we called the "volume factor". As examples, we derive the analytic results for a uniform elastic sphere and for a spherically symmetric Gaussian heterogeneity. We show also the relation

variation of the heterogeneity. Miles has derived the Rayleigh scattering formulas for the P wave incidence. Gubernatis et al. have formulated the problem for a uniform inclusion. Our derivation for a heterogeneity with arbitrary parameter variation is new.

In this chapter, many numerical results and scattering patterns are given to show the general scattering characteristics.

The theory is applied to the interpretation of cross-coupling between SH and SV waves due to scattering by a fracture zone in the vertical seismic profiling experiments in Michigan. The observations agree well in general with the theory.

In chapter 3 the elastic wave scattering theory developed in chapter 2 for a single heterogeneity is extended to the case of random media. Following Haddon, who derived the directional scattering coefficient for P wave incidence, we derive the directional scattering coefficient for both P and S wave incidences. The total scattering coefficient for P wave incidence is also obtained. We find that, in both the spatial scattering pattern and the frequency dependence of scattering coefficients, there are some significant differences between scalar wave scattering and elastic wave scattering. The differences are most striking when the wavelength is comparable to the size of inhomogeneities, which is often encountered in the study of short period seismic body waves. Similar to the deterministic case, the perturbations of the medium parameters can be decomposed into an impedance term and a velocity term. In the forward direction, scattered waves are primarily controlled by velocity perturbations, while backscatted waves are generated mainly by impedance perturbations.

The low and high frequency asymptotics for the directional and total scattering coefficients are also derived. We find that the scalar wave theory

can only be used approximately for the forward scattering problems in the high frequency range, such as the phase and amplitude fluctuations in large seismic arrays. The coda strength problem, which is a backscattering or large-angle scattering problem, must be treated by the full elastic wave theory.

The theory developed here is used to analyze past observations. The measurements on phase and amplitude fluctuations in large seismic arrays are forward scattering experiments, which are only sensitive to rather large scale velocity inhomogeneities and therefore revealed the 10-20 km scale inhomogeneities. The coda generation for local earthquakes is a backscattering experiment, which is most sensitive to the inhomogeneities having scale length comparable to the wavelength. Inferred from the observations in several regions, it seems that the sections of lithosphere in tectonically active regions are rich in small scale (less than 1 km) impedance inhomogeneities.

In chapter 4 the multiple scattering problem is formulated using the radiative transfer theory in order to separate the scattering and intrinsic attenuation. Only the problems of isotropic scattering or strong forward scattering for scalar waves are solved at present. We derive the energy density and energy flux distributions for a point soruce in a random medium. The shapes of the energy density curves depend on the values of medium seismic albedo $B_o = \eta_s/(\eta_s+\eta_a)$, where η_s is the scattering coefficient and η_a is the absorption coefficient. Therefore we can separate absorption and scattering based on the observed energy density - distance curves, especially when $B_o >> 0.5$ (the case of strong scattering).

We apply the theory to the Hindu Kush region. The results suggest that in the frequency range 1.5 Hz-20 Hz, scattering is not the dominant factor in the measured apparent attenuation. The time domain analysis using the

diffusion approximation and single scattering approximation also supports this conclusion. This conclusion implies a frequency dependent Q for this region. The tectonic implication of the results and the possible attenuation mechanism are also discussed.

In the last chapter some conclusions are made and further work is suggested.

I put my two papers on scattering attenuation and a collection of the measured data on coda and S apparent attenuations in different regions over the world in the appendices. I feel that the apparent scattering attenuation is a complicated problem, and is highly controversial and widely open at present. The definition of the scattering attenuation is dependent on the methods of measurement and is unfortunately quite confusing in the literature. Much work is needed to clarify the problem. Here in the appendices I only touched the scattering attenuation of mean power of scalar waves and have some criticism on the mean field formalism used for it by some authors. After the publication of these two papers in 1982 (one is presented in 1980 at AGU fall meeting), more discussion by other authors have appeared in the literature and I believe these discussions will help to advance the study on this topic.

Chapter 2

SCATTERING CHARACTERISTICS OF ELASTIC WAVES BY AN ELASTIC HETEROGENEITY

ABSTRACT

The elastic wave scattering by a general elastic heterogeneity having slightly different density and elastic constants from the surrounding medium is formulated using body-force equivalent method and Born approximation. In low-frequency range (Rayleigh scattering), the scattered field by an arbitrary shaped inclusion having an arbitrary variation of density and elastic constants can be equated to a radiation field from a point source composed of an unidirectional force proportional to the density contrast between the inclusion and the medium, and a force moment tensor proportional to the contrasts of elastic constant. It is also shown that the scattered field can be decomposed into an "impedance-type", which has a main lobe in backscattering direction and no scattering in the exact forward direction, and a "velocity-type" scattered field, which to the contrary has a main lobe in forward scattering direction and no scattering in the exact backward direction.

For Mie scattering we show that, the scattered far-field is a product of two factors. One is that of elastic Rayleigh scattering of a unit volume, the other is a scalar wave scattering factor for the parameter variation function of the heterogeneity which we called "volume factor", of which we derived here the analytic expressions for a uniform sphere and for a Gaussian heterogeneity. We show the relations between volume factors and the 3-D Fourier transform, or 1-D Fourier transform in the case of spherical symmetry, of the parameter

variations of the heterogeneity. The scattering spatial pattern varies depending on various combinations of density and elastic-constant perturbations. Some examples of scattering pattern are given to show the general characteristics of the elastic wave scattering.

The theory is applied to interpret the cross-coupling between SH and SV components of S waves due to scattering by a fracture volume in the VSP experiments in Michigan. The observations agree well with the theory in general.

INTRODUCTION

Elastic wave scattering has become a topic of current interest in both general and exploration geophysics, because of its close relation with various kinds of heterogeneities in elastic media. The earth has been found to be laterally inhomogeneous in every scale and the elastic wave scattering could be the most effective tool to examine these inhomogeneities. In general geophysics, the seismic wave scattering by the heterogeneities near the mantle-core boundary of the earth has been proposed by Haddon and Cleary (1974) to interpret the precursors of PKIKP in seismograms (also see Doornbos 1976). The phase and amplitude fluctuation across a large seismic array (such as LASA or NORSAR) were used to estimate the parameters of velocity inhomogeneities under the arrays based on Chernov's theory of wave scattering in random media (Aki 1973, Capon 1974, Berteussen et al., 1975). Seismic coda waves from local earthquakes were attributed to back-scattering of seismic-waves (Aki 1969, Aki and Chouet 1975) and attempts have been made to infer the properties of local small-scale heterogeneities from their studies (Aki 1982, Sato 1982b, Wu and Aki 1984). Apparent attenuation caused by seismic wave scattering and its relation with the intrinsic absorption were also discussed (Aki 1980a, 1980b, 1982, Sato 1981, 1982a, Wu 1980, 1982a, 1982b, Richards and Menke 1983) and the problem is still widely open. In many of the above-mentioned problems, the solution is obtained by a scalar wave scattering theory without guarantee of the

correctness of the solution. We need to develop full elastic wave treatments for these problems. In exploration geophysics, since the introduction of shear sources and three component geophones, the need for applying elastic wave scattering to the complex object and structure exploration becomes apparent and pressing. Especially in the case of vertical seismic profiling, where the source and receiver arrangements are favorable for receiving wide-angle reflected or scattered waves and the targets are often complicated, seismic wave scattering has vast possibilities of application. Some VSP experiments have been done to examine the explosion-formed fracture volume and hydrofractures (Turpening, 1984, Turpening and Blackway 1984).

Therefore, for both general and exploration geophysics, we need to advance the elastic wave scattering theory in order to model and understand better the scattering phenomena and also to develop some effective algorithms. Elastic wave scattering by a single inclusion in a homogeneous elastic medium is the basis of more advanced scattering theory, though the topic itself is a rather old one. The elastic wave scattering by an elastic spherical inclusion has been studied by several authors. Ying and Truell (1956) and Yamakawa (1962) treated the scattering for plane P-wave incidence, Einspruch et al. (1960) derived the formulas for plane S-wave incidence (Gubernatis et al. 1977b corrected some errors in earlier works). In their method the elastic wave equations (a scalar wave equation and a vector wave equation) were

decomposed into three scalar wave equations for scalar potentials, which were solved in spherical coordinates and the boundary conditions were matched to determine the unknown coefficients. The solutions are infinite series, which converge slowly for large inclusions compared with the wavelength. In addition, for a general elastic sphere, a matrix equation must be solved in order to obtain the expanding coefficients for each term of the series. Therefore there are no explicit expressions for scattered fields and the general characteristics of the spatial scattering pattern have not been exposed. However, in Yamakawa's paper (1962), some results of Rayleigh scattering (when the radius of the sphere is much smaller than the wavelength) for plane P-wave incidence have been shown explicitly. Knopoff (1959a,b) also showed some results for a rigid and unmovable sphere. Because of the infinite rigidity and the infinite density of the sphere in his treatment, the scattering pattern derived there is much simpler and not representative for elastic wave scattering.

Besides the complexity of calculation, the eigenfunction expansion method only works for spherical or circular-cylindrical inclusion (see Morse and Feshbach 1953, Pao and Mao 1973). For a general case of arbitrary shape and arbitrary parameter variation of the inclusion, only approximate methods are expected.

Instead of solving the partial differential equations, Miles (1960) formulated the scattering problem into an equivalent integral equation using the elastodynamic Green's

function derived by Stokes (1849, see also Love 1944 §212 and Rayleigh 1945, §378) and obtained explicit expressions in the case of Rayleigh scattering using Born approximation. This approach was also used by Haddon and Cleary (1974) for the P wave scattering near the mantle-core boundary and by Hudson (1977) for the scattered waves in the coda of P. Gubernatis et al. also formulate the scattering problem of a homogeneous inclusion into an integral equation (1977a) and obtained formulas for the case of Born approximation in the whole frequency range (1977b). In this paper, we follow the approach of integral equation and Born approximation, generalize the formulation to a general elastic heterogeneity of arbitrary shape and arbitrary variation of parameters. We derive the formulas for Rayleigh scattering in terms of equivalent sources having different force and force moments corresponding to the different parameter perturbations. This representation is probably more familiar to geophysicists. In Mie scattering range (when the wavelength is comparable to the size of inclusion), the scattering pattern can be decomposed into two factors. One is the Rayleigh scattering, the other is the "volume factor", which is a generalization of the "shape factor" of Gubernatis et al. for uniform inclusions. To demonstrate the scattering characteristics, we give the numerical results and plot the scattering patterns for a uniform elastic sphere and for a spherically symmetric heterogeneity having Gaussian parameter variations. We will also show that the scattered field can be decomposed into an

"impedance-type" and a "velocity-type" scattered field, they have quite different scattering characteristics.

In the last section we will apply the theory to the cross-coupling between SH and SV components due to scattering by a fracture zone in the VSP experiment in Michigan.

I. RAYLEIGH SCATTERING OF ELASTIC WAVES

In a general inhomogeneous, isotropic elastic medium, the equation of motion for displacement $\vec{U}$ is (Aki and Richards, Ch. 13, 1980)

$$\rho \frac{\partial^2 U_i}{\partial t^2} = (\lambda \nabla \cdot \vec{U})_{,i} + [\mu(U_{i,j}+U_{j,i})]_{,j} , \quad (1.1)$$

where ρ is the density of the medium, λ and μ are the Lame constants. Subscripts before comma denote Cartesian components and subscripts after comma, differentiation with respect to the corresponding Cartesian coordinate. Repeated subscripts imply summation over those subscripts. Suppose the surrounding medium has a set of parameters ρ_o, λ_o, μ_o, and the inclusion,

$$\begin{aligned} \rho &= \rho_o+\delta\rho \\ \lambda &= \lambda_o+\delta\lambda \\ \mu &= \mu_o+\delta\mu \end{aligned} \quad (1.2)$$

where the following conditions are supposed to be satisfied

$$\delta\rho << \rho_o, \ \delta\lambda<<\lambda_o, \ \delta\mu<<\mu_o. \quad (1.3)$$

If we write $\vec{U}$ as the sum of "primary wave" $\vec{U}^o$ and "scattered wave" $\vec{U}^1$:

$$\vec{U} = \vec{U}^o+\vec{U}^1 \quad (1.4)$$

and substitute (1.2) and (1.4) into (1.1), an equation for the scattered wave can be obtained by Born approximation (Aki and Richards (13.21), 1980) in which $|\vec{U}^1|<<|\vec{U}^o|$ is assumed:

$$\rho_o \frac{\partial^2 U^1{}_i}{\partial t^2} - (\lambda_o+\mu_o)(\nabla \cdot \vec{U}^1)_{,i} - \mu_o \nabla^2 U^1{}_i = Q_i, \quad (1.5)$$

where Q_i is the equivalent body force due to the presence of the inclusion:

$$Q_i = -\delta\rho \frac{\partial^2 U^\circ_i}{\partial t^2} + (\delta\lambda+\delta\mu)(\nabla\cdot\vec{U}^\circ)_{,i} + \delta\mu\nabla^2 U^\circ_i \tag{1.6}$$

$$+ (\delta\lambda)_{,i}(\nabla\cdot\vec{U}^\circ)+(\delta\mu)_{,j}[U^\circ_{i,j} + U^\circ_{j,i}].$$

From (1.5), therefore, we can see that the scattered field can be calculated as the radiation field of the equivalent body forces due to the interaction of the primary wave and the inclusion in a homogeneous medium with parameters ρ_o, λ_o, μ_o. The scattering problem has been translated into a radiation problem. In Rayleigh scattering, the problem is quite simple. Since the size of the inclusion is small compared with wavelength involved, the phase differences between the radiation far fields of equivalent body force from different parts of the inclusion can be neglected. The total equivalent body force then can be regarded as a point force whose strength is dependent on the total parameter excesses of the inclusion. The total equivalent single force (unidirectional force) can be obtained by integrating Q_i over the volume of the inclusion. Using integration by parts we get

$$F_i = \int_V Q_i dV = -\int_V \delta\rho \frac{\partial U^\circ_i}{\partial t^2} = \omega^2 \int_V \delta\rho U^\circ_i dV \approx \omega^2 \overline{\delta\rho}\, V U^\circ_i(\vec{x}_o) \tag{1.7}$$

where $\overline{\delta\rho}$ is the average density excess of the inclusion, V is the volume of the inclusion, therefore $\overline{\delta\rho}V$ is the total excess mass,

$$\overline{\delta\rho} = \frac{1}{V}\int_V \delta\rho(\vec{x})dV(\vec{x}), \tag{1.8}$$

and the time dependence of the motion is taken to be $e^{-i\omega t}$. Here again we neglect the phase differences of primary fields for different parts of the inclusion and x_o is taken to be the center of the inclusion. Thus, the equivalent single force comes only from the mass difference which is introduced when the inclusion presents in the otherwise homogeneous medium.

However, the equivalent point force has some moment components in addition to the single force. The moment component M_{ik} can be obtained by

$$M_{ik} = \int_V Q_i x_k dV(\vec{x}) \tag{1.9}$$

Putting (1.6) into (1.9) and using integration by parts, we can get

$$M_{ik} = -\delta_{ik}\,\overline{\delta\lambda}V\,\nabla\cdot\vec{U}^o(\vec{x}_o) - \overline{\delta\mu}V[U^o{}_{i,k}(\vec{x}_o)+U^o{}_{k,i}(\vec{x}_o)], \tag{1.10}$$

where $\overline{\delta\lambda}$ and $\overline{\delta\mu}$ are the average excesses of Lame constants of the inclusion,

$$\overline{\delta\lambda} = \frac{1}{V}\int_V \delta\lambda(\vec{x})dV(\vec{x}) \tag{1.11}$$

$$\overline{\delta\mu} = \frac{1}{V}\int_V \delta\mu(\vec{x})dV(\vec{x})$$

and δ_{ik} is the Kronecker delta.

From (1.10) it can be seen that, the force moment tensor due to $\overline{\delta\lambda}V$ has only diagonal elements and all the elements have the same strength, which corresponds to an "explosion-type" point source. Whereas the moment tensor due to $\overline{\delta\mu}V$ can

have both diagonal and/or off-diagonal elements. Because of the symmetry with respect to i and k, $M_{ik} = M_{ki}$, the diagonal elements correspond to on-line force couples, while the off-diagonal-element pairs correspond to torsion-type double couples (we will show this in detail in the following).

Knowing the equivalent body forces, we can calculate the scattered far field easily (see Aki and Richards, ch. 4, 1980),

$$U_i = F_j * G_{ij} + M_{jk} * G_{ij,k}$$

$$= \frac{1}{4\pi\rho_o\alpha_o^2}\gamma_i\gamma_j\frac{1}{r}F_j(t-\frac{r}{\alpha_o}) - \frac{1}{4\pi\rho_o\beta_o^2}(\gamma_i\gamma_j-\delta_{ij})\frac{1}{r}F_j(t-\frac{r}{\beta_o})$$

$$+ \frac{1}{4\pi\rho_o\alpha_o^3}\gamma_i\gamma_j\gamma_k\frac{1}{r}\frac{\partial}{\partial t}M_{jk}(t-\frac{r}{\alpha_o})$$

$$- \frac{1}{4\pi\rho_o\beta_o^3}(\gamma_i\gamma_j-\delta_{ij})\gamma_k\frac{1}{r}\frac{\partial}{\partial t}M_{jk}(t-\frac{r}{\beta_o}) \qquad (1.12)$$

where U_i is the ith component of displacement of the scattered field, G_{ij} is the elastodynamic Green's function for unbounded, isotropic and homogeneous media, "*" means the convolution operation; r is the distance between the center of inclusion and the observation point, γ_i is the direction cosine of the scattering wave to X_i-axis, and α_o, β_o are the P-and S-wave velocity in the medium respectively. For convenience we have dropped the superscript for scattered field.

I.1 Plane P-wave incidence

When a plane P-wave

$$U^{\circ}_1 = \exp[-i\omega(t-x_1/\alpha_o)]$$
$$U^{\circ}_2 = U^{\circ}_3 = 0 \qquad (1.13)$$

is incident on the inclusion along x direction (we take $x_1 = x$ $x_2 = y$ and $x_3 = z$) where α_o is the P-wave velocity in the medium, we can calculate the equivalent point forces from (1.7) and (1.10):

$$F_1 = \omega^2\overline{\delta\rho}V \exp(-i\omega t),$$
$$F_2 = F_3 = 0$$

$$\underline{\underline{M}} = -i\frac{\omega}{\alpha_o}V \begin{vmatrix} \overline{\delta\lambda}+2\overline{\delta\mu} & 0 & 0 \\ 0 & \overline{\delta\lambda} & 0 \\ 0 & 0 & \overline{\delta\lambda} \end{vmatrix} e^{-i\omega t} \qquad (1.14)$$

Here we took the center of the inclusion at the origin of the coordinates. $\underline{\underline{M}}$ stands for the moment tensor of the equivalent point force. Therefore, for P-wave incidence, the equivalent forces consist of a single force in the incident direction, contributed from the density contrast, and a tensor moment contributed from the contrast of elastic constants. We can see in this case that, $\overline{\delta\lambda}$ contributes an isotropic explosion-type source, while $\overline{\delta\mu}$ functions as an on-line force couple (Fig. 1b).

From (1.12) we can derive the scattered far field:

$U_i = F_j * G_{ij} + M_{jk} * G_{ij,k}$

$$= \frac{\omega^2 V}{4\pi\alpha_o^2}\frac{1}{r}e^{-i\omega(t-r/\alpha_o)}\{\frac{\overline{\delta\rho}}{\rho_o}\gamma_i\gamma_1 - \frac{\overline{\delta\lambda}}{\lambda_o+2\mu_o}\gamma_i - \frac{2\overline{\delta\mu}}{\lambda_o+2\mu_o}\gamma_i\gamma_1^2\}$$

$$+ \frac{\omega^2 V}{4\pi\beta_o^2}\frac{1}{r}e^{-i\omega(t-r/\beta o)}\{\frac{\overline{\delta\rho}}{\rho_o}(\delta_{i1}-\gamma_i\gamma_1) - 2(\frac{\beta_o}{\alpha_o})\frac{\overline{\delta\mu}}{\mu_o}(\delta_{i1}\gamma_1-\gamma_i\gamma_1^2)\} \tag{1.15}$$

If we take the spherical coordinates having polar axis in the incident direction x_1 (i.e. in the direction of particle motion), (Fig. 1a), we can write the scattered P-wave $P_U P_r$ and S-wave $P_U S_{mer}$ as

$$P_U P_r = \sum_{i=1}^{3} U^P{}_i\gamma_i = \frac{V}{4\pi}\frac{\omega^2}{\alpha_o^2}\{\frac{\overline{\delta\rho}}{\rho_o}\cos\theta - \frac{\overline{\delta\lambda}}{\lambda_o+2\mu_o} - \frac{2\overline{\delta\mu}}{\lambda_o+2\mu_o}\cos^2\theta\} \tag{1.16}$$

$$\cdot \frac{1}{r}e^{-i\omega(t-\frac{r}{\alpha_o})}$$

$$P_U S_{mer} = -U^S{}_1\sin\theta + U^S{}_2\cos\theta\cos\phi + U^S{}_3\cos\theta\sin\phi$$

$$= \frac{V}{4\pi}\frac{\omega^2}{\alpha_o^2}(\frac{\alpha_o^2}{\beta_o^2})\{-\frac{\overline{\delta\rho}}{\rho_o}\sin\theta + (\frac{\beta_o}{\alpha_o})\frac{\overline{\delta\mu}}{\mu_o}\sin 2\theta\}\frac{e}{r}^{-i\omega(t-\frac{r}{\beta_o})} \tag{1.17}$$

where the subscript 'r' stands for r-component, 'mer' for meridian component. Because of the symmetry of the problem with respect to the polar axis, there is no latitudinal component of S-wave, i.e. $P_U S_{lat} = 0$.

For acoustic scattering, $\mu=0$, (1.16) agrees with Rayleigh's result (Rayleigh, §296, p. 152, 1896). However, the existence of shear rigidity increases greatly the complexity of the scattering pattern. Fig. 1 gives the

spatial patterns of PUP_r and $PU^s{}_{mer}$ for $\overline{\delta\rho}V$, $\overline{\delta\lambda}V$ and $\overline{\delta\mu}V$ respectively. Since the decompositon of the spatial pattern of PUP_r is not unique, our result is equivalent to that of Miles (1960), but is different in representation. In his case, the scattering pattern by $\delta\mu V$ was expressed as a quadropole plus an isotropic part, while in our case as a dipole. We believe our representation is more natural.

The resultant scattering pattern of an inclusion will exhibit quite different appearances depending on various combinations of $\overline{\delta\rho}$, $\overline{\delta\lambda}$ and $\overline{\delta\mu}$. Fig. 2 and 3 are some examples. Notice that, when $\overline{\delta\lambda}$, $\overline{\delta\mu}$ and $\overline{\delta\rho}$ have the same sign, namely the inclusion is harder and heavier or vice versa softer and lighter, the p-p scattering has always its maximum in the backscattering direction (Fig. 2), because all the scattered field due to $\overline{\delta\lambda}$, $\overline{\delta\mu}$ and $\overline{\delta\rho}$ are in phase in backward direction, as can be seen from (1.16). Also interesting is that, when $\frac{\overline{\delta\rho}}{\rho_o} = \frac{\overline{\delta\lambda}}{\lambda_o} = \frac{\overline{\delta\mu}}{\mu_o}$, namely there is no velocity contrast between the inclusion and the medium ($\delta\alpha/\alpha_o = \frac{1}{2}[-\frac{\delta\rho}{\rho_o} + \frac{\delta\lambda+2\delta\mu}{\lambda_o+2\mu_o}]$), there will be only one main lobe in the backscattering direction, and no forward scattering at all (Fig. 3). We will call this "impedance-type" scattering. When density perturbation $\overline{\delta\rho}$ has opposite sign with that of elastic constants $\overline{\delta\lambda}$ and $\overline{\delta\mu}$, i.e. when the inclusion is lighter and harder than the medium or vice versa, the whole scattering pattern will be turned over in such a way as by swapping the forward and backward direction. In Fig. 3 shows

also the case of $\frac{\overline{\delta\lambda}}{\lambda_o} = \frac{\overline{\delta\mu}}{\mu_o} = -\frac{\overline{\delta\rho}}{\rho_o}$. It can be seen that, when there is no impedance contrast between the inclusion and the medium

$$(\frac{\delta(\rho\alpha)}{\rho_o\alpha_o} = \frac{\delta\rho}{\rho_o} + \frac{\delta\alpha}{\alpha_o} = \frac{\delta\rho}{\rho_o} + \frac{1}{2}[-\frac{\delta\rho}{\rho_o} + \frac{\delta\lambda+2\delta\mu}{\lambda_o+2\mu_o}] = \frac{1}{2}[\frac{\delta\rho}{\rho_o} + \frac{\delta\lambda+2\delta\mu}{\lambda_o+2\mu_o}]),$$

the scattering will have only a main lobe in the forward direction for P wave, and no backscattering. This will be called "velocity type" scattering.

In general, if $\frac{\delta\lambda}{\lambda_o} = \frac{\delta\mu}{\mu_o}$ and $\lambda_o = \mu_o$, we can decompose the scattered field into an "impedance-type" and a "velocity-type" scattered field. Since

$$\frac{\delta\rho}{\rho_o} = \frac{\delta Z_p}{Z_{p_o}} - \frac{\delta\alpha}{\alpha_o},$$

$$\frac{\delta\lambda}{\lambda_o+2\mu_o} = \frac{\delta\mu}{\lambda_o+2\mu_o} = \frac{1}{3}(\frac{\delta Z_p}{Z_{p_o}} + \frac{\delta\alpha}{\alpha_o}), \qquad (1.18)$$

where Z_p is the impedance of P wave, therefore

$$P_U P_r = \frac{V}{4\pi}\frac{\omega^2}{\alpha^2_o}\frac{e}{r}^{-i\omega(t-\frac{r}{\alpha_o})}\{\frac{\overline{\delta Z_p}}{Z_{p_o}}(\cos\theta-\frac{1}{3}-\frac{2}{3}\cos^2\theta)$$

$$- \frac{\overline{\delta\alpha}}{\alpha_o}(\cos\theta+\frac{1}{3}+\frac{2}{3}\cos^2\theta)\}. \qquad (1.19)$$

In a similar way,

$$P_U S_{mer} = -\frac{V}{4\pi}\frac{\omega^2}{\alpha^2_o}(\frac{\alpha_o}{\beta_o})^2\frac{e}{r}^{-i\omega(t-\frac{r}{\beta_o})}\{\frac{\overline{\delta Z_s}}{Z_{so}}(\sin\theta-(\frac{\beta_o}{\alpha_o})\sin 2\theta)$$

$$- \frac{\overline{\delta\beta}}{\beta_o}(\sin\theta+(\frac{\beta_o}{\alpha_o})\sin 2\theta)\}, \quad (1.20)$$

where Z_s is the S wave impedance, $Z_s = \rho\beta$.

I.2 Plane S-wave incidence

When a plane S-wave

$$U^\circ_2 = \exp[-i\omega(t-x_1/\beta_o)]$$
$$U^\circ_1 = U^\circ_3 = 0 \quad (1.21)$$

is incident upon the inclusion along the x-direction and having its particle motion in the y-direction (Fig. 4a), the equivalent forces can be derived from (1.7) and (1.10)

$$F_1 = F_3 = 0,$$

$$F_2 = \omega^2\overline{\delta\rho}V \exp(-i\omega t),$$

$$\underline{\underline{M}} = -i \frac{\omega}{\beta_o} V \begin{vmatrix} 0 & \overline{\delta\mu} & 0 \\ \overline{\delta\mu} & 0 & 0 \\ 0 & 0 & 0 \end{vmatrix} e^{-i\omega t} \quad (1.22)$$

namely a single force F_2 in the direction of particle motion of the incident wave due to density contrast, and a double-couple force in the polarization plane due to the contrast of shear rigidity.

The scattered far field can be obtained from (1.12)

$$U_i = F_j * G_{ij} + M_{jk} * G_{ij,k}$$

$$= \frac{\omega^2 \overline{\delta\rho} V}{4\pi\rho_o} \left\{ \frac{\gamma_i\gamma_2}{\alpha_o^2} \frac{1}{r} e^{-i\omega(t-\frac{r}{\alpha_o})} - \frac{(\gamma_i\gamma_2-\delta_{i2})}{\beta_o^2} \frac{1}{r} e^{-i\omega(t-\frac{r}{\beta_o})} \right\}$$

$$+ \frac{\omega^2}{\beta_o} \frac{\overline{\delta\mu} V}{4\pi\rho_o} \left\{ \frac{-2\gamma_i\gamma_1\gamma_2}{\alpha_o^3} \frac{i}{r} e^{-i\omega(t-\frac{r}{\alpha_o})} \right.$$

$$\left. + \frac{(2\gamma_i\gamma_1\gamma_2 - \delta_{i1}\gamma_2 - \delta_{i2}\gamma_1)}{\beta_o^3} \frac{1}{r} e^{-i\omega(t-\frac{r}{\beta_o})} \right\} \qquad (1.23)$$

We take the direction of particle motion of the incident field (y axis) as the polar axis of the spherical coordinates (Fig. 4). The scattered P wave ${}^sUP_r$ and the scattered S wave ${}^sUS_{mer}$ and ${}^sUS_{lat}$ can be written as

$${}_SU^P{}_r = \sum_{i=1}^{3} U^P{}_i\gamma_i = \frac{V}{4\pi} \frac{\omega^2}{\alpha_o^2} \left\{ \frac{\overline{\delta\rho}}{\rho_o} \gamma_2 - 2\left(\frac{\beta_o}{\alpha_o}\right) \frac{\overline{\delta\mu}}{\mu_o} \gamma_1\gamma_2 \right\} \frac{1}{r} e^{-i\omega(t-\frac{r}{\alpha_o})}$$

$$= \frac{V}{4\pi} \cdot \frac{\omega^2}{\alpha_o^2} \left\{ \frac{\overline{\delta\rho}}{\rho_o} \cos\theta - \left(\frac{\beta_o}{\alpha_o}\right) \frac{\overline{\delta\mu}}{\mu_o} \sin 2\theta \sin\phi \right\} \frac{1}{r} e^{-i\omega(t-\frac{r}{\alpha_o})}, \qquad (1.24)$$

$${}^sUS_{mer} = -U_2 \sin\theta + U_3 \cos\phi \cos\theta + U_1 \sin\phi \cos\theta$$

$$= \frac{V}{4\pi} \frac{\omega^2}{\alpha_o^2} \left(\frac{\alpha_o}{\beta_o}\right)^2 \left\{ -\frac{\overline{\delta\rho}}{\rho_o} \sin\theta + \frac{\overline{\delta\mu}}{\mu_o} (\sin^2\theta - \cos^2\theta) \sin\phi \right\} \frac{1}{r} e^{-i\omega(t-\frac{r}{\beta_o})}$$

$$= -\frac{V}{4\pi} \frac{\omega^2}{\alpha_o^2} \left(\frac{\alpha_o}{\beta_o}\right)^2 \left\{ \frac{\overline{\delta\rho}}{\rho_o} \sin\theta + \frac{\overline{\delta\mu}}{\mu_o} \cos 2\theta \sin\phi \right\} \frac{1}{r} e^{-i\omega(t-\frac{r}{\beta_o})} \qquad (1.25)$$

$${}^sUS_{lat} = -U_3 \sin\phi + U_1 \cos\phi$$

$$= \frac{V}{4\pi}\frac{\omega^2}{\alpha_o^2}\left(\frac{\alpha_o}{\beta_o}\right)^2 \frac{\overline{\delta\mu}}{\mu_o}\cos\theta\cos\phi\,\frac{1}{r}\,e^{-i\omega(t-\frac{r}{\beta_o})}. \qquad (1.26)$$

Note that, the scattered S wave due to $\overline{\delta\mu}V$ is attributed to an equivalent double force-couple. For each single couple, if we take the polar axis of the spherical coordinates parallel to the force direction, there will present only meridian components of S wave. For example, the scattered wave of a single couple M_{12} can be expressed in the spherical coordinates having its polar axis along x-axis as

$$U^s_i = -\frac{1}{4\pi\rho_o\beta^3}(\gamma_i\gamma_1-\delta_{i1})\gamma_2\,\frac{1}{r}\,\frac{\partial}{\partial t}\,M_{12},$$

$$U^s_{mer} = -U_1\sin\theta+U_2\cos\phi\cos\theta+U_3\sin\phi\cos\theta$$

$$= -\frac{1}{4\pi\rho_o\beta_o^3}\,\frac{1}{r}\left(\frac{\partial}{\partial t}\,M_{12}\right)\sin^2\theta\cos\phi$$

$$U^s_{lat} = -U_2\sin\phi+U_3\cos\phi = (-\gamma_2^2\gamma_1\sin\phi+\gamma_3\gamma_2\gamma_1\cos\phi)\frac{1}{4\pi\rho_o\beta_o^3}\,\frac{1}{r}\,\left(\frac{\partial}{\partial t}\,M_{12}\right)$$

$$= 0. \qquad (1.27)$$

Therefore we can plot the scattering patterns contributed from different equivalent forces such as, in Fig. 4, where we decomposed the pattern due to $\overline{\delta\mu}V$ into two parts, each of which corresponds to a pattern due to a single couple. The resultant scattering pattern will be the vector sum of those

three patterns. Fig. 5 to 8 show some examples. The S wave scattering depends only on the contrasts of densities and shear modulus, that is physically expected. As in the case of P wave incidence, the S-S scattering patterns have main lobes in the backscattering direction, if both the density and shear modulus have the same sign. Otherwise the main lobes will turn over to the forward direction (as in Fig. 8). In the same manner as in the P wave incidence, there will be no scattering in the forward direction when $\overline{\frac{\delta\rho}{\rho_o}} = \overline{\frac{\delta\mu}{\mu_o}}$, i.e. when the S wave velocity contrast between the inclusion and the medium vanishes. On the other hand, when $\overline{\frac{\delta\rho}{\rho_o}} = -\overline{\frac{\delta\mu}{\mu_o}}$, namely when the shear wave impedance of the inclusion matches that of the medium, there will be no scattering in the backward direction. Notice that, in the x-y plane (z=o) (polarization plane, see fig. 5), when $\overline{\frac{\delta\mu}{\mu_o}} > \overline{\frac{\delta\rho}{\rho_o}}$ there is a small lobe in the forward scattering direction, having particle motion in the opposite direction against that of the main lobe in backscattering direction. This small lobe will grow bigger and approach the same size as the main lobe when $\overline{\frac{\delta\mu}{\mu_o}}$ becomes much larger than $\overline{\frac{\delta\rho}{\rho_o}}$. When $\overline{\frac{\delta\mu}{\mu_o}} < \overline{\frac{\delta\rho}{\rho_o}}$, the forward lobe will merge with the side lobe into a single lobe. In x-z plane (y=o) (Fig. 6) the meridian component U^s_{mer} is the only non-zero component of the scattered waves. The latitudinal component U^s_{lat}, which comes solely from the transverse (with

respect to the particle motion of the incident wave) equivalent force couple M_{12}, does not appear on x-y and x-z planes. It has two lobes having maxima along y-axis (Fig. 7). We have shown that, for a single force couple, there is no latitudinal component U^s_{lat}. It is the transverse force couple which makes the coupling from the incident field to the scattered latitudinal component U^s_{lat}.

In the similar manner to (1.19), (1.20), the scattered field can be decomposed into an "impedance-type" and a "velocity-type",

$$S_U P_r = \frac{V}{4\pi} \frac{\omega^2}{\alpha_o^2} \frac{1}{r} e^{-i\omega(t-\frac{r}{\alpha_o})} \{\frac{\overline{\delta Z_s}}{Z_{so}} (\cos\theta - (\frac{\beta_o}{\alpha_o})\sin 2\theta \sin\phi) - \frac{\overline{\delta\beta}}{\beta_o} (\cos\theta + (\frac{\beta_o}{\alpha_o})\sin 2\theta \sin\phi)\} \tag{1.28}$$

$$S_U S_{mer} = -\frac{V}{4\pi} \frac{\omega^2}{\alpha_o^2} (\frac{\alpha_o}{\beta_o})^2 \frac{1}{r} e^{-i\omega(t-\frac{r}{\beta_o})} \{\frac{\overline{\delta Z_s}}{Z_{so}} (\sin\theta + \cos 2\theta \sin\phi) - \frac{\overline{\delta\beta}}{\beta_o} (\sin\theta - \cos 2\theta \sin\phi)\}, \tag{1.29}$$

$$S_U S_{lat} = \frac{V}{4\pi} \frac{\omega^2}{\alpha_o^2} (\frac{\alpha_o}{\beta_o})^2 \frac{1}{r} e^{-i\omega(t-\frac{r}{\beta_o})} \{(\frac{\overline{\delta Z_s}}{Z_{so}} + \frac{\overline{\delta\beta}}{\beta_o}) \cos\theta \cos\phi\}. \tag{1.30}$$

For both P wave and S wave incidences, the converted waves (P-S or S-P) have only sidelobes (with respect to the incident direction), while the common-mode scattered waves have always main lobes along the incident direction (either forward or backward direction).

Regarding the scattering strength, the scattered S waves are always stronger than the scattered P waves (suppose $\overline{\delta\lambda} \sim \overline{\delta\mu}$) (see 1.24, 1.25, 1.16, 1.17 or Fig. 2, 5 etc.). Therefore, after a large distance of propagation and scattering, the scattered waves will be composed mostly of S waves.

For an elastic sphere, the volume $V = \frac{4}{3}\pi a^3$, the amplitude of scattered field has a familiar dependence of $\omega^2 a^3$, similar to the acoustic scattering.

II. ELASTIC WAVE SCATTERING OF AN ARBITRARY ELASTIC HETEROGENEITY

In Mie scattering (when the wavelength is comparable with the size of inclusion), the equivalent source of scattering by an inclusion can no longer be regarded as a point source. The phase differences of the incident field at different parts of the inclusion and of the scattered field from different parts of the inclusion can no longer be ignored. Nevertheless, if the total scattered field is still much weaker than the incident field, the Born approximation can be still a useful tool for calculating the scattered field and deriving the scattering characteristics.

Here we formulate the problem for a general arbitrary elastic heterogeneity. The scattered waves can be written using Born approximation as

$$U_i(\vec{x}) = \int_V Q_j(\vec{\xi}) * G_{ij}(\vec{x},\vec{\xi}) dV(\vec{\xi}), \qquad (2.1)$$

where $U_i(\vec{x})$ is the scattered field at point x, G_{ij} is the elastodynamic Green function, Q_i is the equivalent body force (1.6), the integration is over the whole volume. Substituting (1.6) into (2.1) we get

$$U_i(\vec{x}) = \int_V \{[-\delta\rho \frac{\partial^2 U^\circ_j}{\partial t^2} + (\delta\lambda+\delta\mu)(\nabla\cdot\vec{U}^\circ)_{,j} + \delta\mu\nabla^2 U^\circ_j] * G_{ij} dV$$

$$+ \int_V \{(\delta\lambda)_{,j}(\nabla\cdot\vec{U}^\circ) + (\delta\mu)_{,k}[U^\circ_{j,k} + U^\circ_{k,j}]\} * G_{ij} dV. \qquad (2.2)$$

After integrating out the terms with the gradients of elastic constant using integration by parts, we have

$$U_i(\vec{x}) = -\int_V \delta\rho \frac{\partial^2 U^\circ_j}{\partial t^2} * G_{ij}\, dV$$

$$-\int_V [\delta_{jk}\delta\lambda(\nabla\cdot\vec{U}^\circ)+\delta\mu\,(U^\circ_{j,k}+U^\circ_{k,j})]*G_{ij,k}\, dV \qquad (2.3)$$

Compared with (1.12), (1.7) and (1.10), we recognize that the term inside the square brackets of (2.3) with the factor dV is nothing but the equivalent force moment tensor for the scattering of the elementary volume $dV(\vec{\xi})$ with elastic constant perturbations $\delta\lambda(\vec{\xi})$ and $\delta\mu(\vec{\xi})$ in the heterogeneity. Convolved with $G_{ij,k}(\vec{x},\vec{\xi})$, it formed the scattered field by the excess of elastic constants of this volume element. Therefore (2.3) means that the scattered field is a superposition of the scattered fields by all the volume elements of the heterogeneity, each of which is of Rayleigh scattering type expressed by (1.12). Remember that the primary field $U^o_i(\vec{\xi})$ and the Green's function $G_{ij}(\vec{\xi})$ are now position dependent. If we take the Fraunhofer approximation to $G_{ij}(\vec{\xi})$ (see Aki and Richards 1980), (2.3) can be further simplified to

$$U_i = U^P_i + U^S_i$$

$$U^P_i(\vec{x}) = \frac{\omega^2}{4\pi\alpha_o^2}\frac{1}{r}\, e^{-i\omega(t-r/\alpha_o)}\cdot$$

$$\cdot\int_V [\frac{\delta\rho(\vec{\xi})}{\rho_o}\,\gamma_i\gamma_j U^\circ_j(\vec{\xi})+\frac{i}{(\omega/\alpha_o)}\,\frac{\delta\lambda(\vec{\xi})}{\lambda_o+2\mu_o}\,\gamma_i(\nabla\cdot\vec{U}^\circ(\vec{\xi}))$$

$$+\frac{i}{(\omega/\alpha_o)}\,\frac{\delta\mu(\vec{\xi})}{\lambda_o+2\mu_o}\,\gamma_i\gamma_j\gamma_k(U^\circ_{j,k}(\vec{\xi})+U^\circ_{k,j}(\vec{\xi}))]e^{-i\frac{\omega}{\alpha_o}(\vec{\xi}\cdot\hat{x})}$$

$$dV(\vec{\xi})$$

$$U^{S}_{i}(\vec{x}) = \frac{\omega^2}{4\pi\beta_o^2}\frac{1}{r}e^{-i\omega(t-r/\beta_o)}\cdot$$

$$\cdot\int_v [\frac{\delta\rho(\vec{\xi})}{\rho_o}(\delta_{ij}-\gamma_i\gamma_j)U^{\circ}_{j}(\vec{\xi})$$

$$+\frac{1}{(\omega/\beta_o)}\frac{\delta\mu(\vec{\xi})}{\mu_o}(\delta_{ij}-\gamma_i\gamma_j)\gamma_k(U^{\circ}_{j,k}(\vec{\xi})+U^{\circ}_{k,j}(\vec{\xi}))]e^{-i\frac{\omega}{\beta_o}(\vec{\xi}\cdot\hat{x})}$$

$$dV(\vec{\xi}) \qquad (2.4)$$

For plane P wave incidence,

$$P_U P_i(\vec{x}) = \frac{\omega^2}{4\pi\alpha_o^2}\frac{1}{r}e^{-i\omega(t-\frac{r}{\alpha_o})}\cdot$$

$$\cdot\int_v [\frac{\delta\rho(\vec{\xi})}{\rho_o}\gamma_i\gamma_1-\frac{\delta\lambda(\vec{\xi})}{\lambda_o+2\mu_o}\gamma_i-\frac{2\delta\mu(\vec{\xi})}{\lambda_o+2\mu_o}\gamma_i\gamma^2{}_1]e^{i\frac{\omega}{\alpha_o}\xi_1-i\frac{\omega}{\alpha_o}(\hat{x}\cdot\vec{\xi})}dV(\vec{\xi}) \qquad (2.5)$$

$$P_U S_i(\vec{x}) = \frac{\omega^2}{4\pi\beta_o^2}\frac{1}{r}e^{-i\omega(t-r/\beta_o)}$$

$$\cdot\int_v [\frac{\delta\rho(\vec{\xi})}{\rho_o}(\delta_{i1}-\gamma_i\gamma_1)-(\frac{\beta_o}{\alpha_o})\frac{2\delta\mu(\vec{\xi})}{\mu_o}(\delta_{i1}-\gamma_i\gamma_1)\gamma_1]e^{i\frac{\omega}{\alpha_o}\xi_1-\frac{i\omega}{\beta_o}(\hat{x}\cdot\vec{\xi})}$$

$$dV(\vec{\xi}) \qquad (2.6)$$

In the case of plane S wave incidence,

$$S_U P_i(\vec{x}) = \frac{\omega^2}{4\pi\alpha_o^2}\frac{1}{r}\, e^{-i\omega(t-r/\alpha_o)}$$

$$\cdot\int \left[\frac{\delta\rho(\vec{\xi})}{\rho_o}\gamma_1\gamma_2-\left(\frac{\beta_o}{\alpha_o}\right)\frac{2\delta\mu(\vec{\xi})}{\mu_o}\gamma_1\gamma_1\gamma_2\right]e^{i\frac{\omega}{\beta_o}\xi_1-i\frac{\omega}{\alpha_o}(\hat{x}\cdot\vec{\xi})}dV(\vec{\xi}) \tag{2.7}$$

$$S_U S_i(x) = \frac{\omega^2}{4\pi\beta_o^2}\frac{1}{r}\, e^{-i\omega(t-r/\beta_o)}$$

$$\cdot\int_V \left[\frac{\delta\rho(\vec{\xi})}{\rho_o}(\delta_{i2}-\gamma_i\gamma_2)-\frac{\delta\mu(\vec{\xi})}{\mu_o}(\delta_{i1}\gamma_2+\delta_{i2}\gamma_1-2\gamma_i\gamma_1\gamma_2)\right]$$

$$\cdot e^{i\frac{\omega}{\beta_o}\xi_1-i\frac{\omega}{\beta_o}(\hat{x}\cdot\vec{\xi})}dV(\vec{\xi}). \tag{2.8}$$

Comparing these formulas with (1.15) and (1.23), we found that, the scattered far field of a general heterogeneity can be calculated by summing the Rayleigh-scattered fields by all the volume elements, with a phase factor corresponding to the source-scatterer-receiver travel time. This way, we can adopt some numerical methods to calculate the scattered field of an inclusion having arbitrary shape and parameter variation by dividing the inclusion into a number of volume elements smaller than the wavelength.

Suppose $\delta\rho$, $\delta\lambda$ and $\delta\mu$ have the same form of spatial variation. We introduce the parameter variation function $P(\vec{\xi})$ such that

$$\delta\rho(\vec{\xi}) = \delta\rho_o\, P(\vec{\xi}),$$

$$\delta\lambda(\vec{\xi}) = \delta\lambda_o\, P(\vec{\xi}),$$

$$\delta\mu(\vec{\xi}) = \delta\mu_o \, P(\vec{\xi}), \tag{2.9}$$

where $\delta\rho_o$, $\delta\lambda_o$, $\delta\mu_o$, are the parameter perturbations at the center of the heterogeneity and satisfy

$$\delta\rho_o \int_V P(\vec{\xi})dV(\vec{\xi}) = \overline{\delta\rho}\, V, \text{ etc.} \tag{2.10}$$

Putting (2.9) into (2.5) yields

$$P_U P_i(\vec{x}) = \frac{\omega^2}{4\pi\alpha_o^2}\frac{1}{r} e^{-i\omega(t-r/\alpha_o)}\left[\frac{\delta\rho_o}{\rho_o}\gamma_i\gamma_1 - \frac{\delta\lambda_o}{\lambda_o+2\mu_o}\gamma_i - \frac{2\delta\mu_o}{\lambda_o+2\mu_o}\gamma_i\gamma_1^2\right]$$

$$\cdot \int_V P(\vec{\xi}) e^{i\frac{\omega}{\alpha_o}\xi_1 - i\frac{\omega}{\alpha_o}(\hat{x}\cdot\vec{\xi})} dV(\vec{\xi}). \tag{2.11}$$

We recognize that the formula is the same as the Rayleigh scattering with the volume V replaced by a factor

$$\Theta_1(\hat{x}) = \int_V P(\vec{\xi}) e^{i\frac{\omega}{\alpha_o}\xi_1 - i\frac{\omega}{\alpha_o}(\hat{x}\cdot\vec{\xi})} dV(\vec{\xi}). \tag{2.12}$$

We can call $\Theta_1(\hat{x})$ "volume factor". In the case of a uniform inclusion $P(\vec{\xi}) = 1$, it becomes the "shape factor" of Gubernatis et al. (1977b). In this way we can rewrite (2.5)-(2.8) as

$$P_U P_i(\vec{x}) = \frac{1}{r} e^{-i\omega(t-r/\alpha_o)} E_1(\hat{x})\Theta_1(\hat{x}),$$

$$P_U S_i(\vec{x}) = \frac{1}{r} e^{-i\omega(t-r/\beta_o)} E_2(\hat{x})\Theta_2(\hat{x}),$$

$$S_U P_i(\vec{x}) = \frac{1}{r} e^{-i\omega(t-r/\alpha_o)} E_3(\hat{x})\Theta_3(\hat{x}),$$

$$S_U S_i(\vec{x}) = \frac{1}{r} e^{-i\omega(t-r/\beta_o)} E_4(\hat{x})\Theta_4(\hat{x}). \tag{2.21}$$

where E_{1-4} are the elastic wave Rayleigh-scattering factor for a unit volume, Θ_{1-4} are the corresponding volume factors, which are scalar wave scattering patterns:

$$\Theta_n(\hat{x}) = \int_V P(\vec{\xi}) e^{i\omega\vec{\xi}\cdot\vec{S}_n} \, dV(\vec{\xi}). \tag{2.14}$$

$$\vec{S}_1 = \frac{1}{\alpha_o}\hat{x}_1 - \frac{1}{\alpha_o}\hat{x}, \qquad S_1 = |\vec{S}_1| = \frac{1}{\alpha_o} 2\sin\frac{\theta}{2},$$

$$\vec{S}_2 = \frac{1}{\alpha_o}\hat{x}_1 - \frac{1}{\beta_o}\hat{x},$$

$$S_2 = |S_2| = \sqrt{\left(\frac{1}{\alpha_o}\right)^2 + \left(\frac{1}{\beta_o}\right)^2 - \frac{2}{\alpha_o\beta_o}\cos\theta},$$

$$\vec{S}_3 = \frac{1}{\beta_o}\hat{x}_1 - \frac{1}{\alpha_o}\hat{x}, \qquad S_3 = S_2,$$

$$\vec{S}_4 = \frac{1}{\beta_o}\hat{x}_1 - \frac{1}{\beta_o}\hat{x}, \qquad S_4 = \frac{1}{\beta_o} 2\sin\frac{\theta}{2}. \tag{2.15}$$

where $\hat{x}_1$ is the unit vector in x_1-direction, i.e. the incident direction, $\vec{S}_1$-$\vec{S}_4$ are the exchange slowness vectors (Fig. 9) and θ is the scattering angle. Note that (2.14) is in the form of 3-D spatial Fourier transform. Putting $\vec{K}_n = \omega\vec{S}_n$, we have

$$\Theta_n(\hat{x}) = \int_V P(\vec{\xi}) e^{i\vec{K}_n\cdot\vec{\xi}} \, dV(\vec{\xi}) = P_3(\vec{K}_n), \tag{2.16}$$

where $\hat{P}_3(\vec{K}_n)$ is the 3-D Fourier transform of $P(\vec{\xi})$. For a specified scattering direction, the volume factor θ_n is equal to the spatial Fourier component of the parameter variation of the heterogeneity at the corresponding $\vec{K}_n$. If the parameter's spatial variation is spherically symmetrical, i.e. $P(\vec{\xi})$ is only the function of $|\vec{\xi}|=r_1$, we introduce a spherical coordinate (r_1, θ_1, ϕ_1) having the polar axis along $\vec{S}_n$ direction. Then we can integrate out the integral with respect to θ_1 and ϕ_1:

$$\theta_n(\theta) = \int_0^{\infty} \int_0^{\pi} \int_0^{2\pi} P(r_1) e^{i\omega r_1 S_n \cos\theta_1} r_1^2 \sin\theta_1 d\phi_1 d\theta_1 dr_1$$

$$= \frac{4\pi}{\omega S_n} \int_0^{\infty} P(r_1) \sin(\omega S_n r_1) r_1 dr_1 = \frac{-4\pi}{\omega S_n} \frac{1}{2} \frac{\partial}{\partial(\omega S_n)} \qquad (2.17)$$

$$\int_{-\infty}^{\infty} P(r_1) \cos(\omega S_n r_1) dr_1 = -\frac{2\pi}{\omega S_n} \frac{\partial}{\partial(\omega S_n)} \hat{P}(\omega S_n)$$

where $\hat{P}(\omega S_n)$ is the 1-D spatial Fourier transform of the parameter variation $P(r)$.

In the following we will show two examples, a uniform sphere and a local Gaussian type spherical heterogeneity to demonstrate the general scattering characteristics.

1) A uniform sphere

For a uniform sphere, P(r) is a boxcar function. The volume factor turns out as

$$\Theta_n(\theta) = \frac{4\pi}{\omega S_n}\left[\frac{\sin\omega S_n a}{(\omega S_n)^2} - \frac{a}{\omega S_n}\cos\omega S_n a\right]$$

$$= \frac{4\pi a^3}{(\omega S_n a)^2}\left[\frac{\sin\omega S_n a}{\omega S_n a} - \cos\omega S_n a\right], \qquad (2.18)$$

where a is the radius of the sphere. Note that,

$$\frac{\sin(\omega S_n a)}{\omega S_n a} - \cos\omega S_n a \approx \frac{1}{3}(\omega S_n a)^2,$$

$$\Theta_n(\theta) \approx V, \quad \text{when} \quad \omega S_n a \ll 1. \qquad (2.19)$$

In Rayleigh scattering, the phase differences between the volume elements are neglected, so the volume factor is equal to the real volume. For Mie scattering, in general, the volume factor is smaller than the volume because of the interferences between the fields from different volume elements.

Since $S_2 = S_3$, we call

$$\Theta^c \equiv \Theta_2 \equiv \Theta_3 \qquad (2.20)$$

the volume factor of converted wave. The volume factors for P wave scattering and S wave scattering

$$\Theta^P = \Theta_1, \qquad \Theta^S = \Theta_4 \qquad (2.21)$$

have the same angular dependence for same value $\frac{\omega}{c}a$ where c is either the P wave velocity or the S wave velocity. Fig. 10-12 and 13-15 give the volume factors for S wave scattering

Θ^S and for wave converting Θ^C respectively. In plotting, we normalized the values with the volume of the sphere. It can be seen that, for P-P or S-S scattering the volume factor Θ has always the main lobe in the forward scattering direction. In the direction of incident wave propagation, the factor is always equal to one, since all the scattered waves from different volume elements are always in phase along the incident direction. When the volume becomes larger, small backlobe and sidelobes start to appear (Fig. 11,12), but most of the scattered energy for the common-mode scattering (P-P or S-S) will be contained in the main forward lobe. However the situation is quite different for the converted waves. Because the scattered waves have different velocity from the incident waves, destructive interference also occurs in the forward direction. Therefore the volume factor Θ^C along the incident direction will reduce its value and becomes oscillatory with increasing frequencies. The scattering pattern then becomes more complex, and the converted energy diverges to all directions (e.g. Fig. 15) instead of concentrating in the main forward lobe as for the common-mode scattering, when the wavelength goes shorter and shorter.

Note that the Θ's are axially symmetric with respect to x_1-axis (the incident direction).

The general scattering pattern is a combination of $\hat{E(x)}$ and $\Theta(\theta)$, which becomes quite complicated for high frequencies. However, the general feature is to have more scattered energy concentrated in the forward direction. In other words, the forward scattering becomes dominant and the

wave conversions become comparably negligible when the wavelength becomes very short compared to the size of inclusions.

Fig. 16 through 26 show some examples of the scattering patterns for different frequencies in the high frequency range. Note that, for P-P or S-S_{mer} scattering, the main lobe becomes sharper and much bigger than the side lobes when frequency goes higher (Fig. 17 and 22), while the converted waves and cross-coupled waves ($^{s}U^{s}_{lat}$) diverge into many small lobes in all directions and become much smaller compared with the main lobe (Fig. 17,22 and 26). Also remarkable is the "impedance-type" scattering, which does not have a main lobe in the forward direction and has the similar features as the converted or cross-coupled waves (Fig. 18,19,23,24).

Since there is no latitudinal component of scattered S waves in the x-y plane (see 1.26), we took a plane with the common x-axis and having 45° angle with the x-y plane (Fig. 26) to present the changes of the scattering pattern with the increase of frequencies. Fig. 26 gives the patterns in that plane for three frequencies. We can see that, there will be four small lobes of latitudinal component bending close to x-axis when the wavelength becomes shorter, though the x-axis is a node. These four small lobes will give rise to the scattered cross-component (here the z-component) in the nearly forward direction, which might be very useful in detecting the existence of scattering inclusions.

2) A Gaussian spherical heterogeneity

If the parameter variation of a spherical heterogeneity has a Gaussian shape, i.e.

$$P(r) = \exp(r^2/a_o^2) , \qquad (2.22)$$

where a_o is the characteristic length of the heterogeneity. From (2.17) we have

$$\theta_n = (\sqrt{\pi}a_o)^3 \exp[-(\omega S_n a_o)^2/4]. \qquad (2.23)$$

In Fig. 27, θ^P are shown on the upper half plane, θ^C, the lower half plane. Compared with the case of uniform sphere, the patterns for high frequencies are much simpler, though the low-frequency patterns are similar. Because of the smoothness of the parameter variation, small sidelobes do not appear in the high frequency range. The scattered energy gradually concentrates to the forward lobe and becomes narrower and narrower without splitting when frequency goes higher and higher. Therefore the total scattering patterns become also simpler for high frequencies. Fig. 28 and 29 show the patterns of impedance type and velocity type for P wave incidence. Fig. 30 shows the patterns for S wave incidence only for $(\omega/\beta_o)a_o = 10$ to compare with the case of uniform sphere of Fig. 24. The patterns for cross-coupled component $S_U S_{lat}$ are shown in Fig. 31, presented in the same manner as in Fig. 26. The four lobes gradually bend towards the forward direction without splitting when frequency increases.

III. APPLICATION TO THE FRACTURE VOLUME ANALYSIS USING DIFFERENTIAL VERTICAL SEISMIC PROFILING

The single scattering theory developed here can serve as the basis for further developments of the scattering theory in different branches. Statistical treatment can be added to formulate the single scattering theory of elastic random media (see Chapter 3). The multiple elastic wave scattering can also be developed based on the single scattering theory of ela tic waves. Besides, the elastic wave single scattering theory itself can find applications in many practical situations as long as the scattering is not very strong and the propagation distance is not very long, i.e. the requirement for Born approximation is met. As an example we show in this section the application of the theory to the calculation and interpretation of the conversion from SH to SV due to scattering by a fracture volume, when using shear wave VSP (vertical seismic profiling). The detailed description of the experiment and the results is presented in one chapter written by Turpening (1984) of the book "Vertical seismic profiling". In the following we only outline the results and the interpretation using the theory developed here.

The experiment is done in the Michigan Basin, aimed at the study of fracture analysis method using VSP. This method is needed for the assessment of fracturing technique used in the project of extracting oil from the Antrim shale. Fig. 32 shows the arrangement of the experiment. D and C are the source positions on the surface. In well 100 the VSP measurements are taken using GeoSpace downhole wall-locking

geophones, in which the three-componnt 4.5 Hz sensors were installed along with a 40 db amplifier. The source used is a 4.2-in water mortar (Fig. 33), which has a strong SH excitation and can change the polarity of the SH motion easily by rotating the mortar 180° in direction. In the wells around well 300 at the depth about 1300 ft a fracture zone was formed by several explosions. After explosions, the P wave velocity of the Antrim shale was reduced from 3 km/sec to about 2.1 km/sec, and the S wave velocity, from 1.56 km/sec to 1 km/sec. The fracture zone was estimated by the caliper log, VSP velocity and attenuation measurements, along with the fracturing formula to be of 30 m in vertical extent and 19.5 m x 21 m in horizontal extent. The differential VSP is constructed from the comparison of the measurements before and after the fracture zone was formed.

After the fracturing was completed, the measurements in well 100 were repeated for the shotpoints C and D. No noticeable changes are observed on either amplitudes or travel times for both P and S waves, because of the relatively long distances between the source and the target and between the target and the sensors (the distance between D, C and well 100 is about 240 m, the fracture zone is situated in the middle). The only effect recognized of the fracture zone to the transmitted waves is the cross-coupling between the SH and SV components of shear waves. Fig. 34 and 35 show the seismic profile of vertical components before fracturing for the shotpoints C and D respectively. The traces are the overlays for two opposite polarizations of SH source (water mortar).

Fig. 36 and 37 show the after-data for the same conditions. It can be seen from the comparison of before-and after-data that, there are SV waves appearing in the after-traces. These waves are interpreted to be converted from SH waves due to scattering by the fracture volume. There are two ways in which these waves can be distinquished as SV waves from the possible delayed or reflected P waves. First is that they are well within the expected S window, and second, they change their phases by 180° when the SH sources switch the polarizations (the mortar rotates by 180°). The SV waves can be seen clearly having two lobes with a null in the middle. This depolarization or cross-coupling phenomena can be explained by the scattering of elastic heterogeneities. From Fig. 4b we know that the equivalent source of scattering for a small volume of shear rigidity perturbations (δ) is a double couple, which can convert the incident SH wave into SV wave. However, for the Rayleigh scattering this SV component cannot be found in the forward direction. When the volume of the fracture zone is larger than the wavelength, the SV lobes will bend forward because of the constructive interference in the forward direction and destructive interference in the side directions. From Fig. 26 for the uniform sphere model and Fig. 31 for the Gaussian spherical heterogeneity (the perturbation varies Gaussianly along the radius), we can see that, when the heterogeneity is much larger than the wavelength, there will be four narrow lobes near the forward direction. Therefore, the well 100 may just pass through two of these lobes. The locations of the lobes, the polarization

of the lobes can be all explained by the theory. However, the size of the fracture zone inferred by the theory is larger than expected. The closeness of the two lobes (with scattering angle about 15°) requires the diameter of the fracture volume exceeding twice the wavelength, which is not consistent with other measurements. This may be caused by the spherical symmetry of the model, while the fracture volume is estimated as an ellipsoid with its long axis in the vertical direction. The standing ellipsoid is favorable to the constructive interference in the forward direction. Anyhow, the single scattering theory based on Born approximation provides a useful tool for the interpretation of shear wave fracture assessment.

SUMMARY

The Born approximation and the body force equivalent method proved to be useful in calculating the scattered field by an arbitrary elastic inclusion for the case of weak scattering, i.e. when the scattered field is much smaller than the incident field. In low frequency range (Rayleigh scattering) the scattered field is insensitive to the shape and parameter distribution of the inclusion and can be equated to a radiation field from a point source composed of a single force and a force moment tensor. The equivalent single force (unidirectional force) is proportional to the total density excess of the inclusion and is directed along the axis of particle motion of the incident wave (1.14, 1.22 and Fig. 1, Fig. 4). For P wave incidence, the equivalent moment tensor due to $\overline{\delta\lambda}V$ corresponds to an isotropic "explosion type" point force; whereas the moment tensor due to $\overline{\delta\mu}V$ is composed of an on-line force couple (1.14 and Fig. 1). In the case of S wave incidence, the equivalent moment tensor is contributed only from the shear rigidity excess $\overline{\delta\mu}V$, and is composed of a double-couple in the polarization plane of the incident wave (1.22 and Fig. 4).

The scattered field can be decomposed into an "impedance type", which has a main lobe in backscattering direction and no scattering in the exact forward direction, and a "velocity type" scattered field, which to the contrary has a main lobe in forward direction and no scattering in the exact backward direction (1.19, 1.20, 1.28-30 and Fig. 3, Fig. 8). The practical scatterng patterns depend on various combinations of

density and elastic-constant perturbations (1.16, 1.17 and 1.24-26). Examples are given to show the general characteristics of the scattering patterns. For both P wave and S wave incidences, the converted waves (P-S or S-P) have only side lobes (with respect to the incident direction), while the common-mode scattered waves have always main lobes along the incident direction (either forward or backward). Scattered S waves are approximately $(\lambda_o+2\mu_o)/\mu_o$ times stronger than scattered P waves. The frequency dependence of the scattering amplitude will be the familiar $\omega^2 a^3$ for a small elastic sphere.

For Mie scattering, the scattered far-field can be expressed as a product of two factors, i.e. the scattered field of elastic wave Rayleigh scattering multiplied by a "volume factor" which is the scalar wave scattering pattern for the heterogeneity. The "volume factor" can be calculated through (2.14) either numerically or analytically. The derivations for a homogeneous spherical inclusion and for a Gaussian heterogeneity have been carried out (2.18, 2.23). For the sphere, the volume factors for the common-mode scattering (P-P or S-S) have always the main lobe in the forward scattering direction, and will have more energy concentrated in the forward lobe when wavelength becomes shorter, though small sidelobes and backlobes will also appear (Fig. 10-12). However the volume factors for converted waves (P-S or S-P) will have complex spatial patterns and the converted energy will diverge to all directions when wavelength becomes short (Fig. 13-15).

The resultant scattering pattern for a large elastic sphere is a product of the elastic Rayleigh scattering pattern and the volume pattern. Some examples are given to show the different characteristics for common-mode scattering and mode conversion or component-cross-coupling of S waves. The general feature is that in very high frequencies, the forward scattering becomes dominant and the wave conversion and cross-coupling become negligible. However, remarkable is the different behavior of the "impedance type" scattering (Fig. 18, 19, 23 and 24). For the Gaussian heterogeneity, the general features are the same as the sphere. However, because of the smoothness of the parameter variation, the small sidelobes do not appear, resulting in much simpler scattering patterns at high frequencies.

As an example, the theory is applied to the fracture volume analysis using differential vertical seismic profiling. When the SH source is used, two lobes of cross-coupled SV components have been observed near the forward direction, which agree with the theory.

Acknowledgement

I am grateful to Dr. H. Sato for the helpful discussions with him about the use of Born approximation to elastic wave scattering problem when he visited MIT during 1982. Discussions with Dr. R. Turpening about the possibility of applying the cross-coupling effect by scattering to exploration were also very useful. Dr. K. Burrhus helped design and plot the 3-D scattering patterns. Thanks should also be given to them. I am also grateful to the reviewers and the associate editor, who pointed out the works of Gubernatis et al., so that I could revise the paper appropriately. This research is supported partly by the VSP project of Earth Resource Lab. of MIT funded by CGG (Compagnie Générale de Geophysique) and partly by the Advanced Research Project Agency of the Department of Defense, monitored by the Air Force Office of Scientific Research under Contract No. F49620-82-K-0004. This paper is partly (the treatment about the uniform sphere) taken from the report "Vertical seismic profiling research" of the "Earth Resources Laboratory" of Massachusetts Institute of Technology (see Wu 1983). I express here my gratitude to them for allowing me to use the results in the report, and also to Dr. Turpening for allowing me to use his experimental results and his figures.

References

Aki, K., 1969, Analysis of the seismic coda of local earthquakes as scattered waves: J. Geophys. Res., v. 74, p. 615-631.

_____1973, Scattering of P waves under the Montana Lasa: J. Geophys. Res., v. 78, p. 1334, 1346.

_____1980a, Attenuation of shear waves in the lithosphere for frequencies from 0.05 to 25 Hz: Phys. Earth Planet. Inter., v. 21, p. 50-60.

_____1980b, Scattering and attenuation of shear waves in the lithosphere: J. Geophys. Res., v. 85, p. 6496-6504.

_____1982, Scattering and attenuation: Bull. Seis. Soc. Am., v. 72, p. 5319-5330.

Aki, K. and B. Chouet, 1975, Origin of coda waves: source, attenuation and scattering effects: J. Geophys. Res., v. 80, p. 3322-3342.

Aki, K. and P. Richards, 1980, Quantitative Seismology, Ch. 13: San Francisco, W.H. Freeman and Co.

Berteussen, K.A., A. Christofferson, E.S. Husebye and A. Dable, 1975, Wave scattering theory in analysis of P wave anomalies at NORSAR and LASA: Geophys. J.R. astr. Soc., 42, 403-417.

Capon, J., 1974, Characterization of crust and upper mantle structure under Lasa as a random medium: Bull. Seis. Soc. Am., v. 64, p. 235-266.

Doornbos, D.J., Characteristics of lower mantle inhomogeneities from scattered waves: Geophys. J.R. astr. Soc., v. 44, p. 447-470.

Einspruch, N.G., E.J. Witterholt, and R. Trull, 1960, Scattering of a plane transverse wave by a spherical obstacle in an elastic medium: J. appl. phys., v. 31, 5, p. 806-818.

Gubernatis, J.E., E. Domany and J.A. Krumhansl, 1977a, Formal aspects of the theory of the scattering of ultrasound by flows in elastic materials: J. Appl. Phys., v. 48, p. 2804-2811.

Gubernatis, J.E., E. Domany, J.A. Krumhansl and M. Huberman, 1977b, The Born approximation in the theory of the scattering of elastic waves by flows: J. Appl. Phys., v. 48, p. 2812-2819.

Haddon, R.A.W. and J.R. Cleary, 1974, Evidence for scattering of seismic PKP waves near the mantle-core boundary: Phys. Earth and Planet. Int., v. 8, p. 211-234.

Hudson, J.A., 1977, Scattered waves in the coda of P: J. Geophys., v. 43, p. 359-374.

Knopoff, L., 1959a, Scattering of compressional waves by spherical obstables: Geophys., v. 24, 1, p. 30-39.

_____1959b, Scattering of shear waves by spherical obstacles: Geophys., v. 24, 2, p. 209-219.

Love, A.E.H., 1944, A treatise on the mathematical theory of elasticity, 4th ed: New York, Dover.

Miles, J.W., 1960, Scattering of elastic waves by small inhomogeneities, Geophys., 25, 3, 642-648.

Morse, P.M. and H. Feshbach, 1953, Methods of Theoretical Physics: New York, McGraw-Hill.

Pao, Y.H. and C.C. Mow, 1973, Diffraction of elastic waves and dynamic stress concentrations: New York, Crane Russak.

Rayleigh, J.W.S., 1896, The theory of sound, V. II: Dover, 1945 edition.

Sato, H., 1981, Attenuation of elastic waves in one-dimensional inhomogeneous elastic media: Phys. Earth Planet. Int., v. 26, p. 244-245.

_____1982a, Amplitude attenuation of impulsive waves in random media based on travel time corrected mean wave formulism: J. Acoust. Soc. Am., v. 71, p. 559-564.

_____1982b, Attenuation of S waves in the lithosphere due to scattering by its random velocity structure: J. Geophys. Res., v. 87, p. 7779-7785.

Stokes, G.G., 1849, Dynamical theory of diffraction: Cambr. Phil. Soc. Trans., v. 9, p. 1; also Mathematical and Physical Papers, v. 2, p. 243-328.

Turpening, R., 1984, Differential vertical seismic profiling: fracture volume analysis: Ch. 8 of "Vertical seismic profiling", ed. by Balch, A. and M. Lee, Boston, I.H.R.D.C.

Turpening, R. and C. Blackway, 1984, Differential vertical profiling: hydrofrac: ibid, ch. 9.

Wu, R.S., 1980, The attenuation of seismic waves due to scattering in a random medium (abstract): EOS, v. 61, 46, p. 1049.

_____1982a, Attenuation of short period seismic waves due to scattering: Geophys. Res. Lett., v. 9, p. 9-12.

_____1982b, Mean field attenuation and amplitude attenuation due to wave scattering: Wave motion, v. 4, p. 305-316.

_____1983, Scattering characteristics of elastic waves by an elastic inclusion, in "Vertical seismic profiling research": Report of Earth Resources Laboratory, Dept. of Earth, Atmospheric, and Planet. Sci., Mass. Inst. of Tech.

Wu, R.S. and K. Aki, 1984, Elastic wave scattering by a random medium and the small scale inhomogeneities in the lithosphere: submitted to J. Geophys. Res.

Ying, C.F. and R. Truell, 1956, Scattering of a plane longitudinal wave by a spherical obstacle in an isotropically elastic solid: J. appl. phys., v. 27, p. 1087-1097.

Yamakawa, N., 1962, Scattering and attenuation of elastic waves: Geophysical Magazine (Tokyo), v. 31, p. 63-103.

Figure Captions

1. a) Spherical coordinate system for P wave incidence, and b) the scattering patterns for different equivalent forces.
2. Scattering patterns of Rayleigh scattering for plane P wave incidence. The upper half is of P-P scattering, the lower half is of P-S scattering. All the patterns are axially symmetric about the x-axis.
3. Same as Fig. 2. The scattering pattern of "velocity-type" and "impedance type" scattering.
4. a) Spherical coordinate system for S wave incidence, and b) the scattering patterns for different equivalent forces.
5. Scattering pattern of Rayleigh scattering in x-y plane for plane S wave incidence. The upper half is of S-S scattering, the lower half is of S-P scattering. Note that in x-y plane there are only meridian components of scattered S waves.
6. Same as Fig. 5, but in x-z plane.
7. Same as Fig. 5, but in y-z plane.
8. Same as Fig. 5, the scattering pattern of "velocity type" and "impedance type" scattering.
9. The coordinate system for the calculation of volume factors.
10. Volume factors of S wave scattering Θ^S for a uniform sphere for different frequencies.
11. Θ^S, when $\frac{\omega}{\beta_o}a = 2\pi$.

12. Θ^S, when $\frac{\omega}{\beta_o}a = 10$.

13. Volume factors of converted wave Θ^C for a uniform sphere for different frequencies.

14. Θ^C, when $\frac{\omega}{\beta_o}a = 2\pi$.

15. Θ^C, when $\frac{\omega}{\beta_o}a = 10$.

16. Scattering patterns of a uniform sphere for P wave incidence for different frequencies. When $\frac{\delta\lambda}{\lambda_o} = \frac{\delta\mu}{\mu_o} = 2\frac{\delta\rho}{\rho_o}$ and $\lambda_o = \mu_o$. The upper half is of P-P scattering, the lower half is of P-S scattering. All the patterns are axially symmetric about the x-axis.

17. Same as 16 for $\frac{\omega}{\alpha_o}a = 10$.

18. Same as 16, but for $\frac{\delta\lambda}{\lambda_o} = \frac{\delta\mu}{\mu_o} = \frac{\delta\rho}{\rho_o}$, i.e. the "impedance type" scattering.

19. Same as 18, when $\frac{\omega}{\alpha_o}a = 10$.

20. Same as 16, but for $\frac{\delta\lambda}{\lambda} = \frac{\delta\mu}{\mu_o} = -\frac{\delta\rho}{\rho_o}$, i.e. the "velocity type" scattering.

21. Scattering patterns of a uniform sphere in the x-y plane for S wave incidence for different frequencies when $\frac{\delta\mu}{\mu_o} = 2\frac{\delta\rho}{\rho_o}$. The upper half is of S-S scattering, the lower half is of S-P scattering. Note that there exists only the meridian components of scattered S wave.

22. Same as 21 for $\frac{\omega}{\beta_o}a = 10$.

23. Same as 21 but for $\frac{\delta\mu}{\mu_o} = \frac{\delta\rho}{\rho_o}$, i.e. the "impedance type" scattering.

24. Same as 23 for $\frac{\omega}{\beta_o}a = 10$.

25. Same as 21 but for $\frac{\delta\mu}{\mu_o} = -\frac{\delta\rho}{\rho_o}$, i.e. the "velocity type" scattering.

26. Scattering patterns of scattered latitudinal component of a uniform sphere for S wave incidence for different frequencies. The plane has a 45° angle against x-y plane with a common x-axis.

27. Volume factors for a Gaussian heterogeneity. The upper half plane is the case of P-P, the lower half plane is for P-S.

28. Scattering patterns of a Gaussian heterogeneity of impedance type for different frequencies. The upper half plane is for P-P, the lower half plane is for P-S.

29. Same as 28, for velocity type heterogeneity.

30. Same as 28, for $(\omega/\beta_o)a_o = 10$, the upper half plane is for S-S, the lower half plane is for S-P.

31. Scattering patterns of scattered latitudinal component of a Gaussian heterogeneity for S wave incidence. The graphic plane has 45° angle against the polarization plane of the incident wave (x-y plane) with a common x-axis.

32. Schematic diagram of the VSP experiments for the fracture volume analysis. C and D are the shotpoints, the measurements are taken in well 100. The fracture zone is formed by explosions in 301 and its neighboring wells (from Turpening 1984).

33. The SH wave generator used in the experiment, a 4.2-in mortar (from Turpening 1984).

34. Seismic profile of vertical components recorded in well 100 from shotpoint C before fracturing. The SH wave generator is a 4.2-in water mortar. The traces are from two shots with opposite SH orientations. Note that no SV wave occurs (from Turpening 1984).

35. Seismic profile of vertical components recorded in well 100 from shotpoint C before fracturing. The sources are the same as in Fig. 35. Note that no SV wave occurs.

36. The profile after fracturing, recorded in well 100 from shotpoint C. These traces of vertical components are from two shots with opposite SH orientation of the source. Note that clear SV waves can be seen at 2175-2325 ft and 2400-2475 ft. These waves are converted from SH waves due to scattering by the fracture zone (from Turpening 1934).

37. The profile of vertical components after fracturing, from shotpoint D. The two lobes of cross-coupled SV waves can be cleary seen (from Turpening 1984).

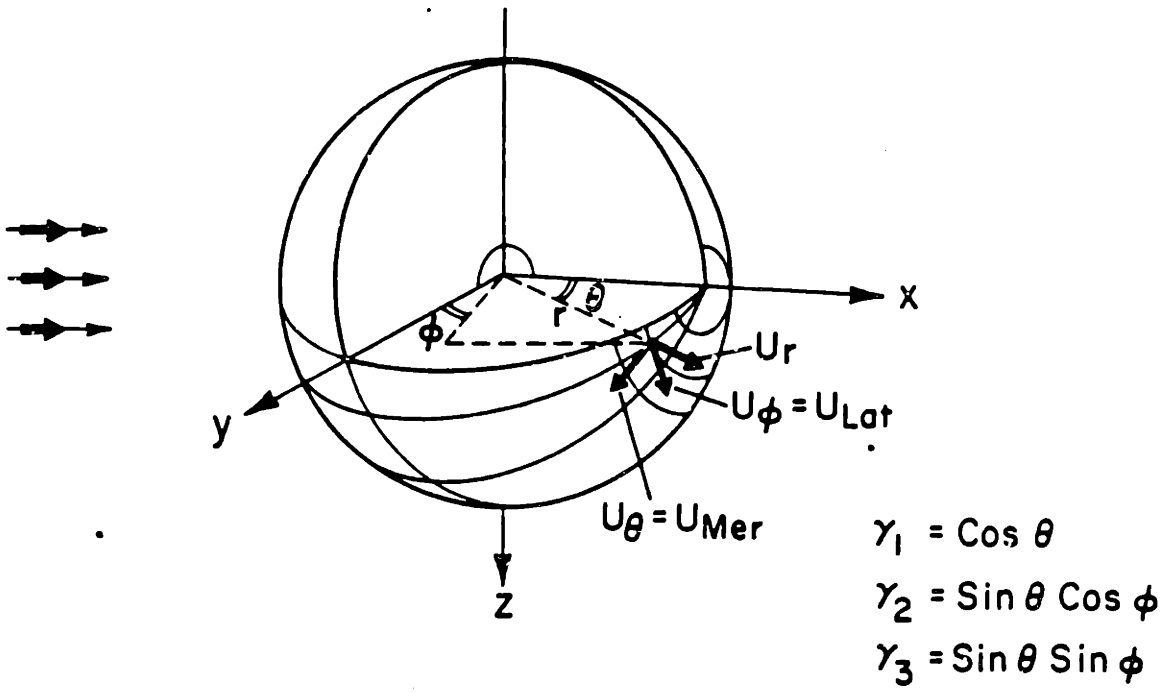

1. a) Spherical coordinate system for P wave incidence,

Elastic-wave Rayleigh scattering

P-wave incidence

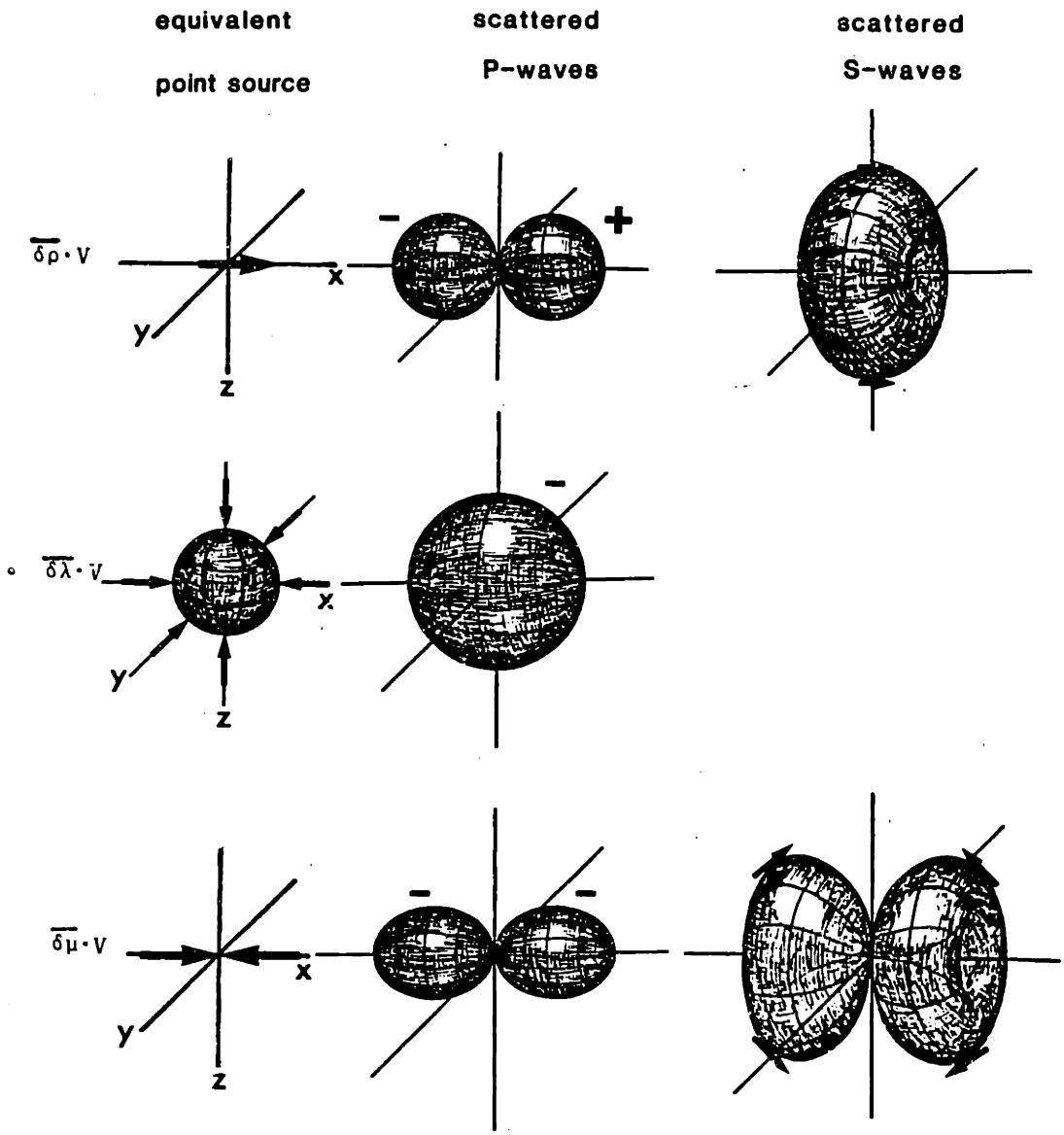

b) the scattering patterns for different equivalent forces.

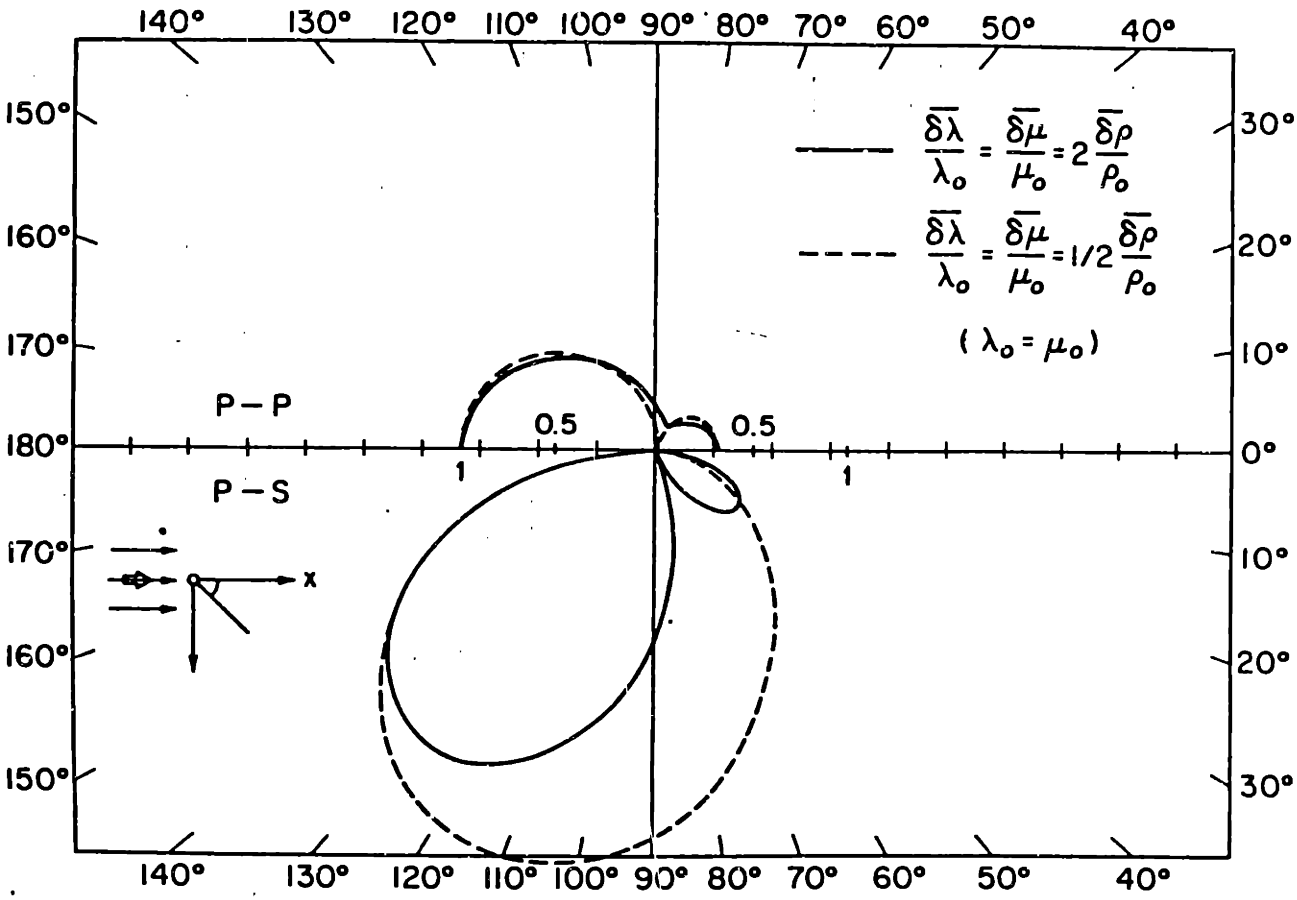

2. Scattering patterns of Rayleigh scattering for plane P wave incidence. The upper half is of P-P scattering, the lower half is of P-S scattering. All the patterns are axially symmetric about the x-axis.

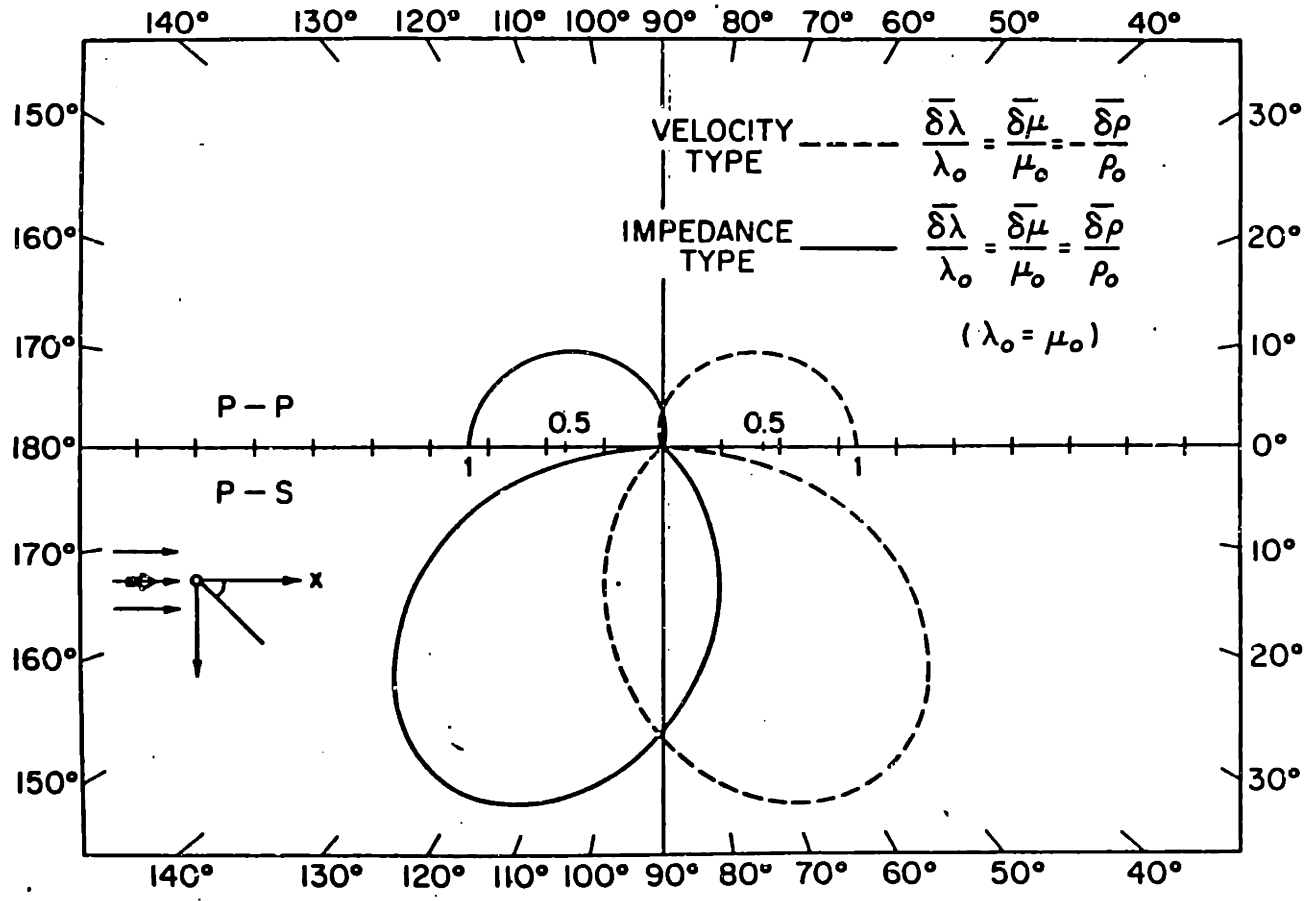

3. Same as Fig. 2. The scattering pattern of "velocity-type" and "impedance type" scattering.

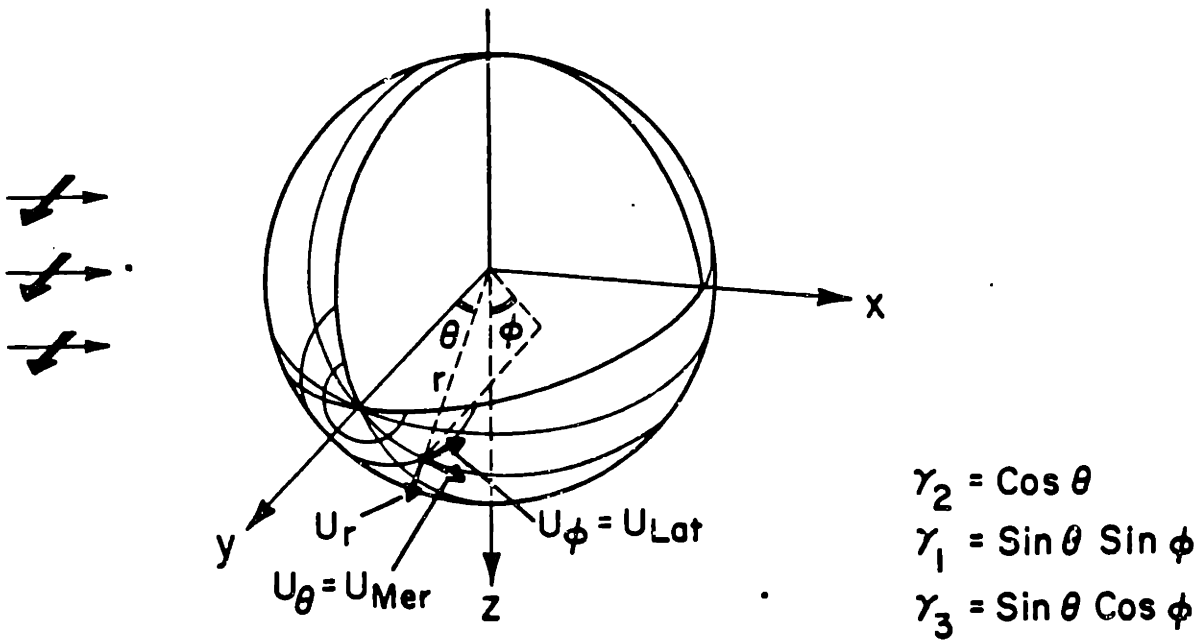

4. a) Spherical coordinate system for S wave incidence,

Elastic-wave Rayleigh scattering

S-wave incidence

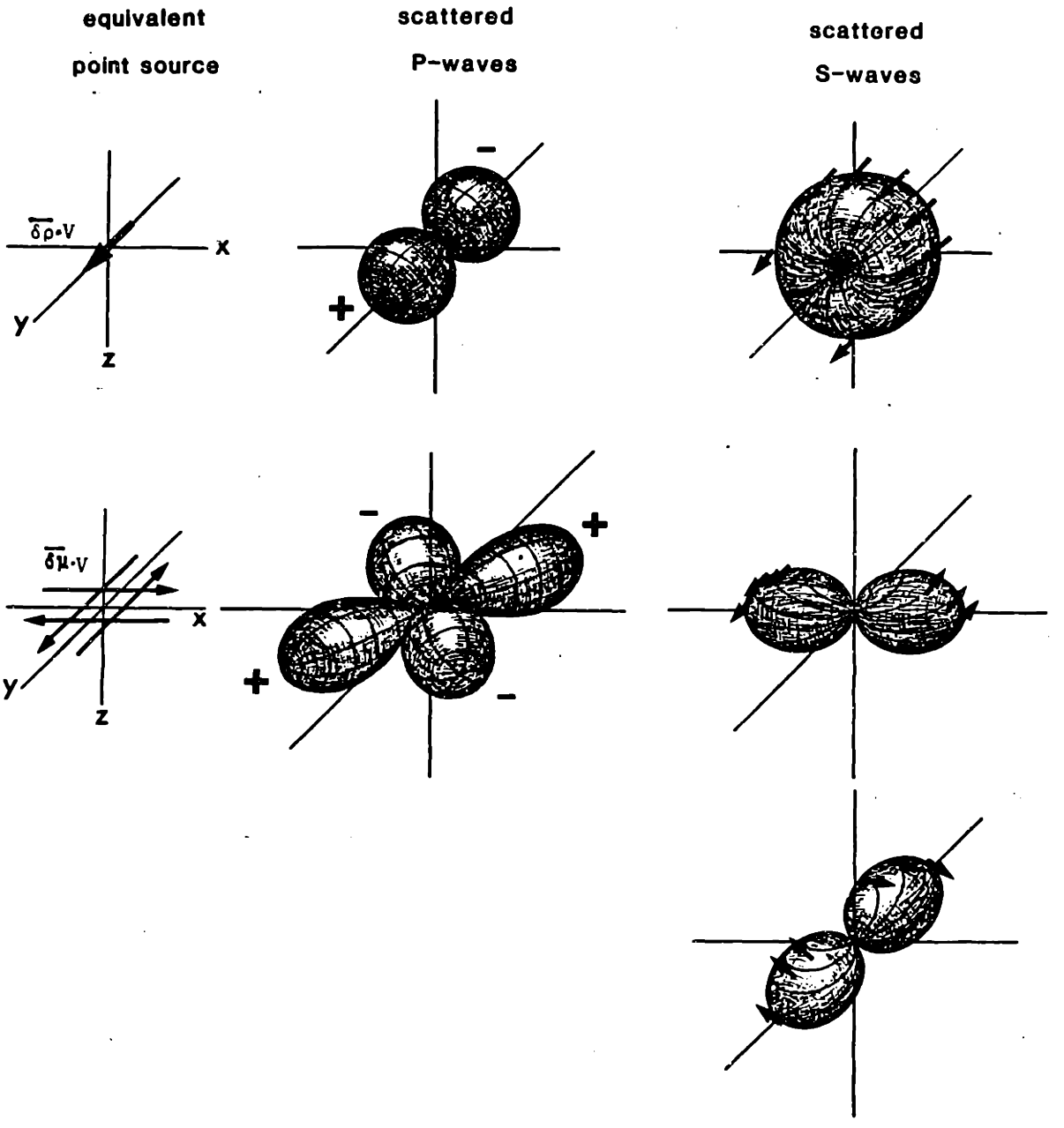

b) the scattering patterns for different equivalent forces.

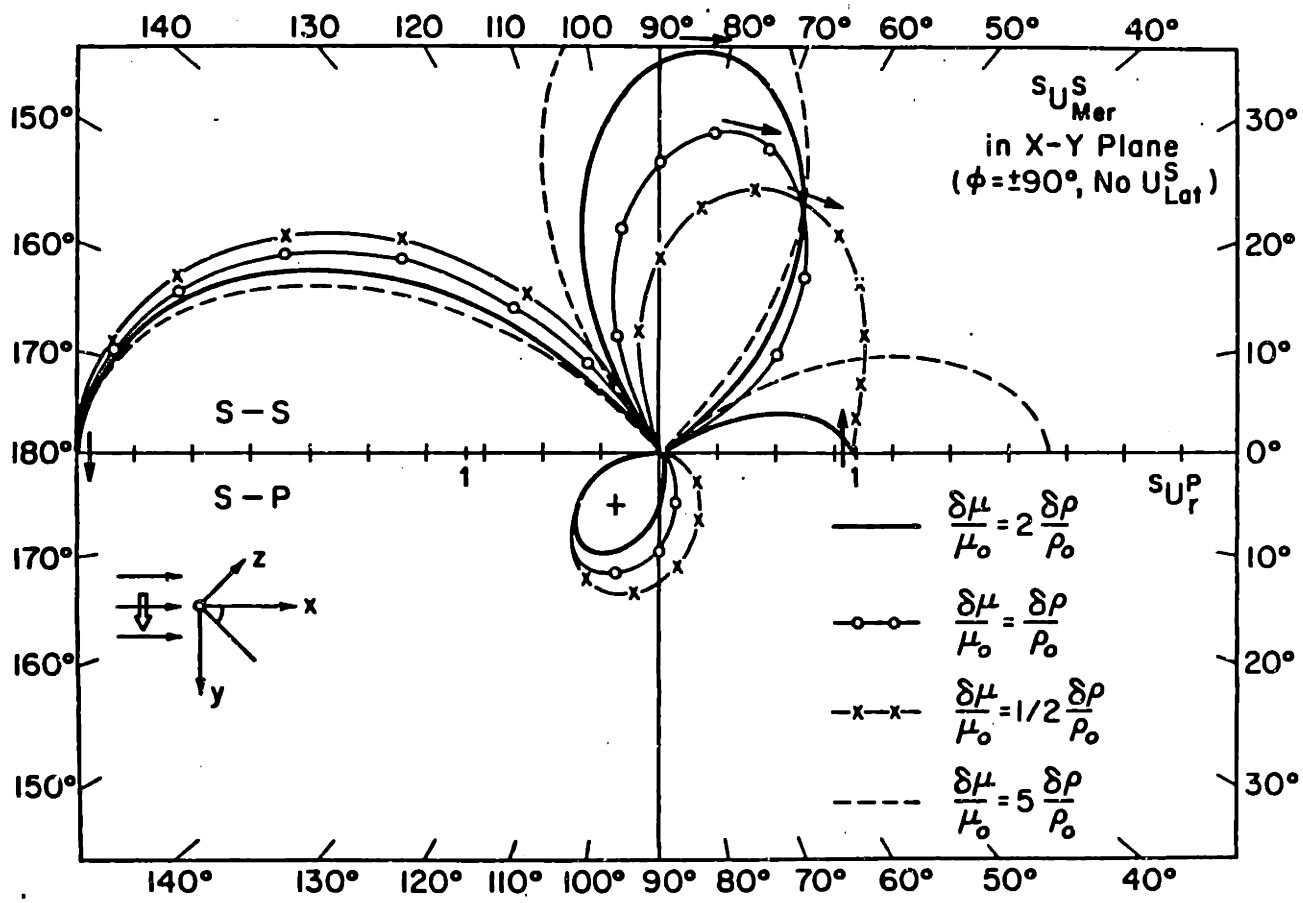

5. Scattering pattern of Rayleigh scattering in x-y plane for plane S wave incidence. The upper half is of S-S scattering, the lower half is of S-P scattering. Note that in x-y plane there are only meridian components of scattered S waves.

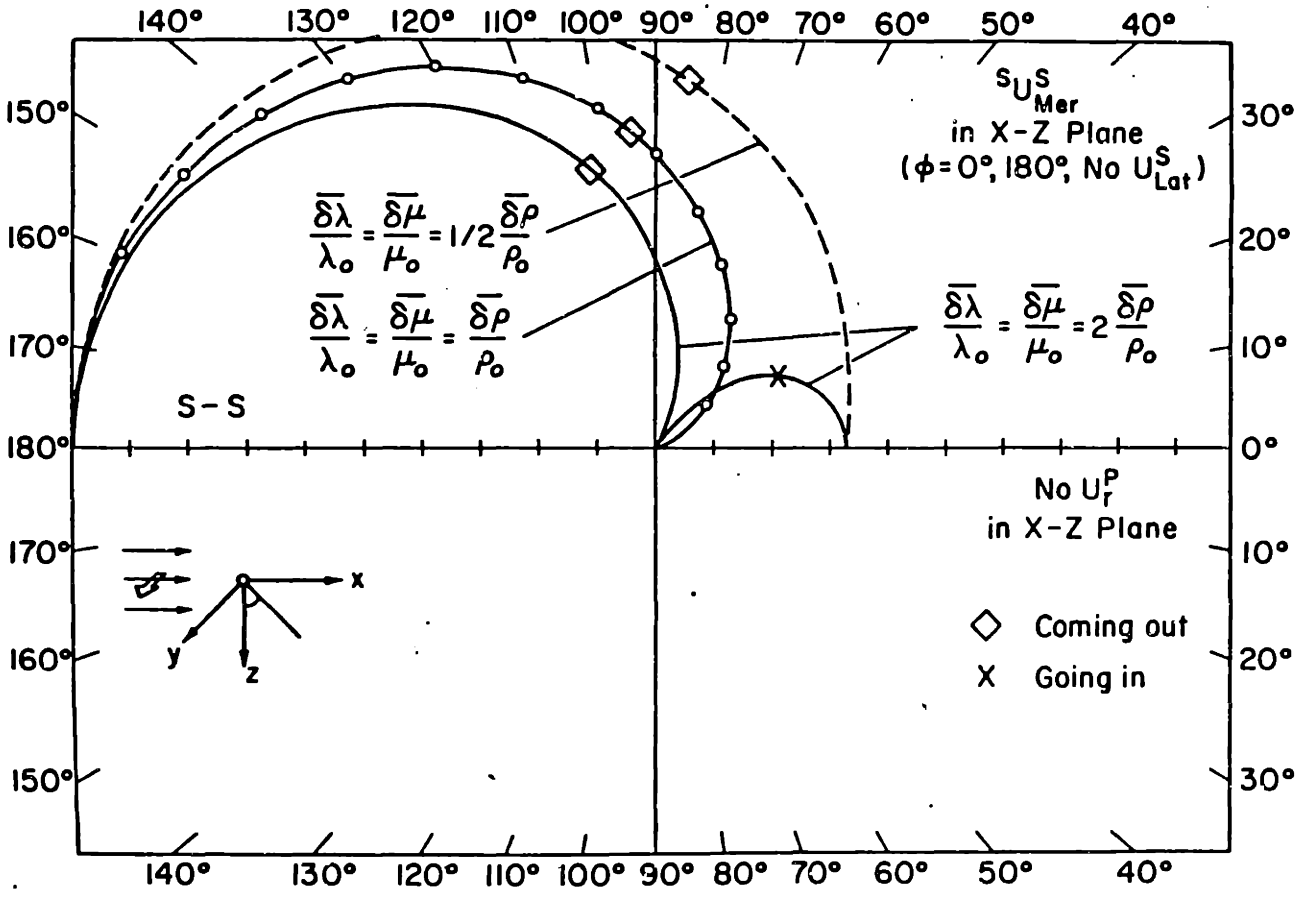

6. Same as Fig. 5, but in x-z plane.

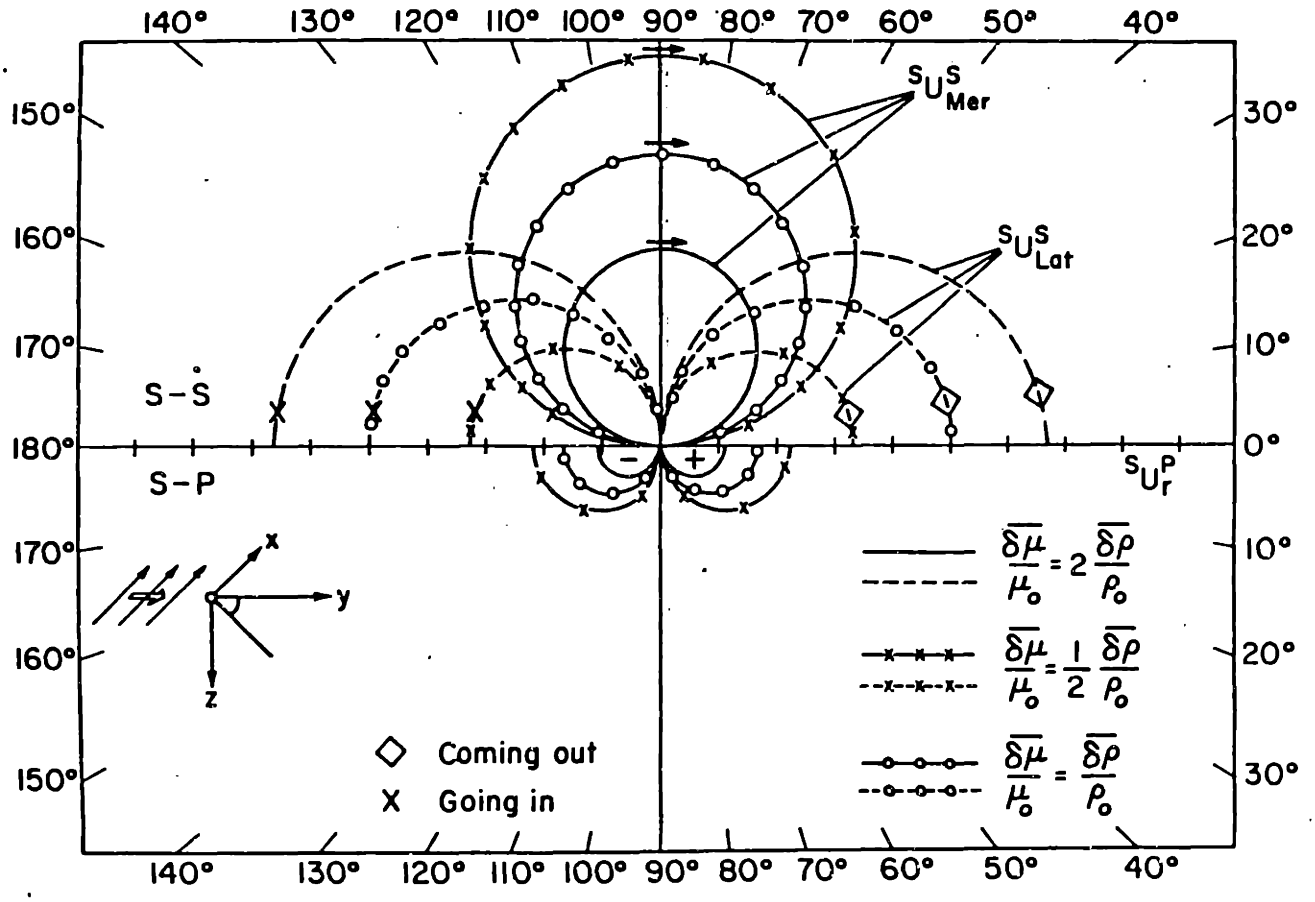

7. Same as Fig. 5, but in y-z plane.

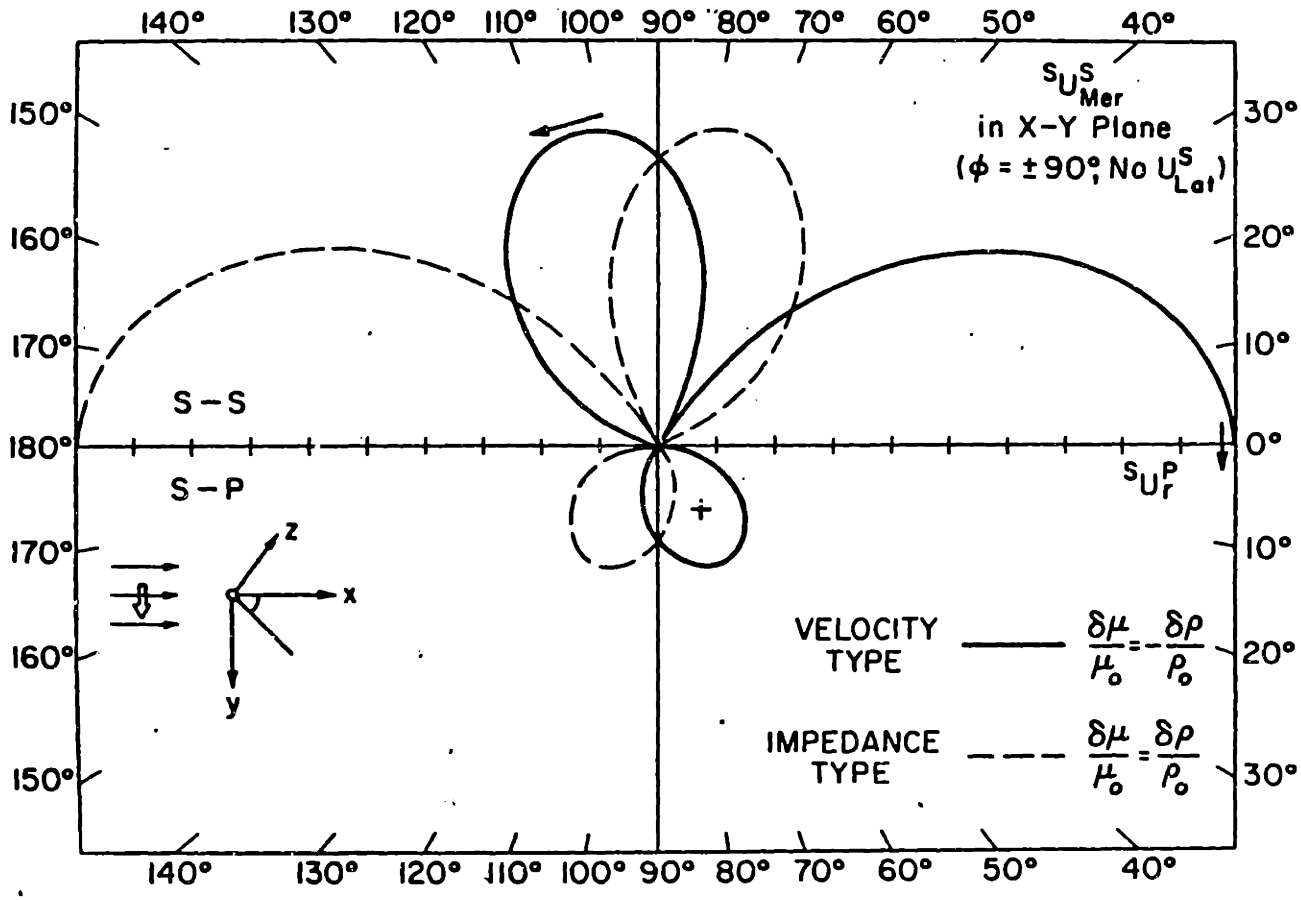

8. Same as Fig. 5, the scattering pattern of "velocity type" and "impedance type" scattering.

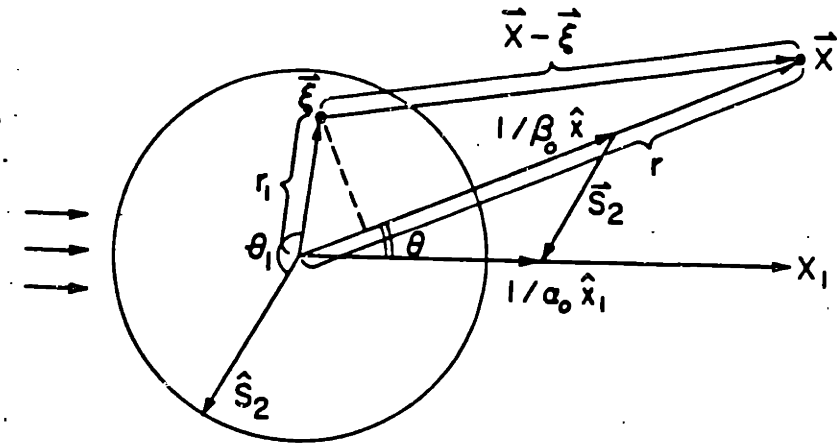

9. The coordinate system for the calculation of volume factors.

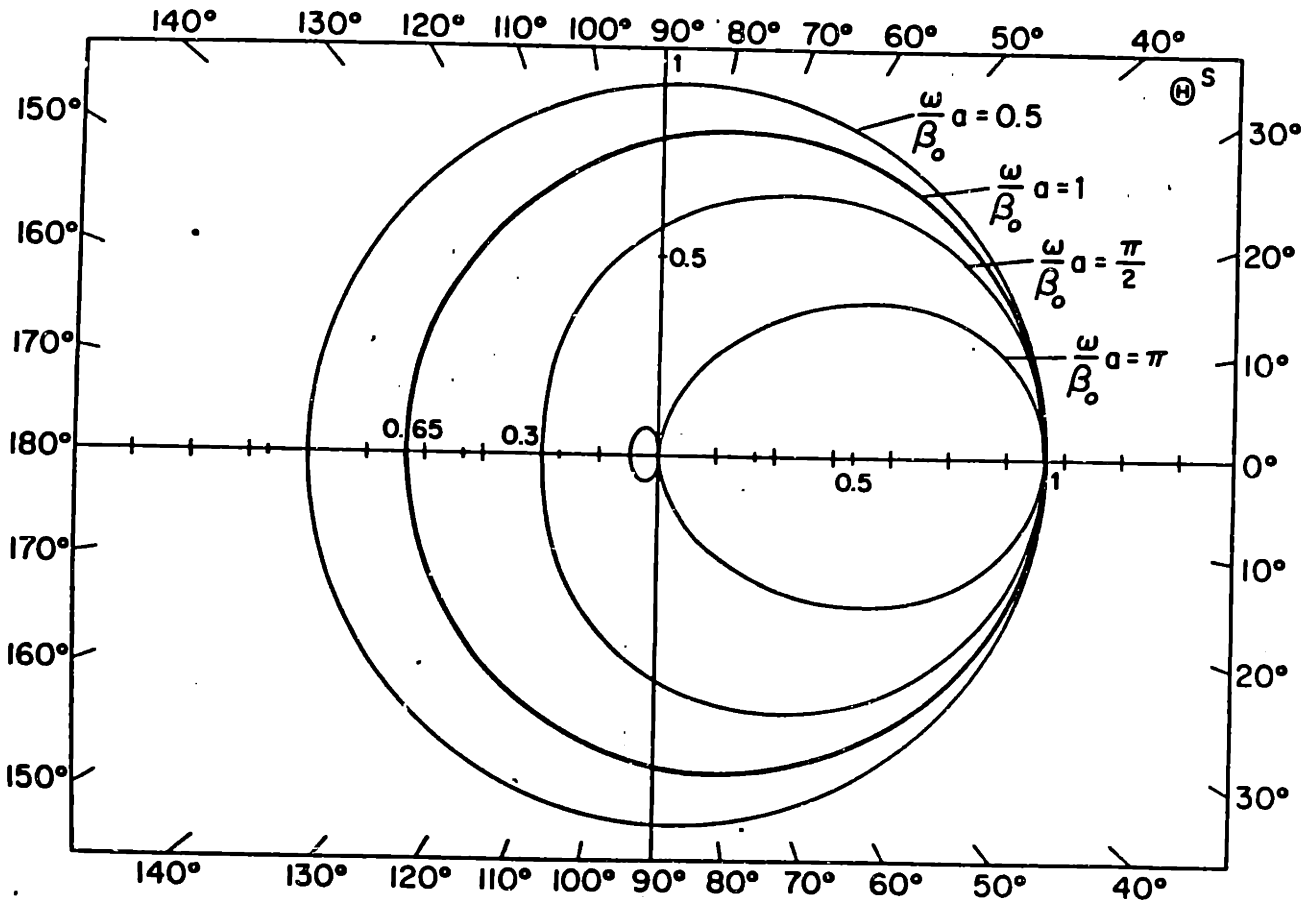

10. Volume factors of S wave scattering Θ^S for a uniform sphere for different frequencies.

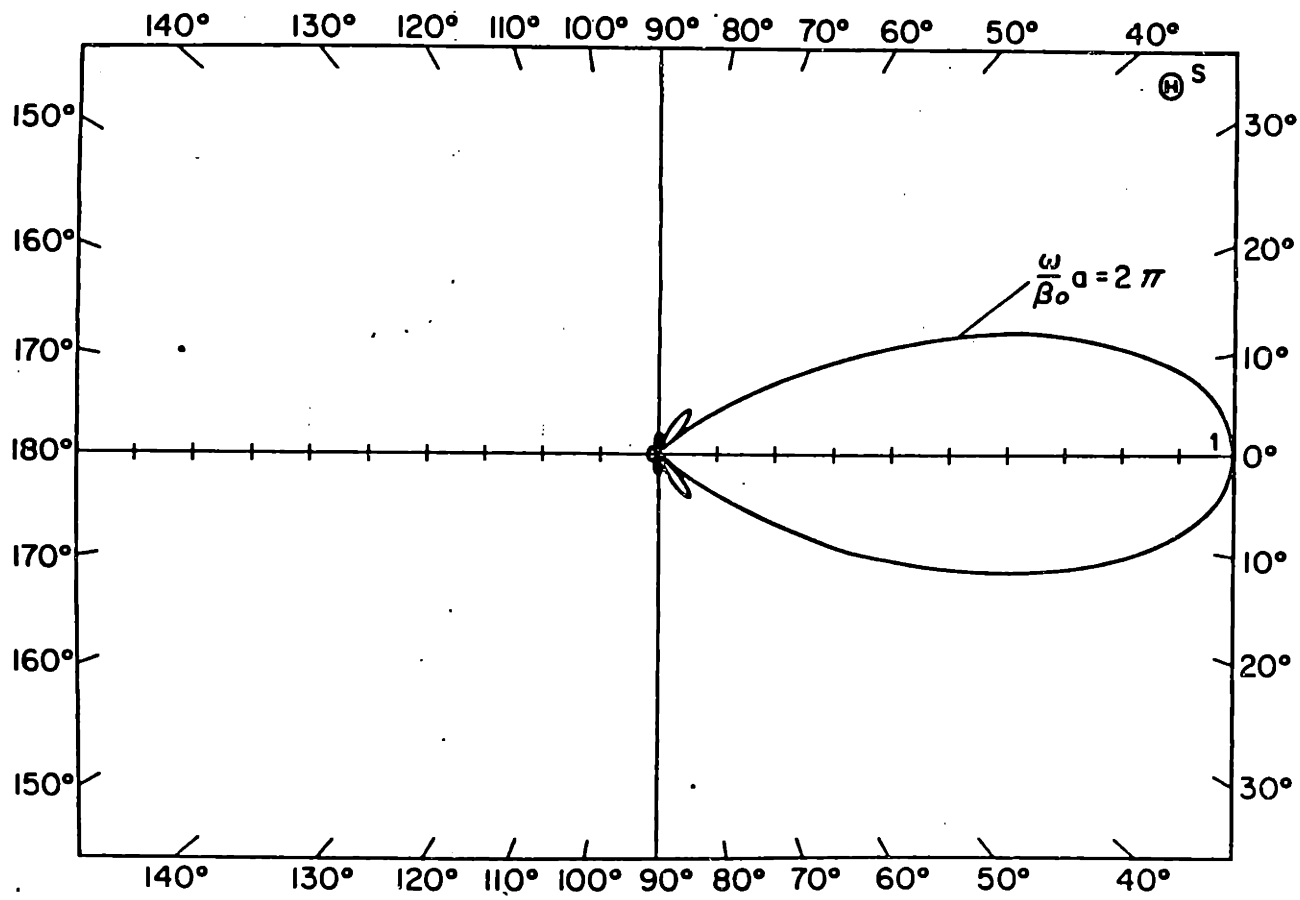

11. θ^S, when $\frac{\omega}{\beta_o} a = 2\pi$.

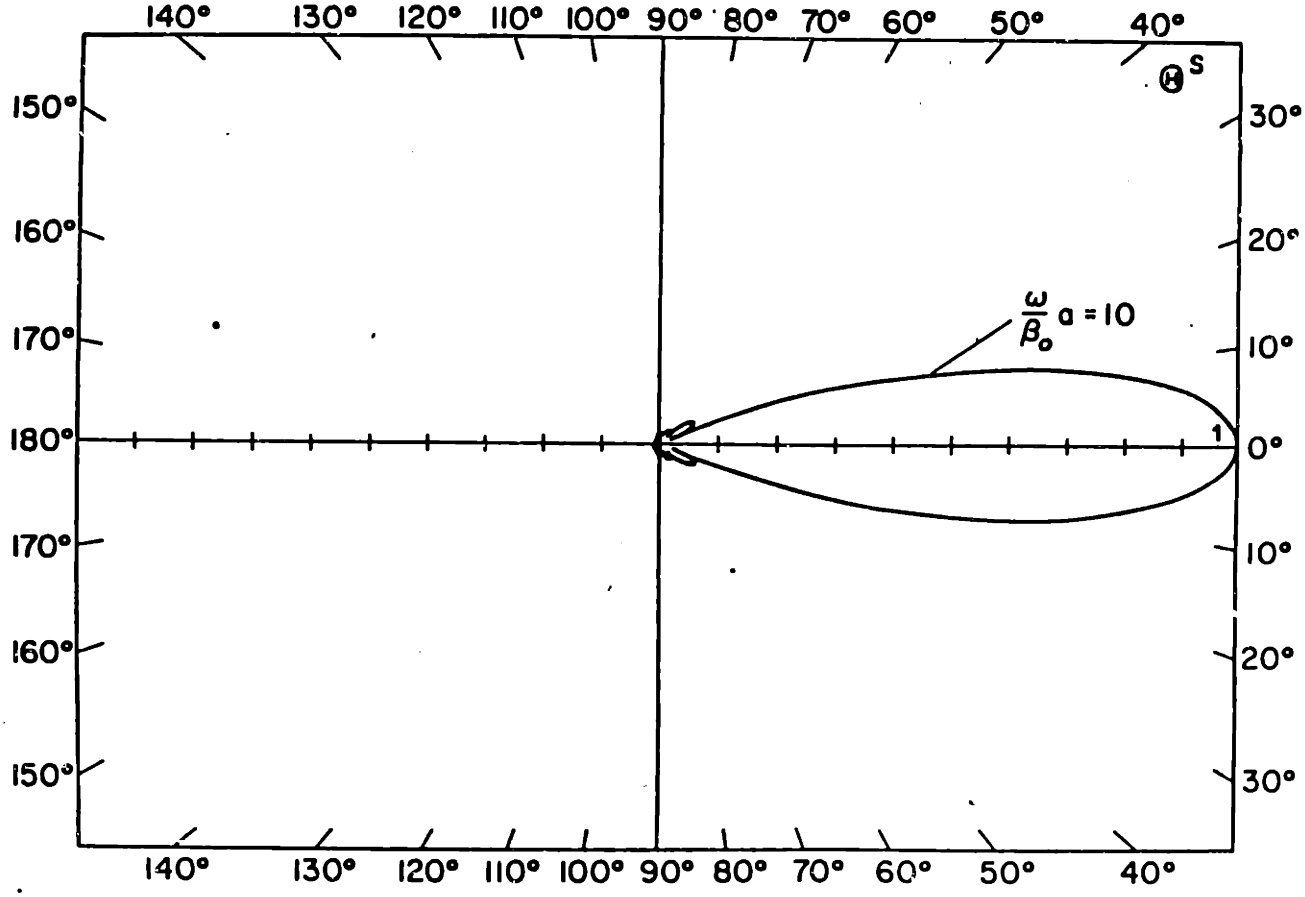

12. Θ^S, when $\frac{\omega}{\beta_o} a = 10$.

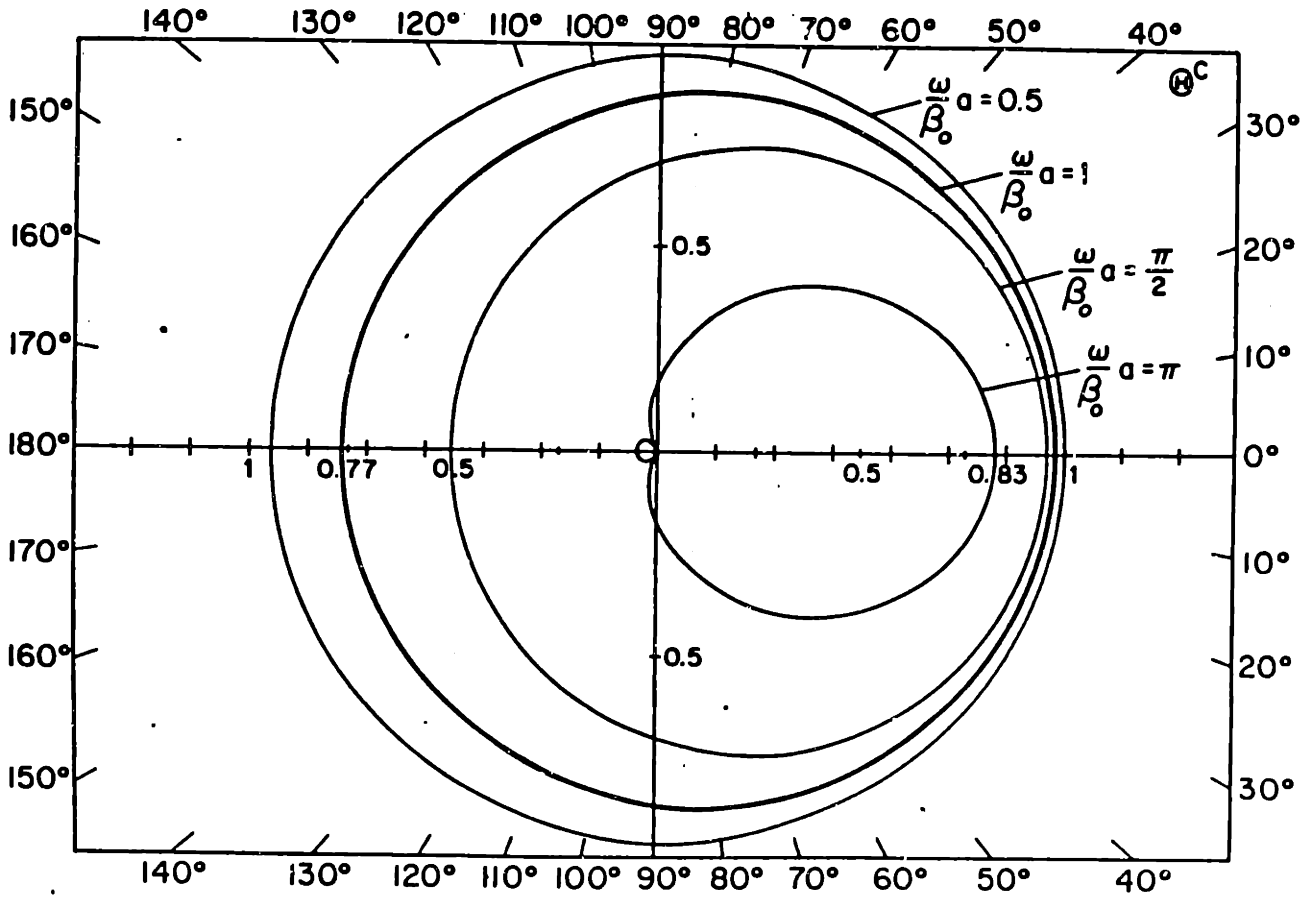

13. Volume factors of converted wave Θ^C for a uniform sphere for different frequencies.

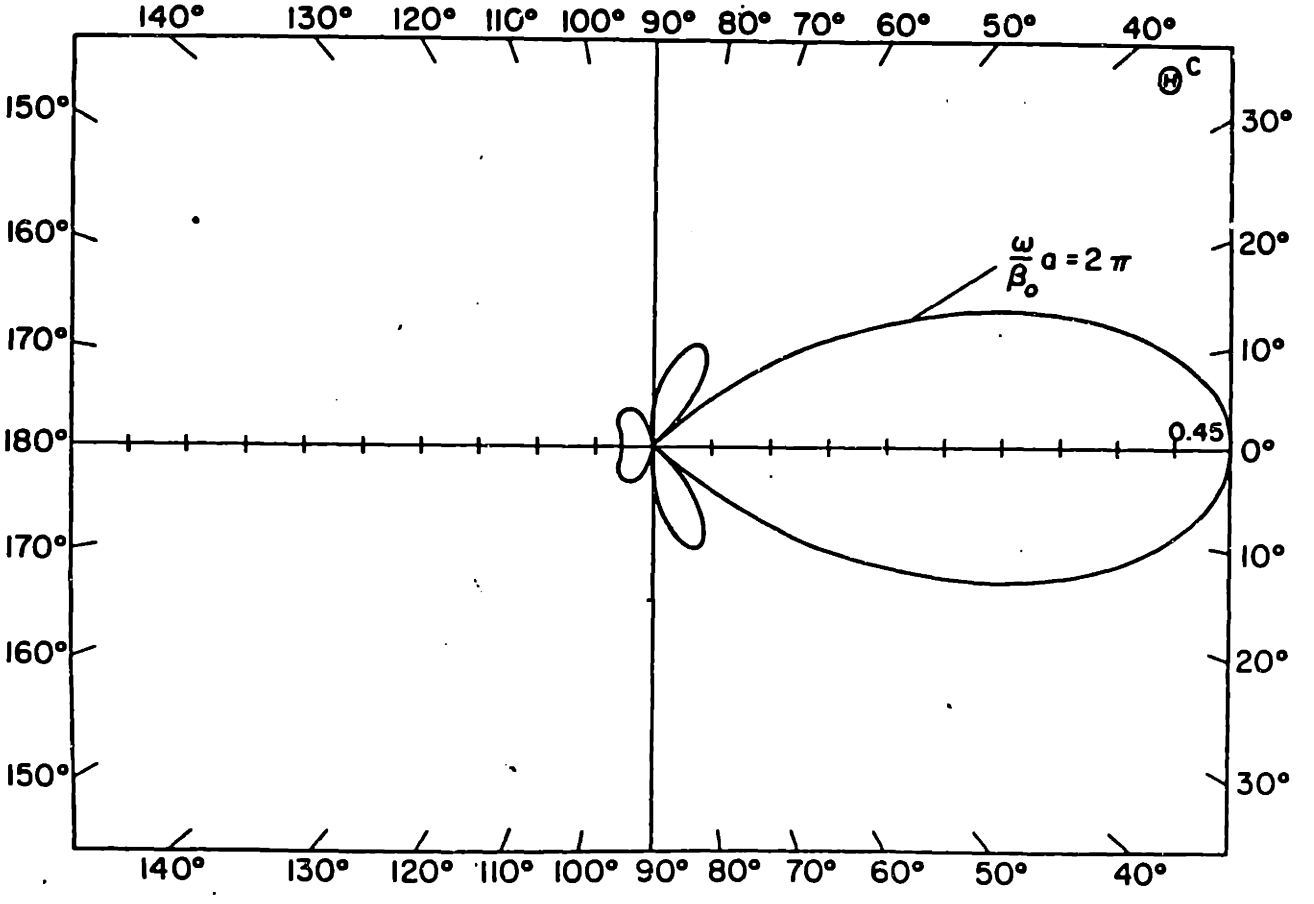

14. θ^c, when $\frac{\omega}{\beta_o} a = 2\pi$.

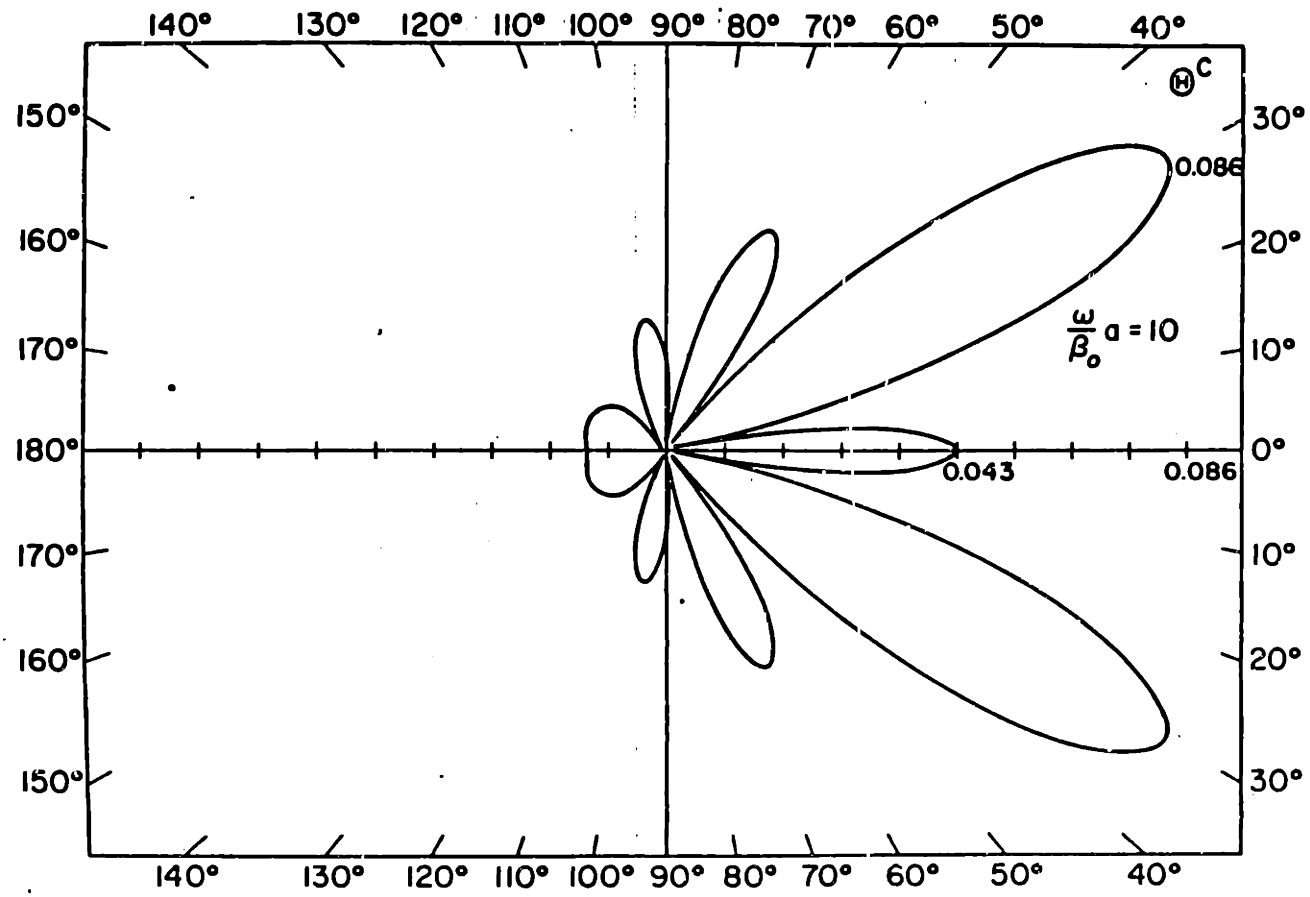

15. θ^C, when $\frac{\omega}{\beta_o}a = 10$.

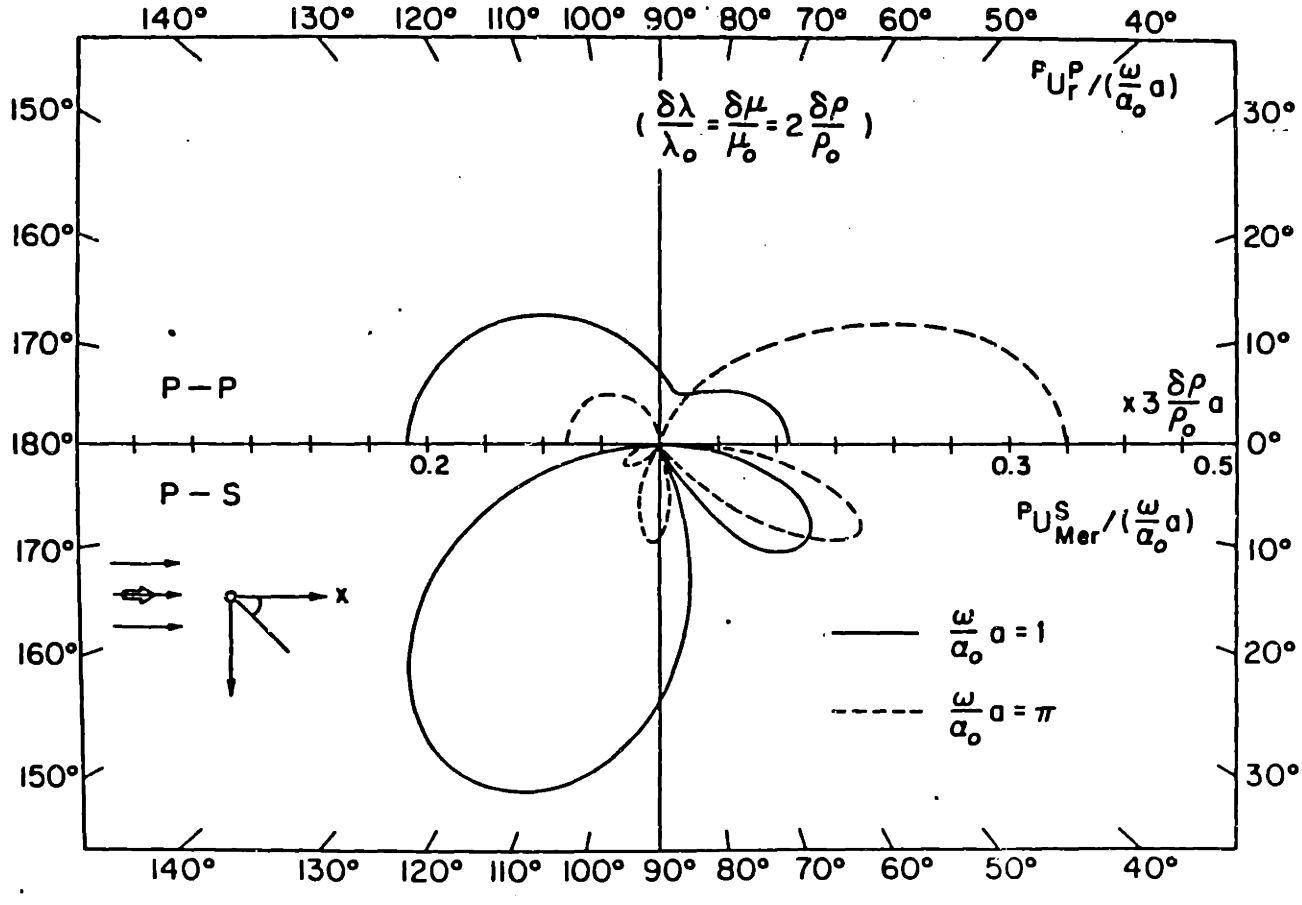

16. Scattering patterns of a uniform sphere for P wave incidence for different frequencies. When $\frac{\delta\lambda}{\lambda_o} = \frac{\delta\mu}{\mu_o} = 2\frac{\delta\rho}{\rho_o}$ and $\lambda_o = \mu_o$. The upper half is of P-P scattering, the lower half is of P-S scattering. All the patterns are axially symmetric about the x-axis.

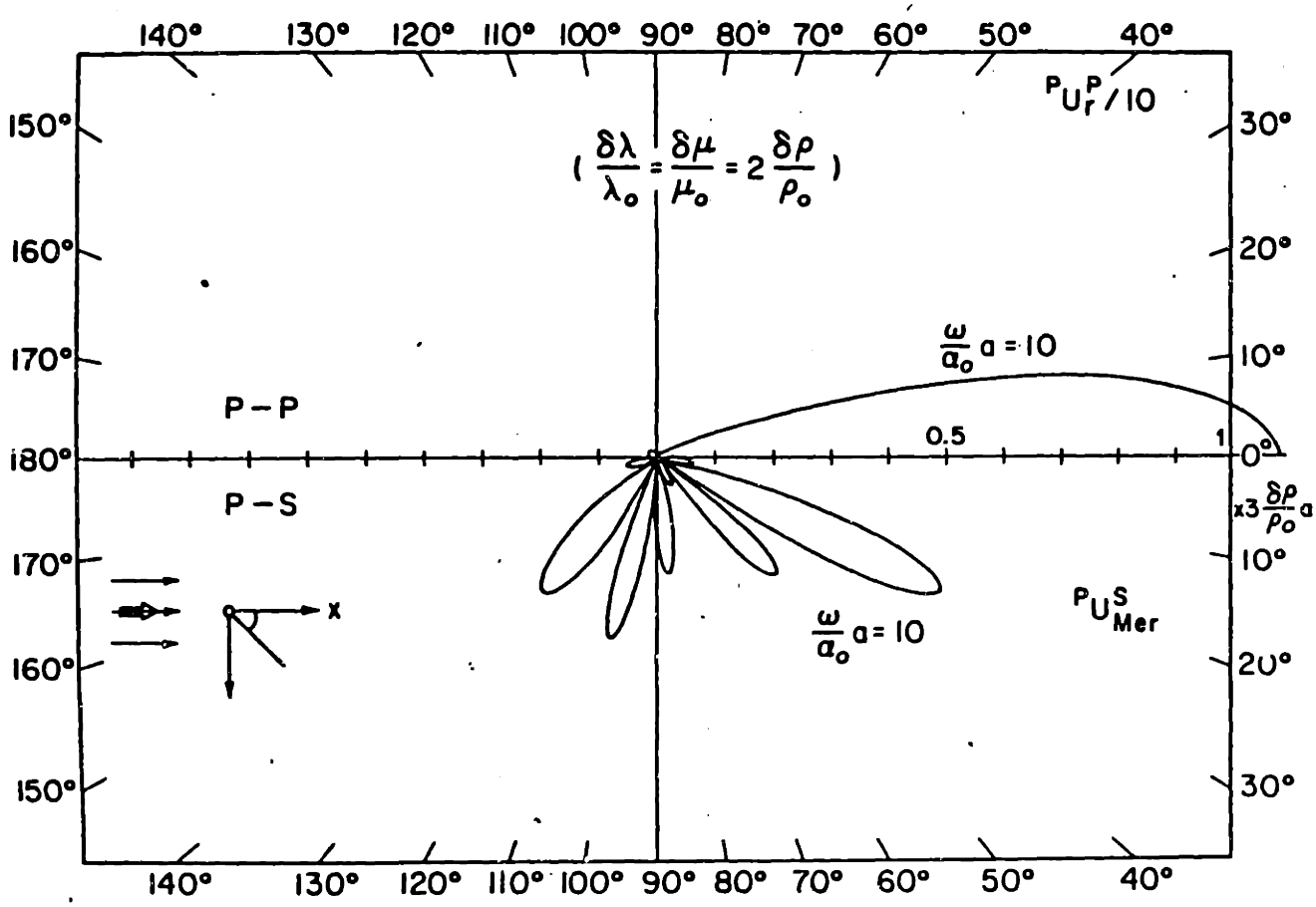

17. Same as 16 for $\frac{\omega}{\alpha_o} a = 10$.

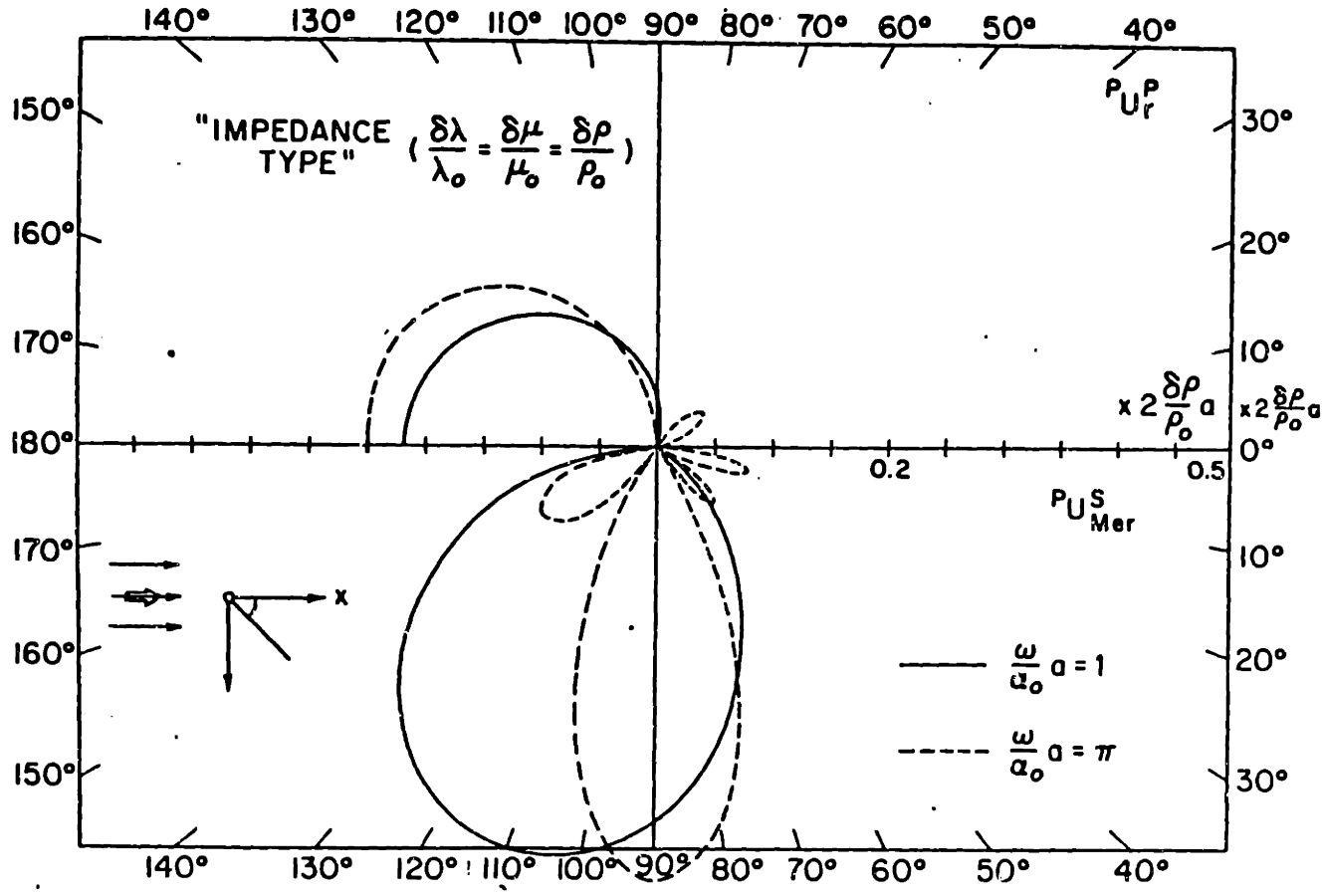

18. Same as 16, but for $\frac{\delta\lambda}{\lambda_o} = \frac{\delta\mu}{\mu_o} = \frac{\delta\rho}{\rho_o}$, i.e. the "impedance type" scattering.

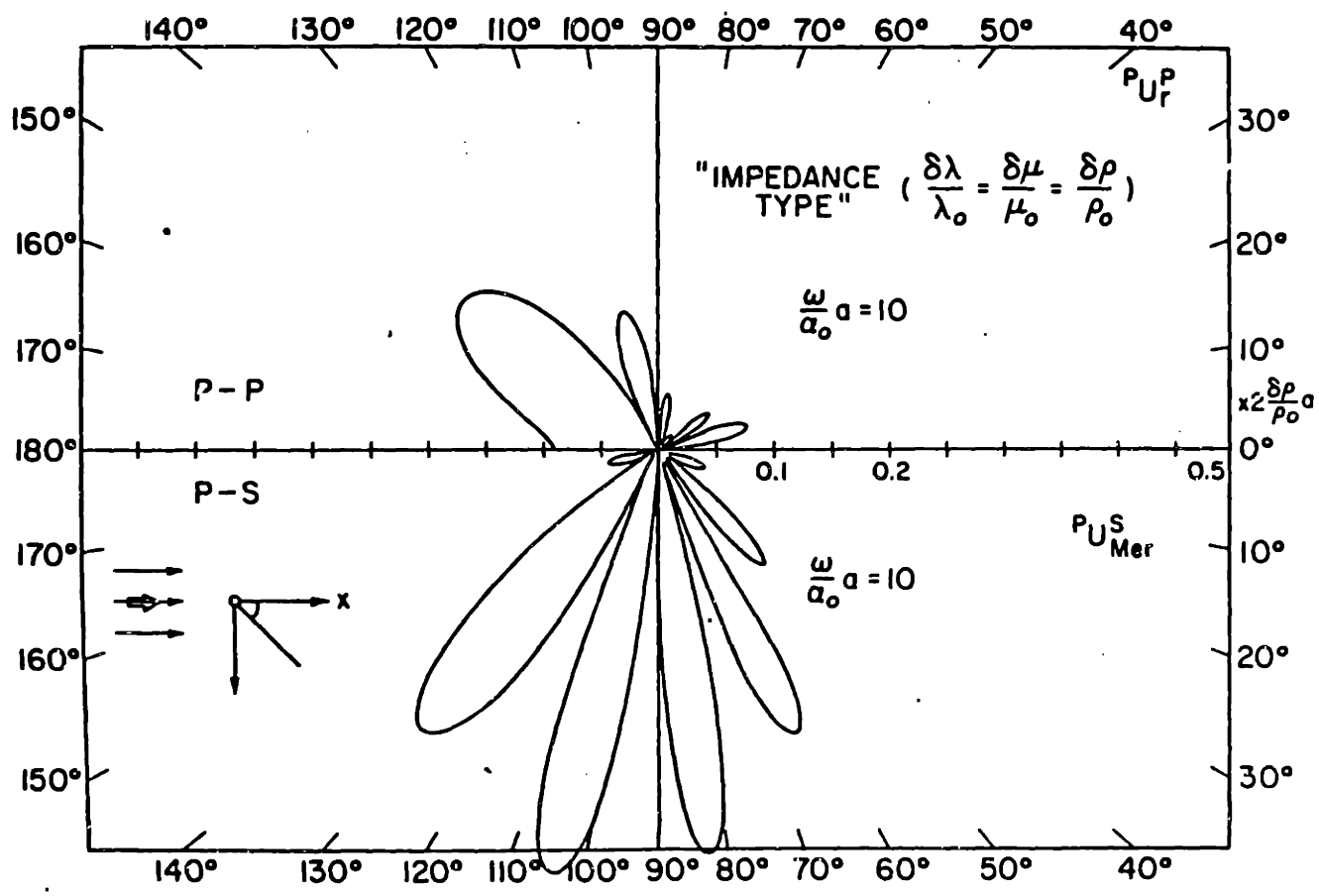

19. Same as 18, when $\frac{\omega}{\alpha_o} a = 10$.

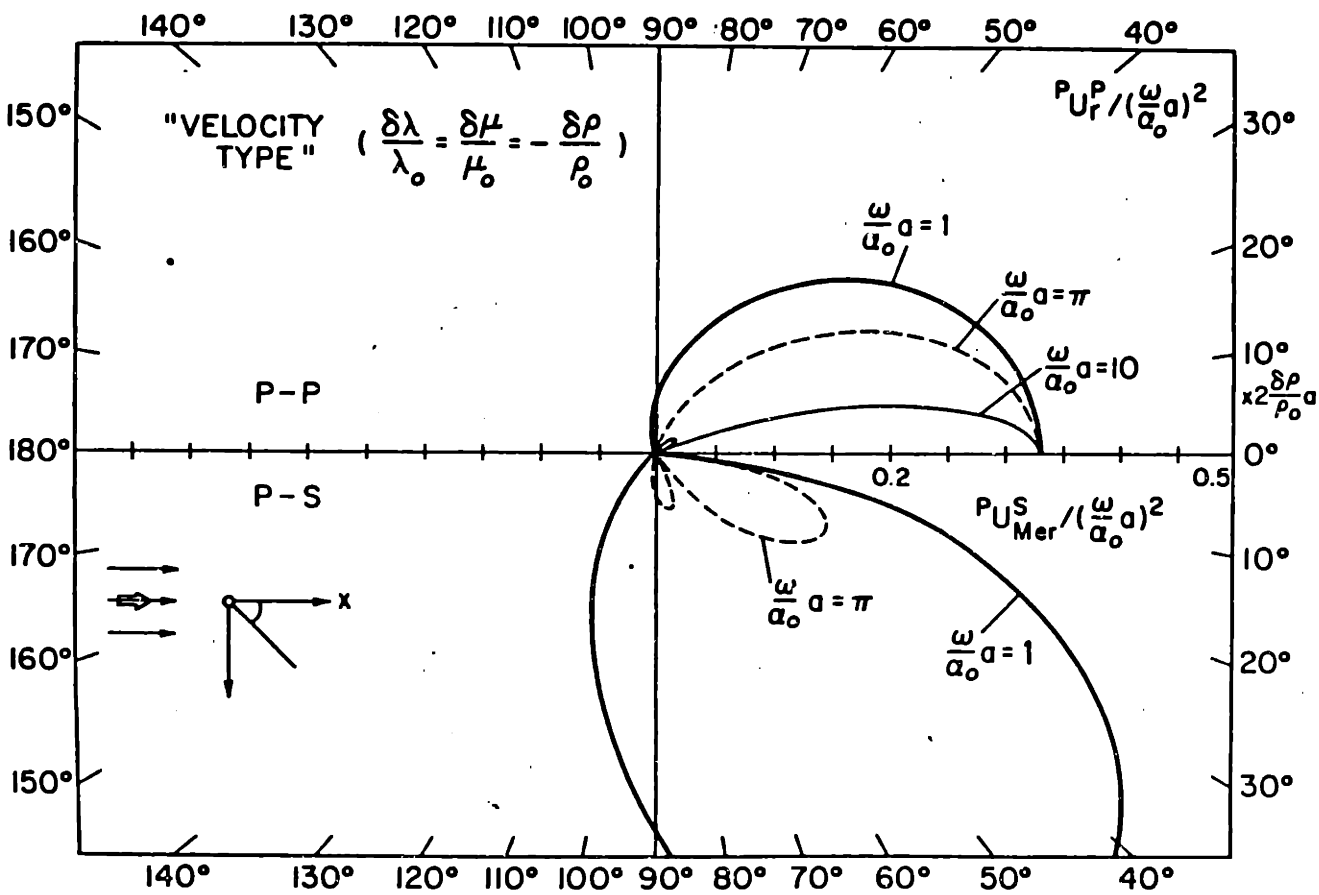

20. Same as 16, but for $\frac{\delta\lambda}{\lambda} = \frac{\delta\mu}{\mu_0} = -\frac{\delta\rho}{\rho_0}$, i.e. the "velocity type" scattering.

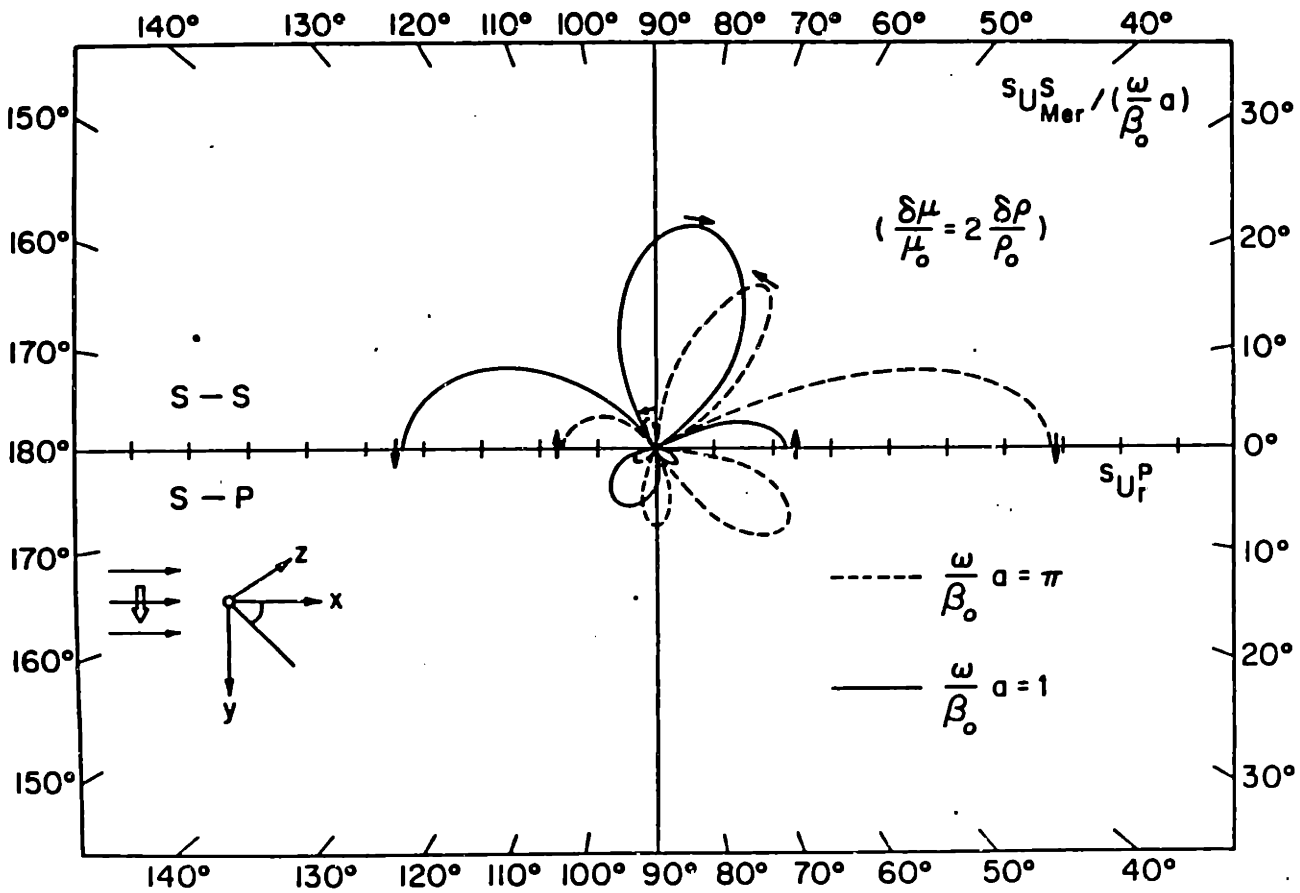

21. Scattering patterns of a uniform sphere in the x-y plane for S wave incidence for different frequencies when $\frac{\delta\mu}{\mu_o} = 2\frac{\delta\rho}{\rho_o}$. The upper half is of S-S scattering, the lower half is of S-P scattering. Note that there exists only the meridian components of scattered S wave.

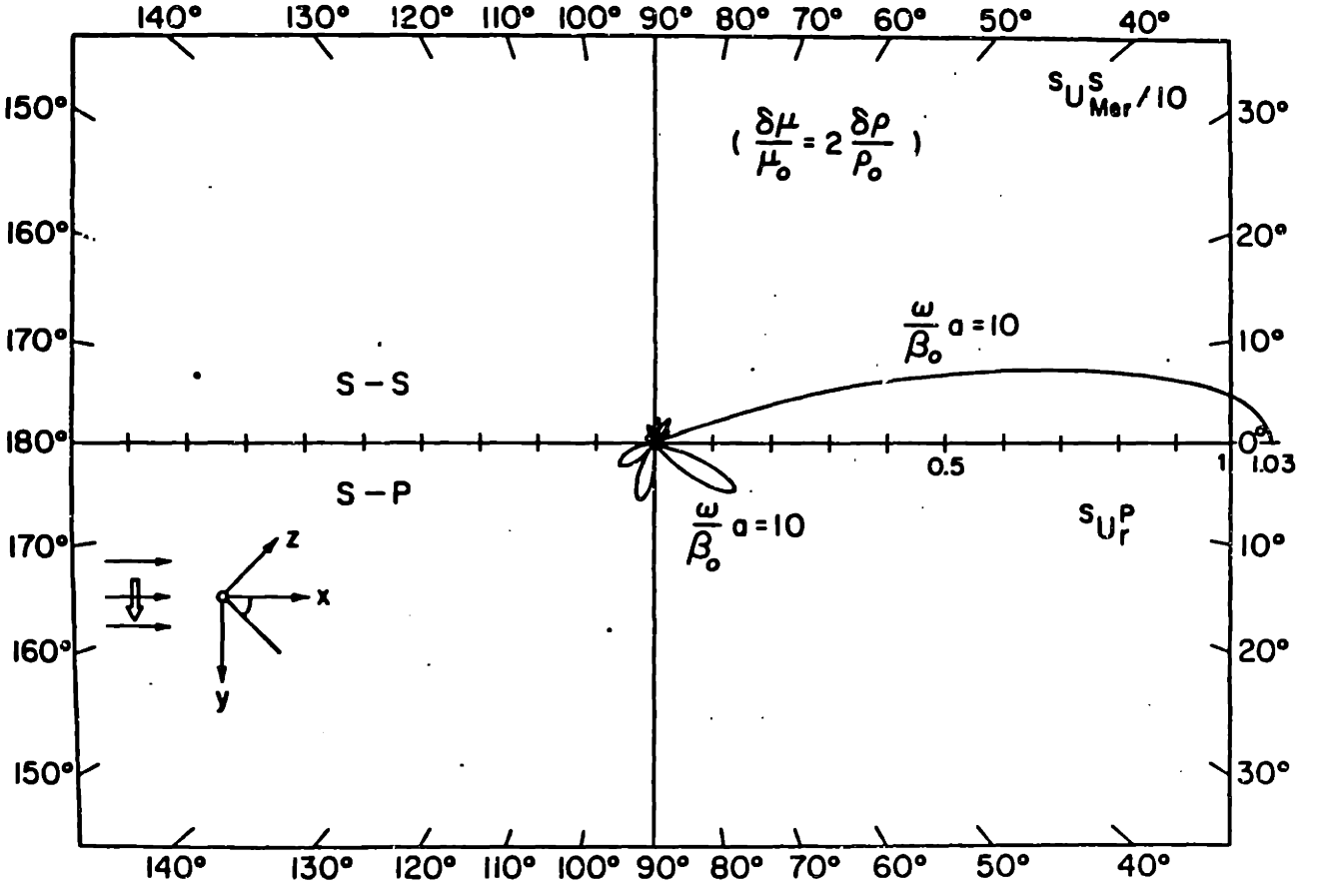

22. Same as 21 for $\frac{\omega}{\beta_o}a = 10$.

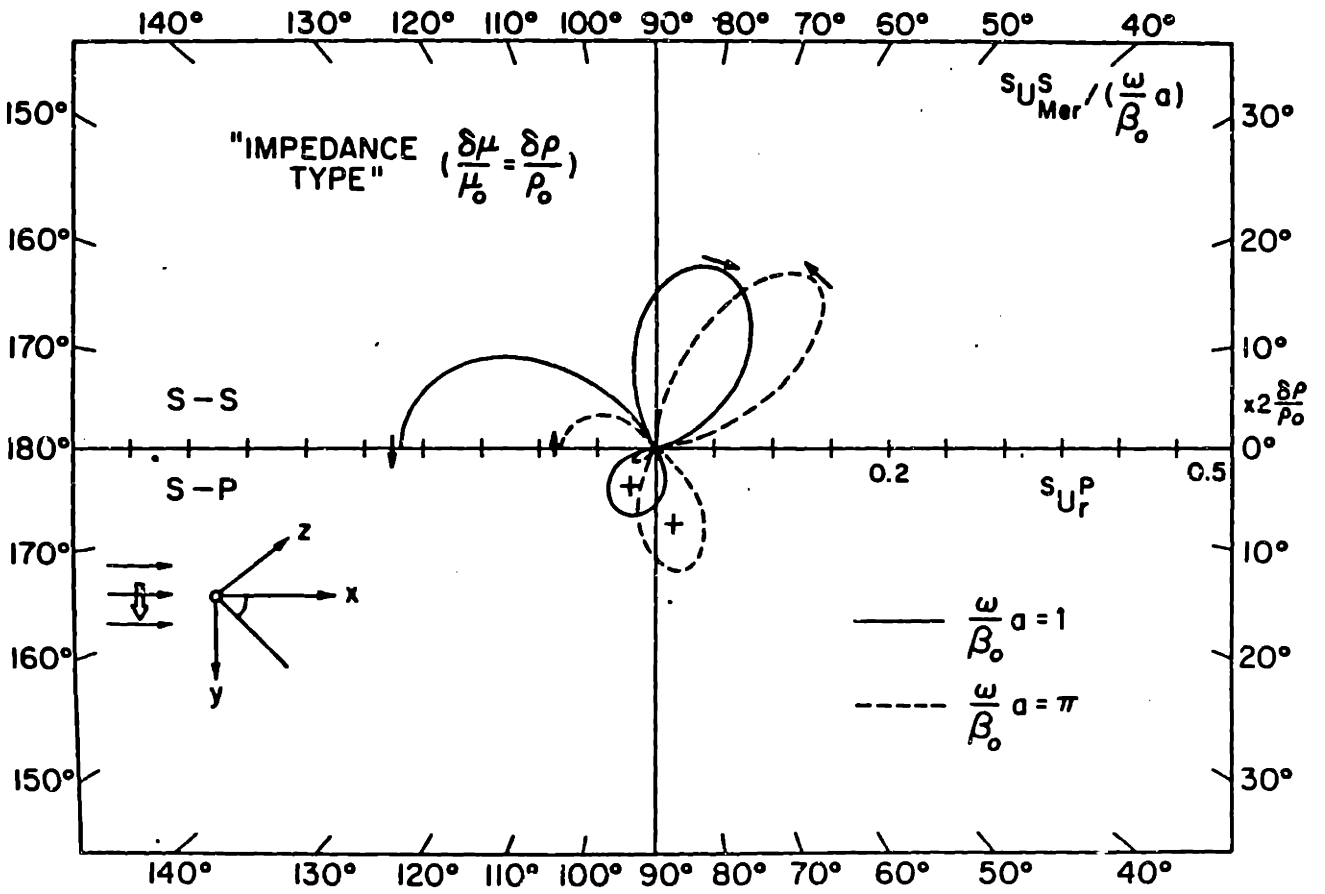

23. Same as 21 but for $\frac{\delta\mu}{\mu_o} = \frac{\delta\rho}{\rho_o}$, i.e. the "impedance type" scattering.

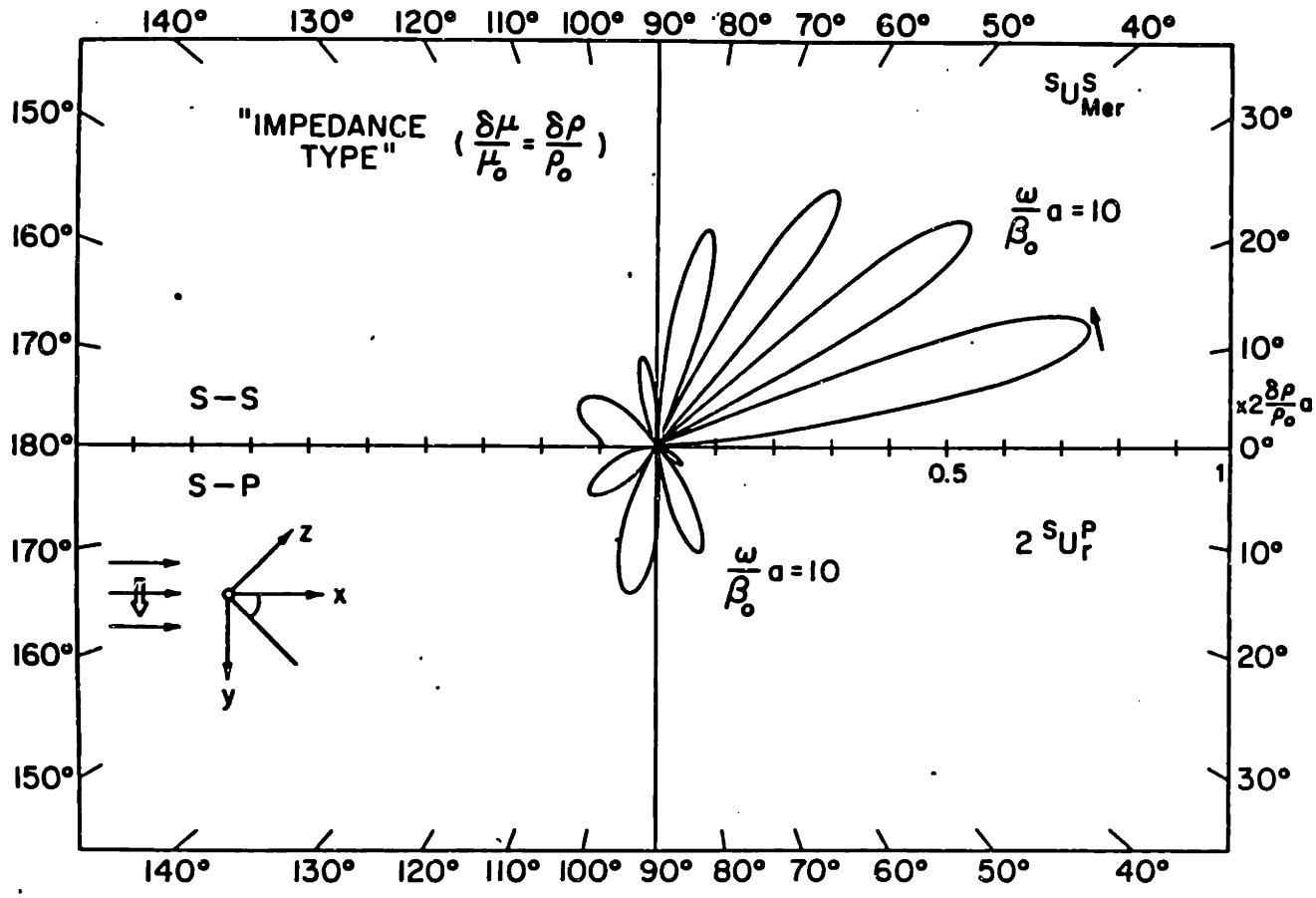

24. Same as 23 for $\frac{\omega}{\beta_o} a = 10$.

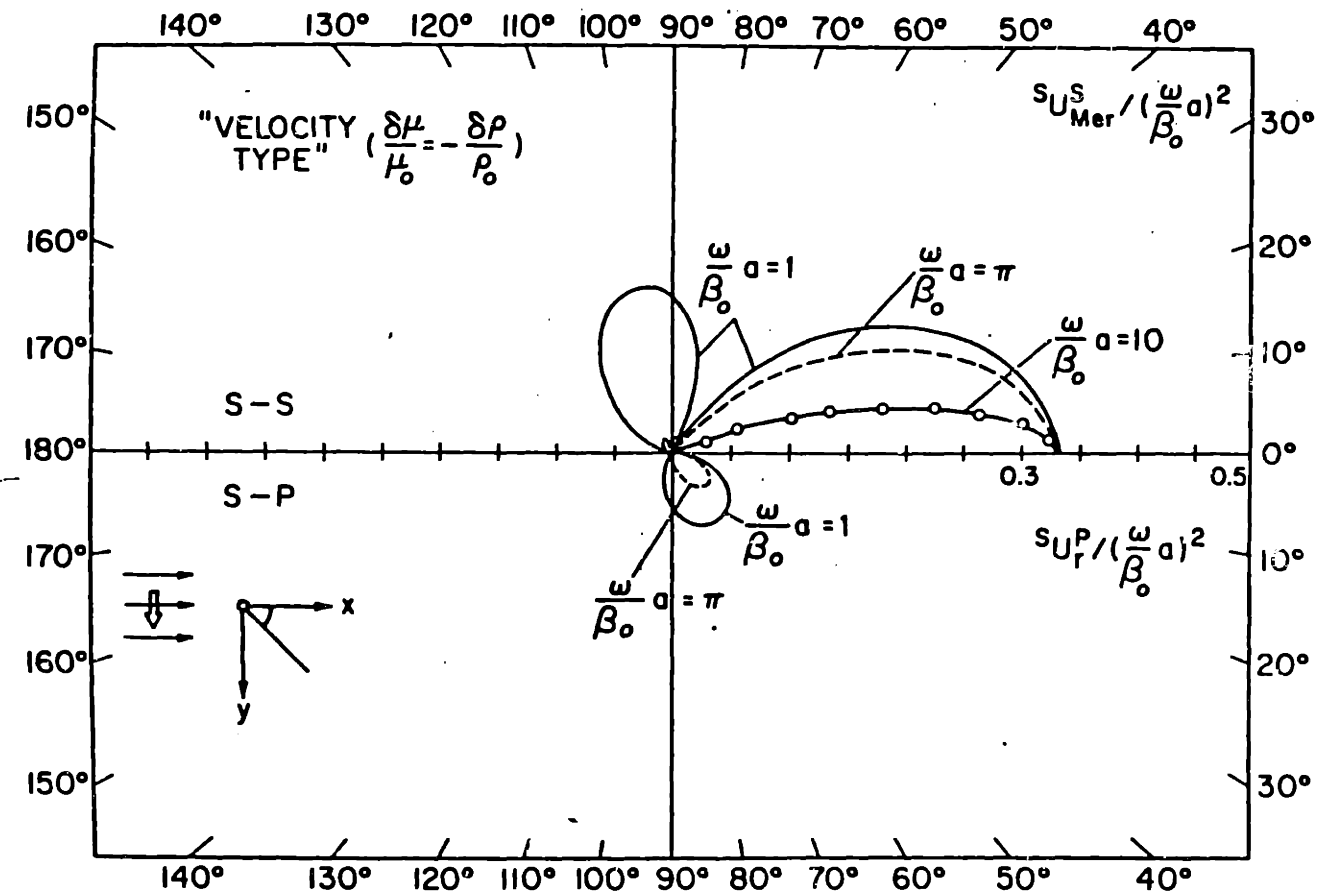

25. Same as 21 but for $\frac{\delta\mu}{\mu_o} = -\frac{\delta\rho}{\rho_o}$, i.e. the "velocity type" scattering.

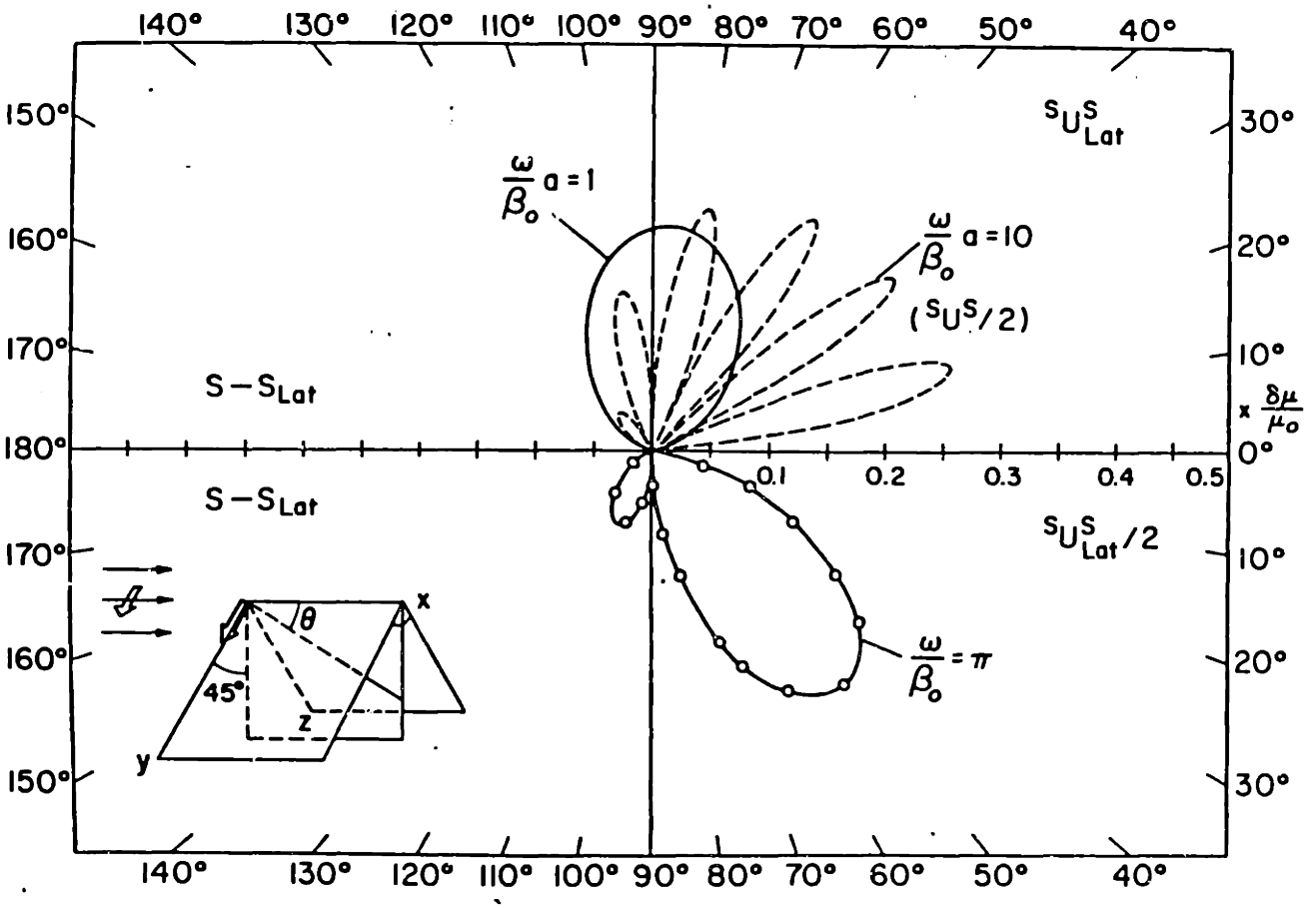

26. Scattering patterns of scattered latitudinal component of a uniform sphere for S wave incidence for different frequencies. The plane has a 45° angle against x-y plane with a common x-axis.

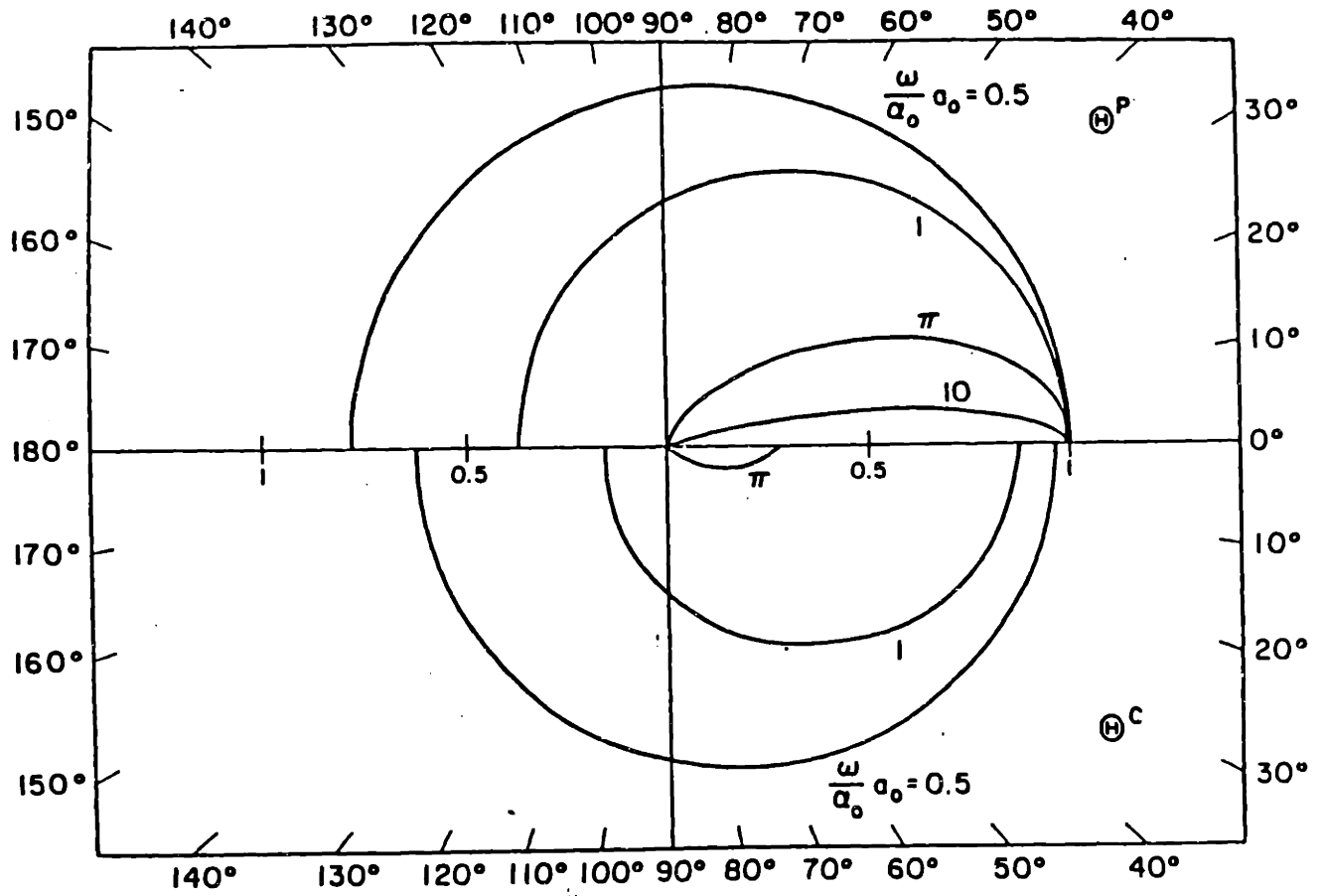

27. Volume factors for a Gaussian heterogeneity. The upper half plane is the case of P-P, the lower half plane is for P-S.

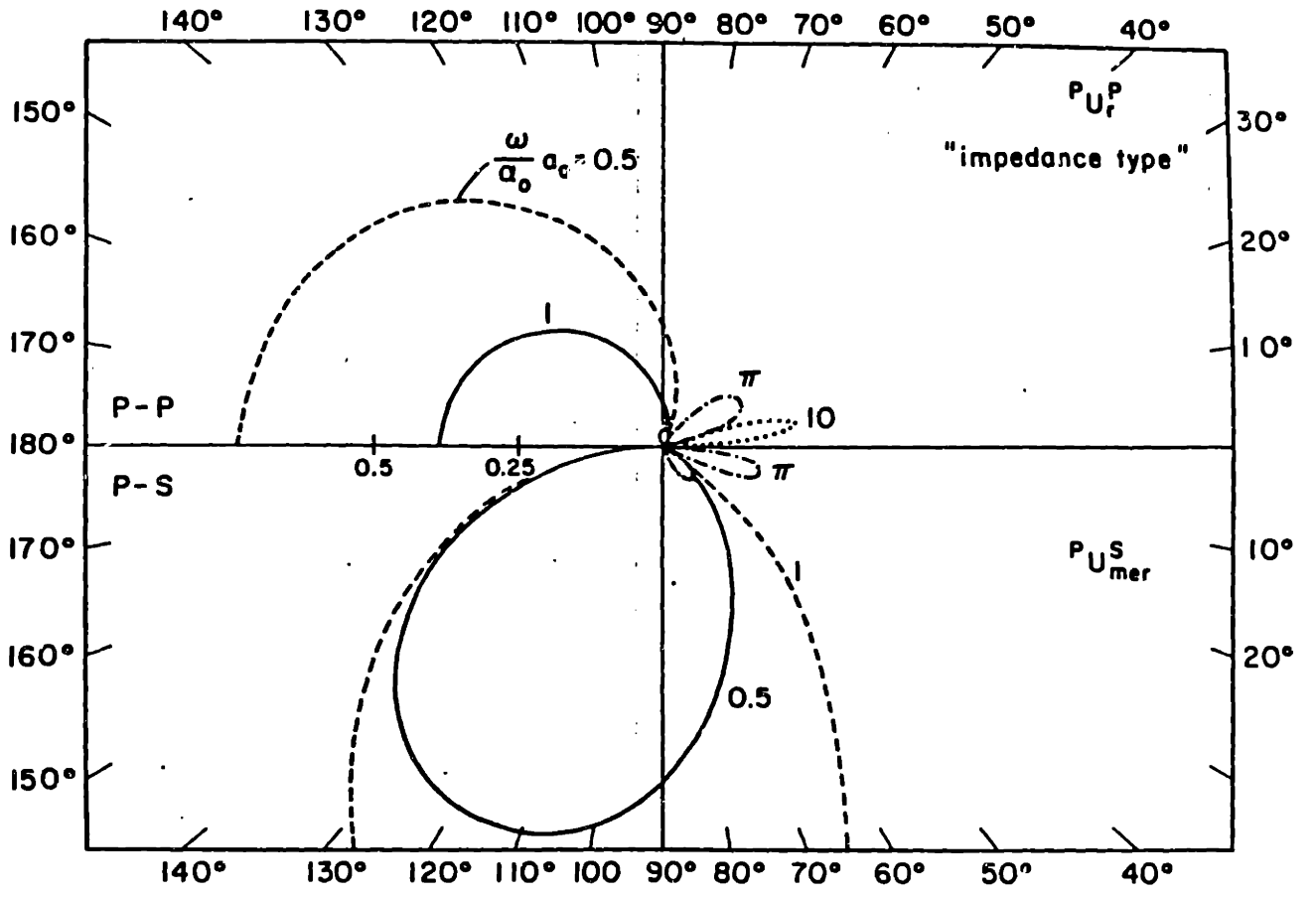

28. Scattering patterns of a Gaussian heterogeneity of impedance type for different frequencies. The upper half plane is for P-P, the lower half plane is for P-S.

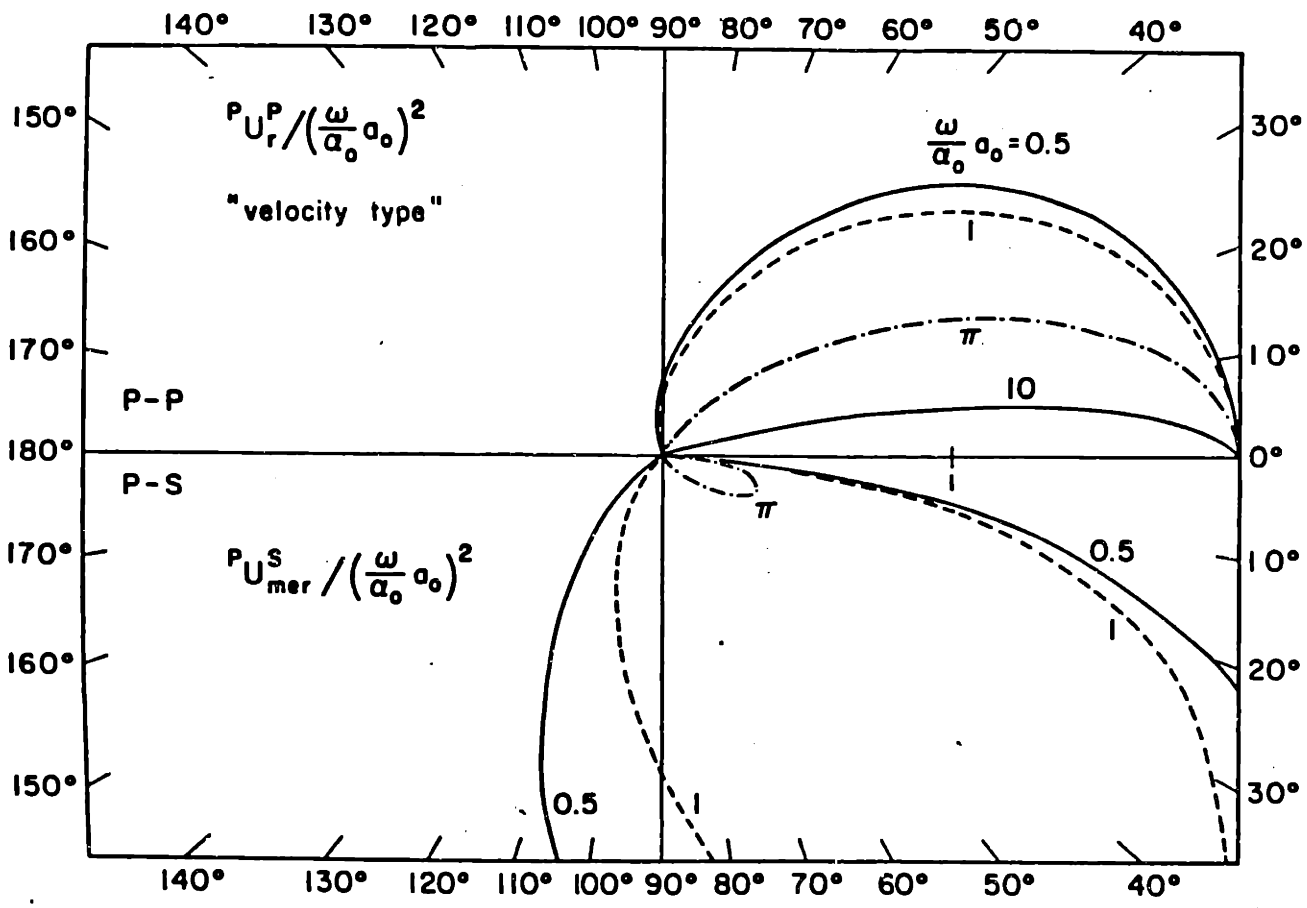

29. Same as 28, for velocity type heterogeneity.

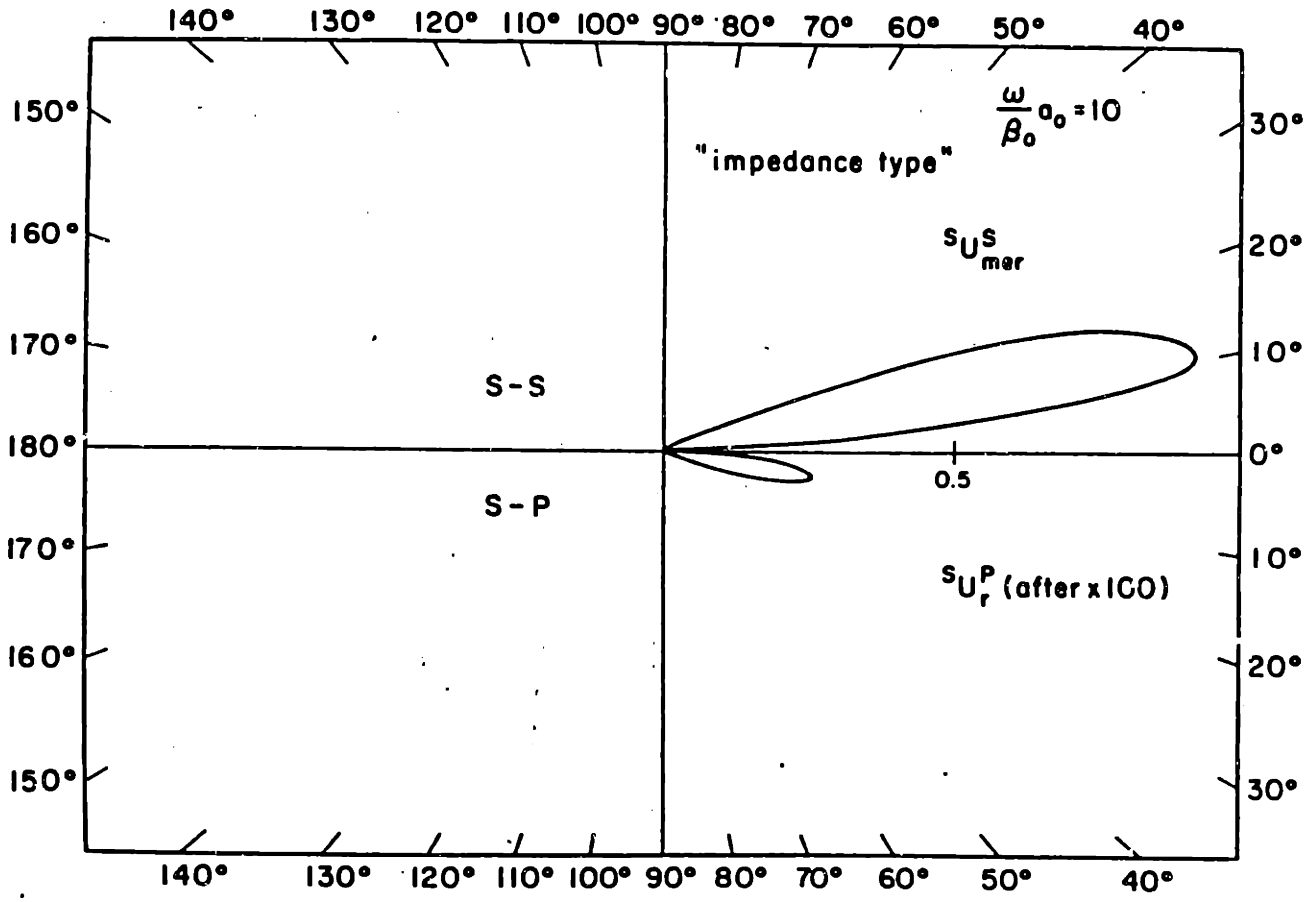

30. Same as 28, for $(\omega/\beta_0)a_0 = 10$, the upper half plane is for S-S, the lower half plane is for S-P.

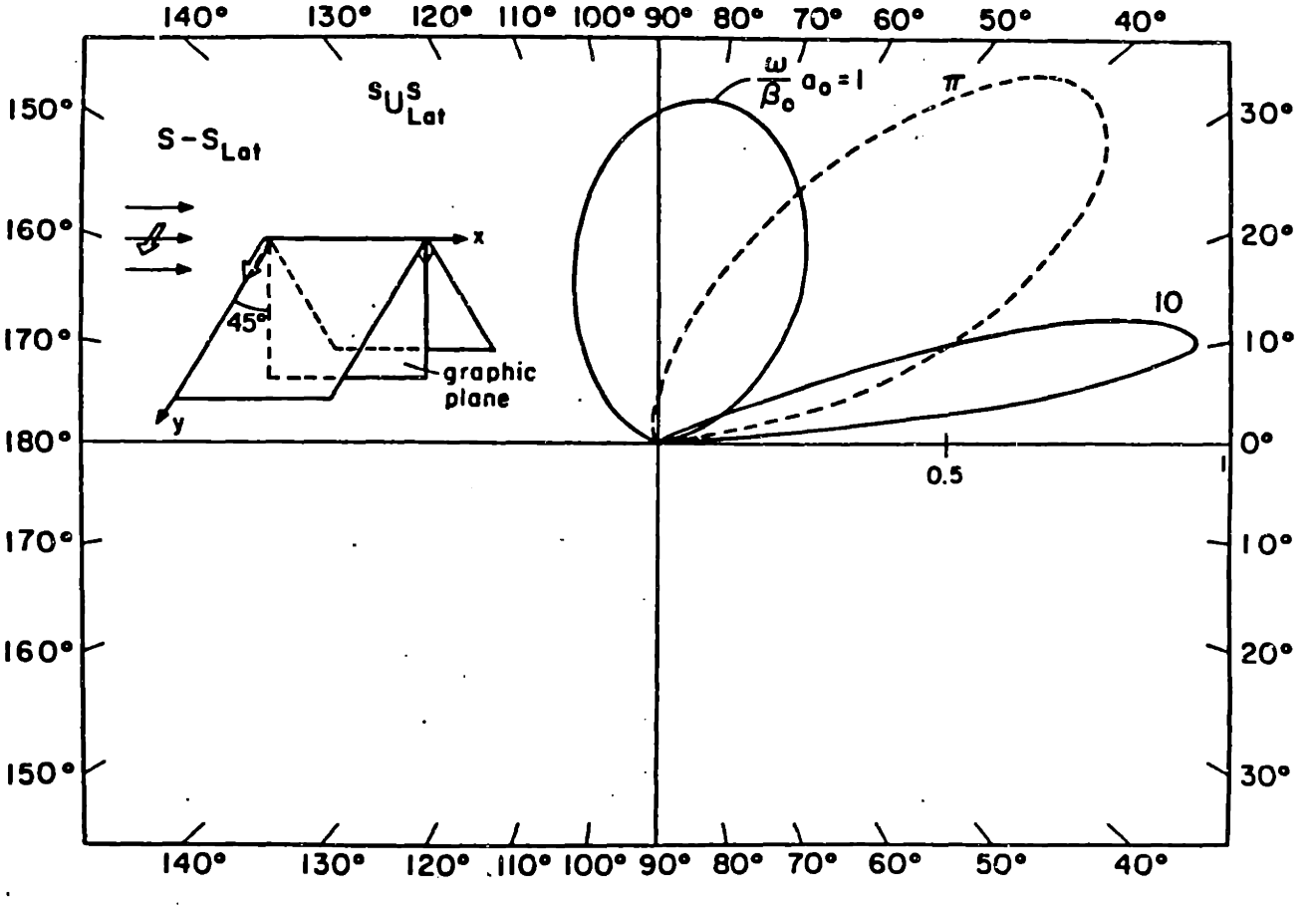

31. Scattering patterns of scattered latitudinal component of a Gaussian heterogeneity for S wave incidence. The graphic plane has 45° angle against the polarization plane of the incident wave (x-y plane) with a common x-axis.

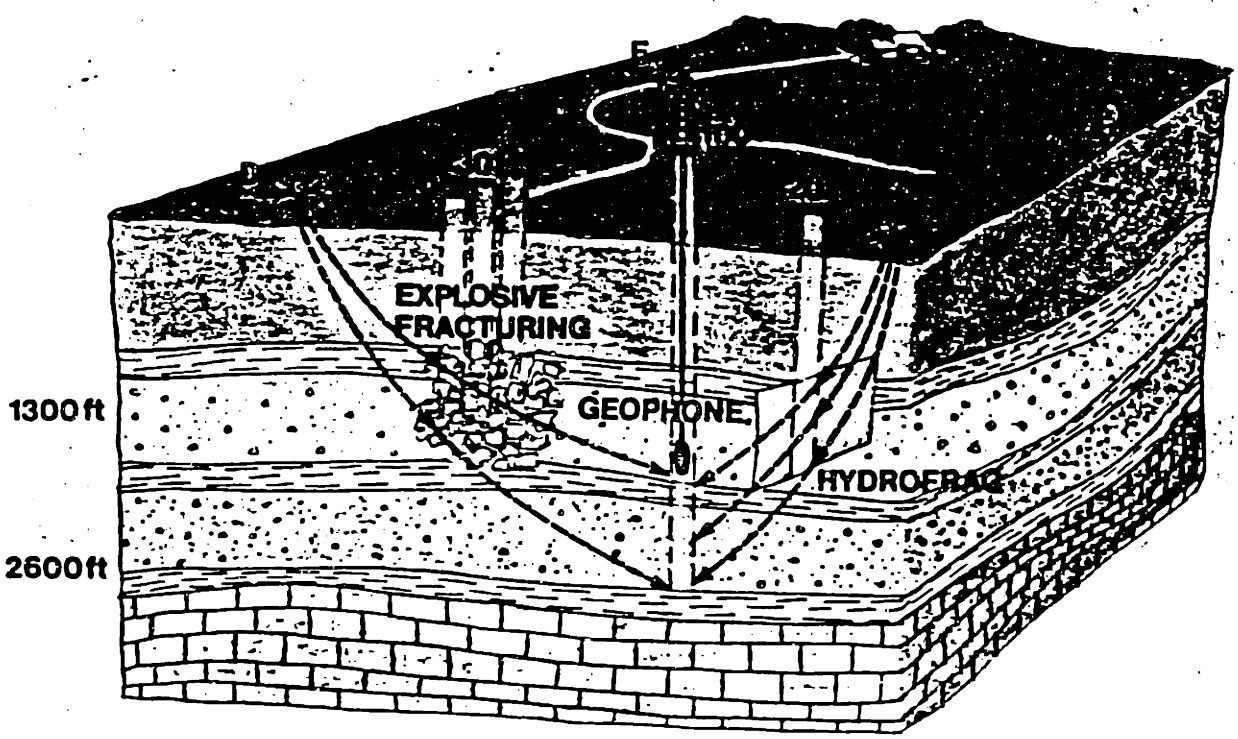

32. Schematic diagram of the VSP experiments for the fracture volume analysis. C and D are the shotpoints, the measurements are taken in well 100. The fracture zone is formed by explosions in 301 and its neighboring wells (from Turpening 1984).

fig. 32

VERTICAL SEISMIC PROFILING

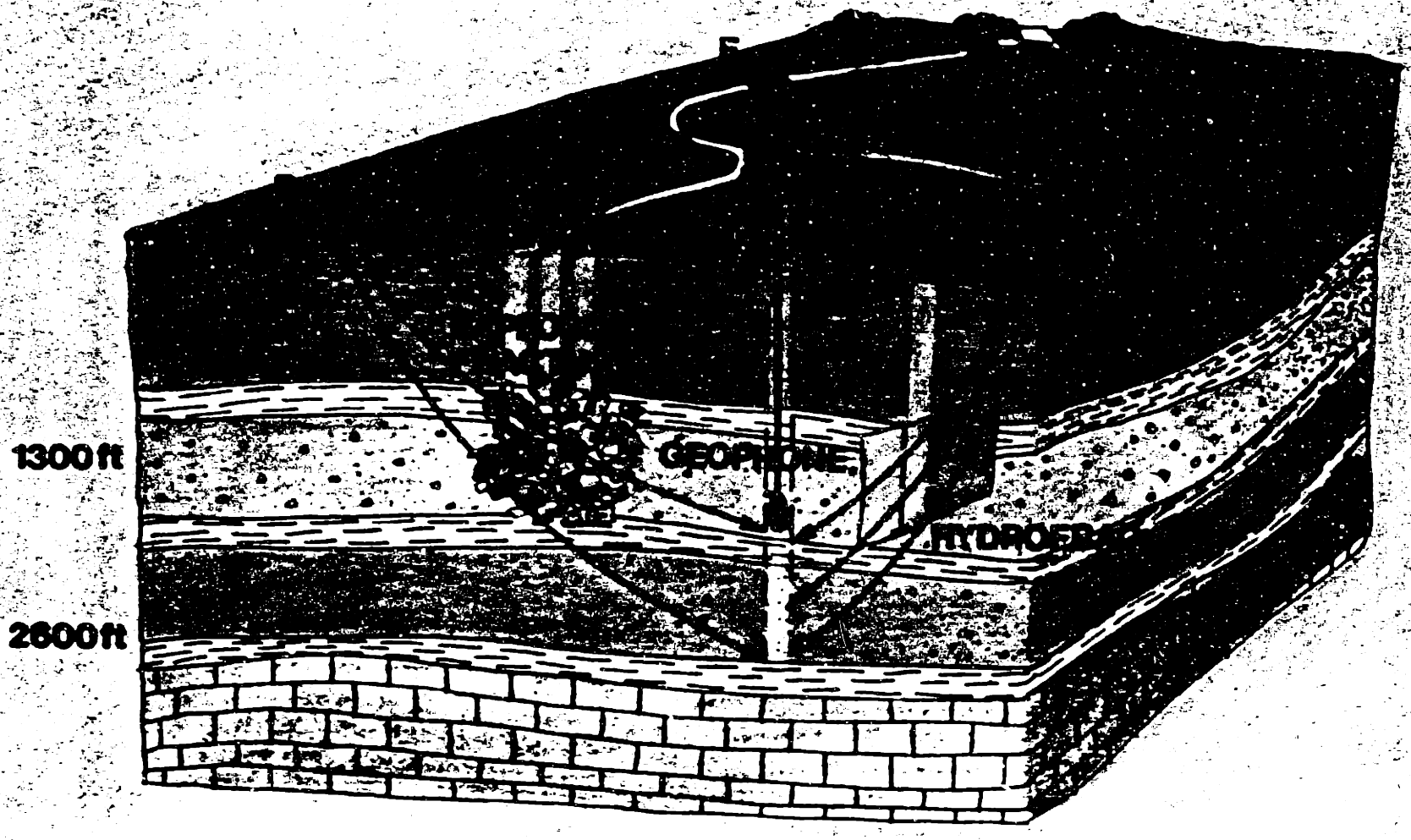

Massachusetts Institute of Technology
Department of Earth & Planetary Sciences

fig. 32

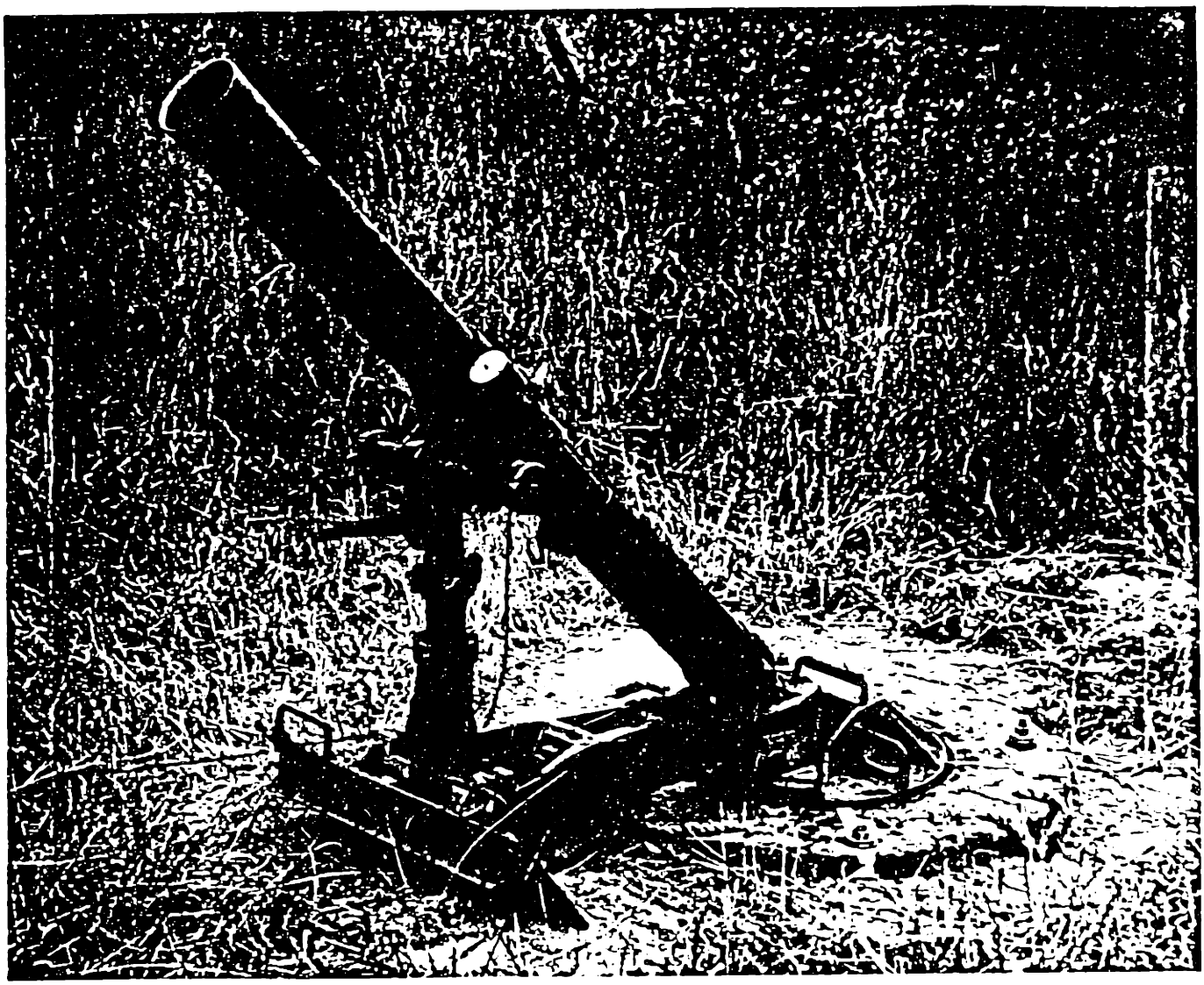

33. The SH wave generator used in the experiment, a 4.2-in mortar (from Turpening 1984).

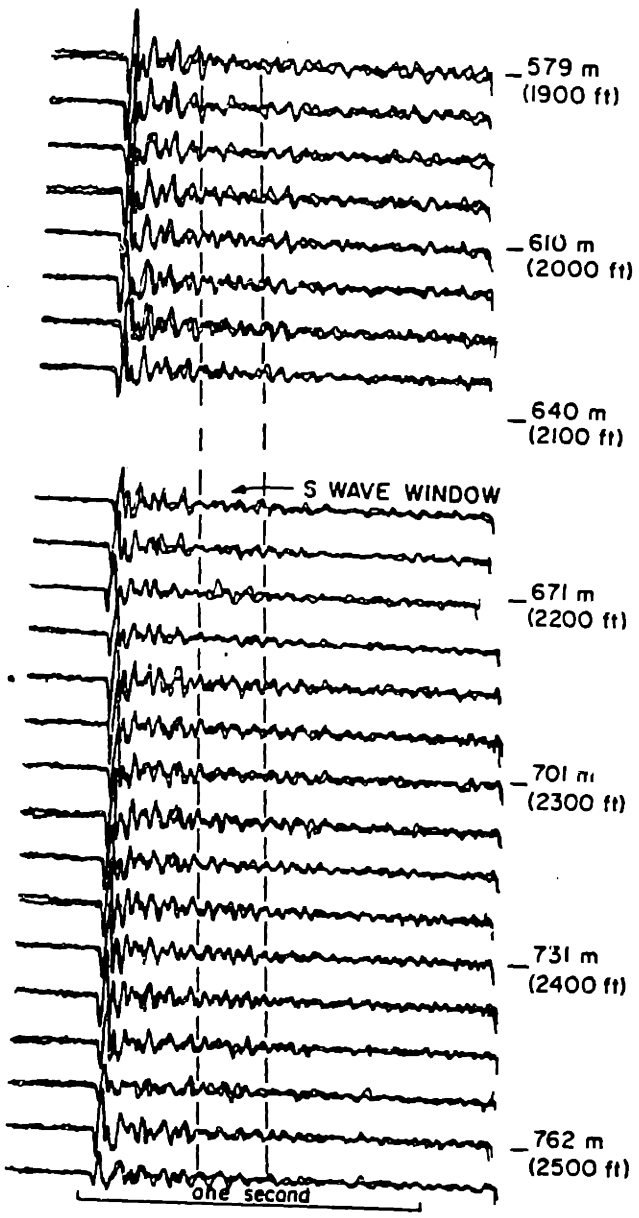

Before Fracturing

Vertical, C

34. Seismic profile of vertical components recorded in well 100 from shotpoint C before fracturing. The SH wave generator is a 4.2-in water mortar. The traces are from two shots with opposite SH orientations. Note that no SV wave occurs (from Turpening 1984).

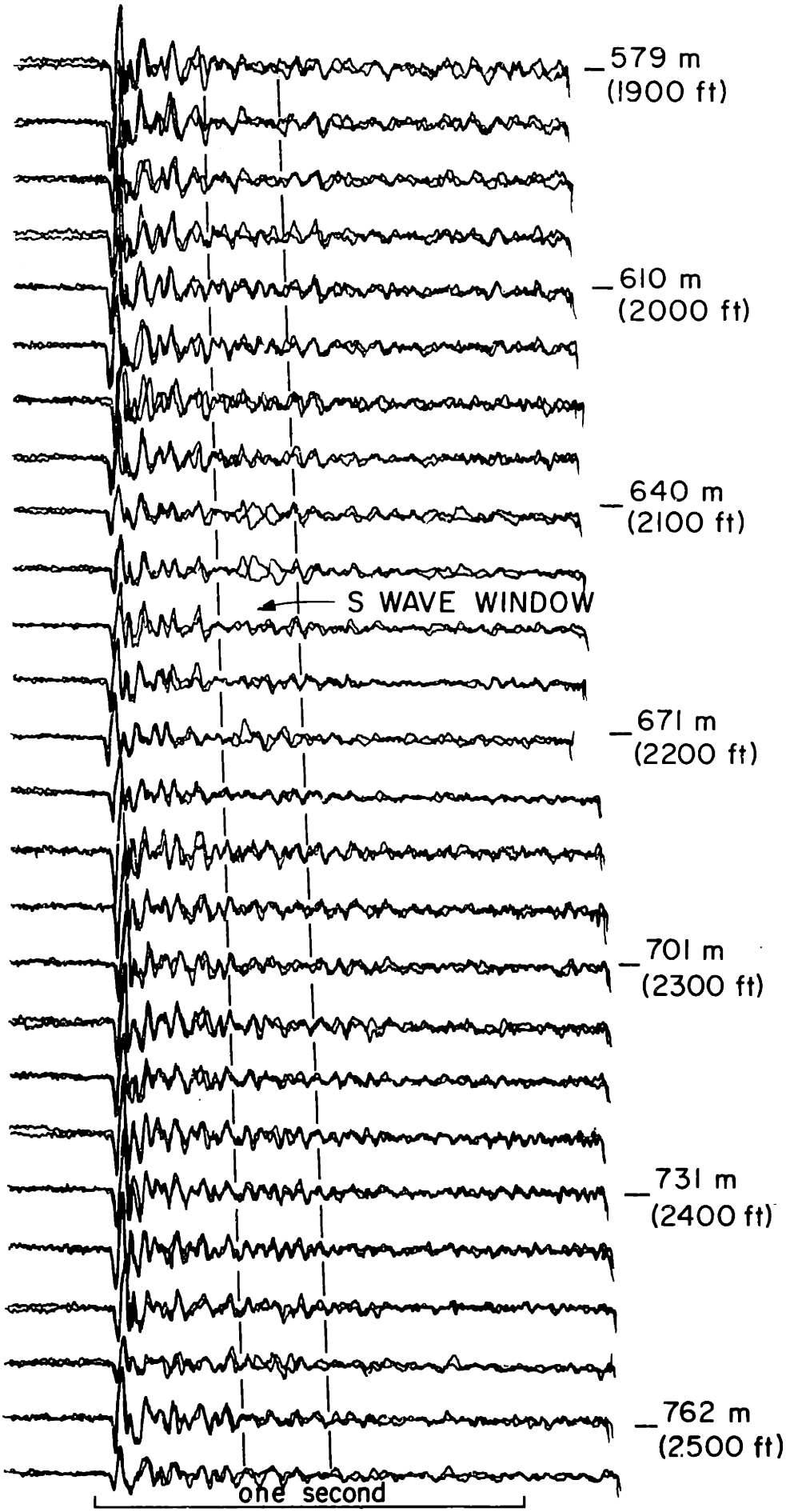
579 m
(1900 ft)
610 m
(2000 ft)
640 m
(2100 ft)
S WAVE WINDOW
671 m
(2200 ft)
701 m
(2300 ft)
731 m
(2400 ft)
762 m
(2500 ft)
one second

C before

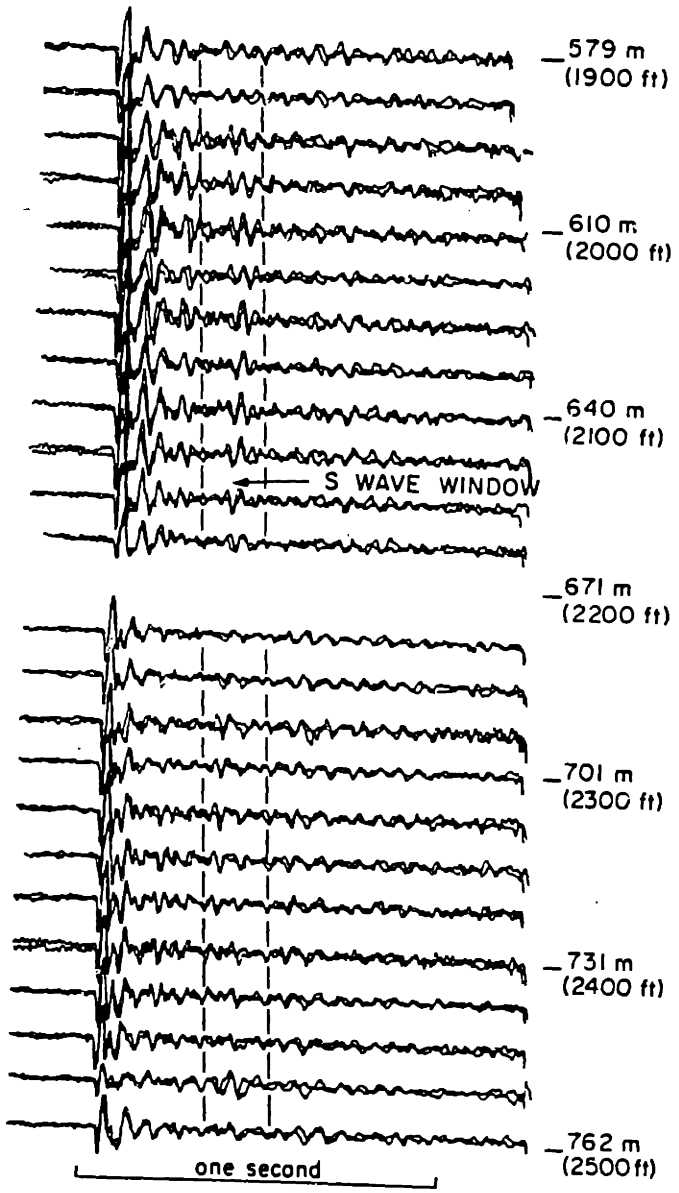

35. Seismic profile of vertical components recorded in well 100 from shotpoint D before fracturing. The sources are the same as in Fig. 35. Note that no SV wave occurs.

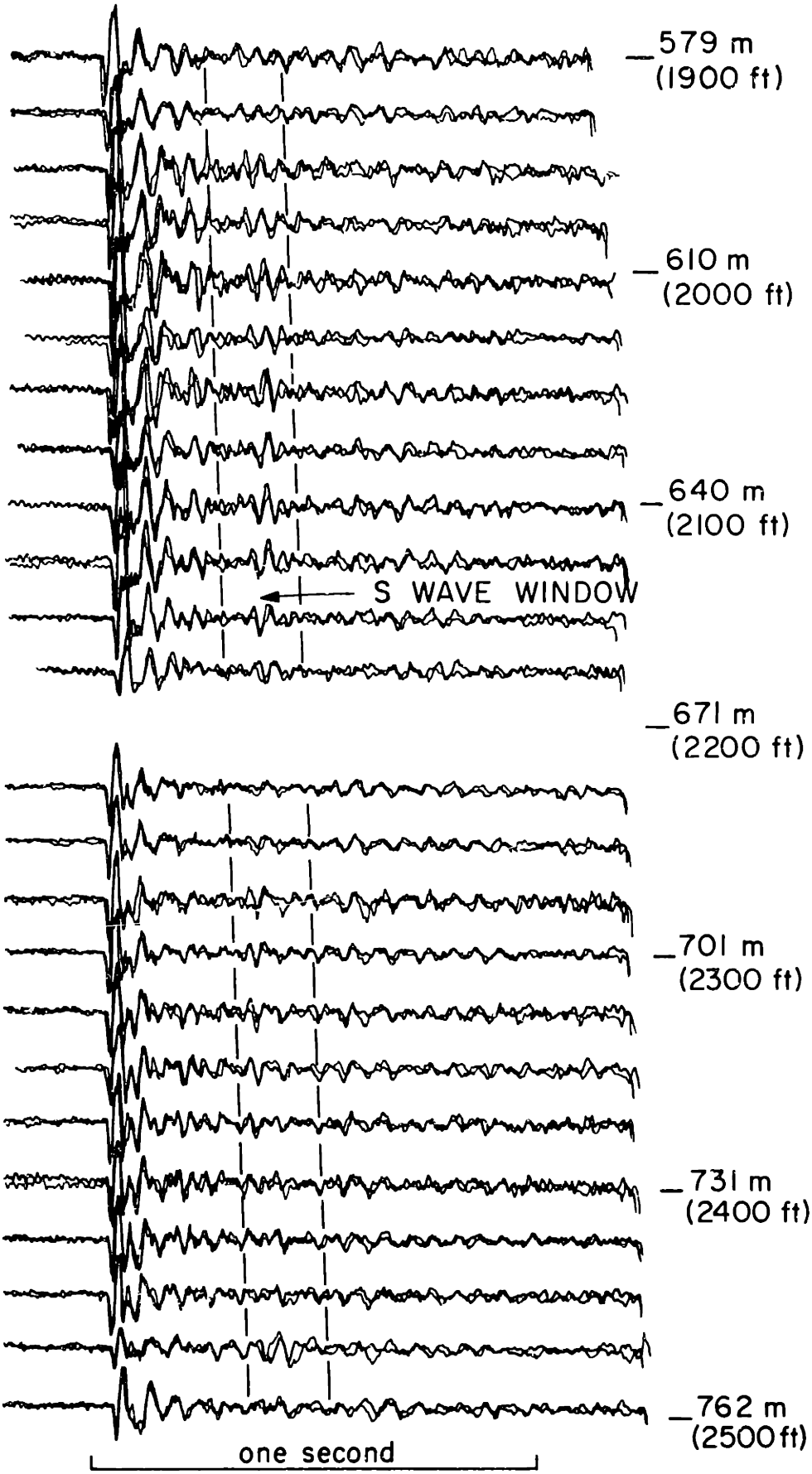
579 m
(1900 ft)
610 m
(2000 ft)
640 m
(2100 ft)
S WAVE WINDOW
671 m
(2200 ft)
701 m
(2300 ft)
731 m
(2400 ft)
762 m
(2500ft)
one second

D before

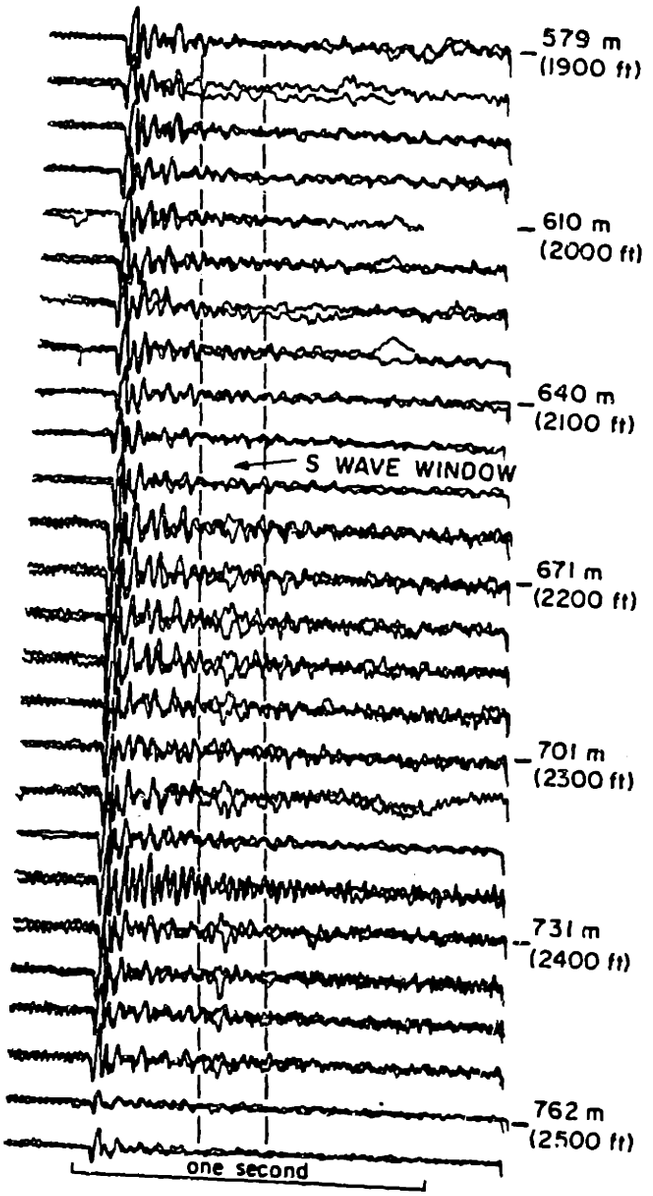

After Fracturing

Vertical, C

36. The profile after fracturing, recorded in well 100 from shotpoint C. These traces of vertical components are from two shots with opposite SH orientation of the source. Note that clear SV waves can be seen at 2175-2325 ft and 2400-2475 ft. These waves are converted from SH waves due to scattering by the fracture zone

fig. 36

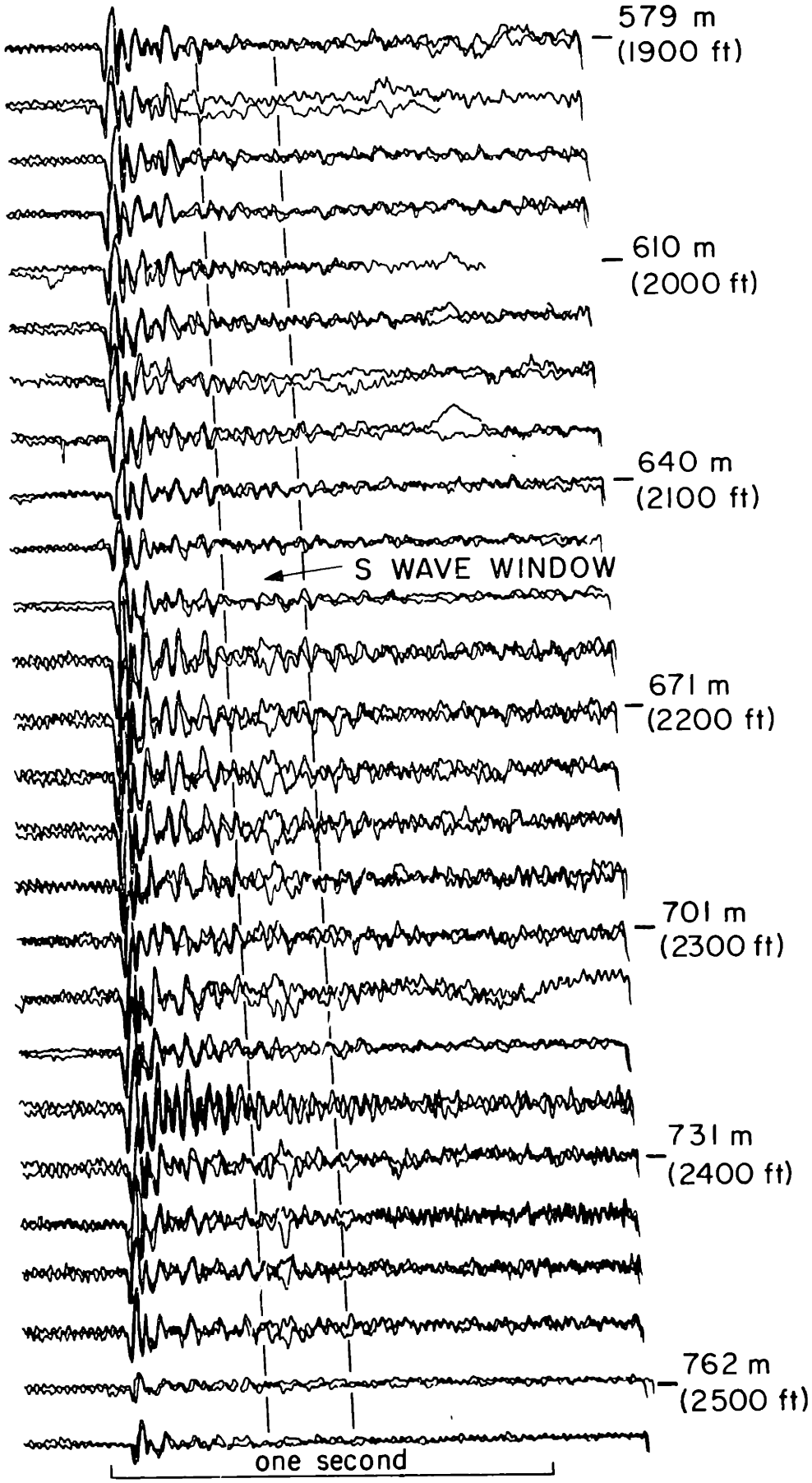

C after

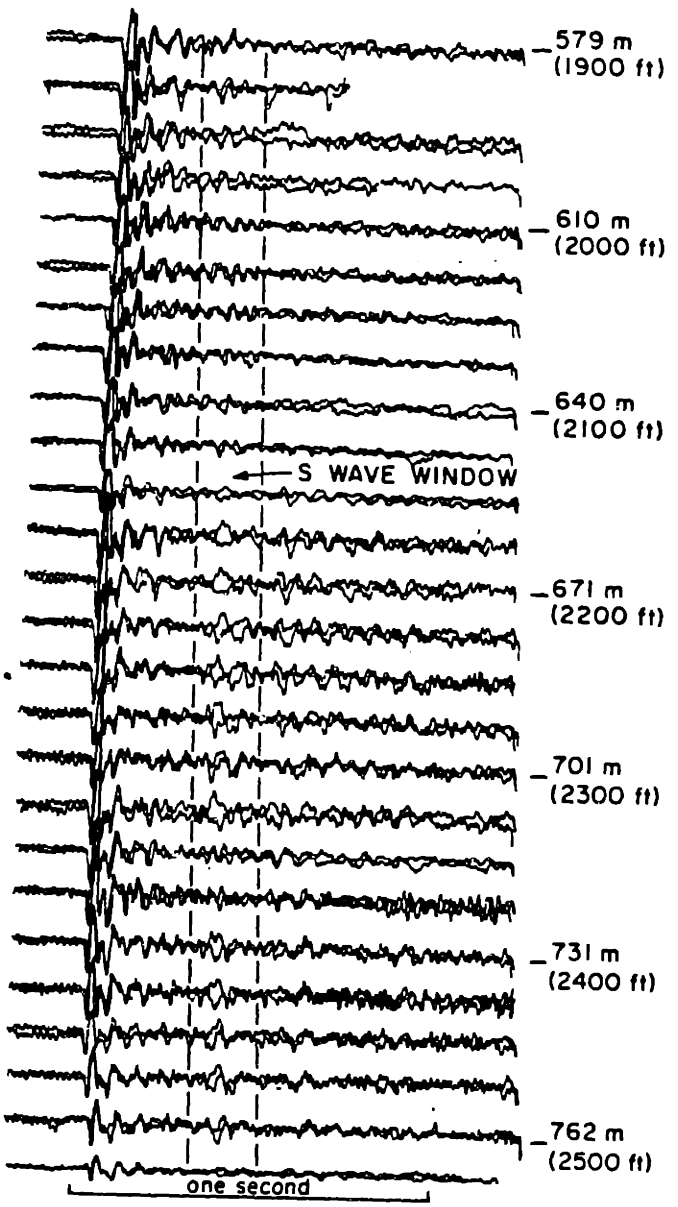

37. The profile of vertical components after fracturing, from shotpoint D. The two lobes of cross-coupled SV waves can be cleary seen (from Turpening 1984).

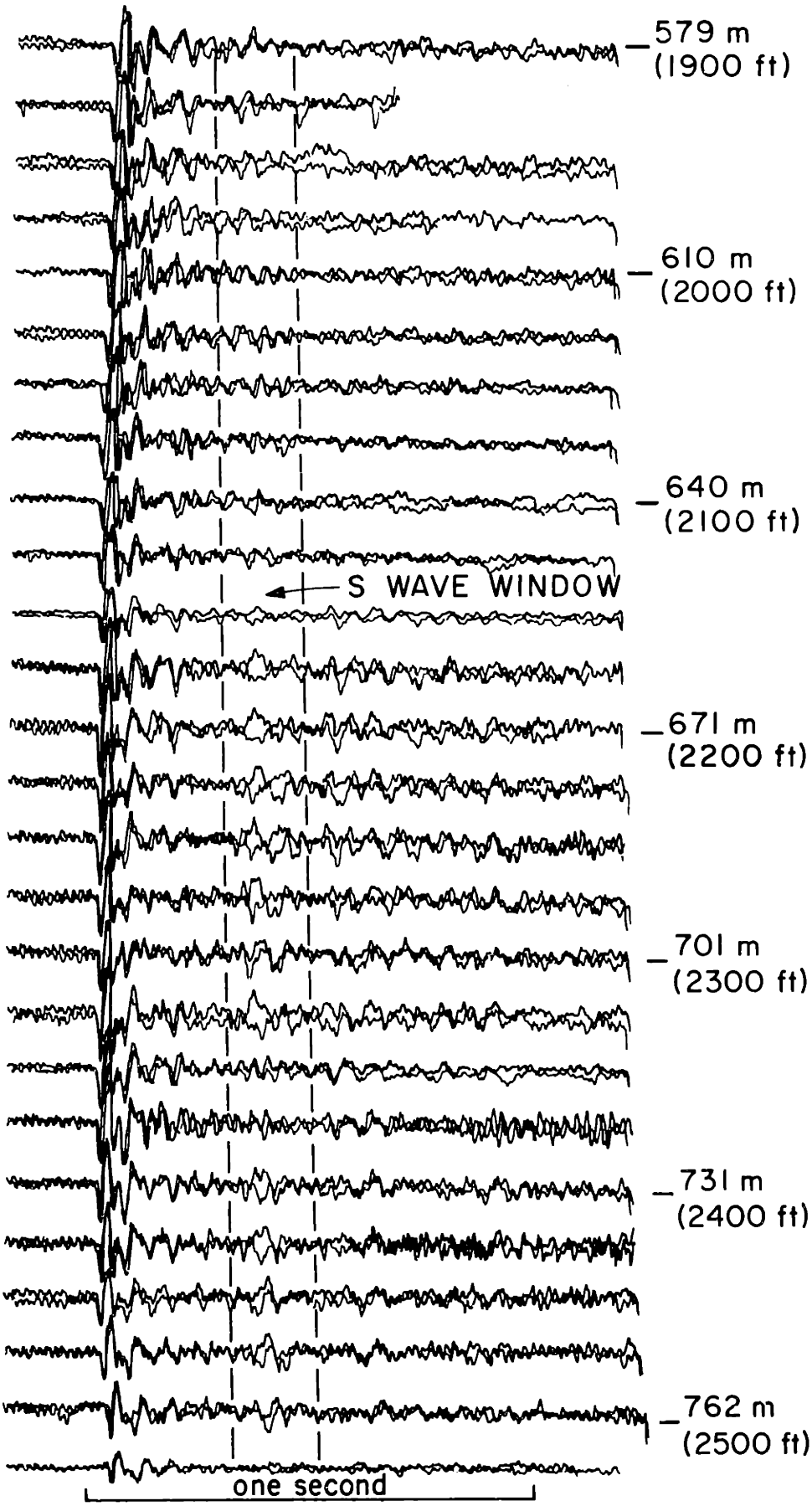
579 m
(1900 ft)
610 m
(2000 ft)
640 m
(2100 ft)
S WAVE WINDOW
671 m
(2200 ft)
701 m
(2300 ft)
731 m
(2400 ft)
762 m
(2500 ft)
one second

D after

Chapter 3

ELASTIC WAVE SCATTERING BY A RANDOM MEDIUM AND THE SMALL SCALE INHOMOGENEITIES IN THE LITHOSPHERE

Abstract

In the study of scattering and attenuation of seismic waves in 3-D heterogeneous media, Chernov's theory on scalar wave scattering in random media has often been used. In this paper we derive the mean square amplitudes of scattered field for P-P, P-S, S-P and S-S scattering by an elastic random medium characterized by perturbations of elastic constants and density using Born approximations. We also obtaine the total scattered power or the scattering coefficient for the case of P wave incidence. We find that, in both the spatial scattering pattern and the frequency dependence of the scattering coefficient, there are some significant differences between scalar wave scattering and elastic wave scattering. This difference is most striking when the wavelength is comparable to the size of inhomogeneities, which is often encountered in the study of short-period seismic body waves. Under certain conditions, the perturbations of the medium parameters can be decomposed into an impedance term and a velocity term. In the forward direction, scattered waves are primarily controlled by the velocity perturbations. For backscattering, scattered waves are generated mainly by impedance perturbations.

We derive the low and high frequency asymptotics for the directional and total scattering coefficients. In the low frequency range, Rayleigh scattering with fourth-power frequency dependence occurs. For the high frequency range, the scattered power for common-mode scattering has a second-power frequency dependence, which is attributed to velocity perturbations, but the power of converted waves reaches a maximum for the case of exponential correlation function. We find that the scalar wave theory can be only approximately used for the forward scattering problem in the high frequency range, such as the phase and amplitude fluctuations in large seismic

arrays. The case of coda wave excitation by local earthquakes, which is a backscattering or a large-angle-scattering problem, must be handled by the full elastic wave theory.

A preliminary analysis of past observations using our theory suggests that the lithosphere may have multiple-scale inhomogeneities. Besides the 10-20 km scale velocity inhomogeneities revealed by the forward scattering observations at LASA nad NORSAR, the lithosphere in tectonically active regions may be rich in small-scale (less than 1 km) inhomogeneities, which may represent randomly distributed faultings.

INTRODUCTION

To study the inhomogeneities in the lithosphere using seismic waves, we need to formulate the scattering and propagation of elastic waves in complex media. Because of the complexity of the lithosphere, an attractive and practical way is to view it as a random medium and attempt to deduce some statistical properties and parameters of its inhomogeneities. The theory of wave propagation and scattering in random media has been well developed in astrophysics, optics, radio physics, and ocean acoustics to deal with light, radio wave and acoustic wave propagation through the atmosphere and ocean (see, e.g., Chandrasekhar, 1950, 1960, Chernov, 1960, Tatarski, 1961, 1971, Flatte et al., 1979). In the past many authors have borrowed the scattering theory of scalar waves in random media from optics and acoustics (Chernov 1960 and Tartarski 1961), and have applied it to deal with the small-scale inhomogeneities in the lithosphere. Aki and his coworkers have successfully applied the single scattering theory of scalar waves to the modeling of the coda generation of local earthquakes (Aki 1969, Aki and Chouet, 1975, Sato 1977). Following the same line, Dainty et al. (1974) explained the lunar seismograms using a wave diffusion model for the strong scattering surface layer of the moon. Single scattering and wave diffusion are two extremes in scattering theory. Recently Gao et al. (1983a,b) has extended the isotropic single scattering coda model to an isotropic multiple scattering model. In addition to coda generation, the scalar wave theory has been also applied to the scattering attenuation problem for short period seismic waves. Aki (1980) applied Chernov's theory to coda waves and found the attenuation of short period seismic waves can be explained by scattering attenuation due to passing through random inhomogeneities. In the calculations he assumed an isotropic single scattering model for scalar waves. Wu has formulated a

forward-multiple-scattering approximation for the scattering attenuation to explain the frequency dependence of S wave and coda attenuation in the high frequency range (Wu 1980, 1982a). Sato (1982a,b) and Korvin (1983) have used some modified mean field approaches in fitting the observed frequency dependence. Some controversy has been raised concerning the use of mean field approach (Wu 1982b, Sata 1982a).

The scalar wave theory has also been used in the phase and amplitude fluctuation problems of tele P waves recorded on large seismic arrays as LASA and NORSAR (Aki, 1973, Capon, 1974, Berteussen et al., 1975). The existnce of velocity inhomogeneities having correlations length 10-20 km, r.m.s. velocity perturbation 2-4% in the lithosphere has been inferred by this application. In addition, the scalar theory can also explain the strong fluctuation of P amplitudes, which is the cause of the instability of the magnitude (yield) estimations of an underground nuclear explosion using direct P amplitudes (Aki et al., 1983).

Despite the succcess in modeling the origin of local coda, and establishing the existence of velocity inhomogeneities of order 10 km size in the lithosphere, the use of the scalar wave theory also brought forth some problems. One is the coda excitation puzzle. As stated by Sato (1982b), the parameters of the random inhomogeneities estimated from the scattering attenuation of the observed data cannot account for the amplitude of coda waves considered as backscattered waves.

In order to know in what circumstances the scalar wave theory can be a good approximation and in what situations it is not applicable, the full elastic wave theory of scattering in random media must be developed. Knopoff and Hudson (1964, 1967) have obtained the asymptotic expressions for the mean square amplitudes of the scattered elastic waves by a random medium for low

and high frequencies using the Born approximation. Haddon (1978) derived the explicit expressions for the incident P waves incidence (see Aki and Richards 1980), and applied them to the interpretation of the precursors to PKIKP as scattered PKP waves by inhomogeneities near the mantle-core boundary (Haddon and Cleary, 1974, see also Doornbos, 1976). Hudson (1977) summarized the development and use of the first order scattering theory (Born approximation) of elastic waves in seismology and gave the expressions of scattered waves in the time domain for incident P wave. Recently Sato (1983) has derived the mean squared amplitudes of scattered fields in frequency domain in terms of density and velocity perturbations by Born approximation. We also need to mention that Karal and Keller (1964) have developed the mean field theory for elastic waves in random media. However, since the seismograms do not record the coherent field or mean field, any comparison between the observations and the mean field predictions should be made with great caution. Some comparisons (e.g. Beaudet 1970) have failed to recognize this and thus did not produce meaningful results.

In the present paper, following an approach similar to Haddon (1978), using equivalent sources and Born approximations for a weakly perturbed random medium, developed by Wu and Aki (1984), we derive the mean square amplitudes of the scattered fields and the directional scattering coefficients of the random medium for the P-P, P-S, S-P and S-S cases. We give the explicit expressions in terms of perturbations of density and Lame constants, and in terms of perturbations of impedances and velocities. We find that the velocity perturbations produce no scattering in the backward direction. On the other hand, there are no scattered waves in the forward directions for impedance perturbations. We obtain the asymptotic expressions for low and high frequency waves. For high frequency waves, i.e. when the wavelength is

much smaller than the correlation length of the random medium, under the small scattering angle approximations, the scalar wave scattering theory considering only the velocity perturbations can be applied approximately to the elastic wave scattering problem. That is why the scalar wave theory has been successfully used for large scale velocity inhomogeneities. On the other hand, for large angle scattering or backscattering, which happen when the wavelength is longer or comparable to the correlation length of the medium, the scalar wave theory is not valid. Therefore the coda strength problem must be solved by the full elastic wave scattering theory.

We derive the total scattered energy or total scattering coefficient for incident P waves to show that the frequency dependence of the total scattered energy can be quite different from the scalar case, especially when the wavelength is comparable to the correlation length.

A preliminary analysis of past observations using our theory suggested that the lithosphere may have multiple-scale inhomogeneities. The phase and amplitude fluctuations observed at LASA and NORSAR revealed the existence of large-scale (10-20 km) velocity inhomogeneities, while the coda wave observations for local earthquakes seem to show the presence of small-scale (less than 1 km) impedance inhomogeneities in tectonically active regions. The parameters of the inhomogeneities will be estimated based on our theory.

I. DIRECTIONAL SCATTERING COEFFICIENTS FOR P WAVE INCIDENCE

Suppose a finite volume of random medium is embedded in a homogeneous elastic medium with density ρ_o and elastic constants λ_o, μ_o. The random medium is characterized by the random perturbations of its parameters from the mean values. We denote the parameters of the random inhomogeneities as

$$\begin{aligned} \rho(\vec{\xi}) &= \rho_o + \delta\rho(\vec{\xi}), \\ \lambda(\vec{\xi}) &= \lambda_o + \delta\lambda(\vec{\xi}), \\ \mu(\vec{\xi}) &= \mu_o + \delta\mu(\vec{\xi}), \end{aligned} \tag{1.1}$$

where $\vec{\xi}$ is the position vector within the volume, and $\rho(\vec{\xi})$ is the density of the random inhomogeneities at $\vec{\xi}$, $\lambda(\vec{\xi})$, $\mu(\vec{\xi})$ are the corresponding Lame constants, $\delta\rho(\vec{\xi})$, $\delta\lambda(\vec{\xi})$ and $\delta\mu(\vec{\xi})$are their perturbations. Here we assume

$$\begin{aligned} \rho_o &= \langle\rho(\vec{\xi})\rangle, \\ \lambda_o &= \langle\lambda(\vec{\xi})\rangle, \\ \mu_o &= \langle\mu(\vec{\xi})\rangle, \end{aligned} \tag{1.2}$$

and

$$\delta\rho \ll \rho_o, \quad \delta\lambda \ll \lambda_o, \quad \delta\mu \ll \mu_o, \tag{1.3}$$

namely the inclusion is a weakly inhomogeneous random medium, where $\langle\ \rangle$ denotes taking mean of a random variable.

A random medium is a large family of innumerable inhomogeneous media. Each member of the family, with a certain probability of existence differs from the others in its detailed structure, but has some common statistical properties of the family. Now we consider one specific member of the random medium, called a realization. Following Wu and Aki (1983), the scattered wave field can be written using body-force equivalence and Born approximation as

$$U_i(\vec{x}) = \int_V Q_j(\vec{\xi}) * G_{ij}(\vec{x},\vec{\xi}) dV(\vec{\xi}), \tag{1.4}$$

where $U_i(\vec{x})$ is the ith component of the scattered wave displacement at the observation point $\vec{x}$, $G_{ij}(\vec{x},\vec{\xi})$ is the elastodynamic Green's function for unbounded media, "*" stands for convolution, $Q_j(\vec{\xi})$ is the jth component of the equivalent body-force of the scattered field at point $\vec{\xi}$ (see Aki and Richards, ch. 13, 1980).

$$Q_j = -\delta\rho \frac{\partial^2 U_j^\circ}{\partial t^2} + (\delta\lambda + \delta\mu)(\nabla\cdot\vec{U}^\circ)_{,j} + \delta\mu\nabla^2 U_j^\circ$$

$$+ (\delta\lambda)_{,j}(\nabla\cdot U^\circ) + (\delta\mu)_{,k}[U^\circ_{j,k} + U^\circ_{k,j}], \qquad (1.5)$$

where U_j° is the jth component of the incident field, subscripts after comma denote differentiation with respect to the corresponding Cartesian coordinate and repeated subscripts imply summation over those subscripts. The integration in (1.4) is over the whole volume of the random medium.

Substituting (1.5) into (1.4) we can get after integration by parts

$$U_i(\vec{x}) = -\int_V \delta\rho \frac{\partial^2 U_j^\circ}{\partial t^2} * G_{ij}\, dV$$

$$- \int_V [\delta\lambda[(\nabla\cdot\vec{U}^\circ)\delta_{jk} + \delta\mu(U^\circ_{j,k}+U^\circ_{k,j})]*G_{ij,k}\, dV, \qquad (1.6)$$

where δ_{jk} is the Kronecker delta.

Suppose the observation point is far from the random medium compared with the size of the random medium, we can make the Fraunhofer approximation to G_{ij} and its derivatives. After some simplification and manipulation (for details see Wu and Aki, 1983) we obtain the scattered far-field as

$$U_i^P(\vec{x}) = \frac{\omega^2}{4\pi\alpha_o^2}\frac{1}{r}e^{-i\omega(t-r/\alpha_o)}$$

$$\cdot\int_V \Big[\frac{\delta\rho(\vec{\xi})}{\rho_o}\gamma_i\gamma_j U_j^o(\vec{\xi}) + \frac{i}{(\omega/\alpha_o)}\frac{\delta\lambda(\vec{\xi})}{\lambda_o+2\mu_o}\gamma_i(\nabla\cdot\vec{U}^0(\vec{\xi}))$$

$$+\frac{i}{(\omega/\alpha_o)}\frac{\delta\mu(\vec{\xi})}{\lambda_o+2\mu_o}\gamma_i\gamma_j\gamma_k(U_{j,k}^o(\vec{\xi}) + U_{k,j}^o(\vec{\xi}))\Big]e^{-i\frac{\omega}{\alpha_o}(\vec{\xi}\cdot\hat{x})}dV(\vec{\xi}) \quad (1.7)$$

$$U_i^S(\vec{x}) = \frac{\omega^2}{4\pi\beta_o^2}\frac{1}{r}e^{-i\omega(t-r/\beta_o)}$$

$$\cdot\int_V \Big[\frac{\delta\rho(\vec{\xi})}{\rho_o}(\delta_{ij}-\gamma_i\gamma_j)U_j^o(\vec{\xi})$$

$$+\frac{i}{(\omega/\beta_o)}\frac{\delta\mu(\vec{\xi})}{\mu_o}(\delta_{ij}-\gamma_i\gamma_j)\gamma_k(U_{j,k}^o(\vec{\xi})+U_{k,j}^o(\vec{\xi}))\Big]e^{-i\frac{\omega}{\beta_o}(\vec{\xi}\cdot\hat{x})}dV(\vec{\xi}), \quad (1.8)$$

where U_i^P and U_i^S are the ith components of the scattered P wave and S wave, $\vec{x}$ is the position vector of the observation point and r is the distance between the observation point and the center of the random medium, $\hat{x}$ is its unit vector and γ_i, its directional cosine with the ith coordinate axis, ω is the circular frequency of the wave field, α_o and β_o are the wave velocity of P and S wave in the surrounding medium respectively.

For a plane P wave incident along the x_1 direction, i.e.

$$U_1^o = \exp[-i\omega(t-x_1/\alpha_o)],$$

$$U_2^o = U_3^o = 0,$$

We obtain the scattered P and S wave as

$$P_U P_i(\vec{x}) = \frac{\omega^2}{4\pi\alpha_o^2}\frac{1}{r}\, e^{-i\omega(t-r/\alpha_o)}$$

$$\int_V \left[\frac{\delta\rho(\vec{\xi})}{\rho_o}\gamma_i\gamma_1 - \frac{\delta\lambda(\vec{\xi})}{\lambda_o+2\mu_o}\gamma_i - \frac{2\delta\mu(\vec{\xi})}{\lambda_o+2\mu_o}\gamma_i\gamma_1^2\right] e^{i\frac{\omega}{\alpha_o}\xi_1 - i\frac{\omega}{\alpha_o}(\hat{x}\cdot\vec{\xi})}\cdot dV(\vec{\xi}), \tag{1.9}$$

$$P_U S_i(\vec{x}) = \frac{\omega^2}{4\pi\beta_o^2}\frac{1}{r}\, e^{-i\omega(t-r/\beta_o)}$$

$$\int_V \left[\frac{\delta\rho(\vec{\xi})}{\rho_o}(\delta_{i1}-\gamma_i\gamma_1) - \left(\frac{\beta_o}{\alpha_o}\right)\frac{2\delta\mu(\vec{\xi})}{\mu_o}(\delta_{i1}-\gamma_i\gamma_1)\gamma_1\right] e^{i\frac{\omega}{\alpha_o}\xi_1 - i\frac{\omega}{\beta_o}(\hat{x}\cdot\vec{\xi})}\cdot dV(\vec{\xi}). \tag{1.10}$$

In a similar way, for a plane S wave incident along the x_1 direction and having its particle motion in the x_2 direction, i.e.

$$\overset{\circ}{U}_2 = \exp(-i\omega(t-x_1/\beta_o)],$$

$$\overset{\circ}{U}_1 = \overset{\circ}{U}_3 = 0,$$

we get

$$S_U P_i(\vec{x}) = \frac{\omega^2}{4\pi\alpha_o^2}\frac{1}{r}\, e^{-i\omega(t-r/\alpha_o)}$$

$$\int_V \left[\frac{\delta\rho(\vec{\xi})}{\rho_o}\gamma_i\gamma_2 - \left(\frac{\beta_o}{\alpha_o}\right)\frac{2\delta\mu(\vec{\xi})}{\mu_o}\gamma_i\gamma_1\gamma_2\right] e^{i\frac{\omega}{\beta_o}\xi_1 - i\frac{\omega}{\alpha_o}(\hat{x}\cdot\vec{\xi})}dV(\vec{\xi}) \tag{1.11}$$

$$S_U S_i(\vec{x}) = \frac{\omega^2}{4\pi\beta_o^2}\frac{1}{r}\, e^{-i\omega(t-r/\beta_o)}$$

$$\int_V \left[\frac{\delta\rho(\vec{\xi})}{\rho_o}(\delta_{i2}-\gamma_i\gamma_2) - \frac{\delta\mu(\vec{\xi})}{\mu_o}(\delta_{i1}\gamma_2+\delta_{i2}\gamma_1-2\gamma_i\gamma_1\gamma_2)\right]$$

$$\cdot\, e^{i\frac{\omega}{\beta_o}\xi_1 - i\frac{\omega}{\beta_o}(\hat{x}\cdot\vec{\xi})}\, dV(\vec{\xi}) \qquad (1.12)$$

Note that, the terms within the square brackets of (1.9), (1.10) (1.11) and (1.12) are the scattered fields for the corresponding elastic-wave-Rayleigh-scattering. That means that the total scattered field is the sum of the Rayleigh-scattered fields by all the volume elements of the inclusion, with phase factors corresponding to the travel time differences among volume elements.

Because the random property of the inclusion, the scattered wave is also a random wave field. In order to calculate the average amplitude of the scattered field, we take the ensemble mean of the square amplitude. For P wave incidence, if we use the spherical coordinates having the polar axis along the direction of particle motion of the incident wave, i.e. the x_1 direction (Fig. 1), (1.9) and (1.10) become

$$P_U P_r(\vec{x}) = \frac{\omega^2}{4\pi\alpha_o^2}\frac{1}{r}\, e^{-i\omega(t-r/\alpha_o)}$$

$$\int_V \left[\frac{\delta\rho(\xi)}{\rho_o}\cos\theta - \frac{\delta\lambda(\vec{\xi})}{\lambda_o+2\mu_o} - \frac{2\delta\mu(\vec{\xi})}{\lambda_o+2\mu_o}\cos^2\theta\right] e^{i\frac{\omega}{\alpha_o}(\hat{x}_1-\hat{x})\cdot\vec{\xi}}\, dV(\vec{\xi}) \qquad (1.13)$$

$$P_U S_{mer}(\vec{x}) = \frac{\omega^2}{4\pi\beta_o^2}\frac{1}{r}\, e^{-i\omega(t-r/\beta_o)}$$

$$\int_V \left[-\frac{\delta\rho(\vec{\xi})}{\rho_o}\sin\theta + \left(\frac{\beta_o}{\alpha_o}\right)\frac{\delta\mu(\vec{\xi})}{\mu_o}\sin 2\theta\right] e^{i\omega\left(\frac{\hat{x}_1}{\alpha_o} - \frac{\hat{x}}{\beta_o}\right)\cdot\vec{\xi}}\, dV(\vec{\xi}). \qquad (1.14)$$

where U_r, U_{mer} are the radial and meridian components of the scattered field respectively. Since the problem is symmetric to the polar axis, there is no latitudinal component. Taking the mean square of (1.13),

$$\langle |P_r U P| ^2 \rangle = \langle P_r U P \cdot P_r U P^* \rangle$$

$$= \frac{\omega^4}{(4\pi)^2 \alpha_o^4} \frac{1}{r^2} \iint_{vv} \left[\cos^2\theta \frac{\langle \delta\rho(\vec{\xi}) \delta\rho(\vec{\eta}) \rangle}{\rho_o^2} + \frac{\langle \delta\lambda(\vec{\xi}) \delta\lambda(\vec{\eta}) \rangle}{(\lambda_o + 2\mu_o)^2} + 4\cos^4\theta \frac{\langle \delta\mu(\vec{\xi}) \delta\mu(\vec{\eta}) \rangle}{(\lambda_o + 2\mu_o)^2} \right.$$

$$\left. - 2\cos\theta \frac{\langle \delta\rho(\vec{\xi}) \delta\lambda(\vec{\eta}) \rangle}{\rho_o(\lambda_o + 2\mu_o)} - 4\cos^3\theta \frac{\langle \delta\rho(\vec{\xi}) \delta\mu(\vec{\eta}) \rangle}{\rho_o(\lambda_o + 2\mu_o)} + 4\cos^2\theta \frac{\langle \delta\lambda(\vec{\xi}) \delta\mu(\vec{\eta}) \rangle}{(\lambda_o + 2\mu_o)^2} \right]$$

$$e^{i\omega \left(\frac{1}{\alpha_o} \hat{x}_1 - \frac{1}{\alpha_o} \hat{x} \right) \cdot (\vec{\xi} - \vec{\eta})} \, dV(\vec{\xi}) dV(\vec{\eta}) \qquad (1.15)$$

Therefore, the mean intensity of the scattered waves, or the mean squared amplitude, will depend on the auto- and cross-correlation of the perturbations of the parameters $\delta\rho(\vec{\xi})$, $\delta\lambda(\vec{\xi})$, $\delta\mu(\vec{\xi})$.

Suppose the random medium is statistical homogeneous and isotropic, and $\delta\rho(\vec{\xi})$, $\delta\lambda(\vec{\xi})$, $\delta\mu(\vec{\xi})$ have similar statistical properties, i.e. they have the same form of correlation functions. Let

$$\left\langle \left(\frac{\delta\rho}{\rho_o} \right)^2 \right\rangle = \langle \varepsilon^2 \rangle,$$

$$\left\langle \left(\frac{\delta\lambda}{\lambda_o} \right)^2 \right\rangle = m^2 \langle \varepsilon^2 \rangle,$$

$$\left\langle \left(\frac{\delta\mu}{\mu_o} \right)^2 \right\rangle = n^2 \langle \varepsilon^2 \rangle,$$

$$\langle \delta\rho(\vec{\xi})\delta\rho(\vec{\eta})\rangle = \langle \delta\rho^2\rangle N(|\vec{\xi}-\vec{\eta}|),$$

$$\langle \delta\lambda(\vec{\xi})\delta\lambda(\vec{\eta})\rangle = \langle \delta\lambda^2\rangle N(|\vec{\xi}-\vec{\eta}|),$$

$$\langle \delta\rho(\vec{\xi})\delta\lambda(\vec{\eta})\rangle = \langle \delta\rho\delta\lambda\rangle N(|\vec{\xi}-\vec{\eta}|),$$

etc. (1.16)

where $N(|\vec{\xi}-\vec{\eta}|)$ is the normalized correlation function of the random parameters. If we taken $\lambda_o = \mu_o$, then

$$\langle \left(\frac{\delta\lambda}{\lambda_o+2\mu_o}\right)^2\rangle = \left(\frac{m}{3}\right)^2\langle\varepsilon^2\rangle$$

$$\langle \left(\frac{2\delta\mu}{\lambda_o+2\mu_o}\right)^2\rangle = \left(\frac{2n}{3}\right)^2\langle\varepsilon^2\rangle \quad (1.17)$$

Introducing correlation coefficient of $\delta\rho$ and $\delta\lambda$,

$$\phi_{\rho\lambda} = \frac{\langle \delta\rho\ \delta\lambda\rangle}{\langle\delta\rho^2\rangle^{1/2}\langle\delta\lambda^2\rangle^{1/2}} \quad (1.18)$$

we can get

$$\frac{\langle \delta\rho(\vec{\xi})\delta\lambda(\vec{\eta})\rangle}{\rho_o(\lambda_o+2\mu_o)} = \frac{m}{3}\,\phi_{\rho\lambda}\,\langle\varepsilon^2\rangle N(|\vec{\xi}-\vec{\eta}|). \quad (1.19)$$

In a similar way,

$$\frac{\langle \delta\rho(\vec{\xi})\delta\mu(\vec{\eta})\rangle}{\rho_o(\lambda_o+2\mu_o)} = \frac{n}{3}\,\phi_{\rho\mu}\,\langle\varepsilon^2\rangle N(|\vec{\xi}-\vec{\eta}|),$$

$$\frac{\langle \delta\rho(\vec{\xi})\delta\mu(\vec{\eta})\rangle}{(\lambda_o+2\mu_o)^2} = \left(\frac{m}{3}\right)\left(\frac{n}{3}\right)\phi_{\lambda\mu}\langle\varepsilon^2\rangle N(|\vec{\xi}-\vec{\eta}|), \quad (1.20)$$

where

$$\phi_{\rho\mu} = \frac{\langle \delta\rho \cdot \delta\mu \rangle}{\langle \delta\rho^2 \rangle^{1/2} \langle \delta\mu^2 \rangle^{1/2}},$$

$$\phi_{\lambda\mu} = \frac{\langle \delta\lambda \cdot \delta\mu \rangle}{\langle \delta\rho^2 \rangle^{1/2} \langle \delta\mu^2 \rangle^{1/2}} \tag{1.21}$$

Therefore (1.15) can be written as

$$\langle |P_r^p U|^2 \rangle = \frac{\omega^4}{(4\pi)^2 \alpha_o^4} \frac{1}{r^2} \langle \varepsilon^2 \rangle \left[\cos^2\theta + \left(\frac{m}{3}\right)^2 + 4\left(\frac{n}{3}\right)^2 \cos^4\theta \right.$$

$$\left. - 2\cos\theta \, \phi_{\rho\lambda}\left(\frac{m}{3}\right) - 4\cos^3\theta \, \phi_{\rho\mu} \left(\frac{n}{3}\right) + 4\cos^2\theta \, \phi_{\lambda\mu}\left(\frac{m}{3}\right)\left(\frac{n}{3}\right) \right]$$

$$\iint_{vv} N(|\vec{\xi} - \vec{\eta}|) e^{i\frac{\omega}{\alpha_o}(\hat{x}_1 - \hat{x}) \cdot (\vec{\xi} - \vec{\eta})} \, dV(\vec{\xi}) dV(\vec{\eta}), \tag{1.22}$$

where $\hat{x}_1$ is the unit vector in x_1 direction. We recognize that, the integration term in (1.22) is just the normalized angular spectral density of the scattered power of a scalar wave, i.e. the normalized scattered power of a scalar wave per unit solid angle by the random volume when the incident wave has a unit power flux density. Since the two point correlation function of the scattered field within the random medium can be written as

$$\begin{aligned} C(\vec{\xi}, \vec{\eta}) &= \langle p(\vec{\xi}) e^{i\omega/\alpha_o \, \vec{\xi} \cdot \hat{x}_1} \cdot p(\vec{\eta}) e^{-i\omega/\alpha_o \, \vec{\eta} \cdot \hat{x}_1} \rangle \\ &= \langle p(\vec{\xi}) p(\vec{\eta}) e^{i\omega/\alpha_o \, \hat{x}_1 \cdot (\vec{\xi} - \vec{\eta})} \rangle \\ &= N(\vec{\xi} - \vec{\eta}) e^{i\omega/\alpha_o \, \hat{x}_1 \cdot (\vec{\xi} - \vec{\eta})} \end{aligned} \tag{1.23}$$

where $p(\vec{\xi})$, $p(\vec{\eta})$ are the normalized random parameters of the medium. Therefore the 3-D Fourier transform of $C(\vec{\xi}, \vec{\eta})$ is

$$P^P(\frac{\omega}{\alpha_o}\hat{x}) = \iiint_{-\infty}^{\infty} C(\vec{\xi},\vec{\eta})e^{-i\frac{\omega}{\alpha_o}\hat{x}_1\cdot(\vec{\xi}-\vec{\eta})}\, dV(\vec{\xi}-\vec{\eta})$$

$$= \iiint_{-\infty}^{\infty} N(\vec{\xi}-\vec{\eta})e^{i\omega(\frac{1}{\alpha_o}\hat{x}_1 - \frac{1}{\alpha_o}\hat{x})\cdot(\vec{\xi}-\vec{\eta})}\, dV(\vec{\xi}-\vec{\eta}) \qquad (1.24)$$

Changing the variables $\vec{\xi}$ and $\vec{\eta}$ in (1.22) into

$$\vec{\nu} = (\vec{\xi}+\vec{\eta})/2, \qquad \vec{\zeta} = \vec{\xi}-\vec{\eta},$$

the integration term in (1.22) becomes

$$\iint_{VV} N(\vec{\xi}-\vec{\eta})e^{i\frac{\omega}{\alpha_o}(\hat{x}_1-\hat{x})\cdot(\vec{\xi}-\vec{\eta})}\, dV(\vec{\xi})dV(\vec{\eta})$$

$$= V\iiint_{-\infty}^{\infty} N(|\vec{\zeta}|)\, e^{i\omega(\frac{1}{\alpha_o})x_1-(\frac{1}{\alpha_o}\hat{x})\cdot\vec{\zeta}}\, dV(\vec{\zeta}) = V\cdot P^P(\frac{\omega}{\alpha_o}\hat{x}). \qquad (1.25)$$

Therefore (1.22) can be written as

$$\langle|^P U_r^P|^2\rangle = \frac{\omega^4}{(4\pi)^2\alpha_o^4}\frac{1}{r^2}\, P_R^P(\hat{x})V\cdot P^P(\frac{\omega}{\alpha_o}\hat{x}), \qquad (1.26)$$

where

$$P_R^P(\hat{x}) = \langle\varepsilon^2\rangle\,[\cos^2\theta+(\frac{m}{3})^2 + 4(\frac{n}{3})^2\cos^4\theta - 2\cos\theta\phi_{\rho\lambda}(\frac{m}{3})$$

$$-4\cos^3\theta\phi_{\rho\mu}(\frac{n}{3}) + 4\cos^2\theta\ \phi_{\lambda\mu}(\frac{m}{3})(\frac{n}{3})], \qquad (1.27)$$

is the direction factor for the Rayleigh elastic wave scattering by a volume element of random medium.

If we define the directional scattering coefficient for P-P scattering $g^{PP}(\hat{x})$ as 4π times of the average scatterd power in $\hat{x}$ direction per unit solid angle by a unit volume of random medium for a unit incident field (i.e. unit power flux density), which differs from the differential scattering

cross-section in electrical science only by a factor 4π,

$$g^{PP}(\theta) = \frac{4\pi r^2}{V} \langle |P_{ij} P_r|^2 \rangle = \frac{1}{4\pi} \frac{\omega^2}{\alpha_o^2} P_R^P(\theta) P^P(\theta) \tag{1.28}$$

When $\delta\rho$, $\delta\lambda$, $\delta\mu$ are totally correlated, i.e. $\phi_{\rho\lambda} = \phi_{\rho\mu} = \phi_{\lambda\mu} = 1$, it turns out

$$\begin{aligned} P_R^P(\theta) &= \langle \varepsilon^2 \rangle (\cos\theta - \frac{m}{3} - \frac{2n}{3} \cos^2\theta)^2 \\ &= \langle (\frac{\delta\rho}{\rho_o} \cos\theta - \frac{\delta\lambda}{\lambda_o + 2\mu_o} - 2 \frac{\delta\mu}{\lambda_o + 2\mu_o} \cos^2\theta)^2 \rangle \quad , \end{aligned} \tag{1.29}$$

which is nothing but the mean square of the Rayleigh elastic wave scattering factor (compared with (1.18) in Wu and Aki, 1983).

Now, we introduce the exchange slowness

$$\begin{aligned} \vec{s}_1 &= \frac{1}{\alpha_o} (\hat{x}_1 - \hat{x}), \\ s_1 &= |\vec{s}_1| = \frac{2}{\alpha_o} \sin\frac{\theta}{2} \quad , \end{aligned} \tag{1.30}$$

where θ is the scattering angle, i.e. the angle between the incident direction and the scattering direction. We get

$$P^P(\theta) = \iiint_{-\infty}^{\infty} N(r) e^{i\omega \vec{s}_1 \cdot \vec{\zeta}} \, dV(\vec{\zeta}) \quad , \tag{1.31}$$

where $r = |\vec{\zeta}|$. Therefore $P^P(\theta)$ is a directional factor of scalar wave scattering, which depends only on the correlation functions of the parameters $N(r)$, son long as all the parameters have the same form of correlation function. Thus (1.28) means that the directional scattering coefficient can be decomposed into two factors, the Rayleigh scattering factor $R(\theta)$ and a scalar scattering factor $P(\theta)$, which is the only factor that depends on the form of correlation function of the random inhomogeneities.

Now we need to specify the form of $N(r)$. Knopoff and Hudson (1964, 1967), and Haddon (1978) used Gaussian correlation functions, which has a

favorable mathematical property of having its all order of derivatives existed. However, it seems to be too smooth to represent the actual inhomogeneities in the earth. Compared with some observations, for example, the bore-hole acoustic velocity log (Wu, 1982a) and the LASA wavefield correlation measurement (Aki, 1973), we found the exponential or Von Karman correlation function fitted the data better. In the following, we will adopt the exponential correlation function

$$N(r) = e^{-r/a} , \tag{1.32}$$

where a is the correlation length.

Putting (1.32) into (1.31), we get

$$P^P(\theta) = 4\pi \int_0^\infty e^{-r/a} \frac{\sin(\omega S_1 r)}{\omega S_1} r dr = 4\pi \frac{2a^3}{[1+(\omega S_1 a)^2]^2} . \tag{1.33}$$

Therefore,

$$g^{PP}(\theta) = 2 \frac{\omega^4}{\alpha_o^4} a^3 \, P_R^P(\theta) \frac{1}{[1+(\omega S_1 a)^2]^2} . \tag{1.34}$$

When $\delta\rho$, $\delta\lambda$, and $\delta\mu$ are totally correlated, i.e. the parameter perturbations are linearly dependent,

$$g^{PP}(\theta) = 2a^3 \frac{\omega^4}{\alpha_o^4} \langle\varepsilon^2\rangle (\cos\theta - \frac{m}{3} - \frac{2n}{3}\cos^2\theta)^2 \frac{1}{[1+(2\frac{\omega}{\alpha_o} a \sin\frac{\theta}{2})^2]^2} . \tag{1.35}$$

When $\frac{\omega}{\alpha_o} a \ll 1$,

$$g^{PP}(\theta) = 2a^3 \frac{\omega^4}{\alpha_o^4} \langle\varepsilon^2\rangle \, P_R^P(\theta) = 2a^3 \frac{\omega^4}{\alpha_o^4} \langle\varepsilon^2\rangle (\cos\theta - \frac{m}{3} - \frac{2n}{3}\cos^2\theta)^2, \tag{1.36}$$

this is the Rayleigh scattering for P-P elastic wave scattering, which has a fourth power frequency dependence and a third power dependence of correlation length. The frequency dependence is equal to the acoustic scattering, but with a more complicated directional pattern.

For high frequencies the directional pattern of (1.35) becomes more complicated, and the frequency dependence will become angle-dependent.

In the linearly dependent case, if $\frac{\delta\lambda}{\lambda_o} = \frac{\delta\mu}{\mu_o}$, we can decompose the perturbations into a velocity term and an impedance term (see Wu and Aki, 1983). (1.29) can be written as

$$P_{RP}(\theta) = \langle(\frac{\delta\rho}{\rho_o}\cos\theta - \frac{\delta\lambda}{\lambda_o+2\mu_o} - \frac{2\delta\mu}{\lambda_o+2\mu_o}\cos^2\theta)^2\rangle$$

$$= \langle(\frac{\delta Z_\alpha}{Z\alpha_o})^2\rangle(\cos\theta - \frac{1}{3} - \frac{2}{3}\cos^2\theta)^2 + \langle(\frac{\delta\alpha}{\alpha_o})^2\rangle(\cos\theta+\frac{1}{3}+\frac{2}{3}\cos^2\theta)^2$$

$$-2\langle\frac{\delta Z_\alpha}{Z\alpha_o}\cdot\frac{\delta\alpha}{\alpha_o}\rangle(\cos\theta - \frac{1}{3} - \frac{2}{3}\cos^2\theta)(\cos\theta+\frac{1}{3}+\frac{2}{3}\cos^2\theta), \qquad (1.37)$$

where $\frac{\delta Z_\alpha}{Z\alpha_o}$ is the P wave impedance perturbation, $\frac{\delta\alpha}{\alpha_o}$ is the P wave velocity perturbation. In the forward direction, $\theta=0$,

$$P_{RP}(0) = 4\langle(\frac{\delta\alpha}{\alpha_o})^2\rangle = 4\tilde{\alpha}^2 , \qquad (1.38)$$

where $\tilde{\alpha} = \langle(\frac{\delta\alpha}{\alpha_o})^2\rangle^{1/2}$ is the perturbation index of velocity α. Therefore the forward scattering coefficient becomes

$$g^{PP}(0) = 8a^3\frac{\omega^4}{\alpha_o^4}\langle(\frac{\delta\alpha}{\alpha_o})^2\rangle = 8a^3\frac{\omega^4}{\alpha_o^4}\tilde{\alpha}^2 . \qquad (1.39)$$

For high frequencies, since $P^P(\theta)$ (1.34) has a very big forward lobe, therefore in the nearly forward direction the main contribution will come from the velocity perturbations. After neglecting the contribution from the impedance perturbations, we can get

$$g^{PP}(\theta\approx o)\approx 2a^3\frac{\omega^4\tilde{\alpha}^2}{\alpha_o^4}\frac{(\cos\theta+\frac{1}{3}+\frac{2}{3}\cos^2\theta)^2}{[1+(2\frac{\omega}{\alpha_o}a\sin\frac{\theta}{2})^2]^2} \approx 8a^3\frac{\omega^4}{\alpha_o^4}\tilde{\alpha}^2\frac{1}{[1+(2\frac{\omega}{\alpha_o}a\sin\frac{\theta}{2})^2]^2} , \qquad (1.40)$$

this result is identical with the Pekeris-Chernov's scalar wave scattering formula (Chernov, 1960, ch. 3, 47). It therefore implies that, whenever the forward scattering is important and dominant, such as in the study of phase and amplitude fluctuation of high-frequency waves propagating in a random medium, the scalar wave scattering theory can be used approximately, and the velocity perturbation of the medium plays the major role in the theory. To the contrary, in the backward direction, i.e. when $\theta=\pi$,

$$P_R P(\pi) = 4\langle(\frac{\delta Z_\alpha}{Z_{\alpha o}})^2\rangle = 4\tilde{Z}_\alpha^2 , \tag{1.41}$$

where $\tilde{Z}_\alpha = \langle(\frac{\delta Z_\alpha}{Z_{\alpha o}})^2\rangle^{1/2}$ is the perturbation index of P wave impedance Z_α. Therefore,

$$g^{PP}(\pi) = 8a^3 \frac{\omega^4}{\alpha_o^4} \tilde{Z}_\alpha^2 \frac{1}{(1+4\frac{\omega^2}{\alpha_o^2} a^2)^2} . \tag{1.42}$$

For low frequencies, i.e. when $\frac{\omega}{\alpha_o}a<<1$,

$$g^{PP}(\pi) \approx 8a^3 \frac{\omega^4}{\alpha_o^4} \tilde{Z}_\alpha^2 , \tag{1.43}$$

while for high frequencies, i.e. when $\frac{\omega}{\alpha_o} a>>1$,

$$g^{PP}(\pi) \approx \frac{1}{2a}\langle(\frac{\delta Z_\alpha}{Z_{\alpha o}}\rangle^2 = \frac{1}{2a} \tilde{Z}_\alpha^2 . \tag{1.44}$$

From (1.41)-(1.43) we can see that, the backscattering coefficient is proportional to the mean square impedance perturbations, i.e. the perturbation index of impedance and is irrelevant to the velocity perturbations. In high frequencies, it is frequency independent for the exponential correlation function. Therefore, in any problems where the backscattering is important or dominant, such as the coda excitation problem, in which the coda waves are

assumed to be composed of backscattered waves from random inhomogeneities according to Aki's model (Aki 1969, Aki and Chouet, 1975, Aki, 1981), the impedance perturbations will play a major role, and the scalar wave scattering theory for the velocity perturbations will no longer be applicable.

In the same way, we can treat the P to S converted waves. From (1.14) we can get

$$\langle |P_U S_{mer}|^2 \rangle = \frac{\omega^4}{(4\pi)^2 \beta_o^4} \frac{\langle \varepsilon^2 \rangle}{r^2} [\sin^2\theta + (\frac{\beta_o}{\alpha_o})^2 n^2 \sin^2(2\theta) - 2(\frac{\beta_o}{\alpha_o}) n \phi_{\rho\mu} \sin\theta \sin 2\theta]$$

$$\iint_{VV} N(|\vec{\xi}-\vec{\eta}|) e^{i\omega(\frac{\hat{x}_1}{\alpha_o} - \frac{\hat{x}}{\beta_o})\cdot(\vec{\xi}-\vec{\eta})} dV(\vec{\xi}) dV(\vec{\eta}) \ . \qquad (1.45)$$

Introduce

$$\vec{S}_2 = \frac{\hat{x}_1}{\alpha_o} - \frac{\hat{x}}{\beta_o} \ ,$$

$$S_2 = |\vec{S}_2| = \sqrt{(\frac{1}{\alpha_o})^2 + (\frac{1}{\beta_o})^2 - \frac{2}{\alpha_o \beta_o} \cos\theta} \qquad (1.46)$$

where θ is the scattering angle. We get the normalized angular power spectral density for converted wave

$$p^c(\theta) = \iiint_{-\infty}^{\infty} N(|\vec{\zeta}|) e^{i\omega \vec{S}_2 \cdot \vec{\zeta}} dV(\vec{\zeta}) = \frac{8\pi a^3}{[1+(\omega S_2 a)^2]^2} \ , \qquad (1.47)$$

for the exponential correlation function.

If $\delta\rho$ and $\delta\mu$ are totally correlated, we can express the directional scattering coefficient for the converted S wave as

$$g^{ps}(\theta) = \frac{1}{4\pi} \frac{\omega^4}{\beta_o^4} P_R^S(\theta) \cdot p^C(\theta)$$

$$= 2a^3 \frac{\omega^4}{\beta_o^4} \langle \varepsilon^2 \rangle (-\sin\theta + (\frac{\beta_o}{\alpha_o}) n \sin 2\theta)^2 \frac{1}{[1+(\omega S_2 a)^2]^2} \ , \qquad (1.48)$$

where $P_R{}^S(\theta)$ is the Rayleigh directional factor for P-S scattering.

When $(\omega/\beta_o)\, a \ll 1$,

$$g^{ps}(\theta) \approx 2a^3 \frac{\omega^4}{\beta_o^4} \langle \varepsilon^2 \rangle (-\sin\theta + (\frac{\beta_o}{\alpha_o}) n \sin 2\theta)^2 , \qquad (1.49)$$

that is the Rayleigh scattering for P-S case. Comparing it with (1.36), we notice that the P-S converted wave powers are almost $(\alpha/\beta)^4$ as stronger than the P-P scattered wave power, same conclusion as derived by Knopoff and Hudson (1964), in which the Gaussian correlation function was used. This should be expected, since the shape is not important for Rayleigh scattering, namely the long period wave cannot recognize the detailed structure having a size smaller than the wavelength. However, the high frequency asymptotics for our case will be quite different from that of Knopoff and Hudson (1967). Note from (1.46) that the minimum value of S_2 is when $\theta=0$,

$$S_2(\min) = \frac{1}{\beta_o} - \frac{1}{\alpha_o}, \quad \text{when} \quad \theta=0 . \qquad (1.50)$$

Therefore, we can get the high frequency asymptotics for (1.48)

$$g^{ps}(\theta) \approx \frac{2\langle \varepsilon^2 \rangle}{a} (-\sin\theta + \frac{\beta_o}{\alpha_o} n \sin 2\theta)^2 \frac{1}{[1+(\frac{\beta_o}{\alpha_o})^2 - 2\frac{\beta_o}{\alpha_o}\cos\theta]^2} ,$$

$$\text{when } \omega(\frac{1}{\beta_o} - \frac{1}{\alpha_o})a \gg 1, \qquad (1.51)$$

which is frequency independent. Although in high frequency range the converted wave power will be much smaller than the common-mode scattered power, but it will reach a constant value as $\omega(\frac{1}{\beta_o} - \frac{1}{\alpha_o}) \gg 1$, contrary to the case of Gaussian correlation functions, in which the converted wave power will quickly decrease to zero when $\frac{\omega}{\beta_o} a \gg 1$. That is because Gaussian correlation function represents some kinds of extremely smooth medium structures, while

exponential correlation function corresponds to certain kinds of discontinuities in the parameter perturbations, resulting in quite different high frequency asymptotic behaviors from each other.

Similar to (1.37), $g^{ps}(\theta)$ can be expressed in terms of impedance and velocity perturbations of S wave:

$$g^{ps}(\theta) = 2a^3 \frac{\omega^4}{\beta_o^4} \{ \langle (\frac{\delta Z_\beta}{Z_{\beta o}})^2 \rangle (\sin\theta - \frac{\beta_o}{\alpha_o}\sin 2\theta)^2$$

$$+ \langle (\frac{\delta\beta}{\beta_o})^2 \rangle (\sin\theta + (\frac{\beta_o}{\alpha_o})\sin 2\theta)^2$$

$$- \langle (\frac{\delta Z_\beta}{Z\beta_o})(\frac{\delta\beta}{\beta_o}) \rangle (\sin\theta - \frac{\beta_o}{\alpha_o}\sin 2\theta)(\sin\theta + \frac{\beta_o}{\alpha_o}\sin 2\theta) \}$$

$$\cdot \frac{1}{[1+(\omega S_2 a)^2]^2} \quad , \tag{1.52}$$

where δZ_β is the S wave impedance perturbation of the random medium.

Fig. 2 to 8 give some examples of the scattering patterns. Fig. 2 shows the Rayleigh directional factors for different parameter combinations (for detailed Rayleigh elastic wave scattering patterns the reader is referred to Wu and Aki, 1983). The upper half are the patterns for P-P scattering. The P-S scattering patterns are put in the lower half plane. Note that, the converted S waves are only side-scattered waves, having very little energy in the forward or backward directions. Fig. 3 gives the scalar wave directional factor for the random medium structure with an exponential correlation function. If $R(\theta)$ can be considered as compositional factor, then $P(\theta)$ can be thought of as a geometrical factor. Same as in Fig. 2, the upper and lower half are for P-P and P-S respectively. Fig. 4 to Fig. 8 give some comparisons

between scalar and elastic wave scattering patterns. In this case, in the upper and lower half plane are shown scalar and elastic scattering patterns respectively. It can be seen that, depending on the parameter combinations, the scattering pattern of elastic waves can be quite different from that of scalar waves.

The decomposition of scattered waves into velocity type and impedance type gives us a promising prospect in estimating the parameter perturbations of an elastic medium. If we can get the velocity perturbation, for example, from the phase and amplitude fluctuations measurements, and derive the impedance perturbation from the coda excitation or other backscattering experiments, then the perturbations of the density and elastic constants can be determined separately. In this way we may get more information about the properties of the inhomogeneities.

However, if the density and elastic-constant perturbations are not totally correlated, the separability of these parameters will degenerate. In the case of total uncorrelation, from (1.26), (1.27) and (1.45), we can write the directional scattering coefficients for P wave and for converted S wave as

$$g^{PP}(\theta) = \frac{\omega^4}{4\pi\alpha_o^4}\langle\varepsilon^2\rangle[\cos^2\theta+(\frac{m}{3})^2+4(\frac{n}{3})^2\cos^4\theta]P^P(\theta) \tag{1.53}$$

$$= \frac{1}{4\pi}\frac{\omega^4}{\alpha_o^4}[\langle(\frac{\delta\rho}{\rho_o})^2\rangle\cos^2\theta+\langle(\frac{\delta\lambda}{\lambda_o+2\mu_o})^2\rangle+4\langle(\frac{\delta\mu}{\lambda_o+2\mu_o})^2\rangle\cos^4\theta]\cdot P^P(\theta)$$

$$g^{PS}(\theta) = \frac{\omega^4}{4\pi\beta_o^4}\langle\varepsilon^2\rangle[\sin^2\theta+(\frac{\beta_o}{\alpha_o})^2n^2\sin^2(2\theta)]\cdot P^C(\theta) \tag{1.54}$$

$$= \frac{\omega^4}{4\pi\beta_o^4}[\langle\frac{\delta\rho}{\rho_o})^2\rangle\sin^2\theta+(\frac{\beta_o}{\beta_o})^2\langle(\frac{\delta\mu}{\mu_o})^2\rangle\sin^2 2\theta]\cdot P^C(\theta)$$

Therefore, the density and elastic-constant perturbations can be no longer separated from the forward scattering and backscattering measurements.

II. Directional Scattering Coefficients for S Wave Incidence

Now we will treat the problem of S wave incidence in x directions in a similar manner. Taking the spherical coordinate system with its polar axis along the direction of particle motion (y axis) (Fig. 9), (1.11) and (1.12) can be written as

$$S_U P_r(\hat{x}) = \frac{\omega^2}{4\pi\alpha_o^2}\frac{1}{r} e^{-i\omega(t-r/\alpha_o)} \tag{2.1}$$

$$\int_V \left[\frac{\delta\rho(\vec{\xi})}{\rho_o}\cos\theta - \frac{\beta_o}{\alpha_o}\frac{\delta\mu(\vec{\xi})}{\mu_o}\sin 2\theta \sin\phi\right] e^{i\frac{\omega}{\beta_o}\xi\left(1-\frac{i\omega}{\alpha_o}(\hat{x}\cdot\vec{\xi})\right)} dV(\vec{\xi}) ,$$

$$S_U S_{mer}(\hat{x}) = \frac{\omega^2}{4\pi\beta_o^2}\frac{1}{r} e^{-i\omega(t-r/\beta_o)} \tag{2.2}$$

$$\int_V \left[\frac{\delta\rho(\vec{\xi})}{\rho_o}\sin\theta + \frac{\delta\mu(\vec{\xi})}{\mu_o}\cos 2\theta \sin\phi\right] e^{i\frac{\omega}{\beta_o}\xi\left(1-\frac{i\omega}{\beta_o}(\hat{x}\cdot\vec{\xi})\right)} dV(\vec{\xi}) ,$$

$$S_U S_{lat}(\hat{x}) = \frac{\omega^2}{4\pi\beta_o^2}\frac{1}{r} e^{-i\omega(t-r/\beta_o)} \tag{2.3}$$

$$\int_V \frac{\delta\rho(\vec{\xi})}{\rho_o}\cos\theta\cos\phi\, e^{i\frac{\omega}{\beta_o}\xi\left(1-\frac{i\omega}{\beta_o}(\hat{x}\cdot\vec{\xi})\right)} dV(\vec{\xi}) ,$$

where $S_U S_{mer}$ and $S_U S_{lat}$ are the meridian component and the latitudinal component of the scattered S wave respectively.

Taking the mean square of the scattered waves, we get

$$\langle|S^{P}_{U_r}|^2\rangle = \frac{\omega^4}{(4\pi)^2\alpha_o^4}\frac{V}{r^2}\langle\varepsilon^2\rangle[\cos^2\theta + (\frac{\beta_o}{\alpha_o})^2 n^2 \sin^2 2\theta \sin^2\phi \tag{2.4}$$

$$-2n\frac{\beta_o}{\alpha_o}\phi_{\rho\mu}\cos\theta \sin 2\theta \sin\phi]\cdot\iiint_{-\infty}^{\infty} N(|\vec{\xi}|)e^{i\omega(\frac{\hat{x}_1}{\beta_o} - \frac{\hat{x}}{\alpha_o})\cdot\vec{\xi}}\, dV(\vec{\xi}),$$

$$\langle|S^{P}_{U_{mer}}|^2\rangle = \frac{\omega^4}{(4\pi)^2\beta_o^4}\frac{V}{r^2}\langle\varepsilon^2\rangle[\sin^2\theta + n^2\cos^2 2\theta \sin^2\phi \tag{2.5}$$

$$+2n\phi_{\rho\mu}\sin\theta \cos 2\theta \sin\phi]\cdot\iiint_{-\infty}^{\infty} N(|\vec{\xi}|)e^{i\omega(\frac{\hat{x}_1}{\beta_o} - \frac{\hat{x}}{\beta_o})\cdot\vec{\xi}}\, dV(\vec{\xi}),$$

$$\langle|S^{P}_{U_{lat}}|^2\rangle = \frac{\omega^4}{(4\pi)^2\beta_o^4}\frac{V}{r^2}\langle\varepsilon^2\rangle n^2\cos^2\theta \cos^2\phi\cdot\iiint_{-\infty}^{\infty} N(|\vec{\xi}|)e^{i\omega(\frac{\hat{x}_1}{\beta_o} - \frac{\hat{x}}{\beta_o})\cdot\vec{\xi}}\, dV(\vec{\xi}), \tag{2.6}$$

where n, $\phi_{\rho\mu}$ are defined as in (1.16) and (1.21). If $\delta\rho(\vec{\xi})$ and $\delta\mu(\vec{\xi})$ are totally correlated, we can obtain the directional scattering coefficients as

$$g^{sp}(\theta,\phi) = \frac{\omega^4}{(4\pi)\alpha_o^4}\langle\varepsilon^2\rangle[\cos\theta - \frac{\beta_o}{\alpha_o} n \sin 2\theta \sin\phi]^2 P^c(\hat{x}), \tag{2.7}$$

$$g^{ss}_{mer}(\theta,\phi) = \frac{\omega^4}{(4\pi)\beta_o^4}\langle\varepsilon^2\rangle[\sin\theta + n\cos 2\theta \sin\phi]^2 P^S(\hat{x}), \tag{2.8}$$

$$g^{ss}_{lat}(\theta,\phi) = \frac{\omega^4}{(4\pi)\beta_o^4}\langle\varepsilon^2\rangle n^2\cos^2\theta \cos^2\phi\, P^S(\hat{x}), \tag{2.9}$$

where

$$P^c(\hat{x}) = \iiint_{-\infty}^{\infty} N(|\vec{\xi}|)e^{i\omega(\frac{\hat{x}_1}{\beta_o} - \frac{\hat{x}}{\alpha_o})\cdot\vec{\xi}}\, dV(\vec{\xi}), \tag{2.10}$$

$$P^S(\hat{x}) = \iiint_{-\infty}^{\infty} N(|\vec{\xi}|)e^{i\omega(\frac{\hat{x}_1}{\beta_o} - \frac{\hat{x}}{\beta_o})\cdot\vec{\xi}}\, dV(\vec{\xi}), \tag{2.11}$$

For exponential correlation function,

$$P^c(\theta_x) = \frac{8\pi a^3}{[1+(\omega S_2 a)^2]^2} \tag{2.12}$$

$$S_2 = \sqrt{(\frac{1}{\alpha_o})^2+\frac{1}{\beta_o})^2 \frac{2}{\alpha_o\beta_o}\cos\theta_x} \ , \tag{2.13}$$

$$P^s(\theta_x) = \frac{8\pi a^3}{[1+(2\frac{\omega}{\beta_o}a \sin\frac{\theta_x}{2})^2]^2} \ , \tag{2.14}$$

where θ_x is the scattering angle, i.e. the angle between the scattering directions and the incident (x_1) directions. In the same way as for the P wave incidence, we can decompose the scattered field into "velocity type" and impedance type," and (2.7) to (2.9) become

$$g^{sP}(\theta,\phi) = \frac{\omega^4}{4\pi\alpha_o^4} \{<(\frac{\delta Z_\beta}{Z\beta_o})^2>[\cos\theta-(\frac{\beta_o}{\alpha_o})\sin 2\theta \ \sin\phi]^2$$

$$+ <(\frac{\delta\beta}{\beta_o})^2>[\cos\theta+(\frac{\beta_o}{\alpha_o})\sin 2\theta \ \sin\phi]^2$$

$$-2<(\frac{\delta Z_\beta}{Z\beta_o})(\frac{\delta\beta}{\beta_o})>[\cos\theta-(\frac{\beta_o}{\alpha_o})\sin 2\theta \ \sin\phi][\cos\theta+(\frac{\beta_o}{\alpha_o})\sin 2\theta \ \sin\phi]\}\cdot P^c(\theta_x) \ , \tag{2.15}$$

$$g^{ss}_{mer}(\theta,\phi) = \frac{\omega^4}{4\pi\beta_o^4} \{<(\frac{\delta Z_\beta}{Z\beta_o})^2>[\sin\theta+\cos 2\theta \ \sin\phi)^2$$

$$+ <(\frac{\delta\beta}{\beta_o})^2>(\sin\theta-\cos 2\theta \ \sin\phi)^2$$

$$-2<(\frac{\delta Z_\beta}{Z\beta_o})(\frac{\delta\beta}{\beta_o})>(\sin\theta + \cos 2\theta \ \sin\phi)(\sin\theta-\cos 2\theta \ \sin\phi)\}\cdot P^S(\theta_x) \ , \tag{2.16}$$

$$g^{ss}_{lat}(\theta,\phi) = \frac{\omega^4}{4\pi\beta_o^4} \{<(\frac{\delta Z_\beta}{Z\beta_o} + \frac{\delta\beta}{\beta_o})^2>\cos^2\theta \ \cos^2\phi\} P^S(\theta_x) \ . \tag{2.17}$$

In the forward direction, i.e. $\theta = \pi/2$, $\phi = \pi/2$, $\theta_x = 0$,

$$g^{sp}(\theta_x=0) = 0,$$

$$g^{ss}_{lat}(\theta_x=0) = 0,$$

$$g^{ss}_{mer}(\theta_x=0) = 8a^3 \frac{\omega^4}{\beta_o^4} \langle(\frac{\delta\beta}{\beta_o})^2\rangle \tag{2.18}$$

In the backward directions, $\theta_x = \pi$, $\theta = \pi/2$, $\phi = -\pi/2$,

$$g^{sp}(\theta_x=\pi) = 0,$$

$$g^{ss}_{lat}(\theta_x=\pi) = 0,$$

$$g^{ss}_{mer}(\theta_x=\pi) = 8a^3 \frac{\omega^4}{\beta_o^4} \langle(\frac{\delta Z_\beta}{Z\beta_o})^2\rangle \frac{1}{[1+4\frac{\omega^2}{\beta_o^2}a^2]^2} . \tag{2.19}$$

We see again that the velocity perturbations and the impedance perturbations for S waves can be separated through forward scattering and backward scattering experiments. Only in the nearly forward scattering direction is the elastic wave scattering identical with a scalar wave scattering with velocity perturbations:

$$g^{ss}_{mer}(\theta_x\approx 0) = 8a^3 \frac{\omega^4}{\beta_o^4} \langle(\frac{\delta\beta}{\beta_o})^2\rangle \frac{1}{[1+(2\frac{\omega}{\beta_o}a \sin\frac{\theta_x}{2})^2]^2} . \tag{2.20}$$

For low frequencies, when $\frac{\omega}{\beta_0} a \ll 1$,

$$P^C(\theta_x) = P^S(\theta_x) = 8\pi a^3 , \tag{2.21}$$

therefore (2.7) to (2.9) become

$$g^{sP}(\theta,\phi) = 2a^3 \frac{\omega^4}{\alpha_o^4} \langle\varepsilon^2\rangle[\cos\theta \frac{\beta_o}{\alpha_o} n \sin 2\theta \sin\phi]^2 = 2a^3 \frac{\omega^4}{\alpha_o^4} S_R{}^P{}_r ,$$

$$g^{ss}_{mer}(\theta,\phi) = 2a^3 \frac{\omega^4}{\alpha_o^4} \langle\varepsilon^2\rangle[\sin\theta + n \cos 2\theta \sin\phi]^2 = 2a^3 \frac{\omega^4}{\alpha_o^4} S_R{}^S{}_{mer} ,$$

$$g^{ss}_{lat}(\theta,\phi) = 2a^3 \frac{\omega^4}{\alpha_o^4} \langle\varepsilon^2\rangle \cos^2\theta \cos^2\phi = 2a^3 \frac{\omega^4}{\alpha_o^4} S_R{}^S{}_{lat} , \qquad (2.22)$$

where ${}^sR^P{}_r$, ${}^sR^s{}_{mer}$, ${}^sR^s{}_{lat}$ are Rayleigh directional factors for the corresponding components. Again we see the Rayleigh scattering features, the scattered power is proportional to the fourth power of frequency and third power of the correlation length. Note also that scattered S wave power are almost $(\frac{\alpha_o}{\beta_o})^4$ times stronger than the scattered P wave power, same as in P wave incidence.

For Rayleigh scattering the backscattering coefficient (2.19) becomes

$$g^{ss}_{mer}(\pi) \approx 8a^3 \frac{\omega^4}{\beta_o^4} \langle(\frac{\delta Z_\beta}{Z_{\beta o}})^2\rangle = 8a^3 \frac{\omega^4}{\beta_o^4} \tilde{Z}_\beta , \qquad (2.23)$$

and the forward scattering coefficient (2.18),

$$g^{ss}_{mer}(0) \approx 8a^3 \frac{\omega^4}{\beta_o^4} \langle(\frac{\delta\beta}{\beta_o})^2\rangle = 8a^3 \frac{\omega^4}{\beta_o^4} \tilde{\beta}^2 , \qquad (2.24)$$

where $\tilde{Z}_\beta = \langle(\frac{\delta Z_\beta}{Z_{\beta o}})\rangle^{1/2}$, $\tilde{\beta} = \langle(\frac{\delta\beta}{\beta_o})\rangle^{1/2}$.

For high frequencies, g^{ss}_{mer} and g^{ss}_{lat} will have complex scattering patterns and varying frequency dependence depending on the scattering angle. However, for the converted waves, we can reach the same conclusion as in P wave incidence, i.e. when $\omega(\frac{1}{\beta_o} - \frac{1}{\alpha_o})a >> 1$, the converted waves have a maximum frequency-independent value (see the discussions after 1.51)

$$g^{sp}(\theta,\phi) \approx \frac{2<\varepsilon^2>}{a}(\frac{\beta_o}{\alpha_o})^4 \frac{[\cos\theta - \frac{\beta_o}{\alpha_o} n \sin 2\theta \sin\phi]^2}{[1+(\frac{\beta}{\alpha_o})^2 - 2\frac{\beta_o}{\alpha_o}\cos\theta_x]^2} \quad . \qquad (2.25)$$

The backscattering coefficient (2.19) becomes in the high frequency range

$$g^{ss}_{mer}(\pi) \approx \frac{1}{2a} \tilde{z}^2_\beta \quad , \qquad \frac{\omega}{\beta_o} a >> 1 \quad . \qquad (2.26)$$

III. TOTAL SCATTERED POWER AND THE SCATTERING COEFFICIENT OF THE MEDIUM FOR P WAVE INCIDENCE

According to the definition of directional scattering coefficient $g(\theta)$ (1.28), the total scattered power for a unit incident field will be

$$W = \iint_{4\pi} \frac{V}{4\pi} g(\theta) d\Omega \ , \tag{3.1}$$

where $d\Omega$ is the differential solid angle, over which $g(\theta)$ is defined. Therefore the scattering coefficient g, defined as the total scattered power by a unit volume of the random medium for a unit incident field (i.e. unit power flux density), will be

$$g = \frac{1}{4\pi} \iint_{4\pi} g(\theta) d\Omega \ . \tag{3.2}$$

By this definition, g has a dimension of 1/length, or area/volume. It has the same meaning as the effective scattering cross-section per unit volume of the scattering medium in the case of discrete scatterers, i.e., $g = n\sigma$, where n is the number of scatterers per unit volume and σ is the average scattering cross-section of the scatterers. However, for a random continuum with a volume V, the scattering coefficient g defined above will be more convenient.

For P wave incidence,

$$g^P = \frac{1}{4\pi} \iint_{4\pi} [g^{PP}(\theta) + g^{PS}(\theta)] d\Omega = g^{PP} + g^{PS} \ . \tag{3.3}$$

As an example, we calculate the case when $\delta\rho$, $\delta\lambda$ and $\delta\mu$ are totally correlated. First we derive g^{PP} by integrating over (1.35)

$$g^{pp} = \frac{1}{4\pi}\iint_{4\pi} 2a^3 \frac{\omega^4}{\alpha_o^4}\langle\varepsilon^2\rangle \frac{(\cos\theta - \frac{m}{3} - \frac{2n}{3}\cos^2\theta)^2}{(1 + 4\frac{\omega^2}{\alpha_o^2}a^2\sin^2\frac{\theta}{2})^2} d\Omega$$

$$= \frac{\langle\varepsilon^2\rangle}{2\pi}\frac{\omega^4}{\alpha_o^4}a^3\int_0^{2\pi} d\phi \int_0^{\pi} \frac{(\cos\theta - \frac{m}{3} - \frac{2n}{3}\cos^2\theta)^2\sin\theta}{(1 + 4\frac{\omega^2}{\alpha_o^2}a^2\sin^2\frac{\theta}{2})^2} d\theta \quad (3.4)$$

Let

$$K = \frac{\omega}{\alpha_o}a, \quad b = 2K^2 = 2\frac{\omega^2}{\alpha_o^2}a^2, \quad \cos\theta = x, \quad (3.5)$$

and using integration by parts we get

$$g^{pp} = \frac{\langle\varepsilon^2\rangle}{a}K^4\{\frac{(1 - \frac{m}{3} - \frac{2n}{3})^2}{b} - \frac{(1 + \frac{m}{3} + \frac{2n}{3})^2}{b(1+2b)}$$

$$- \frac{2}{b}\int_{-1}^{1}[\frac{2(\frac{2n}{3})^2x^3}{1+b-bx} - \frac{2nx^2}{1+b-bx} + \frac{(1+\frac{4mn}{9})x}{1+b-bx} - \frac{\frac{m}{3}}{1+b-bx}]dx\} . \quad (3.6)$$

After laborious but straightforward integration calculations, we get

$$g^{pp} = \frac{\langle\varepsilon^2\rangle}{a}K^4\{\frac{(1- \frac{m}{3} - \frac{2n}{3})^2}{2K^2} - \frac{(1 + \frac{m}{3} + \frac{2n}{3})^2}{2K^2(1+4K^2)} + \frac{2}{3}(\frac{2n}{3})^2\frac{1}{K^4}$$

$$+ (\frac{2n}{3})^2\frac{(1+2K^2)^2}{2K^8} - (\frac{2n}{3})^2\frac{(1+2K^2)^3}{8K^{10}}\ln(1+4K^2) - n\frac{(1+2K^2)}{K^6}$$

$$+ \frac{n}{4}\frac{(1+2K^2)^2}{K^8}\ln(1+4K^2) + \frac{(1 + \frac{4mn}{9})}{K^4}$$

$$- \frac{(1+\frac{4mn}{9})(1+2K^2)}{4K^6}\ln(1+4K^2) + \frac{m}{6}\frac{1}{K^4}\ln(1+4K^2)\} . \quad (3.7)$$

Now let us derive the asymptotic expressions for low and high frequencies.

When $K<<1$, i.e. $b = 2K^2<<1$,

$$\ln(1+2b)\approx 2b-2b^2+\frac{8}{3}b^3-4b^4+\frac{32}{5}b^5-O(b^6) \ .$$

(3.7) can be reduced to

$$g^{PP} = [2(1 - \frac{m}{3} - \frac{2n}{3})^2+4(\frac{m+2n}{3}) - \frac{8}{5}(\frac{2n}{3})^2 - \frac{8}{3}(\frac{m}{3})(\frac{2n}{3})]\langle\varepsilon^2\rangle\frac{\omega^4}{\alpha_o^4}a^3$$

$$= (\frac{2}{3} + \frac{2}{9}m^2 + \frac{8}{45}n^2 + \frac{8}{27}mn)\langle\varepsilon^2\rangle\frac{\omega^4}{\alpha_o^4} a^3 \ . \qquad (3.8)$$

It is Rayleigh scattering, having the fourth power of frequency dependence.

For high frequency, when $K>>1$,

$$g^{PP} \approx \frac{\langle\varepsilon^2\rangle}{a} K^4 \frac{(1 - \frac{m}{3} - \frac{2n}{3})^2}{2K^2} = \frac{\langle\varepsilon^2\rangle}{2}\frac{\omega^2}{\alpha_o^2} a(1 - \frac{m}{3} - \frac{2n}{3}) \ . \qquad (3.9)$$

Remembering that

$$\tilde{\alpha}^2 = \langle(\frac{\delta\alpha}{\alpha_o})^2\rangle = \frac{1}{4}\langle\varepsilon^2\rangle(1 - \frac{m}{3} - \frac{2n}{3})^2 \ , \qquad (3.10)$$

therefore

$$g^{PP} \approx 2\tilde{\alpha}^2 \frac{\omega^2}{\alpha_o^2} a \ . \qquad (3.11)$$

Compare (3.7), (3.8) and (3.11) with Chernov's result for scalar wave theory (Chernov, 1960, (56), (58) and (59) for exponential correlation function):

$$g_{scalar} = 8\tilde{\alpha}^2 \frac{\omega^4}{\alpha_o^4} a^3 \frac{1}{1+4\frac{\omega^2}{\alpha_o^2} a^2} \ , \qquad (3.12)$$

$$g_{scalar} = 8\tilde{\alpha}^2 \frac{\omega^4}{\alpha_o^4} a^3 \ , \qquad \frac{\omega}{\alpha_o} a<<1 \qquad (3.13)$$

$$g_{scalar} = 2\tilde{\alpha}^2 \frac{\omega^4}{\alpha_o^4} a^3 \ , \qquad \frac{\omega}{\alpha} a>>1 \qquad (3.14)$$

We can see that, the high frequency asymptotics are equal for both cases, while in the low frequency and intermediate frequency range the scattering coefficients for elastic waves are more complicated.

The identity of (3.11) with the one of scalar wave scattering (3.14) implies that, in the case of weak perturbation of parameters, the travel time fluctuations in the forward direction will dominate the scattered field when wavelength is very short compared to the sizes of inhomogeneities. That explains also why the scattering coefficient should not be taken as an attenuation coefficient, especially in the high frequency range.

In the same way we now calculate the total scattered S wave power

$$g^{ps} = \frac{1}{4\pi}\iint_{4\pi} g^{ps}(\theta)d\Omega$$

$$= \frac{1}{4\pi}\iint_{4\pi} 2a^3\frac{\omega^4}{\beta_o^4}\langle\varepsilon^2\rangle\frac{(-\sin\theta + \frac{\beta_o}{\alpha_o}\sin 2\theta)^2}{(1+\omega^2 S_2^2 a^2)^2}\,d\Omega\ , \tag{3.15}$$

where

$$S_2 = \sqrt{(\frac{1}{\alpha_o})^2+(\frac{1}{\beta_o})^2-2(\frac{1}{\alpha_o})(\frac{1}{\beta_o})\cos\theta} \tag{3.16}$$

Let

$$K = \frac{\omega}{\alpha_o}a,\quad 2(\frac{\alpha_o}{\beta_o})K^2=b,\quad 1+K^2+(\frac{\alpha_o}{\beta_o})K^2=d\ , \tag{3.17}$$

$$\cos\theta = x\ ,$$

we get

$$g^{ps} = \frac{\langle\varepsilon^2\rangle}{2\pi a}\left(\frac{\alpha_o}{\beta_o}\right)^4 K^4 \int_o^{2\pi} \alpha\phi \int_o^{\pi} \frac{\sin^2\theta+4\left(\frac{\beta_o}{\alpha_o}\right)^2 n^2 \sin^2\theta\cos^2\theta-4\left(\frac{\beta_o}{\beta_o}\right) n \sin^2\theta\cos\theta}{\left[1+K^2+\left(\frac{\alpha_o}{\beta_o}\right)^2 K^2-2\left(\frac{\alpha_o}{\beta_o}\right)K^2\cos\theta\right]^2} \sin\theta d\theta$$

$$= \frac{\langle\varepsilon^2\rangle}{a}\left(\frac{\alpha_o}{\beta_o}\right)^4 K^4 \int_{-1}^{1} \frac{1-x^2+4\left(\frac{\beta_o}{\alpha_o}\right)^2 n^2 (x^2-x^4)-4\left(\frac{\beta_o}{\alpha_o}\right) n (x-x^3)}{(d-bx)^2} dx$$

$$= \langle\varepsilon^2\rangle \left(\frac{\alpha_o}{\beta_o}\right)^4 K^4 \{\frac{2}{b^2}(-2 + \frac{d}{b}\ln\frac{d+b}{d-b})+\frac{4}{b}\left(\frac{\alpha_o}{\beta_o}\right)^2 n^2 (\frac{4}{b} - \frac{2d}{b^2}\ln\frac{d+b}{d-b} - \frac{8}{3b} - \frac{8d^2}{b^3} + \frac{4d^3}{b^4}\ln\frac{d+b}{d-b})$$

$$- \frac{4}{b}\left(\frac{\beta_o}{\alpha_o}\right) n (\frac{-1}{b}\ln\frac{d+b}{d-b} - \frac{6d}{b^2} + \frac{3d^2}{b^3}\ln\frac{d+b}{d-b})\}$$

$$= \frac{\langle\varepsilon^2\rangle}{a}\{\left(\frac{\alpha_o}{\beta_o}\right)^2 (\frac{d}{2b}\ln\frac{d+b}{d-b} - 1) + 2n^2[\frac{2}{3} - \frac{4d^2}{b^2} + (\frac{2d^3}{b^3} - \frac{d}{b})\ln\frac{d+b}{d-b}]$$

$$+ \left(\frac{\alpha_o}{\beta_o}\right) n [\frac{6d}{b} - (\frac{3d^2}{b^2} - 1)\ln\frac{d+b}{d-b}]\} \quad . \qquad (3.18)$$

Let us describe the low frequency approximation. When K<<1,

$$\ln\frac{d+b}{d-b} \approx 2\frac{b}{d} + \frac{2b^3}{3d^3} + \frac{2b^5}{5d^5} + \cdots , \tag{3.19}$$

therefore

$$g^{ps} \approx 4[\frac{1}{3} + \frac{4}{15}(\frac{\beta_o}{\alpha_o})^2 n^2](\frac{\alpha_o}{\beta_o})^4 \langle\varepsilon^2\rangle \frac{\omega^4}{\alpha_o^4} \alpha^3 . \tag{3.20}$$

Considering the factor $(\frac{\alpha_o}{\beta_o})^4$ in (3.20), we conclude that the conversions loss g^{ps} is usually larger than the common-mode scattering loss g^{pp} in Rayleigh scattering range. From (3.20) we can also see that the contribution to g^{ps} from $\delta\rho$ and from $\delta\mu$ are uncorrelated (remembering $\langle(\frac{\delta\mu}{\mu_o})^2\rangle = n^2\langle\varepsilon^2\rangle$), they can be calculated separately. This can be understood from their scattering patterns (1.49), which show that the main lobes of $\delta\rho$ scattering and $\delta\mu$ scattering are in different directions, therefore their cross coupling will be one order smaller than the main lobes.

For high frequencies, when K>>1,

$$\ln\frac{d+b}{d-b} \approx 2\ln(\frac{\alpha_o+\beta_o}{\alpha_o-\beta_o}) = \eta,$$

$$\frac{d}{b} \approx \frac{1}{2}[\frac{\beta_o}{\alpha_o} + \frac{\alpha_o}{\beta_o}] = \xi , \tag{3.21}$$

then

$$g^{ps} \approx \frac{D}{2a}(\frac{\alpha_o}{\beta_o})^2 \langle\varepsilon^2\rangle , \tag{3.22}$$

where

$$D = (\xi\eta-2)+4(\frac{\beta_o}{\alpha_o})^2 n^2(\frac{2}{3} - \xi\eta - 4\xi^2+2\xi^3\eta)$$

$$+ 2(\frac{\beta_o}{\alpha_o})n(6\xi+\eta-3\xi^2\eta) , \tag{3.23}$$

where ξ, η are defined by (3.21).

We can see that the conversions loss reaches a constant value for high frequencies for the case of exponential correlations function, contrary to the case of Gaussian correlation function, in which the conversion loss will diminish for high frequencies (see the discussion following 1.51). If we compare (3.22) with the P-P scattered power g^{pp} at high frequencies (3.11), which has ω^2 dependence, it seems that the conversion loss g^{ps} is negligible. However, we noticed that that ω^2 dependence is only for velocity perturbatins, which will give rise to the travel time fluctuations. It is interesting to note that, if we take out the velocity term in (3.7) (the first term), the rest will reach a constant value for high frequencies. Therefore, the energy loss due to scattering is a more complicated problem in the high frequency range than what the single scattering theory can deal with even qualitatively. At least for the exponential correlation function, the conversion loss cannot be neglected even for high frequencies.

Fig. 10 and 11 show the frequency dependences of P-P and P-S scattering coefficient g^{pp} and g^{ps} respectively. For comparison, in Fig. 10 we also show the frequency dependence of scattering coefficient for scalar wave according to (3.12). We can see that, in the low frequency and intermediate frequency range, the scattering coefficient can behave quite different from the scalar case, depending on the combination of parameter perturbations.

IV. SMALL SCALE INHOMOGENEITIES IN THE LITHOSPHERE REVEALED BY WAVE SCATTERING

In the following we will apply our theory to some past observations. The phase and amplitude fluctuations of P waves over large seismic arrays LASA and NORSAR have been used to infer the velocity inhomogeneities in the lithosphere under these arrays based on the scalar wave scattering theory (Aki, 1973, Capon 1974, Berteussen et al., 1975). The velocity perturbations derived have correlation lengths about 10-20 km (the results by Berteussen et al. are about 15 km for the data of two subarrays, 30-60 km for larger arrays including 5-8 subarrays), with r.m.s. perturbations 1.9%-4%. After that, Aki, Christoffersson and Husebye developed a method of inverting the teleseismic P-time data over a large array to obtain the 3-D velocity structure under the array (Aki et al., 1976, 1977). The method has been applied to more than forty arrays around the world since then, and has confirmed that the velocity inhomogeneities having different scale-lengths exist everywhere being studied in the lithosphere (Aki, 1977, 1981b, 1982). Specifically for LASA, the r.m.s. velocity perturbations have a lower limit 3.1%, and for NORSAR 3.2% from the results of inversion. Therefore, the existence of velocity inhomogeneities having scale-length 10-20 km in the lithosphere has been well accepted.

The success of the above application of scalar wave theory has its own reason. We know that the phase and amplitude fluctuation of transmitted waves for large-scale velocity inhomogeneities (the scale is much larger than the wavelength) is a forward scattering problem under small angle approximation. From (1.40) we know that the scalar wave theory for velocity perturbations can be approximately applied to this problem. On the other hand, the coda generation of local earthquakes and scattering attenuation are problems of

backscattering or full scattering. Some attempts of using scalar wave theory and attributing the coda generation and scattering attenuation to the same velocity inhomogeneities which cause the phase and amplitude fluctuations at large arrays, end up with inconsistency between the parameters of the medium needed to fit the data. In an example given by Sato (1982), the back-scattering coefficients needed to explain the coda strength are more than one order of magnitude higher than that derived from the calculation of scattering attenuation. We will discuss the coda strength problem in more detail in the following.

If we take the single scattering assumptions, then the coda strength is proportional to the backscattering coefficient of the random medium. From (2.19), we know that only the meridian component of scattered waves exists in the backward direction, therefore we will omit the subscript for g^{ss}_{mer},

$$g^{ss}(\pi) = 8a^3 \frac{\omega^4}{\beta_o^4} \tilde{Z}_\beta^2 \frac{1_2}{[1+4\frac{\omega}{\beta_o^2}a^2]^2} , \qquad (4.1)$$

where $\tilde{Z}_\beta$ is the r.m.s. impedance perturbation of S wave. When frequency increases, it reaches its maximum value

$$g^{ss}(\pi) \approx \frac{1}{2a} \tilde{Z}_\beta^2 , \qquad \frac{\omega}{\beta_o} a >> 1 . \qquad (4.2)$$

If we take a≈10 km, same as the velocity inhomogeneities under LASA or NORSAR, it will end up with a very big impedance perturbation index $\tilde{Z}_\beta$ in order to match the observed $g^{ss}(\pi)$. Aki (1980) has determined the back-scattering coefficient to be 0.01 to 0.02 for Kanto, Japan, at frequencies 1.5 to 3 Hz using coda - S ratio method. From (4.2), it would be $\tilde{Z}_\beta$ = 0.45~0.63, if we believe a≈10 km. This is not reasonable. In fact, from our theory, the correlation length for the coda excitation problem should be much

smaller than 10 km derived from the forward scattering experiments. In the following we will discuss this both from the sensitivity of backscattering and forward scattering to the scale of inhomogeneities and from the observed coda power spectra.

For the P-P forward scattering, from (1.40) we get

$$g^{PP}(\theta) \approx \frac{1}{\pi} \frac{\omega^4}{\alpha_o^4} \tilde{\alpha}^2 P^P(\theta) \ , \tag{4.3}$$

where $P^P(\theta)$ is the normalized angular spectral density of the scattered power for scalar waves, which can be written as (1.31)

$$P^P(\theta) = \iiint_{-\infty}^{\infty} N(r) e^{i\omega \vec{S}_1 \cdot \vec{\zeta}} \, dV(\vec{\zeta}) \ , \tag{4.4}$$

where $\vec{S}_1$ is defined by (1.30) and $r = |\vec{\zeta}|$. (4.4) is the 3-D Fourier transform of the correlation function of the random inhomogeneities, therefore $P^P(\theta) = W(\omega \vec{S}_1)$ can be regarded as the 3-D spectral density of the random inhomogeneities. Because of the isotropy of the inhomogeneities, $W(\omega \vec{S}_1) = W(\omega S_1)$ since the spatial frequency ωS_1, is related to the scattering angle θ by (1.30)

$$\omega S_1 = \omega |\vec{S}_1| = \frac{2\omega}{\alpha_o} \sin \frac{\theta}{2} \ , \tag{4.5}$$

therefore, $g^{PP}(\theta)$ for a fixed angle is only related to the 3-D spectral density of the inhomogeneities at the special spatial frequency ωs_1. In the nearby forward directions $\theta \approx 0$, $\omega S_1 \approx 0$, therefore the forward scattering only feels the d.c. component of the random medium, in other words, the forward scattering is most sensitive to the large scale inhomogeneities. On the other hand, for S-S backscattering, which is accepted as the mechanism of coda generation for local earthquakes, we have (from 2.19)

$$g^{ss}(\pi) = \frac{1}{\pi}\frac{\omega^4}{\beta_o^4}\tilde{z}_\beta^2\, P^S(\pi) = \frac{1}{\pi}\frac{\omega^4}{\beta_o^4}\tilde{z}_\beta^2\, W(\omega S_3|_{\theta=\pi}) = \frac{1}{\pi}\frac{\omega^4}{\beta_o^4}\tilde{z}_\beta^2\, W(\frac{2\omega}{\beta_o}) \ , \qquad (4.6)$$

where

$$W(\omega S_3) \iiint_{-\infty}^{\infty} N(r) e^{i\omega \vec{S}_3 \cdot \vec{\zeta}}\, dV(\zeta) \ ,$$

$$\omega S_3 = \omega|\vec{S}_3| = \frac{2\omega}{\beta_o}\sin\frac{\Theta}{2} \ . \qquad (4.7)$$

We can see that the backscattering is only influenced by the spectral density of the inhomogeneities at the spatial frequency $\frac{2\omega}{\beta_o}$, i.e. when the spatial period of the inhomogeneities is equal to half the wavelength of the detecting signal. This is consistent with the physics of scattering. The backscattering has the smallest resolvable length, which cannot be less than the half-wavelength of the wavefield.

Let us look at this problem from another aspect. For a fixed frequency, we know from (2.19)

$$g^{ss}(\pi) \propto \begin{cases} a^3 \ , & \frac{\omega}{\beta_o} a \ll 1 \ , \\ \frac{1}{a} \ , & \frac{\omega}{\beta_o} a \gg 1 \ . \end{cases} \qquad (4.8)$$

Therefore there exists an a_{opt} which has maximum response to the detecting field, if the lithosphere has multiple scale inhomogeneities, which I think we have to accept eventually. By differentiating (2.19) with respect to the correlation length a and equating to zero, we can get a_{opt}

$$\frac{\omega}{\beta_o} a_{opt} \approx \sqrt{\frac{3}{4}} = 0.87 \ ,$$

i.e.

$$a_{opt} \approx 0.14\,\lambda \ .$$

and

$$g^{ss}_{max}(\pi) \approx \frac{0.565}{2\, a_{opt}}\tilde{z}_\beta^2 = 0.28\,\frac{\tilde{z}_\beta}{a_{opt}} \ . \qquad (4.9)$$

From the above analysis, we can expect that the backscattering experiments using short period (around 1 second) S waves have a maximum response to the small scale inhomogeneities having correlation length around 0.5 km.

Fig. 12 shows the responses of inhomogeneities with different correlation lengths to 1 Hz S waves (β_o = 3.5 km/s). The maximum is at a≈0.48 km. For inhomogeneities with correlation length a≈10 km, the backscattering response drops to 1/11.8 of the maximum value.

Fig. 13 gives the frequency dependences of backscattering coefficient for two cases with correlation length a = 0.5 km and a = 10 km. $g^{ss}(\pi)$ for a = 10 km, reaches its maximum at much lower frequency (at about 0.1 Hz) and has also a lower value of maximum coefficient, compared with the case of a = 0.5 km. The dotted line represents the frequency dependency for the case when the medium has inhomogeneities with both scale lengths.

The observations on coda power spectra also support the existence of small scale (less than 1 km) inhomogeneities. Aki (1981a) calculated simultaneously the S and coda spectra for 900 small earthquakes in the Kanto region, Japan, and observed that the coda spectra agree well with the S spectra except for f = 1.5 Hz, where the coda spectra bent down compared to S spectra. That means that, for f>1.5 Hz, $g^{ss}(\pi)$ is almost independent of frequency, which set the upper limit of the scale length of inhomogeneities which cause the generation of local coda waves. Assuming β_o = 3.5 km/s, this critical correlation length a_c ≈ 0.33 km.

Assuming a≈0.3 - 0.5 km for f = 1.5 Hz in (4.1), we can get

$$\tilde{Z}_\beta \approx \begin{cases} 11\% & , \text{ if } g^{ss}(\pi) = 0.01 , \\ 15\%\text{-}16\% & , \text{ if } g^{ss}(\pi) = 0.02 . \end{cases} \tag{4.10}$$

The calculated impedance perturbation index for S waves may have been overestimated because of the simplified single-scattering model in the calculation of $g(\pi)$ from the measured coda power. We will try in the following to correct $g^{ss}(\pi)$ by using a multiple isotropic scattering model for scalar wave derived by Gao et al. (1983), to see its influence on parameter estimation.

Suppose the earthquake is close enough to the station compared with the sampled space by the coda waves, so that we can take it as situating in the same point as the station. If the surrounding infinite random medium is composed of randomly distributed scatterers with isotropic scattering patterns and the distribution of the scatterers is dilute enough so that the Born approximation can be used locally, Gao et al. (1983b) showed that the coda power at time t with central frequency ω can be expressed in considering the multiple scattering in 3-D space as

$$P(\omega|t) = \frac{2gS(\omega)}{\beta}(1+1.23g\beta te^{0.33g\beta t})\frac{e^{-\omega t/Q_e}}{t^2}, \qquad (4.11)$$

where $S(\omega)$ is the source power factor, g is the isotropic scattering coefficient, in the case of discrete scatterers, $g = n_o\sigma$, where n_o is the number of the scatterers per unit volume and σ is the averaged scattering cross-section of the scatterers, and Q_e is equivalent quality factor of the medium extinction coefficient defined by $1/Q_e = 1/Q_i + 1/Q_s$, where Q_i and Q_s are the equivalent Q's for the intrinsic attenuation and the scattering coefficient respectively (see Ch. 4, p. 177). However, if we estimate the backscattering coefficient $g(\pi)$ by using a single-scattering model, as in Aki (1980), the coda power can be expressed as

$$P_s(\omega|t) = \frac{\beta}{2}g(\pi)S(\omega)(\frac{\beta t}{2})^{-2}e^{-\omega t/Q}, \qquad (4.12)$$

where Q is the apparent quality factor of the coda envelope decay, $g(\pi)$ is backscattering coefficient, and $P_s(\omega/t)$ stands for the coda power generated by the single scattering model. Now suppose we have the case of isotropic scattering, then $g(\pi) = g$. From (4.12), if we know the power ratio of coda and source at a specified time t_1, $P_S(\omega|t_1)/S(\omega)$, and Q of the medium, then g can be calculated from (4.12)

$$\hat{g}_{single} = \frac{2}{\beta} \left(\frac{\beta t_1}{2}\right)^2 e^{\omega t_1/Q} \frac{P_S(\omega|t_1)}{S(\omega)} , \qquad (4.13)$$

where $\hat{g}_{single}$ means the estimated g from the single scattering model. In Aki (1980)'s paper, the source factor $S(\omega)$ is obtained through the following equation from the spectral amplitudes of primary S waves and averaged over a large number of earthquakes,

$$|F(\omega)| = \sqrt{S(\omega)} \frac{1}{r} e^{-\frac{\omega r}{2\beta Q_\beta}} , \qquad (4.14)$$

where $|F(\omega)|$ is the spectral amplitude of S wave, r is the distance between the stations and the earthquake, Q_β is the Q factor for S wave.

If the coda power generation is controlled by a multiple scattering process as expressed by (4.11), while we estimate $\hat{g}_{single}$ by using the single scattering model as in (4.13), putting $P_S(\omega|t_1) = P(\omega|t_1)$, and substituting (4.11) into (4.13), we obtain

$$\hat{g}_{single} = g(1+1.23\, g\beta t_1\, e^{-.33 g\beta t_1}) \cdot \exp[\omega t_1 (\frac{1}{Q} - \frac{1}{Q_e})] . \qquad (4.15)$$

Therefore we obtained a relation between the estimated $\hat{g}_{single}$ and the true g. $1/Q$ is usually smaller than $1/Q_e$ and is dependent on the relative magnitudes of scattering coefficient and absorption coefficient. For simplicity, we assume $1/Q \approx 1/Q_e$, which is approximately true for weak scattering, i.e. when the scattering coefficient is smaller than the absorption coefficient (see ch. 4, fig. 3.2 and 3.7). The discrepancy

between g and g_{simple} depends on the value of $g\beta t_1 = \xi$, the ratio of travel distance to the effective mean free path 1/g. When $\xi = 0.5, 1, 2$, $\hat{g}_{single} = 1.73g, 2.71g, 5.76g$ respectively. Therefore, when $\xi > 1$, the discrepancy will be significant. In Aki's calculation (1980), $t_1 = 50$ sec. For $\hat{g}_{single} = 0.01$ and 0.02, we can get $g = 0.0045$ and 0.0065 from (4.15). This correction to the backscattering coefficient is only an approximation, because $g(\theta)$ is not isotropic, the correction may be overdone or underdone. From the corrected $g(\pi)$ values we obtain

$$\tilde{z}_\beta \approx \begin{cases} 7.4\% , & \text{for } g(\pi) = 0.0045 \ (\hat{g}_{single} = 0.01) . \\ 8.6\%\text{-}9.1\% , & \text{for } g(\pi) = 0.0065 \ (\hat{g}_{single} = 0.02) . \end{cases} \qquad (4.16)$$

Table 1 gives the multiple-scattering corrected $g(\pi)$ values and the corresponding equivalent r.m.s. impedance perturbations $\tilde{z}_\beta$ for Area A and B+C in Kanto region, Japan, derived from Table 3 in Aki's (1980) paper. According to Aki (1980), $\hat{g}_{single}$, therefore g also, may have been overestimated by the underestimation of spectral amplitudes of S waves for the case of f > 3 Hz. $\tilde{z}_\beta$ are calculated from g by assuming that the inhomogeneities have the optimum correlation lengths q_{opt} for the specified frequencies, which are also included in the table. These values are not the real values of the perturbation index for the corresponding sizes, because the g value for each frequency may be a combining effect of multiple scale inhomogeneities. We cannot separate the effects from different scale lengths at present. However, it gives some idea of the impedance perturbation strength with scale lengths within the specified range.

What can we say about the properties of these small-scale inhomogeneities? From the backscattering experiment, we can estimate only the average impedance perturbation and the approximate scale length. We will call

these "impedance inhomogeneities". What are they? Might they be intrusions (Dainty 1981)? grain-size of the lithosphere (Aki 1981a)? Most likely they might be faultins and fractures in the lithosphere. This is supported by the recent discovery by Jin (1983), which shows that the coda envelope decay made significant changes before and after the Tangshan earthquake of China. The stress variations before and after a great earthquake might cause changes of the properties of faultings and fractures , resulting in observable differences in coda decay . Therefore, the observation and monitoring of coda spectra and the scattering coefficient g might be able to offer some useful information for both the tectonic activity and the earthquake prediction.

CONCLUSION AND DISCUSSION

By using body-force equivalence and Born approximation, we have derived the mean square amplitudes of the scattered fields and the directional scattering coefficients of the random medium for both P wave and S wave incidence. We obtained expressions in terms of perturbations of density and Lame constants of the medium. The spatial pattern of the scattered powers can be written as a product of two factors, one is the elastic wave Rayleigh scattering pattern of a volume element of the random medium, the other is a scalar-wave scatternig pattern for the whole volume of which are different for common-mode scattering and for mode-conversion scattering.

We found that, under certain conditions, the perturbations can be decomposed into an impedance term and a velocity term (1.37, 1.52, 2.15, 2.16). The velocity perturbations have a main lobe of scattering in the forward direction and no scattering in the exact backward direction. On the other hand, the impedance perturbations have a main backscattering lobe and no scattering in the exact forward direction. We have shown that when the scale lengths of the inhomogeneities are much larger than the wavelength, by the

small angle approximation, the scalar wave theory of velocity perturbations (e.g. Chernov 1960, Tartarski, 1961, 1971, Flatte et al., 1979) can be approximately applied to the forward scattering problems of elastic waves. This includes the phase and amplitude fluctuations over large seismic arrays. To the contrary, the backscattering or large-angle scattering problems must be treated by the theory of elastic wave scattering. It is interesting to note that, in the backward direction or nearly backward direction, the elastic wave scattering problem is similar to a scalar wave scattering problem with only impedance perturbations (1.42).

We derived the low frequency and high frequency asymptotic expressions for the directional scattering coefficients. For low frequencies, it has the common features of Rayleigh scattering: a fourth power frequency dependence and a third power dependence of correlation length. However, the spatial pattern is much more complex than the case of scalar wave or acoustic wave. For high frequencies, the frequency dependences become more complicated and angle-dependent. However, the scattering pattern becomes very simple for the special case of forward scattering (1.39, 2.24), which has a fourth power frequency dependence, and for back-scattering (1.44, 2.23), which is frequency-independent.

The converted waves reach a maximum at high-frequencies for the case of exponential correlation function. This behavior is different from the case of Gaussian correlation function, which represent very smooth structures. In the latter case converted waves diminish for high-frequencies.

In section 3 we derived the total scattered power or total scattering coefficient for P wave incidence. In the low frequency range, it has a fourth power frequency dependence but with a more complicated coefficient than the scalar wave case. In the high frequency range, it coicides with the formulae

for scalar waves in a medium with only velocity perturbations. It implies that, when the wavelength is much shorter than the scale length of the inhomogeneities, the travel time fluctuation will dominate the scattered field. The converted power will reach a constant for high frequencies. It is interesting to note that, if we remove the term with velocity perturbation from the common-mode scattering coefficient, the converted power will be comparable to the common mode scattered power. Therefore the conversion loss can not be neglected even at high frequencies for the case of exponential correlation function.

From the figures shown here, it can be seen that, the elastic wave scattering can be quite different from the scalar wave scattering in the low or intermediate frequency range.

In Section 4 we applied our theory to some previous observations. Since forward scattering is most sensitive to the large scale velocity inhomogeneities, while backscattering has the maximum response from inhomogeneities with scale-lengths comparable to the wavelength, we conclude that the inhomogeneities responsible for local coda generation are not the same velocity inhomogeneities (with a≈10-20 km, $\tilde{\alpha}$ = 1.9-4%) which cause the phase and amplitude fluctuations at large seismic arrays. We estimated the parameters of inhomogeneities in central Japan from the corrected backscattering coefficients using a multiple scattering model developed by Gao et al (1984). For frequencies from 1.5 Hz to 24 Hz, the correlation lengths range from 500 m to 20 m with the r.m.s. impedance perturbations up to 7%-9%. Therefore the lithosphere may have multi-scale inhomogeneities. In addition to the 10-20 km scale velocity inhomogeneities, the lithophere in tectonically active regions may be rich in small scale (less than 1 km) inhomogeneities, which could be randomly distributed faultings and fractures.

References

Aki, K., Analysis of the seismic coda of local earthquakes as scattered waves, J. Geophys. Res., 74, 615-631, 1969.

Aki, K., Scattering of P waves under the Montana Lasa, J. Geophys. Res., 78, 1334-1346, 1973.

Aki, K., Three dimensional seismic velocity anomalies in the lithosphere, method and summary of results, J. Geophys., 43, 235-242, 1977.

Aki, K., Scattering and attenuation of shear waves in the lithospnere, J. Geophys. Res., 85, 6496-6504, 1980.

Aki, K., Source and scattering effects on the spectra of small local earthquakes, Bull. Seismol. Soc. Amer., 71, 1687-1700, 1981a.

Aki, K., 3-D inhomogeneities in the upper mantle, Tectonophys., 75, 31-40, 1981b.

AkI, K., Three-dimensional seismic inhomogeneities in the lithosphere and asthenosphere: Evidence for decoupling in the lithosphere and flow in the asthenosphere, Rev. Geophys. Space Phys., 20, 161-167, 1982.

Aki, K. and B. Chouet, Origin of coda waves: source, attenuation and scattering effects, J. Geophys. Res., 80, 3322-3342, 1975.

Aki, K., A. Christoffersoon and E.S. Husebye, Three-dimensional seismic structure of the lithosphere under Montana LASA, Bull. Seismol. Soc. Amer., 66, 501-524, 1976.

Aki, K., A. Christoffersson and E.S. Husebye, Determination of the three dimensional seismic structure of the lithosphere, J. Geophys. Res., 82, 277-296, 1977.

Aki, K., and P. Richards, Quantitative Seismology, V. I and II, W.H. Freeman and Co., 1980.

Aki, K., R.S. Wu and R.P. Comer, Variability of direct P, stability of P-coda and heterogeneities of the lithosphere, Bull. Seismol. Soc. Amer., in press, 1983.

Beaudet, P.R., Elastic wave propagation in heterogeneous media, Bull. Seis. Soc. Amer., 60, 769-784, 1970.

Berteussen, K.A., A. Christoffersson, E.S. Husebye, and A. Dahle, Wave scattering theory in analysis of P wave anomalies at NORSAR and LASA, Geophys. J.R. astr. Soc., 42, 403-417, 1975.

Capon, J., Characterization of crust and upper mantle structure under Lasa as a random medium, Bull. Seis. Soc. Amer., 64, 235-266, 1974.

Chandrasekhar, S., Radiative Transfer, Dover, 1960 (revised version of 1950).

Chernov, L.A., Wave Propagation in a Random Medium, McGraw-Hill, New York, 1960.

Dainty, A.M., A scattering model to explain seismic Q observations in the lithosphere between 1 and 30 Hz, Geophys. Res. Lett., 8, 1126-1128, 1981.

Dainty, A.M., M.N. Toksoz, K.R. Anderson, P.J. Pines, Y. Nakamura and G. Latham, Seismic scattering and shallow structure of the moon in oceanus procellarum, Moon, 9, 11-29, 1974.

Doornbos, D.J., Characteristics of lower mantle inhomogeneities from scattered waves, Geophys. J.R. astr. Soc., 44, 447-470, 1976.

Flatte, S.M., R. Dashen;, W.H. Munk, K.M. Watson, and F. Zachariasen, Sound transmission through a fluctuating ocean, Cambridge Univ. Press, 1979.

Gao, L.S., L.C. Lee, N.N. Biswas and K. Aki, Comparison of the effects between single and multiple-scattering on coda waves for local earthquakes, Bull. Seis. Soc. Amer., 73, 377-389, 1983a.

Gao, L.S., N.N. Biswas, L.C. Lee and K. Aki, Effects of multiple scattering on coda waves in three-dimensional medium, to be published, 1983b.

Haddon, R.A.W., Scattering of seismic body waves by small random inhomogeneities in the earth, NORSAR Scientific Report No. 3-77/78, 1978.

Haddon, R.A.W., and J.R. Cleary, Evidence for scattering of seismic PKP waves near the mantle-core boundary, Phys. Earth and Planet. Int., 8, 211-234, 1974.

Hudson, J.A., Scattered waves in the coda of P, J. Geophys., 43, 359-374, 1977.

Jin, A.S., Coda, I. durations and backscattering coefficients, Acta Geophysica Sinica (in Chinese), in press, 1983.

Karal, F.C. and J.B. Keller, Elastic, electromagnetic and other waves in a random medium, J. Math. Phys., 5, 537-549, 1964.

Knopoff, L. and J.A. Hudson, Scattering of elastic waves by small inhomogeneities, J. Acoust. Soc. Amer., 36, 338-343, 1964.

Knopoff, L. and J.A. Hudson, Frequency dependence of amplitudes of scattered elastic waves, J. Acoust. Soc. Amer., 42, 18-20, 1967.

Korvin, G., General theorem on mean wave attenuation, Geophys. Trans., 29, 2, 191-202, 1983.

Sato, H., Energy propagation including scattering effect; single isotropic scattering approximation, J. Phys. Earth, 25, 27-41, 1977.

Sato, H., Amplitude attenuation of impulsive waves in random media based on travel time corrected mean wave formalism, J. Acoust. Soc. Amer., 71, 559-564, 1982a.

Sato, H., Attenuation of S waves in the lithosphere due to scattering by its random velocity structure, J. Geophys. Res., 87, 7779-7785, 1982b.

Sato, H., Attenuation of body waves and envelope formation of 3-component seismograms of small local earthquakes in randomly inhomogeneous lithosphere, to be published, 1983.

Tatarskii, V.I., Wave Propagation in a Turbulent Medium, Dover, 1961.

Tatarskii, V.I., The effects of the turbulent atmosphere on wave propagation, 1971.

Wu, R.S., The attenuation of seismic waves due to scattering in a random medium (abstract), EOS, 61, 46, 1049, 1980.

Wu, R.S., Attenuation of short period seismic waves due to scattering, Geophys. Res. Lett., 9, 9-12, 1982a.

Wu, R.S., Mean field attenuation and amplitude attenuation due to wave scattering, Wave Motion, 4, 305-316, 1982b.

Wu, R.S., and K. Aki, Scattering characteristics of elastic waves by an elastic inclusion, submitted to Geophysics, 1984.

Table 1 $\hat{g}_{single}$, g and $\tilde{Z}_\beta$ for Kanto, Japan

center frequency Hz	band-width Hz	$\hat{g}_{single}$ (km^{-1}) area A	$\hat{g}_{single}$ (km^{-1}) area B+C	g (km^{-1}) area A	g (km^{-1}) area B+C	a_{opt} (km)	Z_β (%) area A	Z_β (%) area B+C
1.5	1	0.022	0.024	0.0068	0.0072	0.33	8.9	9.2
3	2	0.02	0.12	0.0065	0.015	0.16	6.1	9.2
6	4	0.04	0.10	0.0093	0.014	0.08	5.1	6.3
12	8	0.06	0.09	0.011	0.013	0.04	3.9	4.3
24	16	0.5	0.36	0.023	0.021	0.02	4.0	3.9

FIGURE CAPTIONS

Figure 1. The spherical coordinate system for P wave incidence.

Figure 2. The spatial patterns of the Rayleigh scattering factor ${}^{P}R^{P}(\theta)$ for different types of perturbations.

Figure 3. The spatial patterns of the scalar wave factor of common-mode scattering $P^{P}(\theta)$ (upper half-plane) and of mode-conversion scattering $P^{C}(\theta)$ (lower half-plane) for different wavelengths.

Figure 4. Comparison of scalar wave scattering and elastic wave scattering for P wave incidence when $K = \frac{\omega}{\alpha_o} = 0.1$.

Figure 5. Same as Fig. 4, where $K = 0.5$.

Figure 6. Same as Fig. 4, where $K = 1$.

Figure 7. Same as Fig. 4, where $K = \pi/2$.

Figure 8. Same as Fig. 4, where $K = 10$.

Figure 9. The spherical coordinate system for S wave incidence.

Figure 10. Frequency dependences of P-P scattering coefficient.

Figure 11. Frequency dependences of P-S scattering coefficient.

Figure 12. Backscattering responses of inhomogeneities with different correlation lengths for 1 Hz wave.

Figure 13. Frequency dependences of backscattering coefficient for inhomogeneities with correlation length $a = 10$ km and $a = 0.5$ km.

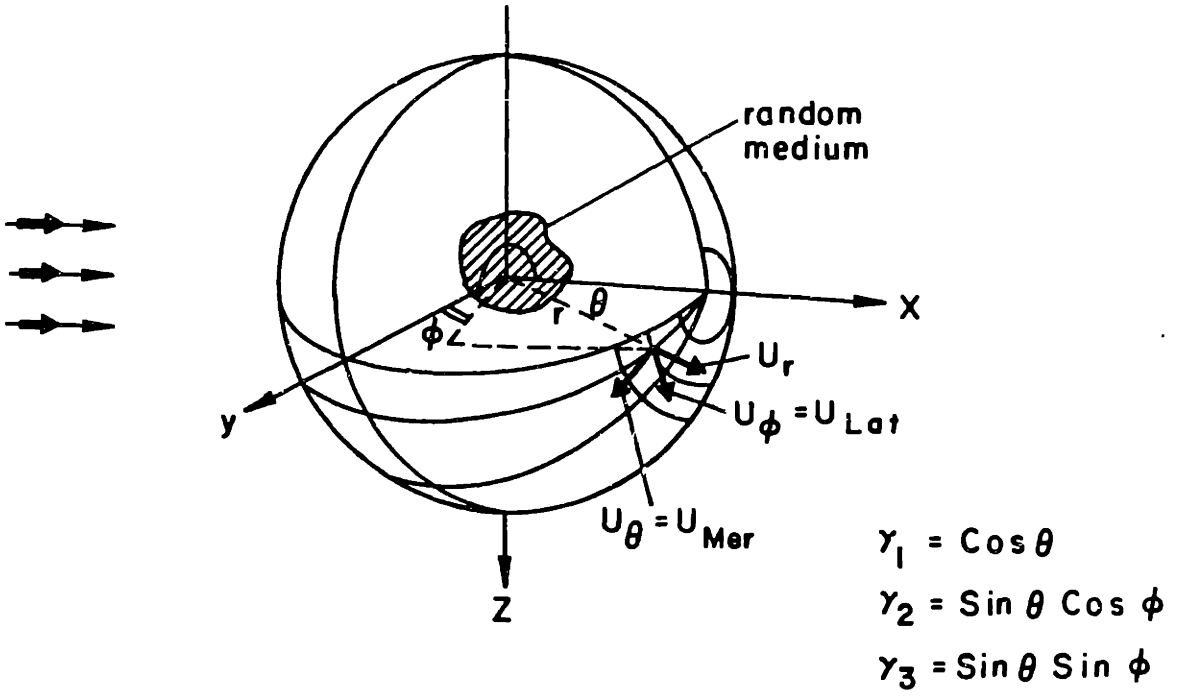

Figure 1. The spherical coordinate system for P wave incidence.

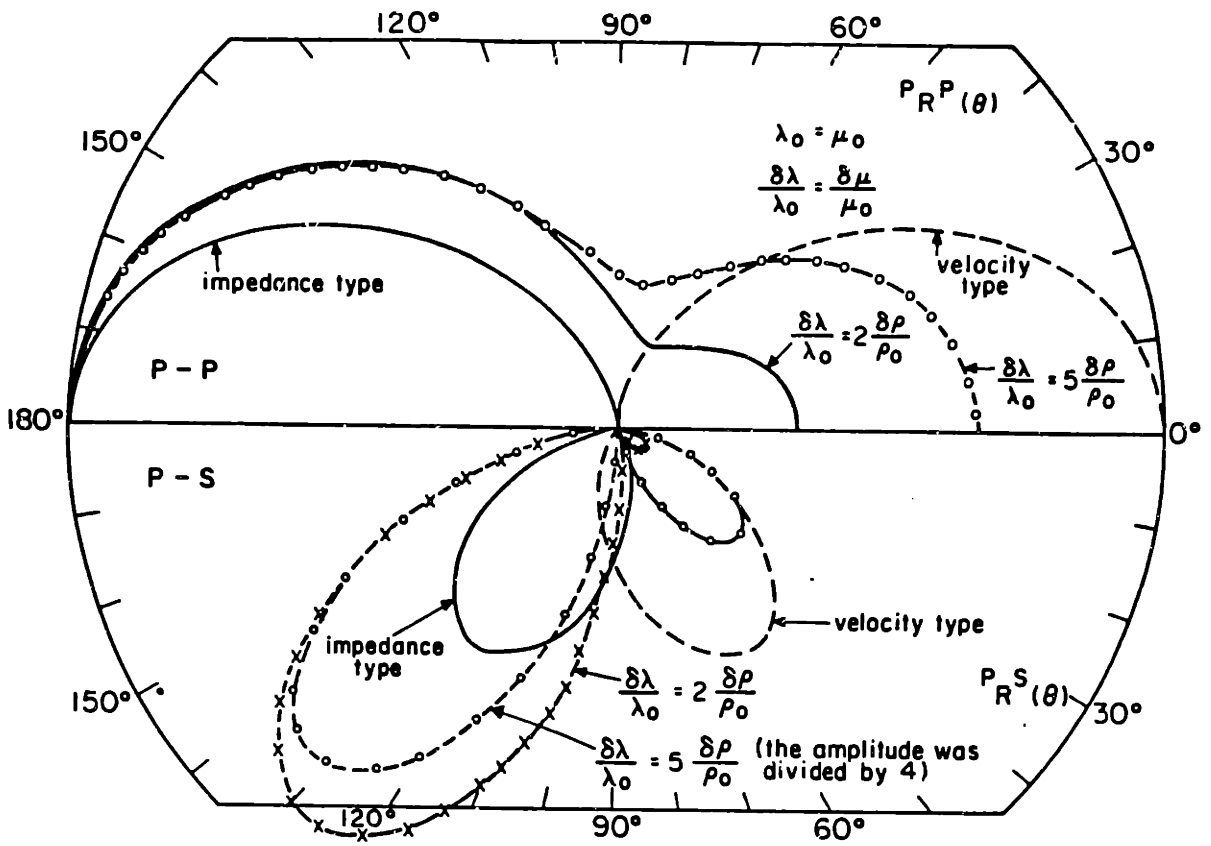

Figure 2. The spatial patterns of the Rayleigh scattering factor $P_R{}^P(\theta)$ for different types of perturbations.

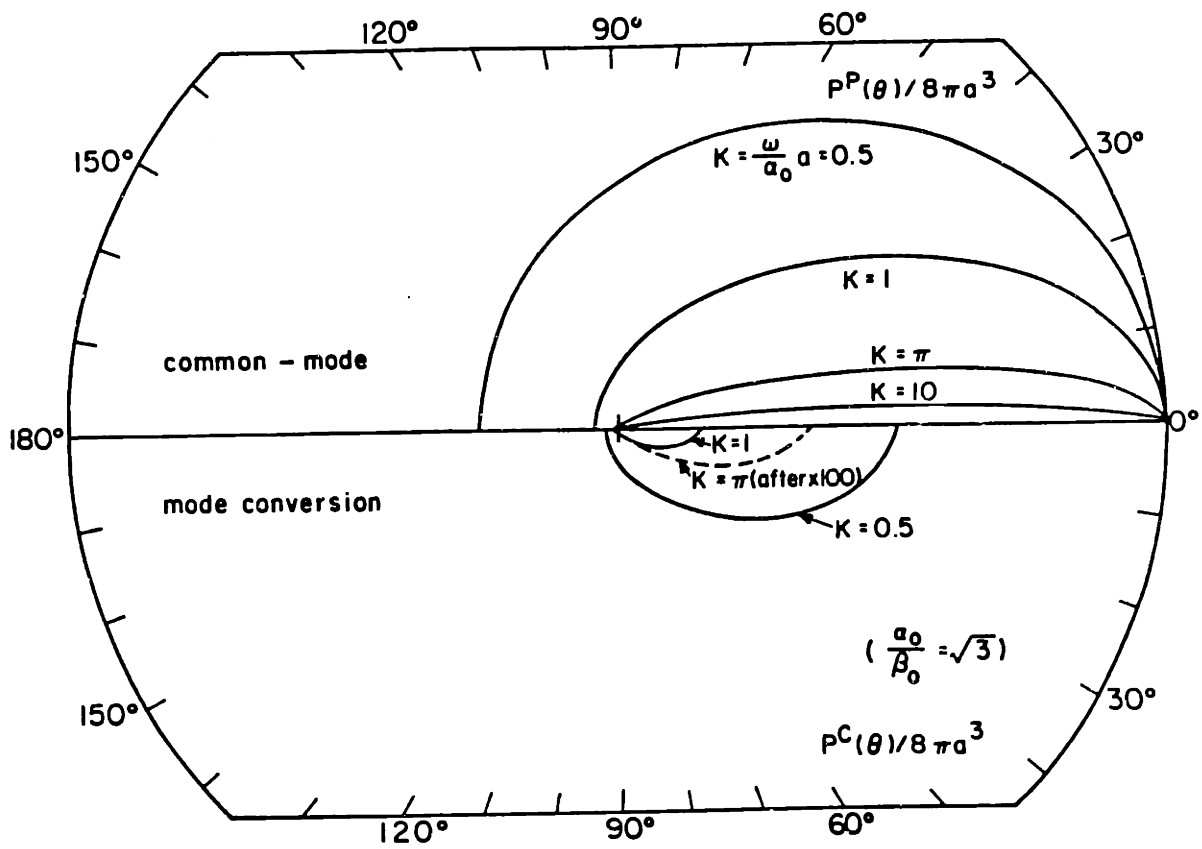

Figure 3. The spatial patterns of the scalar wave factor of common-mode scattering $P^P(\theta)$ (upper half-plane) and of mode-conversion scattering $P^C(\theta)$ (lower half-plane) for different wavelengths.

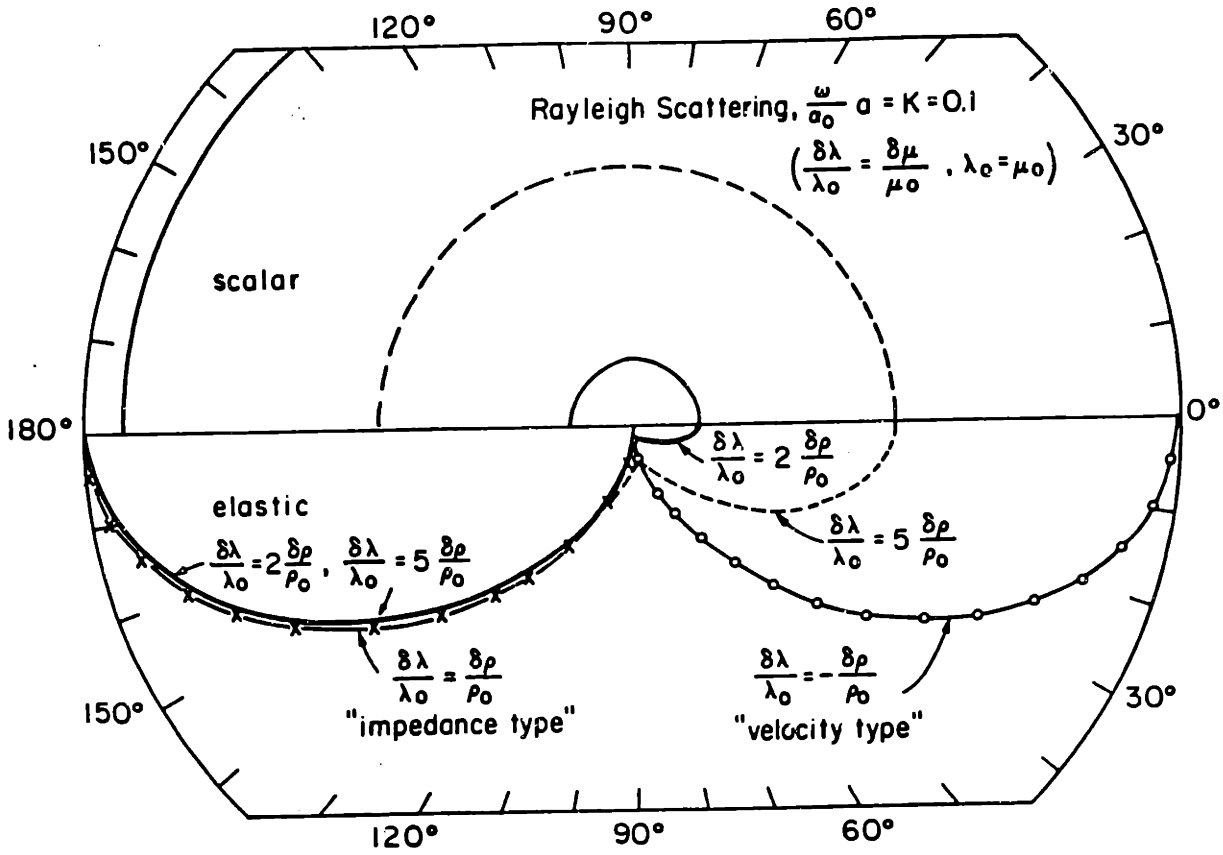

Figure 4. Comparison of scalar wave scattering and elastic wave scattering for P wave incidence when $K = \frac{\omega}{\alpha_0} = 0.1$.

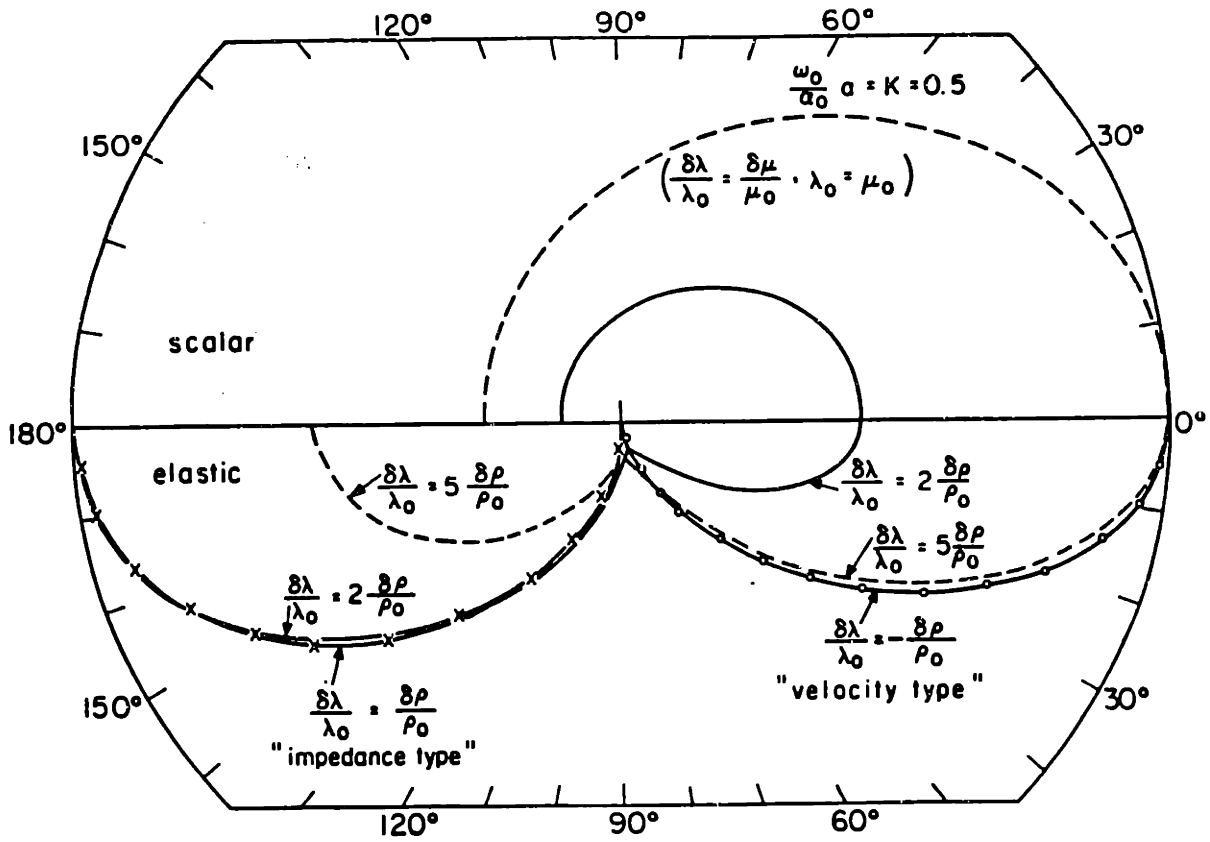

Figure 5. Same as Fig. 4, where K = 0.5.

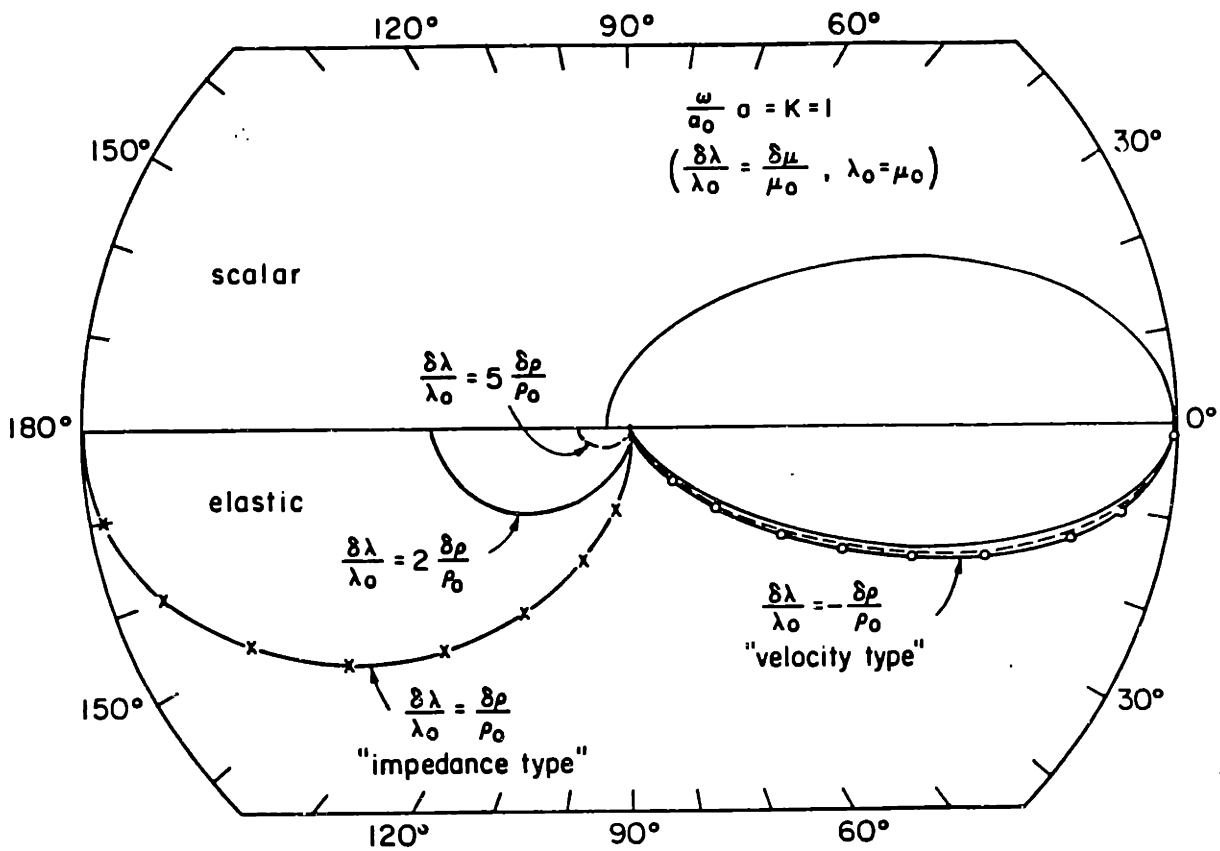

Figure 6. Same as Fig. 4, where K = 1.

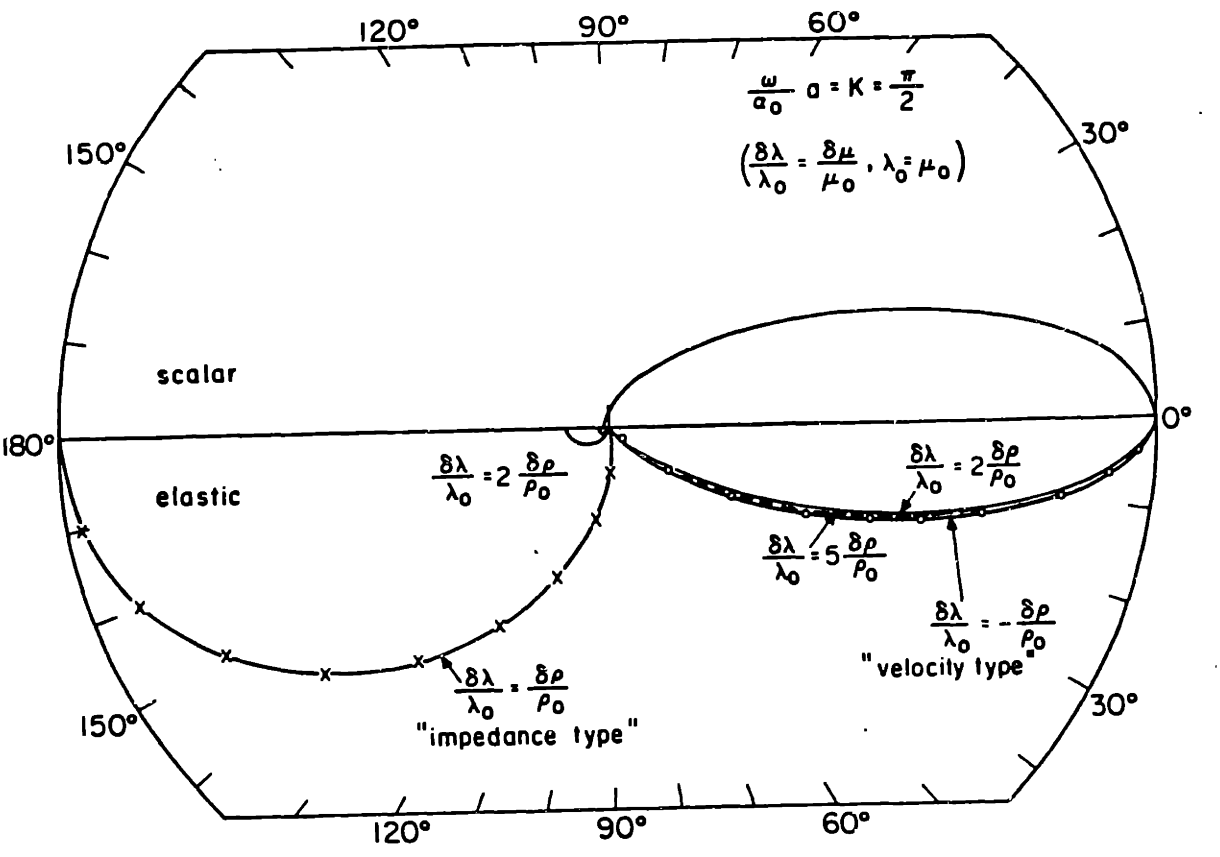

Figure 7. Same as Fig. 4, where $K = \pi/2$.

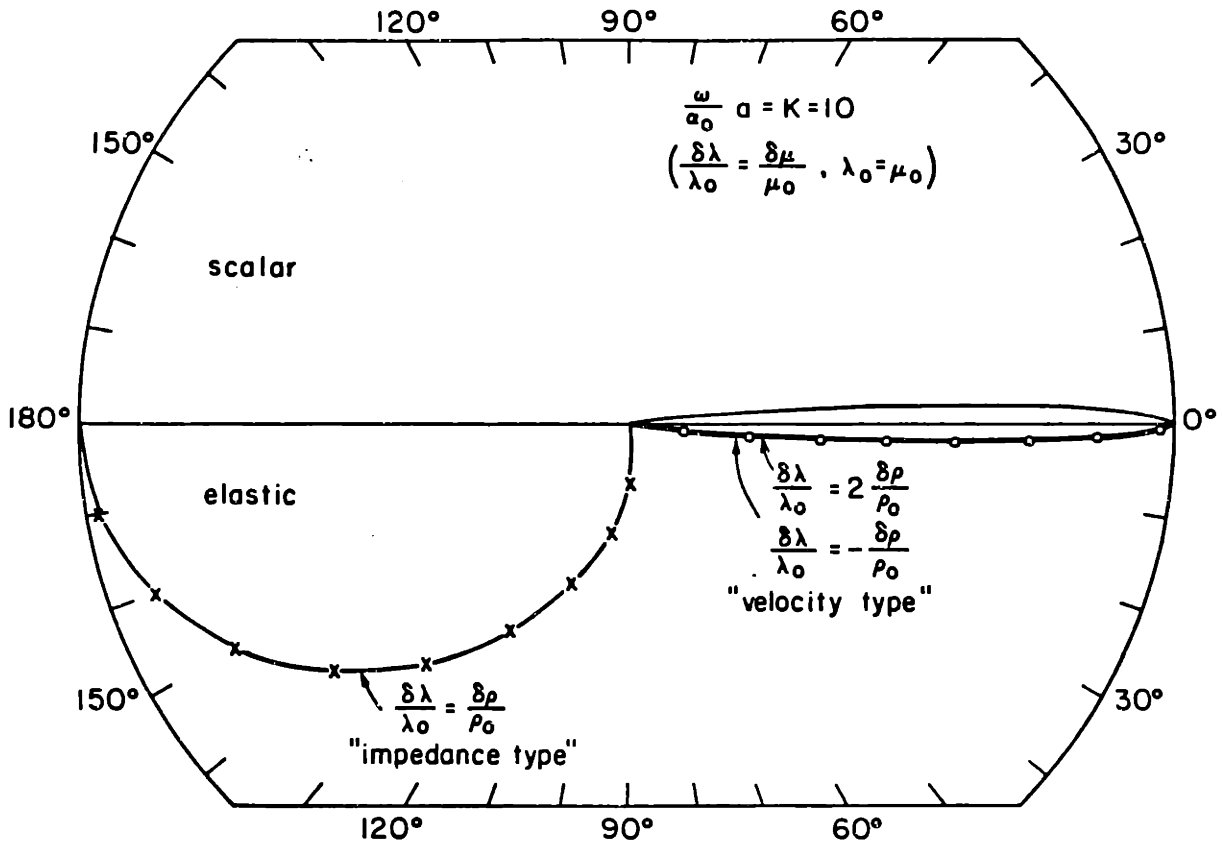

Figure 8. Same as Fig. 4, where K = 10.

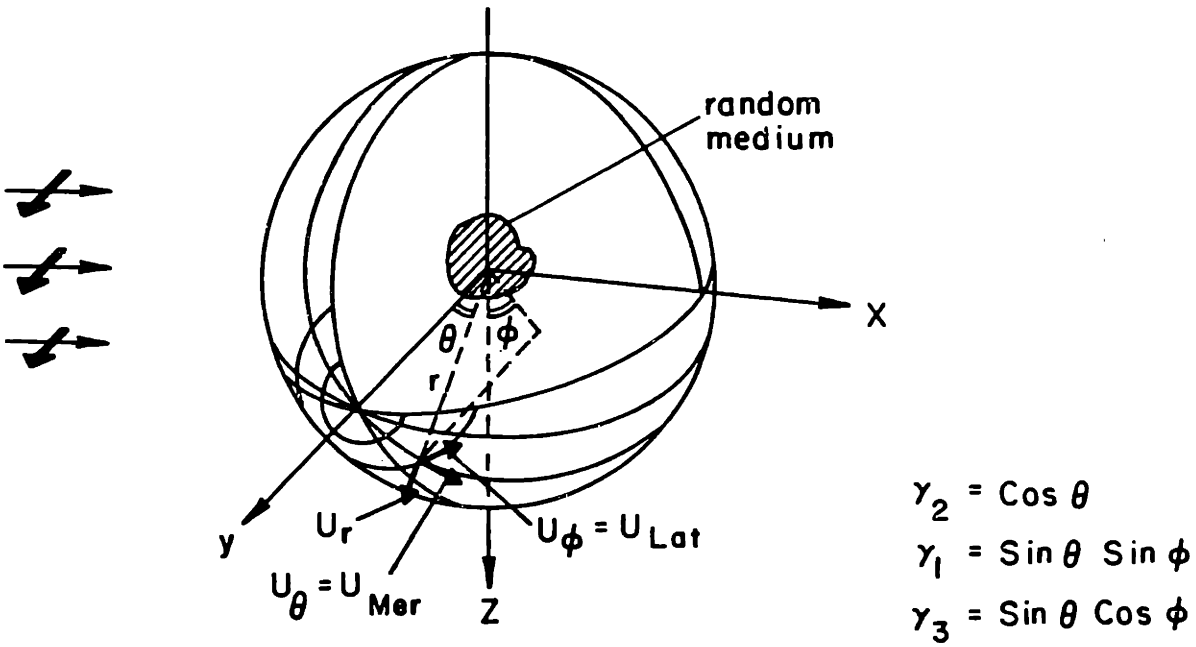

Figure 9. The spherical coordinate system for S wave incidence.

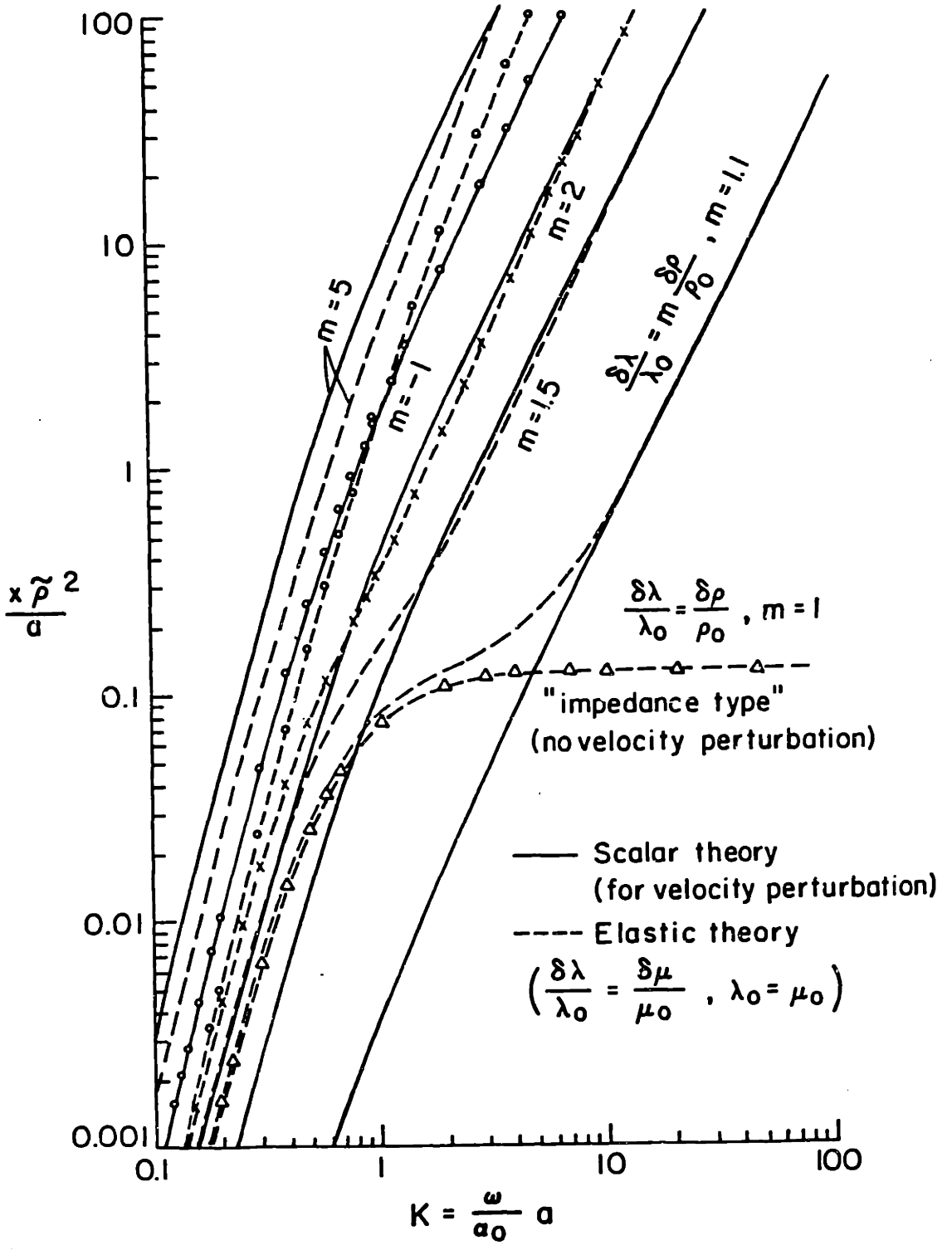

Figure 10. Frequency dependences of P-P scattering coefficient.

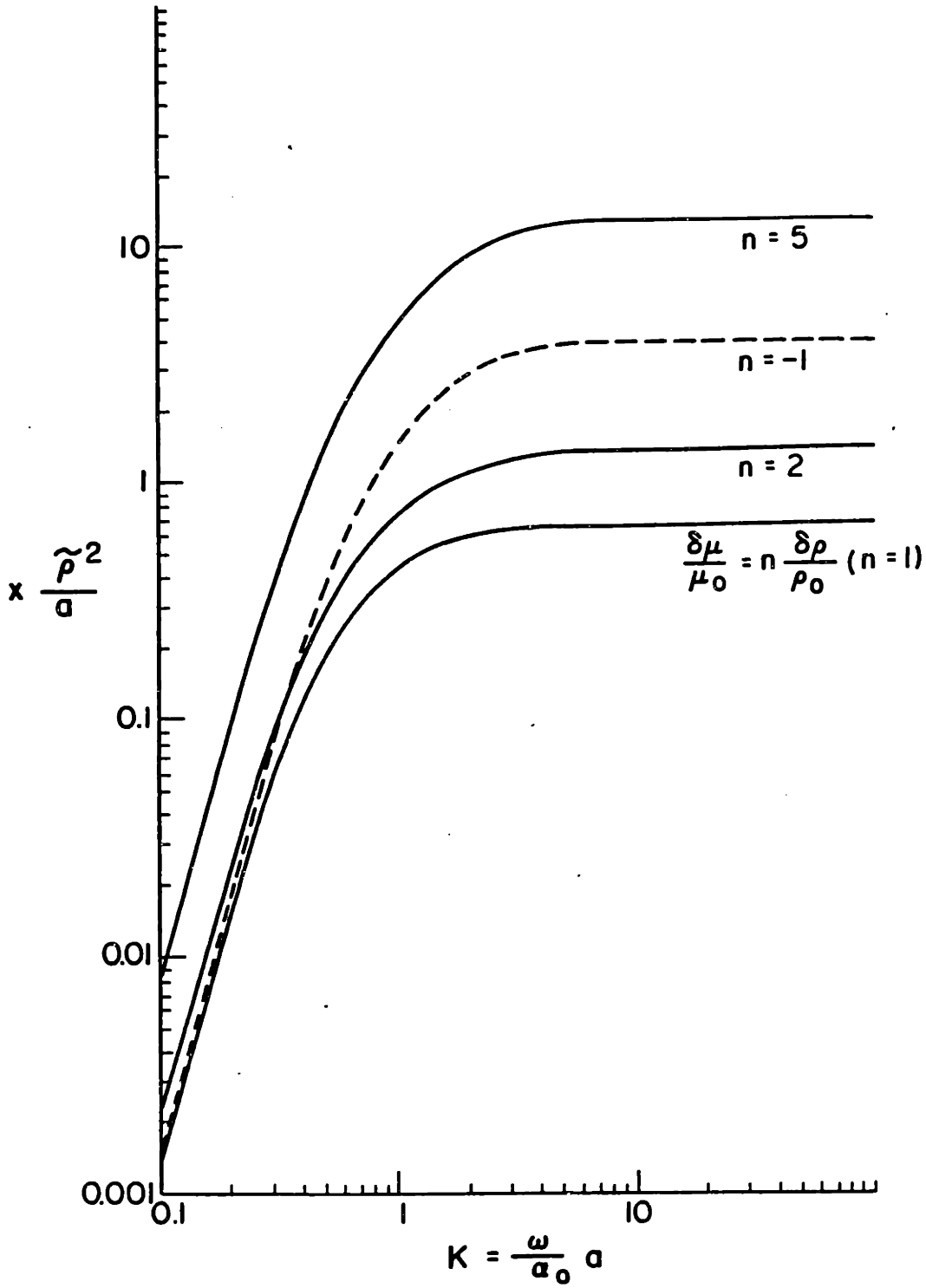

Figure 11. Frequency dependences of P-S scattering coefficient.

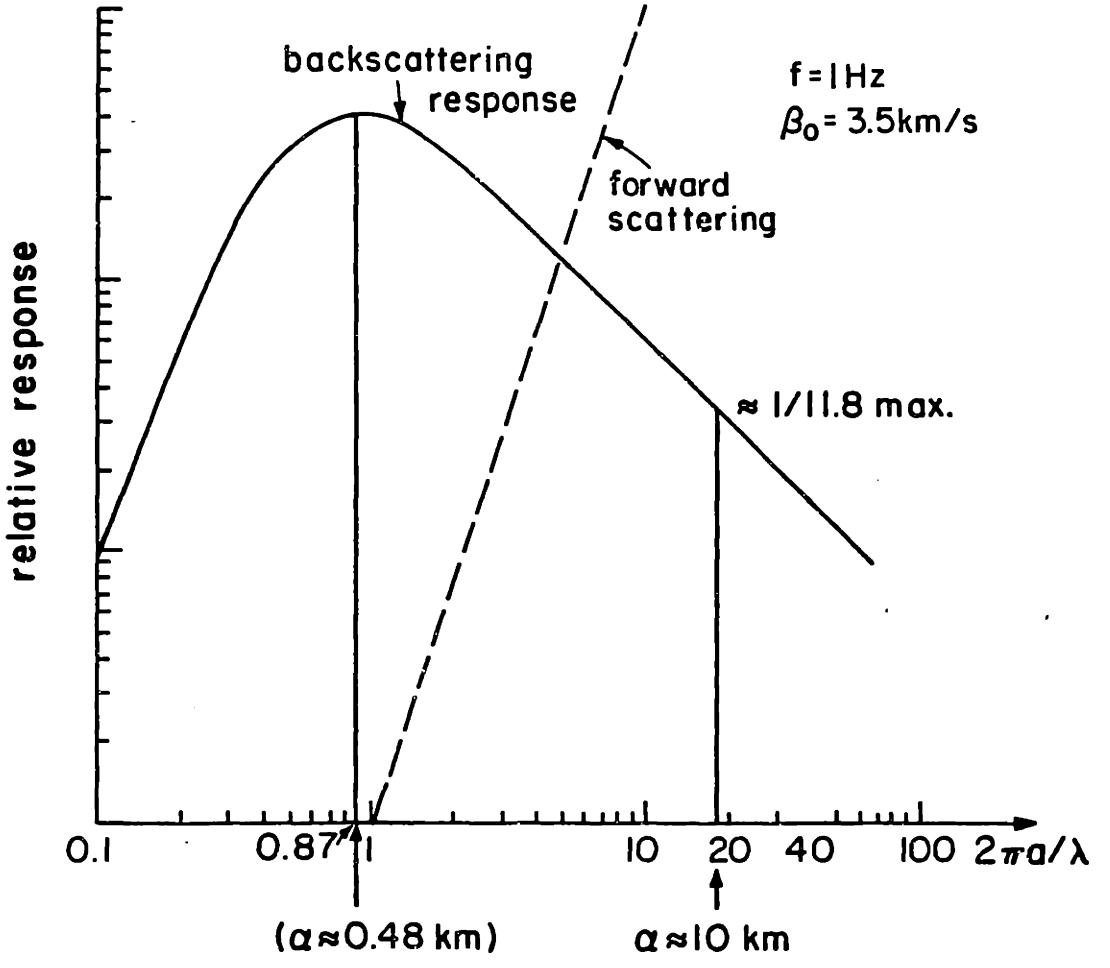

Figure 12. Backscattering responses of inhomogeneities with different correlation lengths for 1 Hz wave.

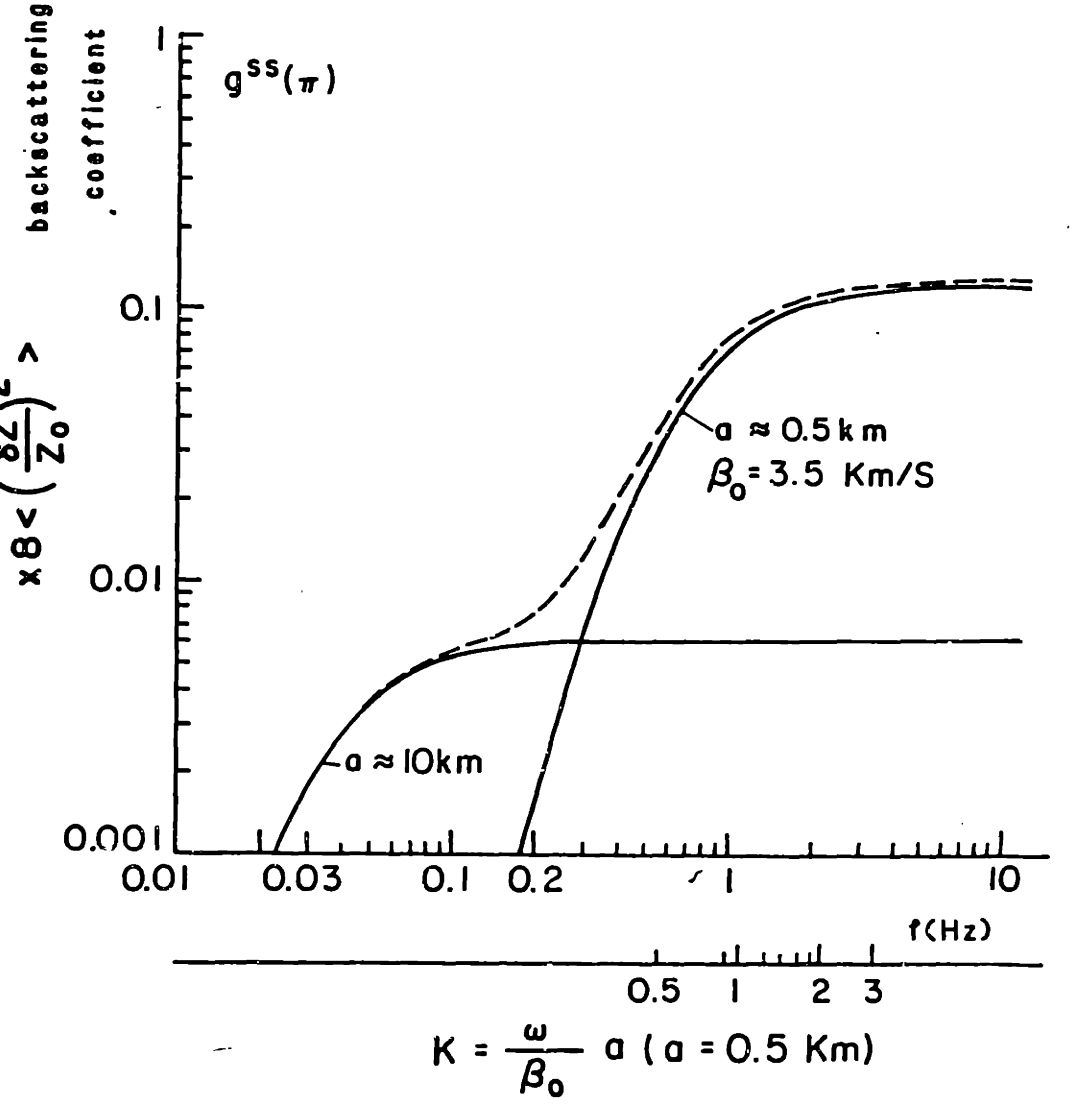

Figure 13. Frequency dependences of backscattering coefficient for inhomogeneities with correlation length a = 10 km and a = 0.5 km.

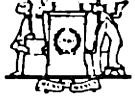

Chapter 4

MULTIPLE SCATTERING AND ENERGY TRANSFER OF SEISMIC WAVES AND THE APPLICATION OF THE THEORY TO HINDU KUSH REGION

Abstract

In order to separate the scattering effect from the intrinsic attenuation, we need a multiple scattering model for the seismic wave propagation in random heterogeneous media. In this paper, we apply the radiative transfer theory to seismic wave propagation and formulate in frequency domain the energy density distribution in space for a point source. We consider the cases of isotropic scattering and strong forward scattering. Some numerical examples are shown. It is seen that the energy density - distance curves have quite different shapes depending on the values of medium seismic albedo $B_o = \eta_s/(\eta_s+\eta_a)$, where η_s is scattering coefficient and η_a is the absorption coefficient of the medium. For high albedo ($B>0.5$) medium, the energy-distance curve is of arch shape and the position of the peak is a function of extinction coefficient of the medium $\eta_e = \eta_s + \eta_a$. Therefore we can separate the scattering and the absorption based on the measured energy density distribution curves.

We also discuss the approximate solutions in time domain: the single scattering approximation and the diffusion approximation. We apply the formulas of diffusion approximation for an arbitrary non-isotropic scattering function to the coda envelope and discuss its relation with the frequency domain solution.

The data from the digital recordings in Hindu Kush region are used as an example of application of the theory. From the derived energy density distribution curves and the discussion on the envelope shapes of the digitally filtered seismograms, we conclude that, in the frequency range 1.5 Hz to 20 Hz, scattering is not the dominant factor in the measured apparent attenuations, i.e. $B_o < 0.5$ in the Hindu Kush region for this frequency range. Due to the insensitivity of the shape of the energy-distance curve for the case $B_o < 0.5$ and the fluctuations of the data, we are not able to obtain the

precise B_o values. Some interesting phenomena at low frequencies (<1.5 hz) and high frequencies (>20 Hz) need to be studied further.

The results obtained in this paper imply a frequency dependent Q. The possible attenuation mechanisms are examined.

The tectonic implication of the results is also discussed. The fact that the high attenuatuion material extends to the depth below 200 km supports the concept of subducted continental crust (and lithosphere) in this region.

Multiple Scattering and Energy Transfer of Seismic Waves and Application of the Theory to Hindu Kush Region

1. INTRODUCTION

Are the measured apparent attenuations for short period seismic waves caused by anelasticity of the media or by scattering of the heterogeneities in the media? Is the single backscattering model a good approximation to the coda envelope decay or do we need a multiple scattering model which will have significant differences in describing the coda behavior from the single backscattering theory? These are long-standing problems. In order to answer these questions, we need to develop certain multiple scattering model for seismic waves and compare the predictions from it with those obtained from the single scattering theory. O'Doherty and Anstey (1971) derived a one-dimensional multiple scattering formulae for a stack of thin layers as

$$|T(\omega)| = e^{-R(\omega)t} , \qquad (1.1)$$

where ω is the angular frequency of the wave, $t = N\tau$ is the travel time of passing through the stack, τ is the travel time for each layer and N is the number of the layers; $T(\omega)$ is the transmission response and $R(\omega)$ is the power spectrum of the reflection coefficient series normalized by the travel time. The exponential form of (1.1) itself exhibits the indiscriminability of the multiple scattering effect from the intrinsic absorption, if we observe only the decay of the transmitted waves. Richards and Menke (1983) did some numerical experiments on this model and discussed some possibilities of using the relation between amplitude spectra and phase spectra, the frequency contents of the coda and that of the main arrival etc. to distinguish the multiple scattering effects of thin layers from the intrinsic attenuation. We note that the formulation of the problem by O'Doherty and Anstey is essentially that of the random slab problem (see Kay and Silverman 1958, Hoffman 1964). The results are presented as the relations of transmitted or

reflected waves with the slab thickness, which do not necessarily represent the amplitude attenuation with distance or the envelope decay with time of seismic waves.

Kopnichev (1977) formulated the double and triple scattering for 2-D and 3-D media in the case of isotropic scattering. Gao et al. (1983, 1984) derived up to seventh order scattering and then obtained the approximate formulas of multiple scattering in time domain for 2-D and 3-D media using curve-fitting technique. However, the formulas derived are for the case in which the source and sensor are located in the same point. On the other hand, the most prominent evidences of multiple scattering would be manifested if the sensor could be situated at some place between the source and the point apart from the source by one mean-free-path of scattering (this will be shown later). Therefore it may be difficult to use these formulas for discriminating the scattering attenuation from the intrinsic attenuation, though the formulation may be very useful in other calculations.

In this paper, we derive the formulation of seismic energy transfer under multiple scattering by using the radiative transfer equation technique developed in the astrophysical optics and the neutron transport theory and explore the possibilities of using this approach to separate the scattering and intrinsic attenuation.

Historically, multiple scattering theory has been developed along two independent approaches: the analytic theory and the transport theory (for review see Ishimaru 1977). Both are based on the statistical treatment of wave propagation in random media. Because the complex heterogeneities are modeled with a random medium, the wavefields propagating therein are also random wavefields. We are interested only in some statistical quantities of the wavefield, such as the mean intensity, phase and amplitude fluctuations,

various correlation functions, pulse spreading, angular broadening, etc. All of these quantities can be obtained from the moments of the random field. The analytic theory starts with basic differential equations such as wave equations and, by introducing the scattering and absorption characteristics of the random heterogeneities, derives the differential or integro-differential equations for the moments of the wavefields. There are basically two branches in the analytic theory: the renormalization method and the small-angle approximation method. In the first branch the renormalization procedure was used for the formal perturbation series and the exact equation for the first moment (the mean field), known as the Dyson equation, and for the second moment (the correlation function), the Bethe-Salpeter equations were derived. These equations are exact in the sense that the multiple scattering of all orders, as well as the diffraction and interference effect are all included in the equations. However, since the operator involved in these equations are in the form of infinite series, there is no solution available at present. Approximations have to be made to the operator before some practical solutions can be obtained. The most widely used approximation is the first order smoothing approximation as called by Frisch (1968) (see also Ishimaru 1978, v. 2), in which the local Born approximation of the fluctuating field (or equivalently the Bilocal approximation to the mean field) is applied to the Dyson equation and the ladder approximation is applied to the Bethe-Salpeter equation. These approximations can be obtained by either the Feynman diagram method or the Bogoliubov smoothing method in the operator form (Frish 1968, Tatarskii 1971, Ishimaru 1978; for the various names of the first order smoothing approximation, see also Wu 1982b, footnote 2). The justification for the use of this approximation has been clarified by Frisch (1968) by introducing the generalized Reynolds number. The basic physical condition for

the valid use of the approximation is the scattered field within a correlation length being weak compared with the incident field. In the case of large scale inhomogeneities, Fante (1982) has shown that a sufficient condition for applying the ladder approximation is the mean free path for multiple scattering being large in comparison with the correlation length of the medium. This condition is usually satisfied in the context of seismic wave scattering in the lithosphere. The first order smoothing approximation to the Dyson equation and Bethe-Salpeter equation can be shown (Frisch 1968) to be equivalent to the Foldy-Twersky system of equations, which have been developed independently for discrete random media, i.e. the media with randomly distributed scatterers. There are still no general solutions for these equations and further approximations are needed to put them into practical use. For small size inhomogeneities, there are some general solutions for the mean field, but no useful results for the second moments (Tatarski 1971, §61, Ishimaru 1978, ch. 14). It has been shown that the first order smoothing approximation of the Dyson and Bethe-Sapeter equations can lead to a radiative transfer equation for the specific intensity which is the 3D spatial Fourier transform of the spatial correlation function of the wavefield when the correlation function is a slowly varying function in space (Barabanenkov 1969, 1971, Tatarskii 1971, §63, Ishimaru 1975, 1978). Similarly, a generalized radiative transfer equation can be derived for the frequency correlation function (Ishimaru 1978). Thereby the link has been established between the analytic theory and the transport theory.

The second branch of the analytic theory includes all the small-angle-scattering methods. Because of the small scattering angle approximation or forward-scattering approximation, the basic starting point of the method is the parabolic wave equation. There are two approaches: parabolic equation

approach and Feynman path integral approach. Tatarskii applies the Markov approximation to the parabolic wave equation, so the theory of Markov process can be used to the study of the problem (Tatarskii 1971). Uscinski, on the other hand, uses the plane wave decomposition and phase-screen technique to the parabolic wave equation (Uscinski 1977). At present, the parabolic equation methods can have only approximate solutions for up to the fourth moment equations. The path-integral approach starts with the Feynman path-integral representation of the parabolic wave equation and makes use of the small scattering-angle approximation and Markov approximation (Dashen 1977, Flatte et al., 1979). It can obtain solutions for any higher order moments for the Gaussian statistics. Flatte et al. have applied this approach to the ocean acoustics and obtained the expressions for phase and intensity fluctuations, various correlations and pulse wandering and spreading etc.

The transport theory (or radiative transfer theory) is a phenomenological approach. It does not start with the wave equation, but deals directly with the energy transport process. Therefore, only energy or intensity arithmetic appears in the theory and no wave interference is considered. This treatment much simplifies the mathematics. Historically it appeared earlier than the analytic theory, and has its root from Boltzmann's equations in the kinetic theory of gases and in the neutron transport theory. It was introduced into astrophysical optics by Schuster (1905), Chandrasekhar (1950) and others and is now widely used in the multiple scattering treatment in the astrophysical optics, ocean acoustics, neutron transport theory, electromagnetic wave remote sensing, marine biology, etc. (Chandrasekhar 1950, Sobolev 1963, Menzel 1966, Davison 1958, Bell and Glasstone 1970, Flatte 1979, Kong et al. 1984, Jerlov 1976). This approach also has its shortcomings. It can only deal with the second moments, it does not account for the diffraction and interference

phenomena. However, there are some new developments recently, which incorporate some wave interference effects into the radiative transfer equation. For example, in deriving the transfer equations from the Bethe-Salpeter equation, beside the ladder terms (which alone will lead to the regular intensity transfer equation), the cyclical diagrams are also included, resulting in a modified radiative transfer equation, which can account for the backscattering enhancement due to the constructive interference effect caused by the double passage of the backscattered waves (Zuniga et al. 1980). So-called "wave radiative transfer theory" based on the second order approximations to the Bethe-Salpeter equation is also under development (Tsang and Ishimaru 1983).

For the coda envelopes or coda energy problems of local earthquakes, it is apparently a wide-angle scattering problem, so that the transport theory is probably the most effective method to treat it at present. In this paper we use the frequency domain formulation mainly from the neutron transport theory and the electromagnetic wave propagation (Davison 1958, Liu and Ishimaru 1974, Fante 1973, Ishimaru 1978) to the energy density decay with distance of the seismic waves from local earthquakes, and discuss the possibility of using the decay curves to evaluate the relative strengths of the intrinsic absorption and the scattering coefficient of the medium in the region studied. Some examples are given for the Hindu-Kush region. The results and their geophysical meaning are also discussed.

2. DEFINITIONS AND NOTATIONS

It is difficult to keep all the notations and terminology in radiative transfer theory without causing ambiguities and contradictions with the traditional notation and terminology in seismology, when the theory is introduced into seismology. I will basically follow Ishimaru (1978) and make some necessary changes to keep the notations self-consistent.

$I(\underline{r},\hat{\Omega})$: Specific intensity or directional intensity. It is the most fundamental quantity in transport theory. It gives the power flowing within a unit solid angle in the direction $\hat{\Omega}$, here $\hat{\Omega}$ is the unit vector, emanated from a unti area perpendicular to $\hat{\Omega}$, in a unit frequency band. The specific intensity is defined for a frequency ω, which is omitted in the notation.

In this paper we consider the S wave and its coda for small local earthquakes. Since the P wave energy is much smaller than the S wave energy for a double-couple point source which is the source model for small earthquakes, we consider here $I(\underline{r},\hat{\Omega})$ as only the S wave energy by neglecting the mode converted energy from P waves. We assume here also that the wave energy described by $I(\underline{r},\hat{\Omega})$ is depolarized, i.e. the energy is equally partitioned between the two orthogonal components of S waves. This agrees generally with the observations. Because of the free surface reflection and the scattering by heterogeneities, the S waves from a double-couple source get quickly depolarized. From the results of this paper, the energy density decay curves for the two orthogonal components are very similar to each other, which further validate the assumptions.

In order to measure the specific intensity (or directional intensity), we need strongly directional sensors, which are not available in the seismological practice. Therefore the specific intensity is not the quantity measured in practice, but is the important concept and quantity for theoretical derivations.

$\bar{I}(\underline{r})$: Average intensity, defined by

$$\bar{I}(\underline{r}) = \frac{1}{4\pi} \int_{4\pi} I(\underline{r},\hat{\Omega}) d\Omega, \tag{2.1}$$

is the intensity at point $\underline{r}$ averaged over all directions.

$E(\underline{r})$: Energy density, defined by

$$E(\underline{r}) = \frac{1}{C}\int_{4\pi} I(\underline{r},\hat{\Omega})d\Omega = \frac{4\pi}{C}\bar{I}(\underline{r}) \quad . \tag{2.2}$$

where C is the wave velocity.

$\underline{J}(\underline{r})$: Flux density vector, defined by

$$\underline{J}(\underline{r}) = \int_{4\pi} I(\underline{r},\hat{\Omega})\hat{\Omega}d\Omega \quad . \tag{2.3}$$

The net flux density in a particular direction $\hat{\Omega}_o$ is defined as $\hat{\Omega}_o \cdot \underline{J}(\underline{r})$. It is the net power transferred along the $\hat{\Omega}_o$ direction across a unit area perpendicular to $\hat{\Omega}_o$. In this paper, we also use the notation for the energy flux density, i.e. the power flux density divided by the wave velocity c.

$S(\hat{\Omega},\hat{\Omega}_o)$: Scattering intensity function of a random medium, which is related to the single scattering amplitude $f(\hat{\Omega},\hat{\Omega}_o)$ of an elementary volume dV of the inhomogeneous medium by

$$S(\Omega,\Omega_o) = \frac{\langle |f(\hat{\Omega},\hat{\Omega}_o)|^2 \rangle}{dV}, \tag{2.4}$$

where $\langle\ \rangle$ denotes taking ensemble average. $S(\hat{\Omega},\hat{\Omega}_o)$ gives the scattered power in $\hat{\Omega}$ direction within a unit solid angle by a unit volume of the random medium for a unit flux density of incident wave in $\hat{\Omega}_o$ direction.

In this paper we will give a unified treatment for both the discrete and the continuous random media. For a discrete random medium composed of randomly distributed scatterers, $S(\hat{\Omega},\hat{\Omega}_o)$ is defined by the scattering characteristics of individual scatterers; while in the case of random continua, we can choose the volume elements small enough so that we can derive the single scattering amplitude $f(\hat{\Omega},\hat{\Omega}_o)$ by the Born approximation.

$g(\hat{\Omega},\hat{\Omega}_o)$: Directional scattering coefficient, defined by

$$g(\hat{\Omega},\hat{\Omega}_o) = 4\pi S(\hat{\Omega},\hat{\Omega}_o) \ . \tag{2.5}$$

for the definition and the derivation for elastic random media, see paper II (Wu and Aki, 1984b).

$\eta_s \equiv g$: Scattering coefficient of the medium defined by

$$\eta_s = \int_{4\pi} S(\hat{\Omega},\hat{\Omega}_o)d\hat{\Omega} = \frac{1}{4\pi}\int_{4\pi} g(\hat{\Omega},\hat{\Omega}_o)d\hat{\Omega} \ , \tag{2.6}$$

which gives the total power loss due to scattering by a unit volume random medium per unit flux density of incident wave under the single scattering assumption.

$\eta_a \equiv b$: Absorption coefficient of the medium, which gives the power loss due absorption by a unit volume random medium per unit flux density of incident wave.

η_e: Extinction coefficient of the medium, defined by

$$\eta_e = \eta_a + \eta_s \tag{2.7}$$

$\ell_o \equiv a$: Correlation length of the random medium.

$L_e = 1/\eta_e$: Extinction length of the medium.

$L_a = 1/\eta_a$: Absorption length of the medium. (2.8)

$L_s = 1/\eta_s$: Scattering length or scattering mean free path of the medium.

D_e: Numerical extinction distance, which is called "optical distance" in optics.

D_a: Numerical absorption distance,

D_s: Numerical scattering distance, defined by

$$\begin{aligned} D_e &= r/Le, \\ D_a &= r/La, \\ D_s &= r/L_s, \end{aligned} \tag{2.9}$$

where r is the travel distance.

B_o: Medium seismic albedo, defined by

$$B_o = \frac{\eta_s}{\eta_e} = \frac{\eta_s}{\eta_s+\eta_a} . \tag{2.10}$$

$D(\hat{\Omega},\hat{\Omega}_o)$: Scattering directivity, defined by

$$D(\hat{\Omega},\hat{\Omega}_o) = \frac{g(\hat{\Omega},\hat{\Omega}_o)}{\eta_s} = \frac{4\pi S(\hat{\Omega},\hat{\Omega}_o)}{\eta_s} \tag{2.11}$$

It is the normalized directional scattering coefficient, and satisfies

$$\frac{1}{4\pi}\int_{4\pi} D(\hat{\Omega},\hat{\Omega}_o) = 1, \tag{2.12}$$

that means its average over all the directions is equal to unit. In the case of isotropic scattering

$$D(\hat{\Omega},\hat{\Omega}_o \equiv 1 . \tag{2.13}$$

Its relation with the "phase function" in the radiative transfer theory (Chandrasekhar 1950, Ishimaru 1978) is

$$D(\hat{\Omega},\hat{\Omega}_o) = B_o p(\hat{\Omega},\hat{\Omega}_o) . \tag{2.14}$$

$p(\hat{\Omega},\hat{\Omega}_o)$: Phase function (see 2.14).

In the case of a discrete random medium having statistically uniformly distributed random scatterers with number density n, we have

$\sigma_d(\hat{\Omega},\hat{\Omega}_o)$: Differential (or directional) scattering cross-section of the scatterers.

$$S(\hat{\Omega},\hat{\Omega}_o) = n\sigma_d(\hat{\Omega},\hat{\Omega}_o). \tag{2.15}$$

σ_s: Scattering cross-section of the scatterers, defined by

$$\sigma_s = \int_{4\pi} \sigma_d(\hat{\Omega},\hat{\Omega}_o)d\Omega \tag{2.16}$$

σ_a: Absorption cross-section of the scatterers.

$\sigma_t=\sigma_s+\sigma_a$: Total cross-section of the scatterers.

η_h: Absorption coefficient of the host medium.

$$\eta_s = n\sigma_s, \tag{2.16}$$

$$\eta_a = n\sigma_a+\eta_h, \tag{2.17}$$

$$D(\hat{\Omega},\hat{\Omega}_o) = \frac{4\pi\sigma_d(\hat{\Omega},\hat{\Omega}_o)}{\sigma_s} \tag{2.18}$$

B_1: Scatterer albedo, defined by

$$B_1 = \frac{\sigma_s}{\sigma_s+\sigma_a} = \frac{\sigma_s}{\sigma_t} . \tag{2.19}$$

Therefore,

$$B_o = \frac{\eta_s}{\eta_s+\eta_a} = \frac{n\sigma_s}{n\sigma_s+n\sigma_a+\eta_h} = \frac{n\sigma_s}{n\sigma_t+\eta_h} . \tag{2.20}$$

When $\eta_h << n\sigma_t$, we have

$$B_o \approx \frac{\sigma_s}{\sigma_t}\left(1-\frac{\eta_h}{n\sigma_t}\right) = B_1\left(1-\frac{\eta_h}{n\sigma_t}\right) . \tag{2.21}$$

For a perfect scattering medium $B_o = 1$.

3. ENERGY DENSITY DISTRIBUTION IN THE CASE OF ISOTROPIC SCATTERING

Knowing the extinction coefficient and scattering coefficient of the medium η_e, η_s and the scattering directivity $D(\hat{\Omega},\hat{\Omega}_o)$ or the scattering intensity function of the medium $S(\hat{\Omega},\hat{\Omega}_o)$ defined by (2.6), (2.7), (2.11) and (2.4), we can obtain the differential equation for the specific intensity $\underline{I}(\underline{r},\hat{\Omega})$, the "equation of transfer" (Chandrasekhar 1950, I, Ishimara 1978, ch. 7):

$$\frac{dI(\underline{r},\hat{\Omega})}{d\ell} = -\eta_e I(\underline{r},\hat{\Omega}) + \int_{4\pi} S(\hat{\Omega},\hat{\Omega}_o) I(\underline{r},\hat{\Omega}_o) d\Omega_o + W(\underline{r},\hat{\Omega})$$

$$= -\eta_e I(\underline{r},\hat{\Omega}) + \frac{\eta_s}{4\pi} \int_{4\pi} D(\hat{\Omega},\hat{\Omega}_o) I(r,\hat{\Omega}_o) d\Omega_o + W(r,\hat{\Omega}) , \qquad (3.1)$$

where $W(\underline{r},\hat{\Omega})$ is the source intensity function, which defines the amount of power emitted from the sources into the direction $\hat{\Omega}$ per unit solid angle. In (3.1), $d\ell$ is the length of a cylindrical elementary volume of unit cross section in the medium with the axis of the cylinder in $\hat{\Omega}$ direction (Fig. 3.1). Therefore the left hand side of (3.1) represents the total change of the specific intensity for a unit travel distance. The first term in right hand side of (3.1) is the loss of power in $\hat{\Omega}$ direction due to absorption and scattering, whereas the second term gives the gain of power in that direction from the scattered waves for the incident intensity from all directions and the third term is the energy supply from the sources. No general analytic solutions are available for (3.1). Some methods such as the Gauss-quadrature can be used to obtain the numerical solutions for a general scattering function. Let us first consider the simplest case of isotropic scattering. In this case the scattering directivity $D(\hat{\Omega},\hat{\Omega}_o) \equiv 1$. Integrating (3.1) over all directions $\hat{\Omega}$, we obtain equation for the average intensity $\bar{I}(\underline{r})$ or the

energy density $E(\underline{r})$ (2.2)

$$\frac{dE(\underline{r})}{d\ell} = -\eta_e E(\underline{r}) + \frac{1}{C}\int_{4\pi}\left[\frac{\eta_s}{4\pi}\int_{4\pi} I(\underline{r},\hat{\Omega}_o)d\Omega_o + W(\underline{r},\hat{\Omega})\right]d\Omega$$

$$= -\eta_e E(\underline{r}) + Q(\ell), \tag{3.2}$$

where C is the wave velocity. (3.2) is in a form of first order differential equation, in which the second term in RHS is the source term

$$Q(\ell) = \frac{1}{C}\int_{4\pi}\left[\frac{\eta_s}{4\pi}\int_{4\pi} I(\underline{r},\hat{\Omega}_o)d\Omega_o + w(\underline{r},\hat{\Omega})\right]d\Omega \ . \tag{3.3}$$

The general solution for (3.2) is

$$E(\underline{r}) = Ae^{-\eta_e \ell} + \int_o^{\ell} Q(\ell_1)e^{-\eta_e(\ell-\ell_1)}d\ell_1 \ , \tag{3.4}$$

where A is a constant.

The energy density (3.4) is composed of two terms. The first term is a simple exponential decay with the extinction coefficient η_e as its attenuation coefficient; this is the coherent energy density E_c or "reduced energy density" (Ishimaru 1978). The second term is therefore the diffuse energy density E_d which is produced by scattering. Applying the initial condition

$$E(\underline{r}_o) = E_{in}, \tag{3.5}$$

where E_{in} is the incident energy, we get

$$E(\underline{r}) = E_c(\underline{r}) + E_d(\underline{r})$$

$$E_c(\underline{r}) = E_{in}\, e^{-\eta_e \ell}$$

$$E_d(\underline{r}) = \int_o^{\ell} Q(\ell_1)e^{-\eta_e(\ell-\ell_1)}\, d\ell_1$$

$$= \frac{1}{C}\int_o^{\ell}\int_{4\pi}\left[\frac{\eta_s}{4\pi}\int_{4\pi} I(\underline{r},\hat{\Omega}_o)d\Omega_o + W(\underline{r},\hat{\Omega})\right]e^{-\eta_e(\ell-\ell_1)}d\Omega d\ell_1 \ . \tag{3.6}$$

In order to calculate the diffuse term (3.8), we need to know the intensity $I(\underline{r},\hat{\Omega}_o)$ which is related to the total energy density. Therefore (3.8) is in the form of integral equation. To carry out the integration with respect to $\hat{\Omega}$, we note that, the intensity gain in the direction $\hat{\Omega}$ within $d\Omega$ are contributed from the intensity of all the volume elements dV_1 at $\underline{r}_1$ within the elementary solid angle, and

$$dV_1 = d\Omega |\underline{r}-\underline{r}_1|^2 d\ell_1 \quad . \tag{3.9}$$

Therefore (3.8) becomes

$$\underline{E}_d(\underline{r}) = \int_V [\eta_s \underline{E}(\underline{r}_1) + \frac{4\pi}{C} \underline{W}(\underline{r}_1,\hat{\Omega})] \frac{e^{-\eta_e|\underline{r}-\underline{r}_1|}}{4\pi|\underline{r}-\underline{r}_1|^2} dV_1 \quad . \tag{3.10}$$

The integration is over the volume of the random medium. The integral equation for the total energy density becomes (see also Ishimaru, 1978, ch. 12).

$$\underline{E}(\underline{r}) = \underline{E}_{in} e^{-\eta_e \ell} + \int_V [\eta_s \underline{E}(\underline{r}_1) + \underline{\varepsilon}(\underline{r}_1,\hat{\Omega})] \underline{\underline{G}}_o(\underline{r}-\underline{r}_1) dV_1 \quad , \tag{3.11}$$

where

$$\underline{\varepsilon}(\underline{r},\hat{\Omega}) = \frac{4\pi}{C} \underline{W}(\underline{r}_1,\hat{\Omega}) \tag{3.12}$$

is the source energy density function, and

$$\underline{\underline{G}}_o(\underline{r}-\underline{r}_1) = \frac{e^{-\eta_e R}}{4\pi R^2} = \frac{e^{-\eta_e|\underline{r}-\underline{r}_1|}}{4\pi|\underline{r}-\underline{r}_1|^2} \quad . \tag{3.13}$$

Integral equation (3.11) can also be derived from the first order smoothing approximation of the Dyson and Bethe-Salpeter equations (Lin and Ishimaru 1974).

From (3.11), the energy density $\underline{E}(\underline{r})$ is totally defined by the incident field, the source-function, and the volume of the random medium. For the problems of seismic coda waves of local earthquakes, the distances between the stations and the sources are short compared to the travel time of coda waves.

As the first approximation, we consider the problem of a point source located in an infinite randomly inhomogeneous medium. The effect of the free surface is like a mirror reflecting the half random space to a whole random space with the upper half space being the mirror image of the lower half space. The limited thickness of the lithosphere, which is supposed to be more heterogeneous than the asthenosphere beneath will have influence on the coda of later part. Further discussion about the limitation of the model will be given later in this paper.

In (3.11), suppose the incident field $E_{in} = 0$ and the point source is located at $\underline{r} = 0$, radiating the total power P_o. Then

$$\underline{\varepsilon}(\underline{r}) = \frac{P_o}{C}\,\underline{\delta}(\underline{r}) = E_o\underline{\delta}(\underline{r}) \tag{3.14}$$

The equation (3.11) becomes

$$\underline{E}(\underline{r}) = E_o\,\frac{e^{-\eta_e r}}{4\pi r^2} + \int_V \eta_s\,\underline{E}(\underline{r}_1)\,\frac{e^{-\eta_e|\underline{r}-\underline{r}_1|}}{4\pi|\underline{r}-\underline{r}_1|^2}\,dV_1$$

$$= E_o\,G_o(\underline{r}) + \int_V \eta_s E(\underline{r}_1)G_o(\underline{r}-\underline{r}_1)dV_1\ . \tag{3.15}$$

This is a Faltung type or convolution type integral equation (Tricomi 1957, Carrier et al. 1966), Fourier transform method can be used for solution. Assuming $E_o = 1$, the solution can be written as (see Davison 1958, Lin and Ishimaru 1974, Ishimaru 1978 (12-21))

$$E(r) = \frac{\eta_e P_d}{4\pi r}\exp(-\eta_e d_o r) + \frac{\eta_e}{4\pi r}\int_1^\infty f(s,B_o)\exp(-\eta_e rs)ds$$

$$= E_d(r) + E_c(r), \tag{3.16}$$

where

$$P_d = \frac{2\, d^2{}_o(1-d^2{}_o)}{B_o(d^2{}_o+B_o-1)}\ , \tag{3.17}$$

and d_o is the diffuse multiplier determined by

$$\frac{B_o}{2d_o}\, \ell n\, (\frac{1+d_o}{1-d_o}) = 1; \tag{3.18}$$

and

$$f(s,B_o) = \{[1-\frac{B_o}{s}\tanh^{-1}(\frac{1}{s})]^2 + (\frac{\pi}{2}\frac{B_o}{s})^2\}^{-1}\ . \tag{3.19}$$

The first term in (3.16) is the diffuse term E_d, which is attributed to the pole residue in the complex spatial frequency plane, and the second term, coherent term E_c is from the branch cut integration.

Fig. 3.2 shows the relation between the diffuse multiplier d_o and the medium albedo B_o. d_o is always less than 1. When distance r is large, especially for large B_o, the diffuse term becomes dominant (see also Fig. 9), and E(r) will be approximately an exponential decay with an apparent attenuation coefficient $d_o\eta_e$, which is less than the extinction coefficient η_e. The degree of reduction depends on the albedo B_o. The diffuse term can also be written as

$$E_d(r) = \frac{\eta_e P_d}{4\pi r}\exp[-(\eta_a+d_s\eta_s)r],$$

$$d_s = \frac{d_o-(1-B_o)}{B_o}\ . \tag{3.20}$$

d_s is a multiplier and $d_s\eta_s$ gives the effective contributions of the scattering coefficient to the apparent attenuations. d_s is also plotted in Fig. 2. Table 1 lists some values of d_o and a_s versus B_o.

The coherent term can also be written as

$$E_c(r) = \frac{\eta_e}{4\pi r} \int_0^1 f(\xi, B_o) \exp\left(\frac{\eta_e r}{\xi}\right) \frac{d\xi}{\xi^2} , \tag{3.21}$$

by setting $\xi = 1/s$ for the convenience of computation. Fig. 3.3 shows the behavior of the two factors of the integrand for different numerical extinction distances $D_e = \eta_e r$ and different medium albedo B_o. $\exp(-D_e/\xi)/\xi^2$ has a sharp peak for small D_e when ξ is small; whereas $f(\xi, B_o)$ is nearly singular for small B_o when ξ is close to 1. Therefore, in doing numerical integration, we used Romberger integration method for three separate segments to take care of the abrupt changes of the integrand at both ends of the interval. The Gauss-Legendre quadrature is also used to check the results. It turned out that the Gauss-Legendre quadrature of order 10 gives fairly good results.

In the following we will show some numerical results of the energy density distribution along the travel path from the source point. In the case of homogeneous media, the decay of energy density with distance is only due to geometric spreading. For a isotropic point source, the decay is $1/4\pi r^2$. Therefore, we normalize the distribution for inhomogeneous media (3.16) by the homogeneous distribution, i.e. multiply both sides of (3.16) with $4\pi r^2$,

$$E_n(r) = 4\pi r^2 E(r) = \eta_e P_d r \exp(-\eta_e d_o r) + \eta_e r \int_0^1 f(\xi, B_o) \exp\left(\frac{\eta_e r}{\xi}\right) \frac{d\xi}{\xi^2}$$

$$= D_e P_d \exp(-d_o D_e) + D_e \int_0^1 f(\xi, B_o) \exp(-D_e/\xi) \frac{d\xi}{\xi^2} , \tag{3.22}$$

where $E_n(r)$ stands for the normalized energy density distribution. Fig. 3.4 gives the results for different medium albedo B_o. The diffuse term and the coherent term are also plotted in the figure for comparison. The coherent term has little changes for different B_o, whereas the diffuse term varies dramatically with B_o, especially when $B_o>0.5$, i.e. when scattering is dominant. This gives the possibility of using the energy density decay curves to calculate the extinction coefficient η_e and the medium albedo B_o, hence to separate the absorption coefficient η_a and the scattering coefficient η_s. In the case of $B_o>0.5$, the diffuse term is dominant. There will be a peak on the E(r) curve, the position of the peak will depend on η_e and B_o of the medium. When $B_o<0.5$, the coherent term is dominant for $D_e<2$. Therefore the shape of the curve is not very sensitive to the change of B_o, so that the separation of scattering from absorption becomes difficult.

By assuming a point source with $E_o=1$, we get E(r) around the peak with values greater than 1, that need some explanation. As shown in Fig. 3.5, the normalized energy density $E_n(r) = 4\pi r^2 E(r)$ represents the energy received by the ring shell (hatched). In a homogeneous medium, if there is no absorption, the energy received will be equal to the source energy. In a scattering medium, the wave energy can go outward and inward across the shell. We denote the outward energy flux by F_r^+ and the inward energy flux by F_r^-. In the figure, we sketched one possible path of multiple scattering. No matter how complicated the path is and how long the time delay is compared to the direct path, the closed ring shell will eventually receive all the energy emitted by the source. There is no escape! Therefore, in this case the F_r^+ is equal to the total energy. However, the shell will also receive the inward scattered energy, so the total received energy $F_r^+ + F_r^-$ is greater than E_o. Of course the net energy flux $F_r^+ - F_r^-$ is always less than E_o. If there exists absorption,

the amount of received energy will depend on the energy balance between the absorption loss and the inward-scattering gain. Near the source, r is small, the ring shell has a small surface area for receiving the inward-scattered energy, so $E_n(r) \approx E_o$. When r increases, the surface area of the shell also increases, so that more inward-scattered energy can be received, resulting in the growth of $E_n(r)$. However, the absorption loss also grows with r due to the increase of the path length. Upon to some distance r, the growth rate of gain is equal to the growth rate of loss, the curve reaches its maximum. Beyond this distance, the absorption loss prevails.

Fig. 3.6 replots the curves of Fig. 4 in a semi-logarithm coordinate system. Fig. 7 and 8 plot some $E_n(r)$ curves for cases of constant absorption and constant scattering respectively. In this paper $b \equiv \eta_a$ $g \equiv \eta_s$. Fig. 3.7 shows the influence of different scattering coefficients on the energy density distribution curve of a constant absorption medium. The distance is normalized by the absorption length of the medium $L_a = 1/\eta_a$. It is seen from the figure that, for large distances compared with the absorption length of the medium, the decay of the energy density is nearly exponential with an apparent attenuation coefficient different from both the extinctions coefficient and the absorption coefficient. In the figure, b is the true absorption coefficient, $\hat{b}$ is the apparent attenuation coefficient measured from the slope of the curve. It can be seen that, for strong scattering ($B_o > 0.5$), the apparent attenuation is much bigger than the absorption coefficient but much smaller than the extinction coefficient (for $B_o = 0.9$, $\hat{b} = 4.5b = 0.45\ \eta_e$). For weak scattering ($B_o < 0.5$), the influence of scattering to the apparent attenuation is less appreciable. When $B_o \approx 0.5$, $\hat{b} = 1.62b$. On the other hand, for small absorption distance ($D_a < 1$), the shape of E(r) curve varies drastically depending on the values of B_o, which provides the

basis for the separation of scattering effect and the absorption effect. Fig. 3.8 in a similar way shows the influence of absorption on the E(r) curve of a constant scattering medium.

In order to compare the relative contributions of the diffuse term and the coherent term, we plot them on Fig. 3.9 and Fig. 3.10 with the distance normalized by the extinction length L_e and scattering length L_s respectively.

Now, we will derive the radial energy flux density $J_r(r)$. We know the energy conservation relation (see Ishimaru 1978, (7.28))

$$\underline{\underline{\text{div}}}\ \underline{\underline{J}}(r) = -\frac{\eta_a}{C}\int_{4\pi} \underline{\underline{I}}(r,\hat{\Omega})d\Omega + \frac{1}{C}\int_{4\pi} \underline{\underline{W}}(r,\hat{\Omega})d\Omega, \tag{3.23}$$

where $\underline{J}(\underline{r})$ is the energy flux density vector, C is the wave velocity and $W(\underline{r},\hat{\Omega})$ is the source intensity. For isotopic scattering in the source free region

$$\text{div}\ \underline{J}(\underline{r}) = \eta_a E(r). \tag{3.24}$$

In view of the spherical symmetry, there is no transverse component of $\underline{J}(\underline{r})$, therefore (3.24) becomes

$$\underline{\underline{\text{div}}}\ \underline{\underline{J}}(r) = \frac{1}{r^2}\frac{\partial}{\partial r}(r^2 J_r) = -\eta_a E(r)\ . \tag{3.25}$$

Then

$$J_r = -\frac{\eta_a}{r^2}\int_0^r E(r)r^2dr = \frac{\eta_a}{r^2}\int_r^\infty E(r)r^2dr \tag{3.26}$$

Normalizing J_r by the homogeneous case, we get

$$J_{nr}(r) = 4\pi r^2 J_r(r) = \eta_a \int_r^\infty 4\pi r^2 E(r)dr = \eta_a \int_r^\infty E_n(r)dr\ . \tag{3.27}$$

Substituting (3.22) into (3.27) yields

$$J_{nr}(r) = 4\pi r^2 J_r(r)$$

$$= (1-B_o)\{\frac{P_d}{d_o}(D_e+\frac{1}{d_o})\exp(d_o D_e) + \int_o^1 f(\xi,B_o)(1-\frac{D_e}{\xi})\exp(-D_e/\xi)d\xi \qquad (3.28)$$

Fig. 3.11 and 3.12 give some numerical results with the distance normalized by the extinction length and by the absorption length respectively, together with the results for the forward scattering approximation (see next section). It can be seen that the radial net flux is always smaller than the source energy E_o. However, the radial energy flux is difficult to measure in the practice of seismology. The reason is the difficulty of separating the inward and outward energy flow. Nevertheless, the comparison between E(r) and $J_r(r)$ helps us understand the multiple scattering process.

4. STRONG FORWARD SCATTERING: THE CASE OF LARGE SCALE INHOMOGENEITIES

From the analysis of coda generations for local earthquakes, we conclude that the lithosphere in tectonically active regions may be rich in small scale heterogeneities (less than 1 km) (paper II). On the other hand, by measuring the phase and amplitude fluctuations in large seismic arrays as LASA and NORSAR, large scale velocity inhomogeneities (10-20 km) underneath the arrays were revealed (Aki 1973, Capon 1974, Berteusson et al. 1975). Therefore, the lithosphere may have multi-scale inhomogeneities. For short period seismic waves (around 1 Hz), the scattering by the small scale heterogeneities may be in the Rayleigh and Mie scattering region. From the elastic scattering pattern (paper I, II), we may approximately use the isotropic scattering approximation. However, for the large scale velocity inhomogeneities, the forward scattering is dominant. The energy density distribution with distance will be quite different from the case of isotropic scattering. Since most of the scattered energy is concentrated in the forward direction within a small cone, the focussing and defocussing, diffraction interference phenomena become important. Most of the scattered energy arrives at the receiver point with much shorter travel paths, so that the energy delay due to scattering is much less severe than the case of isotropic scattering. From a reasoning similar to that in Fig. 3.5, we can see that, the normalized energy density decay curve will not have a peak of value greater than 1. Because the inward scattered energy is much less than the outward scattered energy, the energy density which is $J_r^+ + J_r^-$, where J_r^+ and J_r^- is the outward and inward radial energy flux respectively, will have no too much difference from the net energy flux $Jr = J_r^+ - J_r^-$. In the following, let us examine what can be obtained from the theory available in transport theory.

Fante (1973) has solved the transport equation under the forward scattering approximation, and Ishimaru (1978, ch. 13) has a lucid derivation and discussion on it. Here we only draw some main threads for understanding. Since

$$\frac{dI(\underline{r},\hat{\Omega})}{d\ell} = \hat{\Omega}\cdot\text{grad } I(\underline{r},\hat{\Omega}), \tag{4.1}$$

where $d\ell$ is the length of an elementary segment in $\hat{\Omega}$ direction (Fig. 3.1), the transport equation (3.1) can be written as

$$\hat{\Omega}\cdot\text{grad}I(\underline{r},\hat{\Omega}) = -\eta_e I(\underline{r},\hat{\Omega})+\eta_s \int_{4\pi} D(\hat{\Omega},\hat{\Omega}_o)I(\underline{r},\hat{\Omega}_o)d\Omega_o+w(\underline{r},\hat{\Omega}) . \tag{4.2}$$

Because the scattered energy is mostly confined within a small angle in the forward direction, we choose the z-axis of the cartesian coordinates as this direction, and approximate (4.2) through the following steps.

$$\hat{\Omega} = l\hat{x} + m\hat{y} + n\hat{z} , \tag{4.3}$$

where x, y and z are the unit vectors in x, y and z-axis respectively, and l,m,n, the corresponding direction cosines. In the spherical coordinate system with z-axis as its polar axis (Fig. 4.1)

$$l = \sin\theta\cos\phi,\ m = \sin\theta\sin d,\ n = \cos\theta . \tag{4.4}$$

Because the angle with z-axis θ is always small, we have approximations

$$n = \cos\theta \approx 1$$

$$d\Omega \approx nd\Omega = dldm = d\underline{s},$$

$$\int_{4\pi} d\Omega \approx \int_{-\infty}^{\infty} dl \int_{-\infty}^{\infty} dm = \int d\underline{s},$$

$$\hat{\Omega}\cdot\text{grad } I(\underline{r},\hat{\Omega}) \approx \frac{\partial}{\partial z}I(z,\underline{\rho},s)+\underline{s}\cdot\nabla_t I(z,\underline{\rho},s), \tag{4.5}$$

where

$$\underline{r} = x\hat{x}+y\hat{y}+z\hat{z} = \underline{\rho} + z\hat{z},$$

$$\underline{r} = l\hat{x}+m\hat{y}, \quad \nabla t = \frac{\partial}{\partial x}\hat{x}+\frac{\partial}{\partial y}\hat{y} . \tag{4.6}$$

Note that $\underline{s}$ is not a unit vector. Because θ is a small angle, the magnitude of $\underline{s}$ is much smaller than 1.

By these approximations (4.2) becomes

$$\frac{\partial}{\partial z} I(z,\underline{\rho},\underline{s}) + \hat{s}\cdot\nabla_t I(z,\underline{\rho},\underline{s})$$

$$= -\eta_e I(z,\underline{\rho},\underline{s}) + \frac{\eta_s}{} \int\int_{-\infty}^{\infty} D(\underline{s}-\underline{s}')I(z,\underline{\rho},\underline{s}')d\underline{s}'+W(z,\underline{\rho},\underline{s}) . \tag{4.7}$$

here $D(\hat{\Omega},\hat{\Omega}_o)$ is assumed only as a function of $\hat{\Omega}-\hat{\Omega}_o$. Since most of the energy is confined within a small angle with z-axis, the integration limits for l and m are extended to $\pm\infty$ without introducing any significant change.

Again (4.7) can be solved by the Fourier transform method (Fante 1973, Ishimaru 1978, ch. 13), the general solution for $W(z,\underline{\rho},\underline{s}) = 0$ is

$$I(z,\underline{\rho},s) = \frac{1}{(2\pi)^4} \int d\underline{k} \int d\underline{q} \exp(-i\underline{k}\cdot\underline{\rho}-i\underline{s}\cdot\underline{q})I_o(\underline{k},\underline{q}+\underline{k}z)K(z,\underline{k},\underline{q}) , \tag{4.8}$$

where

$$I_o(\underline{k},\underline{q}) = \iint I_o(\underline{\rho},\underline{s})\exp(i\underline{k}\cdot\underline{\rho}+i\underline{s}\cdot\underline{q})d\underline{\rho}d\underline{s} \tag{4.9}$$

is the double Fourier transform of the incident intensty $I_o(\underline{\rho},\underline{s})$ at z=0, and

$$K(z,\underline{k},\underline{q}) = \exp\{\int_o^z \eta_e[1-\frac{B_o}{4\pi} D(\underline{q}+\underline{k}(z-z'))]dz'\} \tag{4.10}$$

where

$$D(\underline{q}) = \iint_{-\infty}^{\infty} D(\underline{s})\exp(i\underline{s}\cdot\underline{q})d\underline{s} \ . \tag{4.11}$$

There is no general explicit expression for (4.8) for a general scattering directivity D(s). If we approximate the strong forward scattering pattern by a Gaussian function,

$$D(\underline{s}) \approx 4\xi\exp(-\xi s^2) \tag{4.12}$$

where ξ is a parameter proportional to $(\ell_o/\lambda)^2$, and ℓ_o is correlation length of the random medium, λ is the wavelength, substituting into (4.11) and (4.10) yields

$$D(\underline{q}) = 4\pi\exp(\frac{q^2}{4\xi}) \ , \tag{4.13}$$

$$K(z,\underline{k},\underline{q}) = \exp\{ \int_o^z \eta_e[1-B_o\exp(\frac{-q^2}{4\xi})]dz'\} \ . \tag{4.14}$$

Since most of the energy is confined within a small cone along z-axis, we consider the case of a plane incident wave

$$I_o(\underline{\rho},\underline{s}) = I_o\delta(\underline{s}) \ , \tag{4.15}$$

$$I_o(\underline{k},\underline{q}) = (2\pi)^2 I_o\delta(\underline{k}). \tag{4.16}$$

From (4.8) we have

$$I(z,\underline{\rho},\underline{s}) = \frac{I_o}{(2\pi)^2}\int d\underline{k}\int d\underline{q}\ \exp(-i\underline{k}\cdot\underline{\rho}-i\underline{s}\cdot\underline{q})\delta(\underline{k})\exp[-\eta_e z+\eta_s z\ \exp(\frac{-q^2}{4\xi})]. \tag{4.17}$$

When the scattering distance is large, i.e. $\eta_s z \gg 1$, the main contributions to the integral in (4.17) come from the integrands with small q's. We can set

$$\exp(\frac{-q^2}{4\xi}) \approx 1- \frac{q^2}{4\xi} \ . \tag{4.18}$$

Therefore

$$I(z,\underline{\rho},\underline{s}) \approx \frac{I_o\xi}{\pi\eta_s z}\exp[-\eta_a z - \frac{\xi s^2}{\eta_s z}] \ . \tag{4.19}$$

$$E(z,\underline{\rho}) = J(z,\underline{\rho}) = \int I(z,\underline{\rho},s)d\underline{s} = I_o e^{-\eta_a z} . \qquad (4.20)$$

We see that, under forward scattering approximation, the energy density decay with distance is only due to the absorption. That is because, in the approximation, we neglect the backscattering and the path length differences between the direct path and the multiple scattering paths by letting $\cos\theta \sim 1$. In Fig. 3.11 and Fig. 3.12 we plot the energy flux J(r) of strong forward scattering vs. that of the isotropic scattering. If we consider the lengthening of travel paths by multiple forward scattering, the decay curve could be somewhere between these two extremes.

(4.19) gives the angle distribution of intensities. The incident wave has only intensity in z-direction, after scattering by the medium, the intensities with different directions have a Gaussian distribution and the width of the angle distribution broadens with distance. The loss due to the scattering of energy to other directions is compensated by the gain of scattered energy from other directions. Therefore there is no energy loss except absorption. However, in order to calculate the real energy attenuation, we have to take the backscattered energy into account. Wu (1982a, see appendix C) uses a simple renormalization procedure and sums up all the energy scattered into the back halfspace as the energy loss. This procedure is similar to DeWolf's "Cumulative Forward-Scatter Single-Backscatter Approximation" in calculating the backscattering strength (DeWolf 1971). Since the backscattered energy is much smaller than the forward scattered energy, the second backscattered energy (from the backward direction into the forward direction) is one order smaller than the single backscattered energy. Therefore the single backscattering loss with the renormalization of the total forward energy could be a reasonable approximation of the scattering attenuation for the harmonic wave field.

From the above analysis, in the case of strong forward scattering due to large scale inhomogeneities, the shape of the energy density decay curve is insensitive to the medium albedo B_o and the separation of scattering attenuation from absorption becomes more difficult. However, because the scattering loss is much smaller than the isotropic case, we can have some constraint on the possible scattering attenuation from the strength of inhomogeneities. The shape of the seismogram evelope in time domain can also give constraints on the possible values of albedo B_o. We will discuss this later in this paper.

5. SEISMIC WAVE SCATTERING AND ATTENUATION IN HINDU KUSH REGION

In this section we will calculate the energy density distribution with travel distances for the small earthquakes in the Hindu Kush region. The data used are from the digital recordings from two stations in that area. Between 11 June and 13 July, 1977, 11 smoked paper recorders and 4 digital event detector recorders were operated around the Hindu Kush Mountains of Northeastern Afghanistan. The organization and operation of the field work as well as the seismicity and tectonics of that region are described by Roecker (1981), Chatelain et al. (1980) and Roecker et al. (1982). Fig. 5.1 is the map view of the earthquake distribution and the station locations. In Fig. 5.2, the events are divided into groups with 50 km depth intervals. The digital numbered events were recorded digitally on magnetic tapes, which have been used by Roecker et al. (1982) to calculate the coda Q and S wave Q in that region using Aki's single station methods. Table 5.1 lists these events. We will use some of those events to calculate the energy distribution along the travel path.

The digital event recorders were of the event detector type (for details see Prothero 1976). When the received signal exceeded the pre-set level the recorders were triggered to record the event on magnetic tapes. The buffer of the instruments also allowed us to record one second data proceeding the triggering signal. Each digital station had four seismometers, three components with high gain and a low-gain vertical component. The natural period of the seismometers was 4 seconds. The preamplifier had a gain 20 db or 40 db (low gain or high gain). The amplifier had a gain 52 db or 58 db, with a 3 pole, low-pass, antialiasing filter having a corner frequency of 32 hz. The response of the whole system is shown in Fig. 5.3. After amplification the signal was digitized at 128 samples per second, multiplexed

and then recorded if the recorder was triggered. The events recorded usually were greater than magnitude 3, with the exception of a few close earthquakes, due the pre-set trigger level.

Because there are only a few stations, it is difficult to get the energy density-distance relation from a single event. We will use a single station method. The seismograms of different events with different distances from the station will be Fourier-transformed to get the spectral density of the energy density E(r) for the corresponding source-sensor distances. In order to have a common source factor for all the events, we use the coda spectral density of these events as the reference levels. From observations, it is generally acknowledged that the coda level, at the travel time greater than twice the S wave travel time, has a very stable relation with the source energy and does not change with the locations of the events. This can be explained by the theory of coda generation in which the coda waves are assumed to be formed by the backscattered S waves from the heterogeneities in the local region of the lithosphere (Aki 1969, Aki and Chouet 1975). A received signal can be considered as a product of three factors:

received signal = source factor x path factor x station factor. (5.1)

Because the coda energy at a specified time interval is assumed to be the sum of backscattered wave energy from the heterogeneities in all the directions, therefore the path factor has been averaged over all the directions, which is much more stable than the path factor of the direct path.

In the calculations, we took the reference coda travel time as t_o = 70 sec. However, for the very close events, some seismograms are shorter than 70 sec, while for the distant events, 70 sec is smaller than twice the S wave travel times. We need to do extrapolations. The guideline for choosing coda time t_c is to have it greater than twice the S travel time and as close as

possible to 70 sec. In order to convert the coda level of each t_c to the reference level of t_o = 70 sec, we use the empirical averaged coda envelope decay for each frequency obtained by Roecker (1982) for this region. When $t>2t_s$, where t_s is the S travel time, the coda envelope decay can be fitted by

$$P(\omega|t) = P_o(\omega) \frac{1}{t^2} \exp(-b_t t), \tag{5.2}$$

where $P(\omega|t)$ is the coda power spectral density at frequency ω, at time t, $P_o(\omega)$ is a constant, b_t is the attenuation rate and

$$b_t = \beta b, \tag{5.3}$$

where b is the attenuation coefficient and β is S wave velocity. For the single backscattering model, $P_o(\omega)$ is found to be (Aki and Chouet 1975)

$$P_o(\omega) = \frac{2g(\pi)S(\omega)}{\beta}, \tag{5.4}$$

where $g(\pi)$ is the backscattering coefficient and $S(\omega)$ is the source power. For our purpose, it is not necessary to specify $P_o(\omega)$, we need only use the empirical relation (5.2). If we set $t = t_o$ as the reference coda travel time, then

$$P(\omega|t_o) = P_o(\omega) \frac{1}{t_o^2} \exp(-b_t t_o) . \tag{5.5}$$

Suppose we measure the coda power $P(\omega|t_c)$ at time t_c, the correction for reducing $P(\omega|t_c)$ to $P(\omega|t_o)$ is then

$$P(\omega|t_o) = P(\omega|t_c) \left(\frac{t_c}{t_o}\right)^2 \exp[-b_t(t_o-t_c)] . \tag{5.6}$$

We can also use $P_o(\omega)$ as the reference level:

$$P_o(\omega) = P(\omega|t_o) \cdot t_o^2 \exp(b_t t_o) . \tag{5.7}$$

In Fig. 5.4, the solid line is the averaged attenuation-frequency relation obtained by Roecker, the dotted line is the smoothed version being used for calculations.

We choose two stations PEN and CHS (Fig. 5.1), because there were many close events for both stations to confine the energy-distance curves. In Table 5.2 and 5.3 the events used for calculations are listed in the order of distances. The events were located using the arrival times on smoked paper records.

To calculate the spectral density, we use the fast Fourier transform algorithm, and average the spectral densities over the specified bandwidths. In order to compare with the previous results obtained using the filtering method by other authors, we take the frequencies as octave and with bandwidths 2/3 of the central frequencies. Table 5.4 lists the 14 central frequencies and their corresponding attenuation values. We use a 32 second window for the S wave Fourier transforms. Fig. 5.5 shows some examples of the seismograms at station PEN for different hypocenter distances, from which we can see that the 32 second window will include most of the S wave energy. In the figure, for each event first gram is the low gain vertical (Z) component, the rest are high gain Z, E-W, and N-S components respectively. In order to avoid the Gibbs phenomena of the rectangular window, we use a 1 second cosine taper for both edges of the window. For the reference coda spectrum, we use an 8 second Hamming window for Fourier transforms.

Fig. 5.6 shows the obtained $4\pi r^2 E(r)$ curves from the station PEN. Totally 31 events are used and the events are grouped according to their distances. From left to right, the curves are of Z, EW and NS components. In the upper part, they are for f = 0.25, 0.5 and 1 kz; in the middle, f = 1.5-8 hz; in the bottom, f = 12-45 hz. Except for the low frequencies f<1 hz, the curves can almost be fitted with straight lines. We calculated the apparent attenuations for different frequencies for the EW components and listed in the Table 5.5.

Because of the fluctuations of the measured curves and the insensitivity to albedo B_o when $B_o<0.5$, we can not determine exactly the values of B_o for each frequency. However, we can get some constraints on the B_o values from the comparison between the measured and the theoretical curves.

Since Aki introduced the single station method using S-coda ratios to measure the apparent attenuations of short period body waves (Aki, 1980a), various attenuation mechanisms have been examined to interpret the observations, especially the frequency dependence of the apparent attenuations. After discussing different attenuation mechanisms, Aki proposed two most promising candidates: thermoelasticity and scattering (Aki 1980a). However, it seems only the scattering mechanism survived in the literature. Dainty (1981) proposed a scattering model with a constatn Q medium and attributed the observed attenuation as the sum of the intrinsic attenuations and the single scattering coefficient. Assuming an intrinsic Q_i=2000, he matched the observed data in Kanto, Japan by Aki (1980a) well with the theoretical calculations. Let us test this model usign our theoretical calculatuions and the data in Hindu-Kush. Fig. 5.7 gives the possible energy density distribution curves for different frequencies if we assume the constant Q model (Q_i = 2000) and use the values of apparent Q in Kanto region obtained by Aki. Due to the low intrinsic attenuation at low frequencies, the medium albedo B_o will be very high, if we attribute the observed apparent attenuations mainly to scattering. However, from Fig. 5.7 and Fig. 3.6, we see that the $E_n(r)$ curves for B_o 1 are of arch shape, only approach approximately exponential curves when distances are much greater than the extinction length L_e. Compare the prediction of Fig. 5.7 with Fig. 5.6, they do not agree in general. More detailed comparison is shown in Fig. 5.8 for the Hindu-Kush data. The apparent attenuations b obtained from the curves in Fig. 5.6 are listed in Table 5.5. For the highest frequency f = 45 hz,

$\hat{b}$ = 0.03/km. If we assume this is totally due to the intrinsic absorption, the equivalent Q_i will be around 2500. From this Q_i, we can obtain the approximate B_o, d_o, and L_e for each frequency (also listed in Table 5.5) based on the measured $\hat{b}$ values. In Fig. 5.8 the prediction of the constant Q model with B_o = 0.9 is compared with the measured data of f = 1.5 hz and 2 hz. There is no match between them. Comparing with other theoretical curves of different B_o's, we found that the observations may be fitted with curves of B_o<0.5. Since the fluctuation in the data and the insensitivity of the curve to B_o for B_o<0.5, we can not determine the B_o value precisely. For the frequencies above 1.5 hz, we can have the similar conclusions (see Fig. 5.6). Therefore, the constant Q_i model may not represent the real medium in Hindu-Kush region. Because the apparent attenuations and their frequency dependence for some tectonically active regions (e.g. California, Kanto region of Japan, etc.) are alike, we might expect that these analyses would be applicable to that region. However, we need to apply the method to other regions before we can draw any conclusions.

More careful studies are needed for the energy distribution curves of low frequencies (f<1 hz). The curves at these frequencies (Fig. 3.6) have the interesting arch shapes, which might indicate the existence of strong scattering at these frequencies. However, these curves are more fluctuating, which may be caused by the interference, and therefore are less reliable. Another consideration is the influence of surface waves and guided waves (higher mode Rayleigh and Love waves), which is stronger at low frequencies. Fig. 5.9 shows two examples of seismograms of events having distances about 100 km from the station (A34: r = 104 km, depth = 4.57 km; A08: r = 124 km, depth 16.27 km). The strong low frequency components following immediately the S arrivals are apparent. This may evidence the strong multiple scattering

at these low frequencies. Another positive indication of multiple scattering is emerged when we compare with the decay curves of direct S amplitudes. In Fig. 5.10 these decay curves are shown for f = 0.25, 0.5, and 1 hz, the S wave power spectra are calculated by Fourier transform using a 4 second Hamming window. These curves are more regular and are not of arch shape. That is because when the window for S wave is very narrow, the multiple-scattered waves, which have longer travel times, are not included. In 5.11 we also plot the calculated apparent attenuations from both the direct S and the total S decay curves for comparisons (the smoothed coda attenuation curve is also plotted). Above 1.5 hz, the attenuation of the total S wave is smaller than that of the direct S wave. This may be due to the inclusion of part of the scattered energy in the former case. However, the differences between these two cases are small in general, which further suggest that, the scattering is not the dominant factor in the apparent attenuation for these frequencies. Again a noticeable different behavior at low frequencis ($f<1.5$ hz) is presented. For these frequencies, the attenuations of direct S waves are smaller than that of the total S waves. Note that the attenuations of the total S waves are estimated from only the later part of the energy distribution curves.

If we take the energy curves for $f<1$ hz as controlled by multiple scattering. A rough estimation by comparing with the theoretical curves (Fig. 3.6) can be made about the medium scattering parameters. For the vertical component, we have

f	L_e(km)	B_o	L_s(km)	L_a(km)	Q_i(equivalent)
0.25	33.3	0.99	33.7	3330	1494
0.5	28.3	0.99	28.6	2830	2540
1	50	0.9	56	500	898

In the case of the EW component,

f	L_e(km)	B_o	L_s(km)	L_a(km)	Q_i(equivalent)
0.25	25	0.99	25.3	2500	1122
0.5	26.7	0.99	26.9	2670	2396
1	40	0.90	44	400	718

It is interesting to note that, at 0.25 and 0.5 hz, the estimated Q_i are close to the proposed intrinsic Q for the constant Q model. Although this may be only a numerical coincidence, we would like to report it here for further study.

Fig. 5.12 shows the 4 r E(r) curves obtained from station CHS. The events used are listed in Table 5.3. The general conclusions drawn from the analysis of the results of station PEN hold true also for CHS.

6. DIFFUSION APPROXIMATION IN TIME DOMAIN, THE CONSTRAINT OF SEISMOGRAM ENVELOPE ON THE SCATTERING STRENGTH

Another approach for studying the scattering and attenuation of seismic waves is to formulate the problem of energy transfer in the time domain and compare the envelopes of seismograms with the theoretical predictions. However, from the author's knowledge, the complete solution of energy transfer in time domain is not available at present. Nevertheless, there are approximate solutions for the weak scattering and the strong scattering. In the weak scattering case, when the propagation distance is smaller than the scattering mean free path, the single scattering approximation can be used. Aki and Chouet (1975) developed a single backscattering model, Sato (1977) derived the formulation for isotropic scattering and discussed subsequently the influence of non-isotropic scattering (Sato 1982). In the case of strong scattering, when the scattering coefficient is much greater than the absorption coefficient ($B_0 >> 0.5$), and the propagation distance is much greater than the scattering mean free path, the diffusion approximation can be used to approximate the envelope variation in time domain. In the following, we discuss the diffusion approximation and seek the constraint of the observed envelopes on the medium scattering properties.

When the scattering mean free path is much shorter than the absorption length in the medium, the energy transfer can be approximated by a diffusion equation (see Morse and Feshbach, 1953, §2.4)

$$\frac{\partial}{\partial t} P(r,t) \approx d\nabla^2 P(r,t) - b_t P(r,t) + q(t), \qquad (6.1)$$

where $P(r,t)$ is the power at distance r and time t; b_t is the absorption rate

$$b_t = bc,$$

where b is the absorption coefficient and c is the wave velocity; $q(t)$ is the source; and d is the diffusivity

$$d = \frac{c}{3\eta_d} , \tag{6.3}$$

where η_d is the effective extinction coefficient for the diffusion process. In the case of isotropic scattering $\eta_d = \eta_e$. For non-isotropic scattering, in the case of discrete random media

$$\eta_d = n\sigma_a + n\sigma_m, \tag{6.4}$$

where n is the number density of the scatterers, σ_a is the absorption cross-section of the scatterers, σ_m is defined by

$$\sigma_m = \int_{4\pi} \sigma_d(\hat{\Omega})(1 - \cos\theta)d\Omega , \tag{6.5}$$

where $\sigma_d(\hat{\Omega})$ is the differential scattering cross-section (2.15), θ is the scatterng angle. σ_m is called the "momentum transfer cross section" by Morse and Feshbach (1953, p. 188). The solution of (6.1) for a point impulsive source is (Morse and Feshbach, 1953)

$$P(r,t) = \begin{cases} 0, & t<0 \\ \dfrac{1}{(4\pi dt)^{3/2}} \exp[-(r^2/4dt)-b_t t], & t>0 . \end{cases} \tag{6.6}$$

Ishimaru (1978) formulated the problem using the equations for the two-frequency mutual coherency functnion and derived the two-frequency equation of transfer. Under the diffusion approximation, a solution similar to (6.6) for a point impulsive source was obtained

$$P(r,t) \approx \frac{r}{\sqrt{4\pi d}\ t^{3/2}} \exp[-(r^2/4dt)-b_t t], \tag{6.7}$$

where d is the same as (6.3), but with η_d defined by

$$\eta_d = n\sigma_m, \tag{6.8}$$

instead of (6.4). However, since σ_a is assumed very small, there will be no big difference between (6.8) and (6.4) except for very strong forward scattering. In the following we will discuss the case of $\sigma_m >> \sigma_a$, therefore

(6.8) will be used, which can be written as

$$\eta_d = \eta_s (1-\bar{\gamma}), \tag{6.9}$$

where η_s is the scattering coefficient, and $\bar{\gamma}$ is the mean scattering angle cosine

$$\bar{\gamma} = \frac{1}{\sigma_s} \int_{4\pi} \sigma_d(\hat{\Omega})\cos\theta \, d\Omega$$

$$= \frac{1}{4\pi} \int_{4\pi} D(\hat{\Omega})\cos\theta \, d\Omega, \tag{6.10}$$

where $D(\hat{\Omega})$ is the scattering directivity (2.11).

Note that, the quantity

$$\eta_s\bar{\gamma} = \frac{\eta_s}{4\pi} \int_0^{2\pi} d\phi \int_0^{\pi} D(\theta\ \phi)\cos\theta \sin\theta \, d\theta, \tag{6.11}$$

where θ, ϕ consistute the spherical coordinates with the polar axis in the incident direction, is the net scattering power flux in the incident direction. This part of the scattered power will join the incident power flow, and does not contribute to the diffusion process. In the case of isotropic scattering, $\bar{\gamma} = 0$, the net scattering power flow in the incident direction is zero, so that $\eta_d = \eta_s$. In the case of strong backscattering, $-1<\bar{\gamma}<0$, so $\eta_d>\eta_s$. Vice versa, for the case of strong forward scattering, $0<\bar{\gamma}<1$, $\eta_d<\eta_s$.

From (6.6), we know there is a peak in the power flow curve, which is approximately at the maximum of the exponent of the exponential term, i.e. at

$$t_m = r \frac{1}{\sqrt{4dbt}} = t_o \frac{\sqrt{3}}{2} \sqrt{1-\bar{\gamma}} \sqrt{\frac{\bar{\tau}_a}{\tau_s}} = t_o \frac{\sqrt{3}}{2} \sqrt{\frac{\bar{\eta}_d}{\eta_a}}$$

$$= t_o \frac{\sqrt{3}}{2} \sqrt{1-\bar{\gamma}} \sqrt{\frac{\bar{B}_o}{1-B_o}} \tag{6.12}$$

where

$$t_o = r/c, \tag{6.13}$$

and

$$\tau_a = 1/b_t, \quad \tau_s = 1/\eta_s c \ , \tag{6.14}$$

are the absorption time and the scattering mean free time respectively. Therefore, the arrival time of the peak of the power flow is proportional to the square root of the ratio between the absorption time and the scattering mean free time. For strong forward scattering, $\sqrt{1-\bar{\gamma}} < 1$, the power peak will arrive earlier than the case of isotropic scattering; in the case of strong backscattering, $\sqrt{1-\bar{\gamma}} > 1$, the peak will arrive later.

Note that, under diffusion approximation, the apparent attenuation, when $t\,\tau_s >> t_o^2$, is approaching to the absorption coefficient η_a; while in the exact solution in frequency domain (3.16) it approaches $d_o\eta_e$ or $\eta_a + d_s\eta_s$. The multiplier d_o or d_s varies depending on B_o. Only in the case of $B_o \to 1$, the apparent attenuation approaches η_a.

From the peak time we can derive the ratio η_d/η_a after doing correction of $t^{3/2}$, while measuring apparent attenuation will determine approximately η_a. Therefore the shape of the envelope provides all the parameters of diffusion scattering.

If we assume a constant Q model, from table 5.5, we have $B_o > 0.79$ for $f < 6$ hz. Therefore, the diffusion approximation could be applied to the wave energy transfer for frequencies below 6 hz. Based on the estimated scattering parameters in Table 5.5, we list in Table 6.1 the predicted arrival times of peak power for different frequencies. Except for the strong forward scattering case, the peak arrival times have a large delay up to several times of the direct travel time. This contradicts the observations on earthquake seismograms or explosion-source seismograms on the earth. The travel time fluctuations for local earthquakes are usually less than 10-20% and the direct S waves can be easily recognized for these frequencies in general. The

observed seismograms are not of diffusion type in the frequency range 1-10 hz. Fig. 6.1 shows the diffusion type envelope curves according to (6.6) at f = 2 hz for different scattering patterns (the envelopes should be symmetric about the time axis). Since we neglected the $t^{-3/2}$ term in deriving (6.12), the peak times in Fig. 6.1 are different from the predictions in Table 6.1. However, the envelopes exhibit the typical diffusion characteristics. These diffusion type envelopes have been observed on the moonquake seismograms and on the seismograms of model experiments in laboratories. In Fig. 6.2, the 3-component seismograms for two events on the moon are shown (the figures are from Latham et al. 1971). The first event (upper seismograms) is believed to be a meteoroid impact, corresponding to the case of shallow source; the second event is considered to be a deep moonquake (below the strong scattering layer). These diffusion type seismograms are due to the existence of the high Q, strong scattering layer below the moon surface (Dainty et al., 1974, Dainty and Toksoz, 1981). Fig. 6.3 shows the seismograms from the model experiment in the laboratory (Dainty et al., 1974). (a) is the seismogram with a homogeneous plate as the propagation medium; while (b) shows the diffusion type seismogram for the case when the plate has many grooves as scatterers.

In order to compare with Fig. 6.1, we select two events A06 (Depth 103 km) and A15 (depth 118 km), which have distances around 200 km from station PEN and CHS. From Fig. 3.9 we know that, the diffuse term will dominate after the travel distance exceeds twice the extinction distance for $B_0 = 0.9$. Therefore the seismograms for these two events should be of diffusion type, if the parameters in Table 6.1 are true, i.e. the constant Q model is true. Fig. 6.4 and 6.5 show the filtered seismograms for these two events at different stations. The digital filter is a six pole, zero-phase, Butterworth filter, the central frequencies are 0.375, 0.75, 1.5, 3, 6, 12, 24, and 46 hz, the

bandwidth is 2/3 of the central frequency for each band (see Roecker, 1982). From these figures, we do not see the diffusion type seismograms at low frequencies. In Fig. 6.6 we plot the envelope decay curves for event A15 as an example. The power decay curves are calculated by the moving window spectral analysis with an 8 second Hamming window and at a 5 second interval. On the left are the vertical components, right, the EW components. These envelope curves are typical for the events in this region (see Roecker 1982). They are not of diffusion type except for some very high frequency components (f>20 hz, we will discuss this later). In fact these curves fit the single isotropic model fairly well. The energy density E(r,t) of the isotropically scattered body waves at time t and at distance r from a point source can be expressed as (Sato 1977)

$$E(r,t) = \frac{n\sigma_s W_o}{4\pi r^2} K\left(\frac{t}{t_s}\right) , \qquad (6.15)$$

where t_s is the direct wave (here S wave) travel time, n, the number density and σ_s the scattering cross-section of the scatterers. W_o is the source factor, and

$$K(\xi) = \frac{1}{\xi} \ln\left[\frac{\xi+1}{\xi-1}\right] . \qquad (6.16)$$

The time function $K(t/t_s)$ is a pure geometric spreading factor for the single isotropic scattering model, which is plotted in Fig. 6.7 for the distance of event A15 to CHS (r=221.85 km). Fig. 6.8 shows the power decay curves after making the corresponding geometric spreading correction, i.e. dividing the curves in Fig. 6.6 by $K(t/t_s)$. We can see that, after this geometric correction, the power decay curves are fairly linear, which is of exponential decay due to attenuation.

To compare with Fig. 6.1, we need to examine the case of strong forward scatternig more carefully. The curve of $\bar{\gamma}$=0.5 is calculated by assuming the same scattering coefficient η_s as the isotropic scattering case. Because more energy is concentrated in the forward direction, the effective scattering coefficient for diffusion η_d becomes smaller than η_s (see (6.9)). In our case we estimated η_s from the apparent attenuation measurement in frequency domain (section 5). Since we calculated the power spectral densities for the total S waves, the net scattering power flux (6.11) is included, so that the forward scattering power flux does not contribute to the apparent attenuation. Therefore, the estimated scattering coefficient is closer to η_d than to η_s, if we consider the apparent attenuatuion is mainly due to the scattering loss. By this consideration, the curve for strong forward scattering in Fig. 6.1 should have a shape close to the isotropic case with a η_d closer to, but a a η_s greater than the isotropic case. Secondly, if the peak of the power flow is near the direct arrival time, the more elaborated diffusion formulae should be appealed (Ishimaru 1978), which will incorporate the direct travel time into the formulation. At any rate, if the apparent attenuation obtained in section 5 is taken as mainly from scattering loss, the envelope curve should be similar to a diffusion type curve of isotropic scattering.

From above comparison and analysis, combining with the results obtained in section 5, we can conclude that, in the frequency range 1.5-20 hz, the scattering is not the dominant factor of the measured apparent attenuation. In other words, the scattering coefficients is smaller than the absorption coefficients at these frequencies in the lithosphere of this region.

More careful study is also needed for the case of frequencies higher than 20 hz. From Fig. 6.4, 6.5 we notice that, at these high frequencies the seismograms become spindle-shaped as pointed out by Tsujura and Aki (see Aki

1980b). These are of diffusion type. For some stations, the P and S phase can no longer be clearly separated, which means also strong scattering and conversion. Since the attenuation coefficients are high at these frequencies, the scattering coefficients must be also high. This strong scattering for high frequencies may be caused by the near surface very small scale heterogeneities. Regarding Fig. 6.6, 6.8, we can find that the decay curves of m and n band (f=32 and 45 hz) have flat tops, different from the other bands.

The time domain analysis has the advantage of easy comparison with the data, because each seismogram is one experiment, unlike the energy density distribution curve in frequency domain, which need many events covering a distance range. However, in order to perform more complete analysis, we need to develop more accurate theory and model. Besides, the shape of the envelope is also sensitive to the slip direction of the earthquake source, that makes the analysis more complicated. At any rate, the combinations of time domain and frequency domain analysis will make the analysis more informative and reliable.

7. DISCUSSION

ATTENUATION MECHANISM?

From the calculations and comparisons in frequency domain and the analysis in time domain, we conclude that scattering is not the dominant factor for the measured apparent attenuations on S waves or coda waves in the frequency range 1.5-20 Hz in this region. This leads to a frequency dependent Q (intrinsic). Then the question arises: Why is the intrinsic Q so low and frequency dependent? What is the mechanism?

The frequency dependence of Q value and the attenuation mechanism for short period seismic waves is a highly controversial topic at present (for review, see Jackson and Anderson 1970, Lundquist 1979, Minster 1980, Toksoz and Johnston 1981, and Clements 1982). Therefore we can only have some speculations based on some observations.

Since the Q values are very high at high frequencies (above 20 Hz) as inferred from the measured apparent attenuations (Table 5.5), we assume the lithosphere in this region is made of dry rocks. Any absorption mechanism involved with pore fluid is excluded. However, the well-known mechanisms for dry rocks, such as the frictional sliding along crack surfaces (Walsh, 1966), the linear and nonlinear mechanism connected with the motion of dislocations (Mzson 1969, 1971), all favor the frequency independent Q. Besides, people argued that, in the deep crust, the cracks are all closed by the high confining pressure there. Some experiments also showed that, the friction loss is amplitude dependent, for the low strain amplitude encountered in seismology, the friction loss is not important (Winkler et al. 1979). The thermally activated attenuation mechanism allows a frequency dependent Q, However, the corner frequency for the " absorption band " is much higher than 100 hz for the case of lithosphere (Anderson and Given 1982, Cormier

1982). Only above this frequency Q starts to increase. This does not agree with the observations on the attenuation of lithosphere. In addition, this mechanism can not explane the strong regional variation of the observed attenuation. Therefore, from the measured frequency dependent Q for short period seismic waves, we need to reconsider some other attenuation mechanisms. The mentioned mechanisms for dry rocks are all "microscopic" compared with the wavelength and are for the fresh rocks or "healthy" rocks. How about the "wounded" rocks and the "Macroscopic" mechanisms? In the tectonically active regions, earthquakes left numerous "wounds": faulting, fracture zones, etc. Because the healing process is very slow, the population of the "wounds" maintains in certain level. These faultings or fracture zones behave differently from the "healthy" rocks. They may scatter and absorb the seismic energy in the same time. Therefore, if we assume the perfect rock, namely the unwounded lithosphere has a high Q, then the medium albedo B_o is mainly determined by the scatterer's albedo B_1 (see 2.21). From our measurements and calculations, these scatterers seem to have a frequency independent attenuation constant, i.e. a frequency dependent Q. The absorption mechanism is still unknown and needed to study further. However, since these faultings are generally comparable to the wavelengths, the frequency dependence will be more complicated than that of the "micro-cracks".

Other macroscopic mechanisms, such as the couple stress effect related to scattering (Yildiz 1984) should also be examined.

There are some observations supporting the idea of "weak zone" (faulting or fracture zone) related absorption and scattering. The VSP (Vertical Seismic Profiling) experiments in Michigan basin have shown that, after the fracture zone was formed by explosions, both the velocity decrease and attenuation increase for the transmitted waves have been oberved (Turpening, 1984) in addition to the cross-coupling between SH and SV components of S

waves due to scattering by the fracture zone (see Chapter 2, §3). Another example is the change in attenuation and scattering properties of the medium after a swarm as reported by Suyehiro (1968). High attenuation to the transmitted seismic waves by the swarm region especially for high-frequencies (above 40 Hz) was observed after the Matsushiro earthquake swarm (in central Japan). Stronger scattering can also be inferred from the richness of the coda in the seismograms after the swarm. This can be explained by the formation of a fracture zone due to the swarm.

From the above examples, it seems that the "wounds" or "scars" (faultings or fractures) in the medium behave like both scatterers and absorbers. In fact the scattering and absorption may be closely related, both involve the surface or boundary frictional sliding, if the sizes of the macro-scale boundaries are comparable with the wavelength.

Since the boundary friction is strongly dependent on the local stress, so that the scattering and attenuation should be also stress dependent. There are observations from which the strong variations of coda envelope and duration before and after big earthquakes have been noticed (Jin 1983, Del Pezzo et al. 1983). This variation could be caused by the stress changes before and after the big earthquakes. Temporal variations of coda Q also were reported by Chouet (1979) and Rhea (1983).

From our results and conclusion in this paper, the problem of coda strength becomes sharper. According to Sato's calculation (1982), the coda strength is much higher than expected from the velocity perturbations inferred from the coda attenuation, even if we attribute the apparent attenuation totally to scattering. As pointed out by Wu and Aki (1984, see ch. 3) this puzzle can be partly solved by treating the excitation problem using the formulas of elastic wave scattering instead of scalar wave scattering. In

the theory of elastic wave scattering, the scattering due to impedance contrasts behaves quite differently from that due to velocity contrasts. In addition, more accurate methods of measuring the coda strength and a better model for the coda apparent attenuation are also needed to solve the problem. Besides, the scattering and attenuation mechanism by the "wounds" and "scars" due to earthquakes in the lithosphere may also help to solve the problem. The scattering strength by these scatterers may not observe the formulas for the volume velocity perturbations. The equivalent impedance perturbations for these scatterers may be higher than that of the volume inhomogeneities.

TECTONIC IMPLICATIONS

In the following we discuss briefly the tectonic implications of our results for this region.

From our results, the intrinsic attenuation is high in general, and surprisingly, this high attenuation extends to the depth of 200 km to 300 km. It can be seen from Fig. 5.6 and 5.12 that, the linearity of the $4\pi r^2 E(r)$ curves extend to the deepest events. This supports the idea that the thick continental crust (along with the lithosphere) have subducted to the mantle beneath the continent of Eurasia (Roecker 1981, ch. 6). Fig. 7.1 (from Roecker, 1981) shows the vertical variations of P (upper figure) and S (lower figure) velocity from the results of 3D velocity inversion, along with the seismicity in the region. From the contour plots we can see that the active seismic zone coincides with the low velocity region, in contrast to the typical high velocity region associated with the oceanic subduction plate. Therefore, we should expect high attenuation for this subducted continental lithosphere. In summary, the high apparent attenuations for the total S wave and their extension to the depth below 200 km obtained in this paper support the concept of thick subducted continental lithosphere.

SUGGESTION FOR FURTHER STUDIES

It is interesting and beneficial to apply the method to other regions to see the relative importance of absorption and scattering for different regions. Especially the comparison between the results for the tectonically stable regions, such as New England area or the central U.S., and that for the active regions such as the results obtained here for Hindu Kush or that for California, will give us deeper understanding about scattering and attenuation as well as more information about the tectonic activities.

Further improvements on the scattering theory and modeling are also needed, such as the influences of the radiation pattern of the source, the finite thickness of the lithosphere, the anisotropy of the inhomogeneities, etc. Of course, full treatment of elastic wave scattering in both the frequency domain and the time domain are highly desired.

Acknowledgement

I am grateful to Dr. S. Roecker for allowing me to use his data tapes and for his careful reading of the manuscripts and the helpful discussions. I also thank all the people involved in the field work and data processing of the Hindu Kush experiment. Without their work, the application of the theory to this region is not possible.

References

Aki, K., 1969, Analysis of the seismic coda of local earthquakes as scattered waves, J. Geophys. Res., 74, 615-631.

Aki, K., 1973, Scattering of P waves under the Montana Lasa, J. Geophys. Res., 78, 1334-1346.

Aki, K., 1980a, Attenuation of shear waves in the lithosphere for frequencies from 0.05 to 25 Hz, Phys. Earth Planet. Int., 21, 50-60.

Aki, K., 1980b, Scattering and attenuation of shear waves in the lithosphere, J. Geophys. Res., 85, 6496-6504.

Aki, B. and B. Chouet, 1975, Origin of coda waves: source, attenuation and scattering effects, J. Geophys. Res., 80, 3322-3342.

Anderson, D.L. and J.W. Given, 1982, Absorption band Q model for the earth, J. Geophys. Res. ,87,3893-3904.

Barabanenkov, Y.N., 1969, On the spectral theory of radiation transport equations, Sov. Phys., JETP, 29, 679-684.

Bell, G.I. and S. Glasstone, 1970, Nuclear Reactor Theory, New York, Van Nostrand Reinhold.

Berteussen, K.A., A. Christoffersson, E.S. Husebye, and A. Dahle, 1975, Wave scattering theory in analysis of P wave anomalies at NORSAR and LASA, Geophys. J. Roy. astr. Soc., 42, 403-417.

Capon, J., 1974, Characterization of crust and upper mantle structure under Lasa as a random medium, Bull. Seis. Soc. Am., 64, 235-266.

Carrier, G.F., M. Krook and C.E. Pearson, 1966, Functions of a complex variable, ch. 7, McGraw-Hill, New York.

Chandrasekhar, S., Radiative Transfer, Dover, 1960 (revised version of 1950).

Chatelain, J.L., S.W. Roecker, D. Hatzfeld, and P. Molnar, 1980, Microearthquake seismicity and fault plane solutions in the Hindu Kush region and their tectonic implications, J. Geophys. Res., 85, 1365-1387.

Chernov, L.A., 1960, Wave Propagation in a Random Medium, McGraw-Hill, New York.

Chouet, B., 1979, Temporal variations in the attenuation of earthquake coda near Stone Canyon, California, Geophys. Res. Lett., 6, 3.

Clements, J.R., 1982, Intrinsic Q and its frequency dependence,Phys. earth plenet. int., 27,289-299.

Dainty, A.M., A scattering model to explain seismic Q observations in the lithosphere between 1 and 30 Hz, Geophys. Res. Lett., 8, 1126-1128, 1981.

Dainty, A.M., M.N. Toksoz, K.R. Anderson, P.J. Pines, Y. Nakamura, and G. Latham, Seismic scattering and shallow structure of the moon in oceanus procellarum, Moon, 9, 11-29, 1974.

Dainty, A.M. and M.N. Toksoz, 1981, Seismic codas on the earth and the moon: a comparison, Phys. Earth Planet. Int., 26, 250-260.

Dashen, R., 1979, Path integrals for waves in random media, Stanford Research Inst. Tech. Report JSR 76-1, also J. Math. Phys., 20, 894-920 (1979).

Davison, B., 1957, Neutron Transport Theory, Oxford Univ. Press, London.

Del Pezzo, E., F. Ferulano, A. Giarusso, and M. Martini, 1983, Seismic coda Q and scaling law of the source spectra at the Aeolian Islands, Southern Italy, Bull. Seis. Soc. Am., 73, 97-108.

DeWolf, D.A., 1971, Electromagnetic reflection from an extended turbulent medium: cumulative forward-scatter single-backscatter approximation, IEEE Trans. Ant. Prop., AP-19, 254-282.

Fante, R.L., 1973, Propagation of electromagnetic waves through turbulent plasma using transport theory, IEEE Trans. Ant. and Prop., AP-21, 750-755.

Flatte, S.M., R. Dashen, W.H. Munk, K.M. Watson, and F. Zachariasen, Sound transmission through a fluctuating ocean, Cambridge Univ. Press, 1979.

Frisch, V., 1968, Wave Propagation in Random Media, Probabilistic Methods in Applied Mathematics, Vol. 1, Academic Press, New York, 76-198.

Gao, L.S., L.C. Lee, N.N. Biswas and K. Aki, 1983, Comparison of the effects between single and multiple-scattering on coda waves for local earthquakes, Bull. Seis. Soc. Amer., 73, 377-389.

Gao, L.S., N.N. Biswas, L.C. Lee and K. Aki, 1984, Effects of multiple scattering on coda waves in three-dimensional medium, to be published.

Hoffman, W.C., 1964, Wave propagation in a general random continuous medium, Proc. Symp. Appl. Math., 16, 117-144.

Ishimaru, A., 1975, Correlation functions of a wave in a random distribution of stationary and moving scatterers, Radio Sci., 10, 45-52.

Ishimaru, A., 1977, Theory and application of wave propagation and scattering in random media, Proc. of IEEE, 65, 1030-1061.

Ishimaru, A., 1978, Wave propagation and scattering in random media, V. 1 and 2, Academic Press, New York.

Ishimaru, A., 1978, Diffusion of a pulse in densely distributed scatterers, J. Opt. Soc. Am., 68, 1045-1050.

Jacksom,D.D. and D.L. Anderson, 1970, Physical mechanisms of seismic attenuation, Rev. geophys. space phys., 8, 1-63.

Jerlov, M.G., 1976, Marine Optics, Elsevier, New York.

Jin, A.S., Coda, I. Durations and backscattering coefficients, Acta Geophysica Sinica (in Chinese), in press, 1983.

Kay, I. and R.A. Silverman, 1958, Multiple scattering by a random stack of dielectric slabs, Nuovo Cimento (10) 9, suppl., 625-645.

Kong, J.A., Tsang, L. and R. Shin, 1984, Theory of Microwave Remote Sensing, Wiley-Interscience, New York.

Kopnichev, Y.F. 1977, The role of multiple scattering in the formation of a seismogram's tail, Isvestiya Academy of Science, USSR, Physics of the Solid Earth, 13, 394-398.

Latham, G.V., M. Ewing, J. Dorman, D. Lammlein, F. Press, N. Toksoz, G. Sutton, F. Duennebier, and Y. Nakamura, 1971, Moonquakes and lunar tectonism, Science, 174, 687-692.

Lin, J.C. and A. Ishimaru, 1974, Multiple scattering of waves by a uniform random distribution of discrete iotropic scatterers, J. Acoust. Sco. Am., 56, 1995-1700.

Lundquist,G.M., 1979, The frequency dependence of Q, ph. D. thesis, U. of Colorado, Boulder, Colorado.

Mason, W.P., 1969, Internal friction mechanism that produces an attenuation in the earth's crust proportional to frequency, J. Geophys. Res., 74, 4963-4966.

Mason, W.P., 1971, Internal friction at low frequencies due to dislocation: applicatins to metals and rock mechanics, in Physical Acoustics, v. 8, W.P. Mason and R.N. Thurston, eds., Academic Press, New York.

Menzel, D.H., ed., 1966, Selected Papers on the Transfer of Radiations, New York, Dover.

Morse, P.M. and H. Feshbach, 1953, Methods of Theoretical Physics, New York, McGraw-Hill.

O'Doherty, R.F. and N.A. Anstey, 1971, Reflections on amplitudes, Geophys. Prospecting, 19, 430-458.

Rautian, T.G. and V.I. Khalturin, 1978, The use of coda for determination of the earthquake source spectrum, Bull. Seis. Soc. Am., 68, 923-948.

Rhea, S., 1983, Analysis of digital data from local Charleston, S.C., earthquakes, Earthquake Notes, 54, 32.

Richard, P.G. and W. Menke, 1983, The apparent attenuation of a scattering medium, Bull. Seis. Soc. Am., 73, 1005-1021.

Roecker, S.W., 1981, Seismicity and tectonics of the Pamir-Hindu Kush region of central Asia, Ph.D. Thesis, Massachusetts Institute of Technology, Cambridge, MA.

Roecker, S.W., B. Tucker, J. King, and D. Hatzfeld, 1982, Estimates of Q in central Asia as a function of frequency and depth using the coda of locally recorded earthquakes, Bull. Seis. Soc. Am., 72, 129-149.

Sato, H., 1977, Energy propagation including scattering effect; single isotropic scattering approximation, J. Phys. Earth, 25, 27-41.

Sato, H., 1982a, Coda wave excitation due to nonisotropic scattering and nonspherical source radiation, J. Geophys. Res., 87, 8665-8674.

Sato, H., 1982b, Attenuation of S waves in the lithosphere due to scattering by its random velocity structure, J. Geophys. Res., 87, 7779-7785.

Schuster, A., 1905, Radiation through a foggy atmosphere, Astrophys. J., 2, 1-22.

Sobolev, V.V., 1963, A Treatise on Radiative Transfer, Princeton, NJ, Van Nostrand.

Suyehiro, S., 1968, Change in earthquake spectrum before and after the Matsushiro Swarm, Papers in Meteorology and Geophysics, 19, 3, 427-435.

Tatarskii, V.I., 1971, The effects of the turbulent atmosphere on wave propagation.

Toksoz,M.N. and D.H. Johnston,(ed.), 1981, Seismic attenuation, Geophysics reprint series, NO.2, SEG.

Tricomi, F.G., 1957, Integral Equations, New York, 22-26.

Tsang, L. and A. Ishirmau, 1983, Backscattering enhancement for random discrete scatterers, to be published.

Turpening, R., 1984, Differential vertical seismic profiling: fracture volume analysis in "Vertical seismic profiling", ed. by Balch, A. and M. Lee, I.H.R.D.C., Boston.

Uscinski, B.J., 1977, The elements of wave propagation in random media, McGraw-Hill.

Walsh, J.B., 1966, Seismic wave attenuation in rocks due to friction, J. Geophys. Res., 71, 2591-2599.

Winkler, K., A. Nur, and M. Gladwin, 1979, Friction and seismic attenuation in rocks, Nature, 227, 528-531.

Wu, R.S., 1980, The attenuatuion of seismic waves due to scattering in a random medium (abstract), EOS, 61, 46, 1049.

Wu, R.S., 1982a, Attenuation of short period seismic waves due to scattering, Geophys. Res. Lett., 9, 9-12.

Wu, R.S., 1982b, Mean field attenuation and amplitude attenuation due to wave scattering, Wave Motion, 4, 305-316.

Wu, R.S., and K. Aki, 1984, Scattering characteristics of elastic waves by an elastic heterogeneity, Geophyics, in press.

Wu, R.S. and K. Aki, 1984, Elastic wave scattering by a random medium and the small scale inhomogeneities in the lithosphere, J. Geophys. Res., in press.

Yildiz, A., 1984, Macroscale attenuation of seismic waves, preprint.

Zuniga, M., J.A. Kong and L. Tsang, 1980, Depolarization effects in the active remote sensing of random media, J. Appl. Phys., 51, 2315-2325.

Table 3.1. The Diffuse Multipliers d_o and d_s

B_o	0.1	0.2	0.3	0.4	0.5	0.6	0.7	0.8	0.9	0.95	0.99
d_o	0.997	0.987	0.969	0.944	0.910	0.866	0.807	0.728	0.611	0.519	0.374
d_s	0.97	0.94	0.90	0.86	0.82	0.78	0.72	0.66	0.57	0.49	0.37

Table 5.1

DATE	ORIGIN TIME	LAT N	MIN	LON E	MIN	DEPTH (KM)	EVENT NO.	MAG
77 616	1616 55.26	36	31.76	70	16.13	102.26	16	3.9
77 617	8 6 32.45	35	23.30	69	28.05	1.49	18	2.4
77 617	1714 20.46	36	32.89	70	57.20	197.00	19	3.8
77 617	1930 38.16	35	43.12	69	40.23	77.98	20	3.7
77 617	22 1 47.14	36	30.00	71	14.24	112.19	21	3.6
77 618	528 43.58	34	54.80	69	55.45	1.87	23	2.5
77 618	753 35.31	34	39.56	70	34.71	1.42	24	2.4
77 618	9 3 40.71	34	34.30	72	48.84	340.70	25	5.3
77 618	1150 22.64	36	6.23	69	23.71	131.94	26	3.3
77 618	2320 3.27	35	59.24	70	38.49	112.21	27	3.5
77 620	148 49.52	36	5.63	70	26.43	98.55	28	4.3
77 620	4 5 56.23	36	7.01	70	26.17	105.32	29	4.0
77 620	1156 30.60	36	30.35	70	18.96	215.02	30	3.8
77 620	2335 16.51	35	30.68	69	3.71	2.50	31	3.1
77 621	316 2.84	36	38.92	71	18.30	98.13	32	3.7
77 621	2133 46.80	36	33.34	71	22.42	159.81	33	4.3
77 622	832 21.95	36	35.21	70	53.23	232.49	02	4.1
77 622	1430 58.92	36	10.33	69	19.52	4.57	34	3.9
77 623	934 59.59	36	27.15	71	14.84	136.57	03	3.5
77 623	2054 13.26	36	2.75	70	32.94	106.25	04	3.5
77 624	2358 0.19	36	31.68	70	22.24	218.87	05	4.6
77 624	2243 57.24	36	11.90	69	17.27	9.65	35	3.3
77 626	824 11.00	36	18.48	70	55.67	119.35	36	3.4
77 626	1833 58.79	36	47.06	71	23.74	155.28	37	3.5
77 627	759 14.12	36	27.88	70	50.11	127.75	38	3.3
77 628	1034 26.75	36	7.26	70	32.94	100.00	39	3.6
77 628	1520 4.70	36	10.48	71	8.95	86.02	40	2.9
77 628	1623 51.79	37	11.84	71	25.61	108.66	41	3.4
77 628	17 3 36.25	35	17.53	69	16.85	8.68	42	2.1
77 629	636 27.30	36	21.49	71	10.14	105.56	43	3.5
77 629	1031 4.37	36	28.76	71	18.43	138.44	44	3.4
77 629	1521 33.18	37	27.39	72	21.65	221.95	45	4.3
77 629	1540 1.48	34	46.64	70	58.65	2.04	46	2.5
77 629	16 6 30.59	36	24.00	71	9.33	103.31	06	4.7
77 630	220 47.74	36	29.06	70	26.98	219.25	07	4.1
77 630	338 34.03	36	37.07	71	17.14	86.83	47	3.5
77 630	1353 29.92	36	17.64	71	11.71	98.83	48	3.4
77 7 1	348 32.15	34	38.56	70	28.55	16.27	08	4.5
77 7 1	1444 10.80	36	28.05	71	6.59	264.91	09	4.9
77 7 1	1627 3.09	36	14.58	70	19.05	108.83	49	3.0
77 7 2	330 48.81	36	34.45	70	39.80	174.84	50	4.1
77 7 2	2028 19.63	35	13.97	69	25.26	8.32	51	2.2
77 7 2	2111 49.19	35	59.39	70	43.29	93.93	52	3.2
77 7 3	17 0 4.91	36	56.43	71	2.82	76.67	53	3.0
77 7 4	614 15.39	36	32.71	71	21.16	122.09	54	3.5
77 7 4	824 3.03	36	19.90	69	33.71	134.72	55	3.6
77 7 4	1128 47.08	36	26.39	70	12.86	221.59	10	4.6

77	7	4	2041	5.58	36	11.73	69	26.72	128.00	56	3.3
77	7	4	21 1	56.74	37	31.97	72	0.62	157.19	11	4.7
77	7	5	14 7	12.46	36	29.72	69	47.10	271.19	57	2.9
77	7	6	055	22.50	36	39.45	71	5.04	229.10	58	3.9
77	7	6	1328	56.27	37	4.49	71	34.93	96.33	59	3.4
77	7	6	1659	8.76	36	17.72	69	50.94	9.46	60	3.0
77	7	7	620	43.34	36	25.26	70	37.26	228.86	61	4.1
77	7	8	130	36.15	36	38.20	71	8.46	214.61	12	4.0
77	7	8	525	26.60	36	41.86	71	12.24	230.79	13	4.7
77	7	8	7 2	10.28	36	31.90	71	20.23	94.37	62	3.3
77	7	8	950	6.99	36	41.21	71	12.71	233.80	63	3.8
77	7	9	1141	13.94	35	30.46	68	52.81	38.00	64	2.7
77	7	9	1211	40.56	37	36.71	71	45.78	129.68	65	3.7
77	7	9	1616	39.67	36	28.06	71	12.71	143.71	66	3.3
77	710		028	19.08	35	41.93	68	38.41	3.74	67	3.6
77	710		1347	18.52	35	6.83	69	21.09	17.57	69	2.3
77	710		1612	22.07	35	31.28	69	13.05	17.04	70	3.6
77	711		11 2	56.61	36	26.37	71	20.63	104.40	14	3.9
77	711		1224	5.07	36	45.50	71	28.64	188.43	72	3.6
77	711		1651	7.33	36	28.89	71	9.82	118.48	15	4.2
77	712		11 7	59.16	36	32.53	70	58.27	192.49	73	4.3
77	712		1518	28.82	36	12.21	69	15.96	5.57	74	3.8
77	712		1718	2.32	36	16.59	70	40.23	103.88	75	3.7

Table 5.2

Events Used in the Calculations for PEN in the Order of Distances (31 events)

Point No. in curve	Event No.	Distance (km)	Depth (km)	Magnitude	P travel time (sec.)	S travel time (sec.)	Reference coda time t_c (sec.)	Record length (sec.)
1	A42	11.12	8.68	2.1	7.29	11.83		44
	A51	12.10	8.32	2.2	7.54	12.26	31.5	34
2	A69	21.52	17.57	2.3	7.54	12.52	31.5	40
	A18	22.03	1.49	2.4	9.55	15.62	20.5	18
3	A70	37.76	17.04	3.6	10.10	17.03	34.1	38
	A31	39.15	2.5	3.1	11.67	19.42	41.7	40
4	A64	63.09	38.0	2.7	11.42	19.79	40.4	38
	A23	65.15	1.87	2.5	15.04	25.38	42.0	36
5	A67	80.75	3.74	3.6	16.86	28.66	60.7	60
6	A20	100.16	77.98	3.7	15.94	27.87		54
	A34	104.68	4.57	3.9	19.81	33.91	73.8	82
	A35	107.97	9.65	3.3	19.67	33.76		68
	A74	108.33	5.57	3.8	20.16	34.56		80
7	A08	124.88	16.27	4.5	21.06	36.39		158
	A68	175.74			24.21	42.61		60
8	A04	178.52	106.25	3.5	24.78	43.42	78.7	70
	A39	179.28	100.0	3.6	24.9	43.56		64
9	A16	196.42	102.36	3.9	27.16	47.47	84.0	70
	A75	197.95	103.88	3.7	27.36	47.83		64
10	A06	234.53	103.31	4.7	31.95	55.72	105.9	134
	A15	247.35	118.48	4.2	33.41	58.51	107.5	158
11	A03	259.49	136.57	3.5	34.71	61.11		62
	A50	295.83	174.84	4.1	34.46	61.07		90
	A10	271.40	221.59	4.6	35.57	63.1	109.4	258
12	A05*	278.65	218.87	4.6	36.52	64.75		234
	A07	279.0	219.25	4.1	36.56	64.82	100.5	76
	A73	283.65	192.49	4.3	37.22	65.96		90
13	A02	310.97	232.49	4.1	40.23	71.32	102.1	78
14	A13*	329.59	230.79	4.7	42.47	75.29		246
	A09*	339.32	264.91	4.9	43.36	77.06		302
15	A25	472.39	340.70	5.3	58.59	104.48	132.2	96

*high gain records were clipped, only low gain vertical component has been used.

Table 5.3

Events Used in the Calculations for CHS in the Order of Distances (22 events)

Point No. in curve	Event No.	Distance (km)	Depth (km)	Magnitude	P travel time (sec.)	S travel time (sec.)	Record Length (sec.)
1	A46	8.47	2.04	2.5	1.55	2.63	
2	A24	47.77	1.42	2.4	12.85	21.48	
	A08	59.54	16.27	4.5	12.98	22.09	
	A04	181.43	106.25	3.5	27.08	42.69	
3	A28	184.08	98.55	4.3	25.55	44.64	
	A39	184.42	100.00	3.6	28.59	44.74	
	A29	189.83	105.32	4.0	26.9	46.03	
	A06	206.22	103.31	4.7	28.42	49.64	
	A14	211.85	104.40	3.9	29.54	50.88	
4	A34	220.58	4.57	3.9	34.71	60.37	
	A15	221.85	118.48	4.2	30.33	53.19	
	A74	226.84	5.57	3.8	35.41	61.63	
	A16	230.02	102.26	3.9	31.4	54.74	
	A66	235.26	143.71	3.3	31.33	56.0	
5	A50	266.53	174.84	4.1	34.67	60.89	
	A73	273.54	192.49	4.3	35.65	61.65	
	A12	296.55	214.61	4.0	38.17	65.84	
6	A10	297.63	221.59	4.6	37.62	65.62	
	A05	298.40	218.87	4.6	39.10	65.58	
	A02	306.54	232.49	4.1	39.11	66.00	
7	A09	323.59	264.91	4.9	41.13	70.13	
8	A11	352.37	157.19	4.7	46.24	78.24	

Table 5.4 The Central frequencies used and the corresponding attenuation values of coda waves

Band no.	Central frequency	Coda Q_c (observed)	Coda Q_c (smoothed)	Coda b_t (observed)	Coda bt (smoothed)	Coda b (smoothed)
a	0.25	24.0	24.0	6.5×10^{-2}	6.5×10^{-2}	1.86×10^{-2}
b	0.5	47.9	44.2	6.6	7.10	2.03
c	1	83.2	81.0	7.6	7.76	2.22
d	1.5	89.1	115.4	10.6	8.17	2.33
e	2	107.2	148.3	11.7	8.47	2.42
f	3	125.9	211.3	15.0	8.92	2.55
g	4	190.5	271.6	13.2	9.26	2.64
h	6	281.8	386.8	13.4	9.75	2.78
i	8	446.7	497.2	11.3	10.11	2.89
j	12	707.9	708.2	10.7	10.65	3.04
k	16	933.3	910.2	10.8	11.04	3.16
l	24	1174.9	1296.6	12.8	11.63	3.32
m	32	1698.2	1666.6	11.8	12.06	3.45
n	45	2238.7	2244.0	12.6	12.60	3.60

Table 5.5 Apparent attenuations for the EW components of station PEN and the estimated values of seismic albedo B_o's, if we assume a constant Q (=2500) medium

f	$\eta_a = \omega/\beta\ Q^{-1}$ (Q = 2500)	La(km) (for Q=2500)	$\hat{b}$ (measured)	$\eta_a/\hat{b}$	B_o	d_o	L_e (km)
0.5	0.036×10^{-2}	2778	1.00 x 10-2	0.036	≈0.96	0.5	50
1	0.072	1389	1.38	0.052	0.95	0.5	36
2	0.144	694	1.50	0.096	0.90	0.6	40
3	0.215	465	1.60	0.134	0.87	0.6	38
6	0.431	232	2.03	0.212	0.79	0.7	34
12	0.862	116	2.50	0.345	0.66	0.8	31
24	1.72	58	2.73	0.63	0.37	0.95	35
45	3.23	31	3.00	1.08	0	1	33

Table 6.1 The Predicted arrival time of the peak power by the diffusion approximation based on the assumed constant Q(=2500) model and the estimated parameters in Table 5.5.

f (hz)	absorption time τ_a (sec.)	mean free time τ_s (sec.)	$d(1-\bar{\gamma})$ (km^2/sec)	Albedo B_o	L_e	Arrival time of peak power t_m/t_o		
						$\bar{\gamma}$ = -0.5	0	0.5
0.5	793.7	14.9	60.8	0.96	50	5.20	4.24	3.0
1	396.8	10.8	44.1	0.95	35	4.62	3.77	2.67
2	198.4	12.7	51.9	0.90	40	3.18	2.60	1.84
3	132.9	12.5	51.0	0.87	38	2.74	2.24	1.58
6	66.3	12.3	50.2	0.79	34	2.06	1.68	1.19

Figure Captions

3.1 The derivation of the transfer equation for the specific intensity $I(\underline{r},\hat{\Omega})$.

3.2 The diffuse multipliers d_o and d_s as functions of B_o (the medium seismic albedo).

3.3 The behavior of the integrand of the integral for the coherent term.

3.4 The normalized energy density distribution curves $4\pi r^2 E(r)$, where r is the propagation distance from the point source. At the top are the curves of the diffuse term, at the bottom are that of the coherent term; in the middle are the curves of the sum of the two term. Here D_e is the numerical extinction distance, $L_e = 1/\eta_e$ is the extinction length of the medium, $\eta_e = \eta_s + \eta_a$ is the extinction coefficient, where η_s and η_a are the scattering coefficient and the absorption coefficient respectively. $B_o = \eta_s/(\eta_s+\eta_a)$ is the medium seismic albedo.

3.5 The schematic diagram of a possible multiple scattering path compared with the direct path. The hatched shell of unit thickness will receive the energy $4\pi r^2 E(r)$.

3.6 The normalized energy distribution curves $4\pi r^2 E(4)$ in the semi-logarithmic scale.

3.7 The energy distribution curves with the numerical absorption distance $D_a = r/La$, where $L_a = \eta_a$ is the absorption length of the medium. $\hat{b}$ is the apparent attenuation coefficient obtained from the slope of the curve. B_o is the medium albedo.

3.8 The energy distribution curves with the numerical scattering distance $D_s = 4/L_s$, where $L_s = 1/\eta_s$ is the scattering length of the medium. B_o is the medium albedo.

3.9 The relative strengths of the diffuse term E_d and the coherent term E_c at different extinction distances $D_e = r/L_e$ for different medium albedo B_o, where $L_e = 1/\eta_e$ is the extinction length of the medium.

3.10 Same as 3.9, at different scattering distances $D_s = r/L_s$, where $L_s = 1/\eta_s$ is the medium scattering length.

3.11 The normalized radial energy flux density $4\pi r^2 J_r(r)$ for the isotropic scatternig case and the strong forward scattering case.

3.12 Same as 3.11. The distance is the numerical absorption distance $D_s = r/L_a$, where $L_a = 1/\eta_a$ is the absorption length of the medium.

4.1 The derivation for the case of strong forward scattering approximation. z is along th forward direction. $\underline{r}$ is the position vector, $\underline{\rho}$ is the position vector in the transverse plan; $\hat{\Omega}$ is the unit vector in the scattering direction, and $\underline{s}$ is projection of $\hat{\Omega}$ in the transverse plan.

5.1 Map view of seismicity in the Hindu Kush as determined by Chatelain et al. (1980). The digital stations are indicated by open stars, and the smoked paper stations by solid diamonds.

5.2 Map view of all the Hindu Kush seismicity on smoked paper stations, divided into 50 km depth intervals. Locations of events recorded on the digital recorders are denoted by numbers used in Table 5.1 (from Roecker 1982).

5.3 The overall response of the digital recorder (from Roecker 1981).

5.4 The averaged coda attenuation rate $b_t = \beta b$, where β is the shear wave velocity, b is the attenuation coefficient. The solid line is obtained by Roecker (1982) for the shallow events, and the dotted line is the smoothed curve used in this paper.

5.5 Some seismograms for different hypocenter distances at station PEN. A42, r = 11.12 km, A67, r = 8.75 km; A16, r = 196.42 km; A02, r = 310.97 km.

5.6 Energy distribution curves $4\pi r^2 E(r)$ obtained from the data at station PEN. From left to right: Z, EW and NS components. From top to bottom: f = 0.25-1 Hz, f = 1.5-8 Hz, and f = 12-45 Hz.

5.7 The predicted $4\pi r^2 E(r)$ curves by the constant Q (=2000) model for different frequencies, if the measured apparent attenuation in Kanto, Japan by Aki (1980a) is assumed as the sum of the absorption coefficient and the scattering coefficient (Dainty 1981).

5.8 The comparison between the observed $4\pi r^2 E(r)$ for f = 1.5 and 2 hz at station PEN in Hindu Kush and the theoretical predictions for different B_0's. The curve of B_0 = 0.9 is the prediction from the constant Q (=2500) model, which does not match with the observation.

5.9 Examples of seismograms at station PEN (A34: r = 104 km, depth = 4.57 km; A08: r = 125 km, depth = 16.27 km), which show strong low frequency components immediately after the direct S).

5.10 The energy density curves $4\pi r^2 E(r)$ for direct S waves at f = 0.25, 0.5 and 1 Hz for station PEN. The curves are calculated using a 4 sec Hamming window for the direct S arrivals. Compare to fig. 5.6. No arch shape appears here.

5.11 Apparent attenuations derived from the slopes of the energy density curves (Fig. 5.6) for station PEN, together with the average coda attenuations and the direct S attenuations.

O: for EW component, total S

X: for Z component, total S

Δ: Z component, direct S (4 sec. window).

Note: For f<1Hz, the apparent attenuations are calculated by using only the last part of the curves (Fig. 5.6).

5.12 The energy density curves $4\pi r^2 E(r)$ for station CHS. From left to right: Z component and EW component. From top to bottom: f = 0.25-1 Hz, f = 1.5-8 Hz, and f = 12-45 Hz.

6.1 The seismogram envelopes of S waves predicted by the diffusion approximation for the case of f = 2 Hz, $B_0 = 0.9$ ($Q_i = 2500$). $\bar{\gamma}$ is the mean scattering angle cosine defined by (6.10).

6.2 The seismograms of moonquakes. The event on the top is supposed to be a meteoroid impact; the bottom event is believed to be a deep moonquake (from Latham et al., 1971).

6.3 The seismograms from the model experiment in laboratory (Dainty et al., 1974).

a) The seismogram with the homogeneous plate.

b) The seismogram when the plate has many grooves as scatterers.

6.4 The band-pass filtered seismograms of A06 (r = 235 km, depth = 103 km) for the stations CHS, FRA, JOR and PEN. From top to bottom: f = 0.375, 0.75, 1.5, 3, 6, 12, 24, 46 Hz.

6.5 The band-pass filtered seismograms of A15 (r = 247 km, depth = 118 km) for the stations CHS, PEN and JOR. From top to bottom: f = 0.375, 0.75, 1.5, 3, 6, 12, 24, 46 Hz.

6.6 The envelope decay curves of A15 (r = 247 km, depth = 118 km) for station PEN. From left to right: Z component and EW component. From top to bottom: f = 0.25, 0.5 Hz; f = 1-8 Hz; f = 12-45 Hz.

6.7 The theoretical envelope decay curve for the single isotropic scattering in a lossless medium according to Sato (1977). The envelope decay is a pure geometric spreading effect. The distance between the source and sensor is taken as 247 km (as the case of A15 to PEN).

6.8 The coda decay curves at station PEN for A15 after the geometric correction. The corrections were done by taking the ratios of the curves in Fig. 6.6 and that in Fig. 6.7. Note that, the curves for f = 1-20 Hz can be approximately fitted with straight lines, which means that, the scattering at this frequency range can be approximated by the single scattering theory.

7.1 Contour plot of the vertical variations in velocity inferred from 3D inversions, along with the seismicity in the region. The North-South cross section is made along 69°E. Locations of earthquakes occuring between 68°E and 70°E are indicated by closed circles. Percent changes in P and S wave velocities are shown in the upper and lower parts of the figure, respectively (from Roecker 1981).

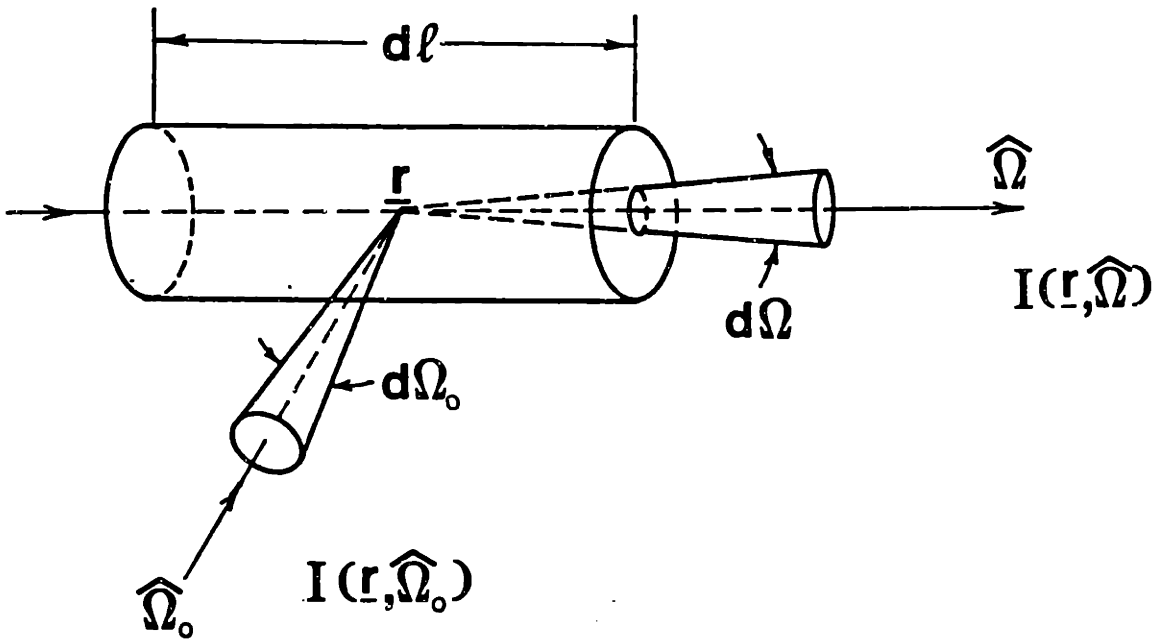

3.1 The derivation of the transfer equation for the specific intensity $I(\underline{r},\hat{\Omega})$.

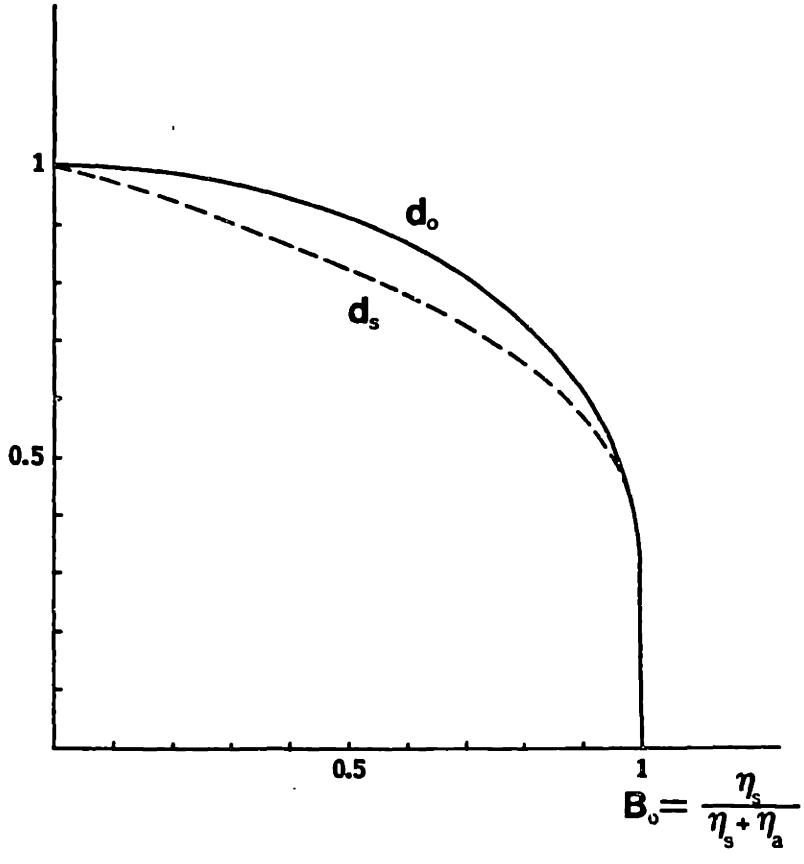

3.2 The diffuse multipliers d_o and d_s as functions of B_o (the medium seismic albedo).

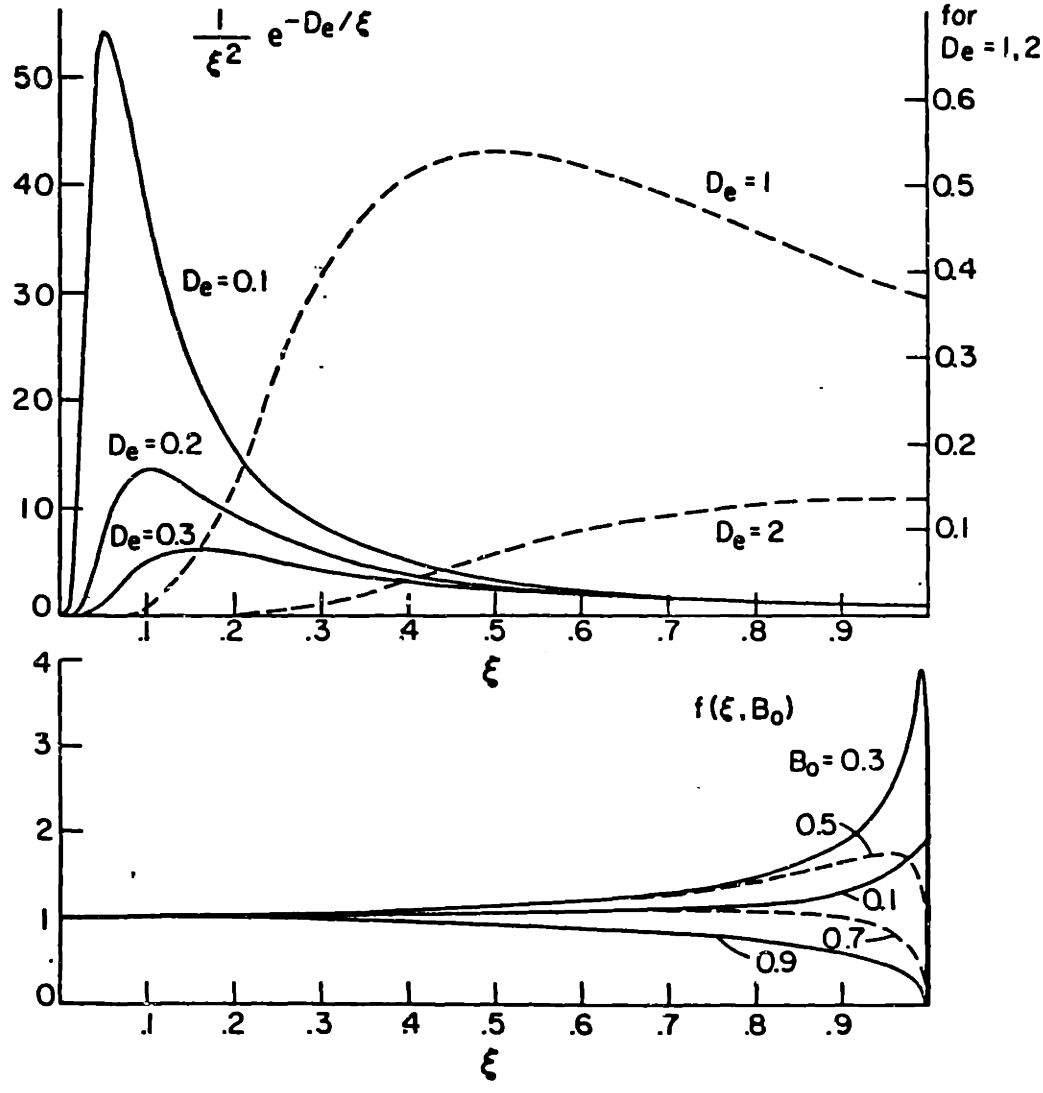

3.3 The behavior of the integrand of the integral for the coherent term.

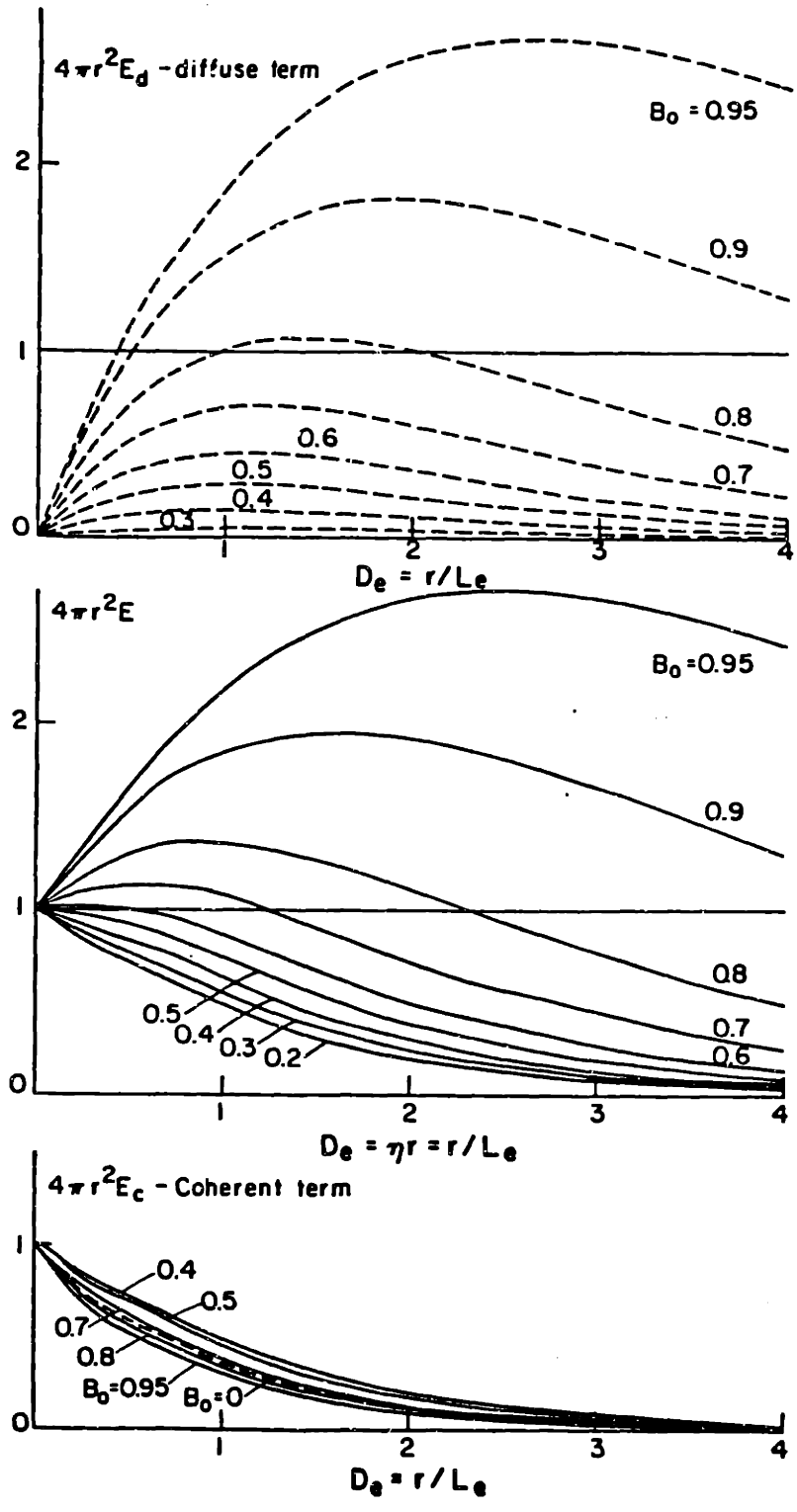

3.4 The normalized energy density distribution curves $4\pi r^2 E(r)$, where r is the propagation distance from the point source. At the top are the curves of the diffuse term, at the bottom are that of the coherent term; in the middle are the curves of the sum of the two term. Here D_e is the numerical extinction distance, $L_e = 1/\eta_e$ is the extinction length of the medium, $\eta_e = \eta_s + \eta_a$ is the extinction coefficient,

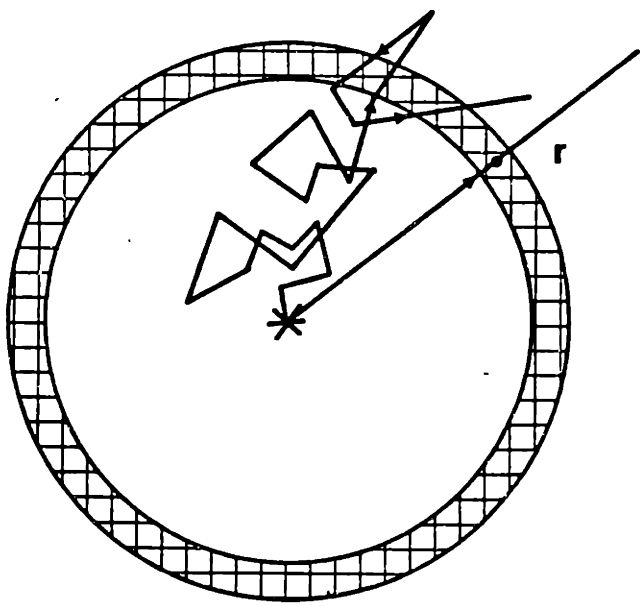

3.5 The schematic diagram of a possible multiple scattering path compared with the direct path. The hatched shell of unit thickness will receive the energy $4\pi r^2 E(r)$.

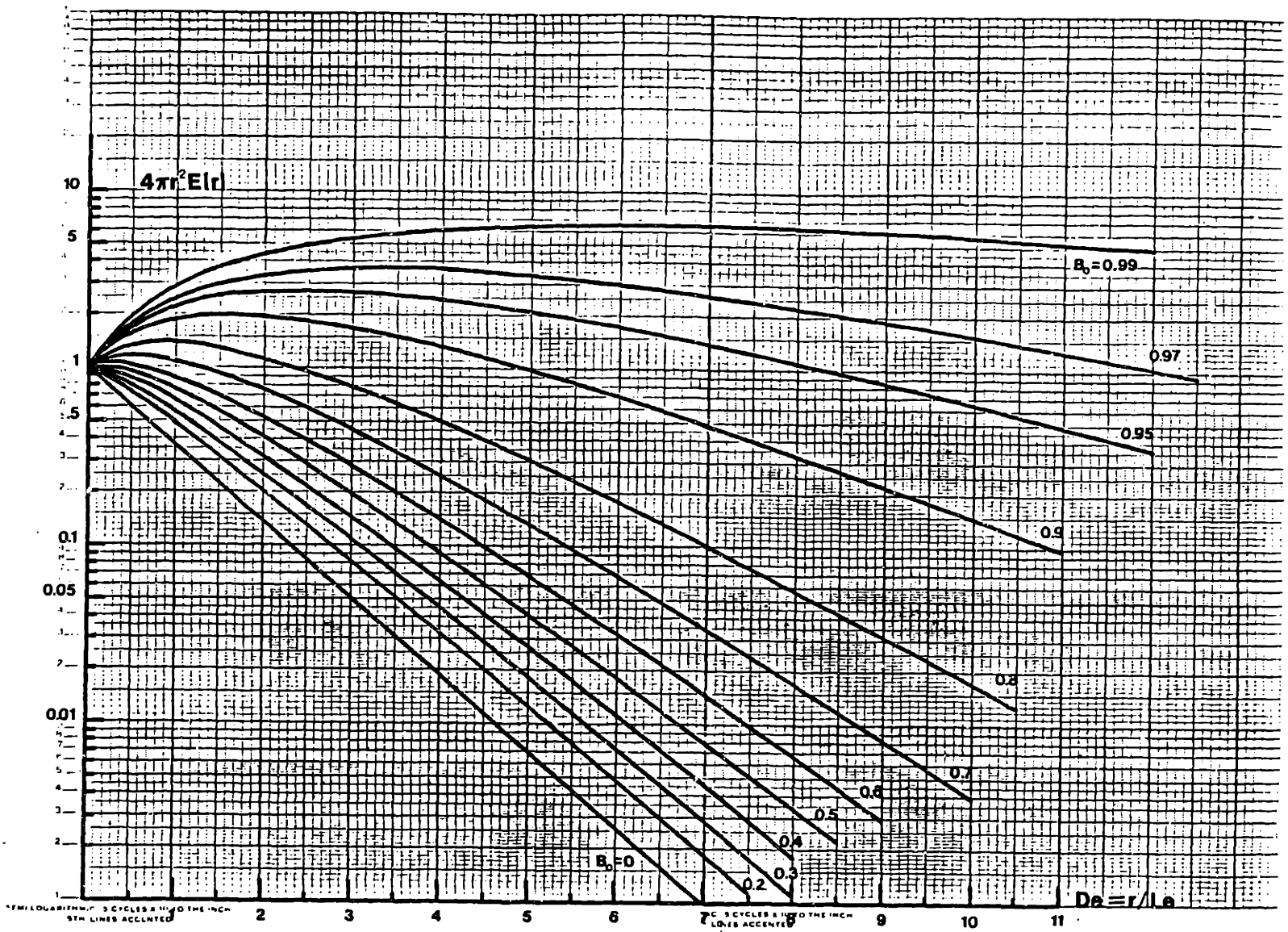

3.6 The normalized energy distribution curves $4\pi r^2 E(4)$ in the semi-logarithmic scale.

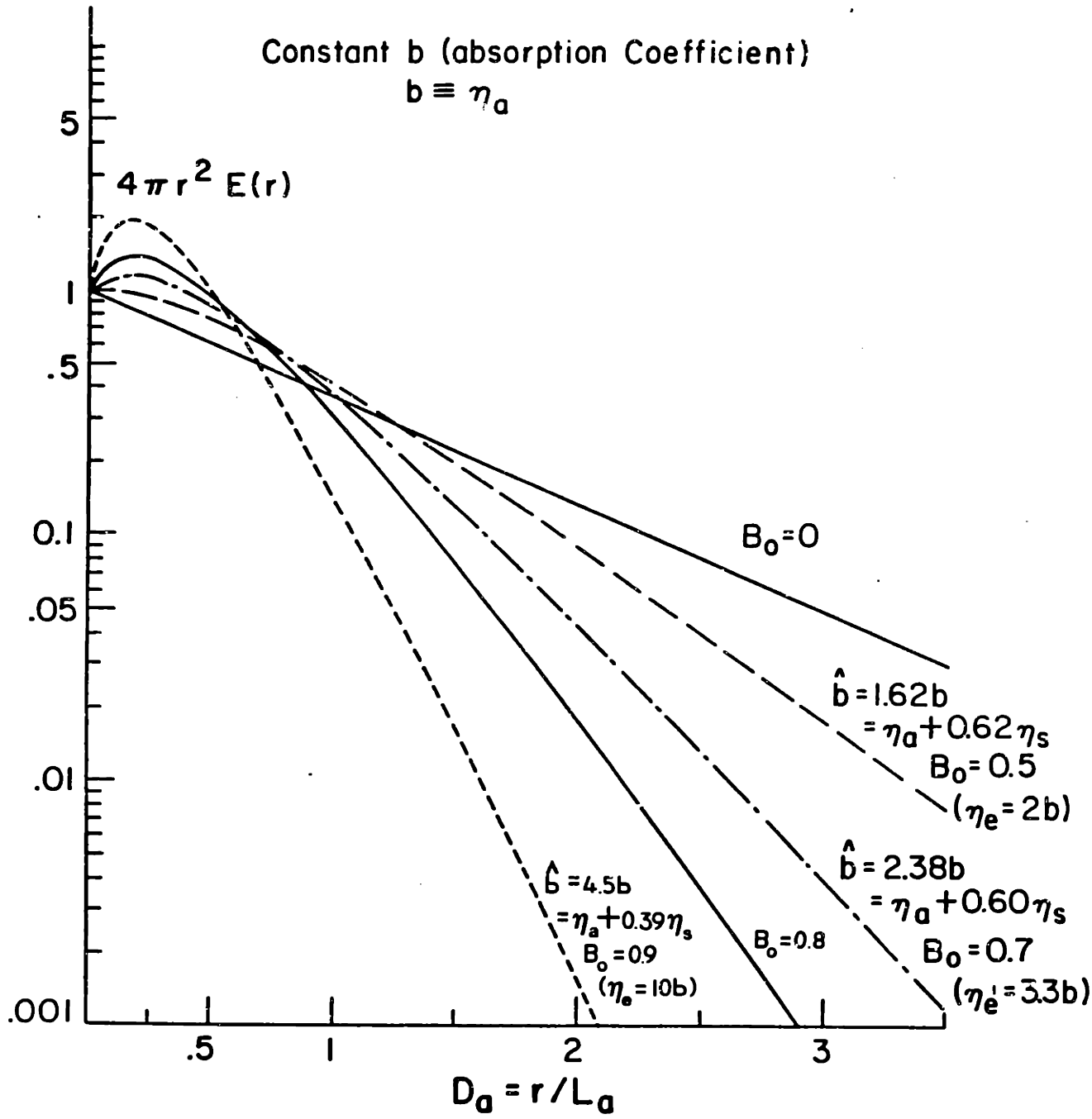

3.7 The energy distribution curves with the numerical absorption distance $D_a = r/La$, where $L_a = \eta_a$ is the absorption length of the medium. $\hat{b}$ is the apparent attenuation coefficient obtained from the slope of the curve. B_o is the medium albedo.

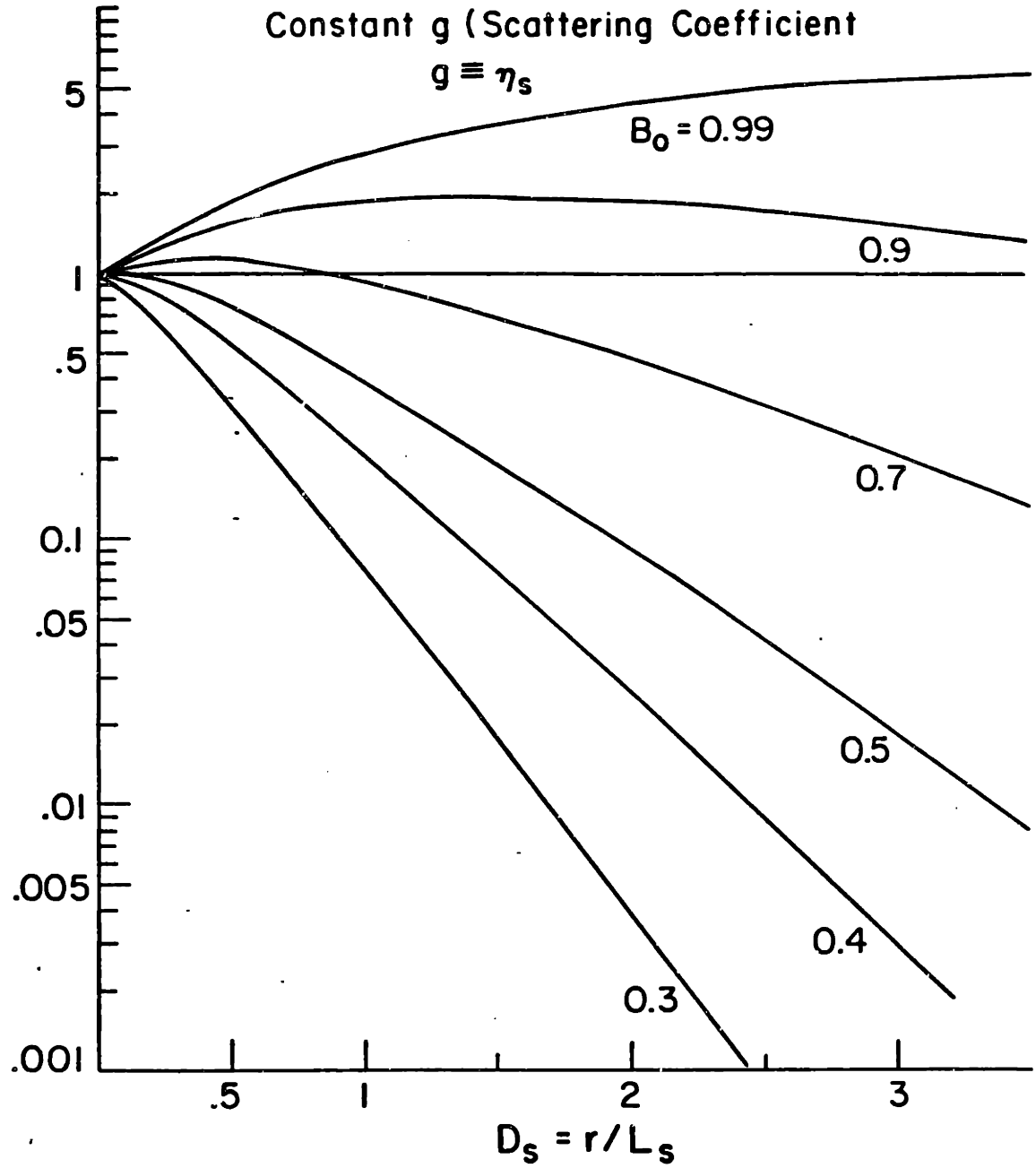

3.8 The energy distribution curves with the numerical scattering distance $D_s = 4/L_s$, where $L_s = 1/\eta_s$ is the scattering length of the medium. B_o is the medium albedo.

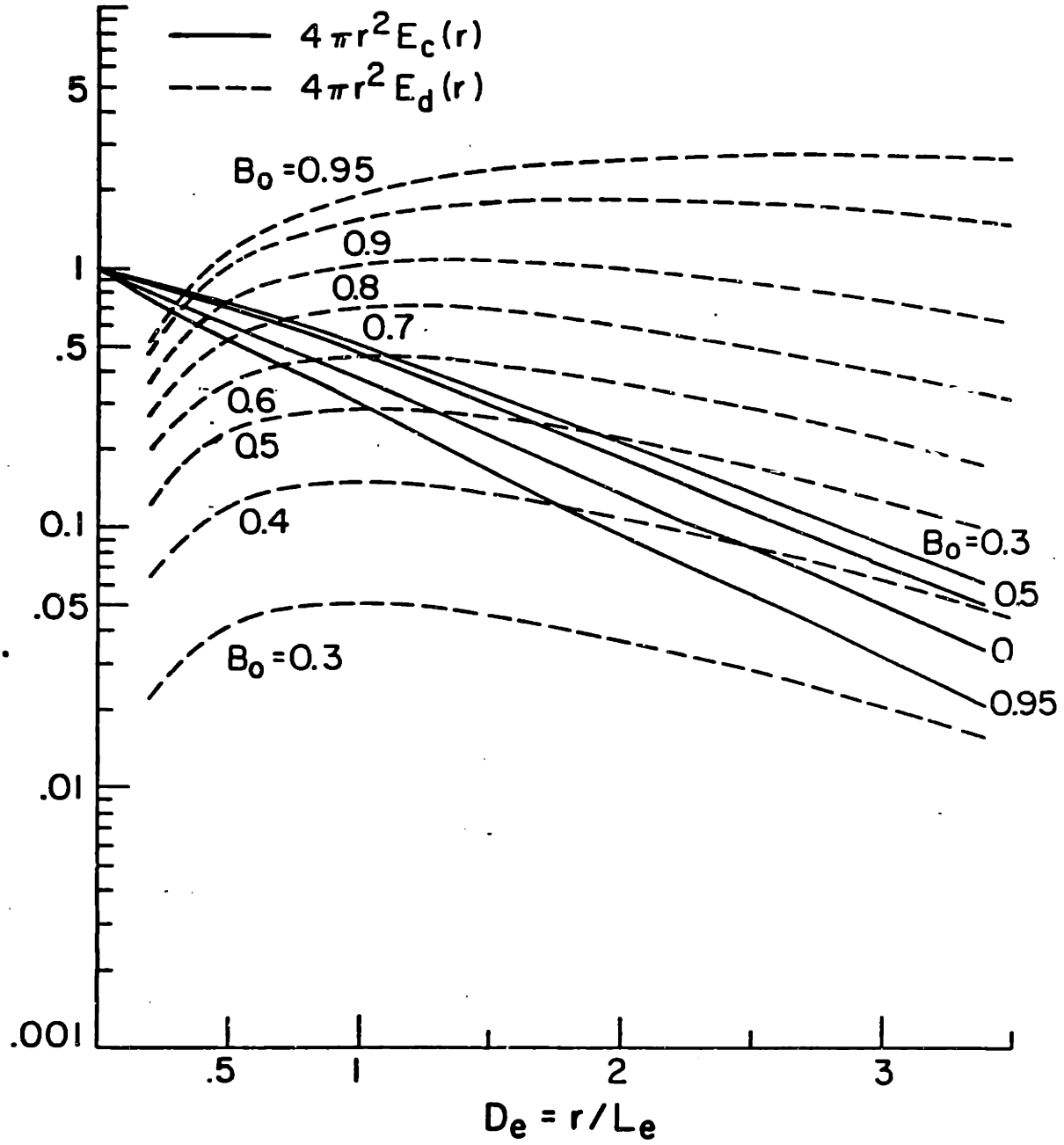

3.9 The relative strengths of the diffuse term E_d and the coherent term E_c at different extinction distances $D_e = r/L_e$ for different medium albedo B_o, where $L_e = 1/\eta_e$ is the extinction length of the medium.

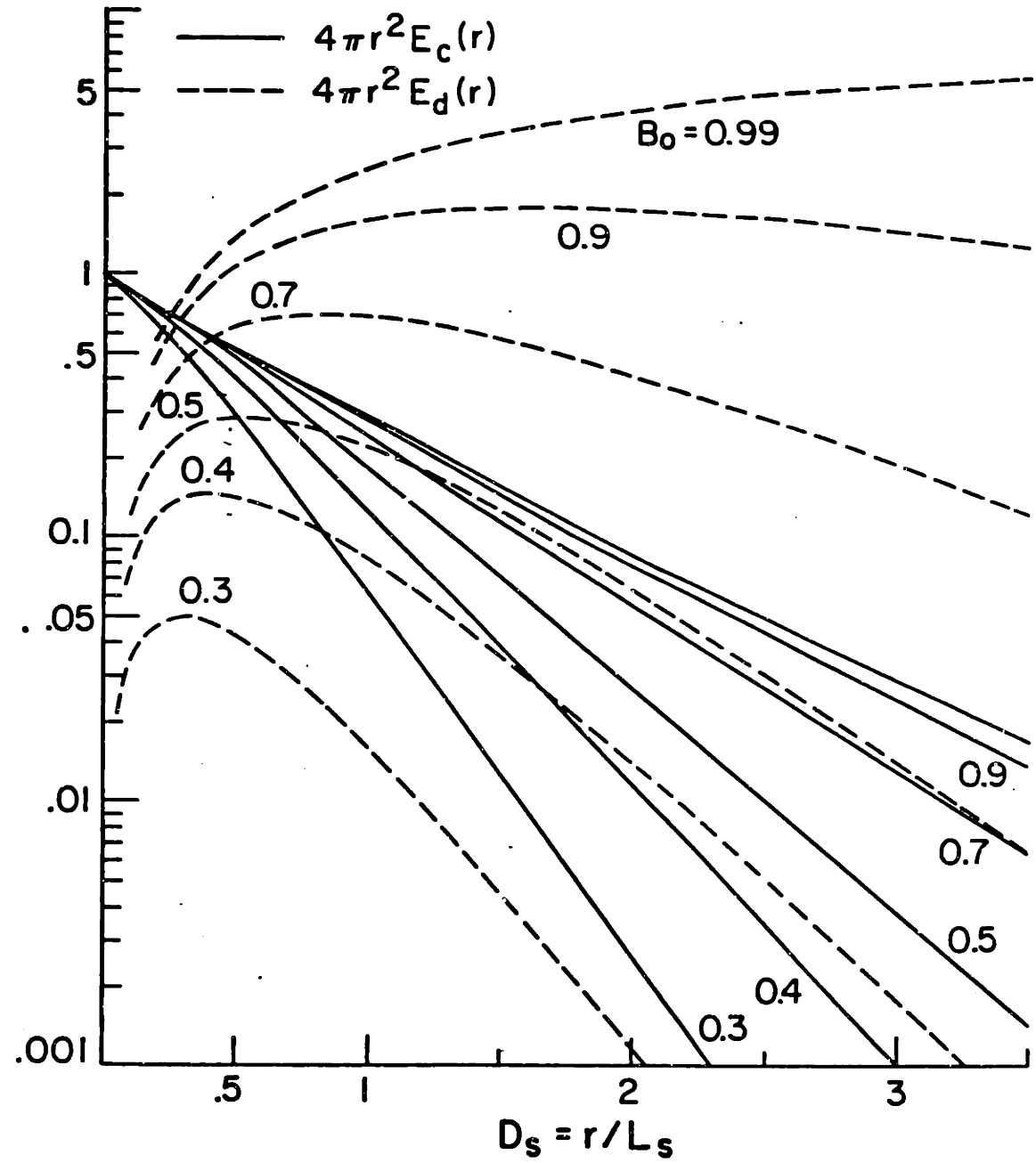

3.10 Same as 3.9, at different scattering distances $D_s = r/L_s$, where $L_s = 1/\eta_s$ is the medium scattering length.

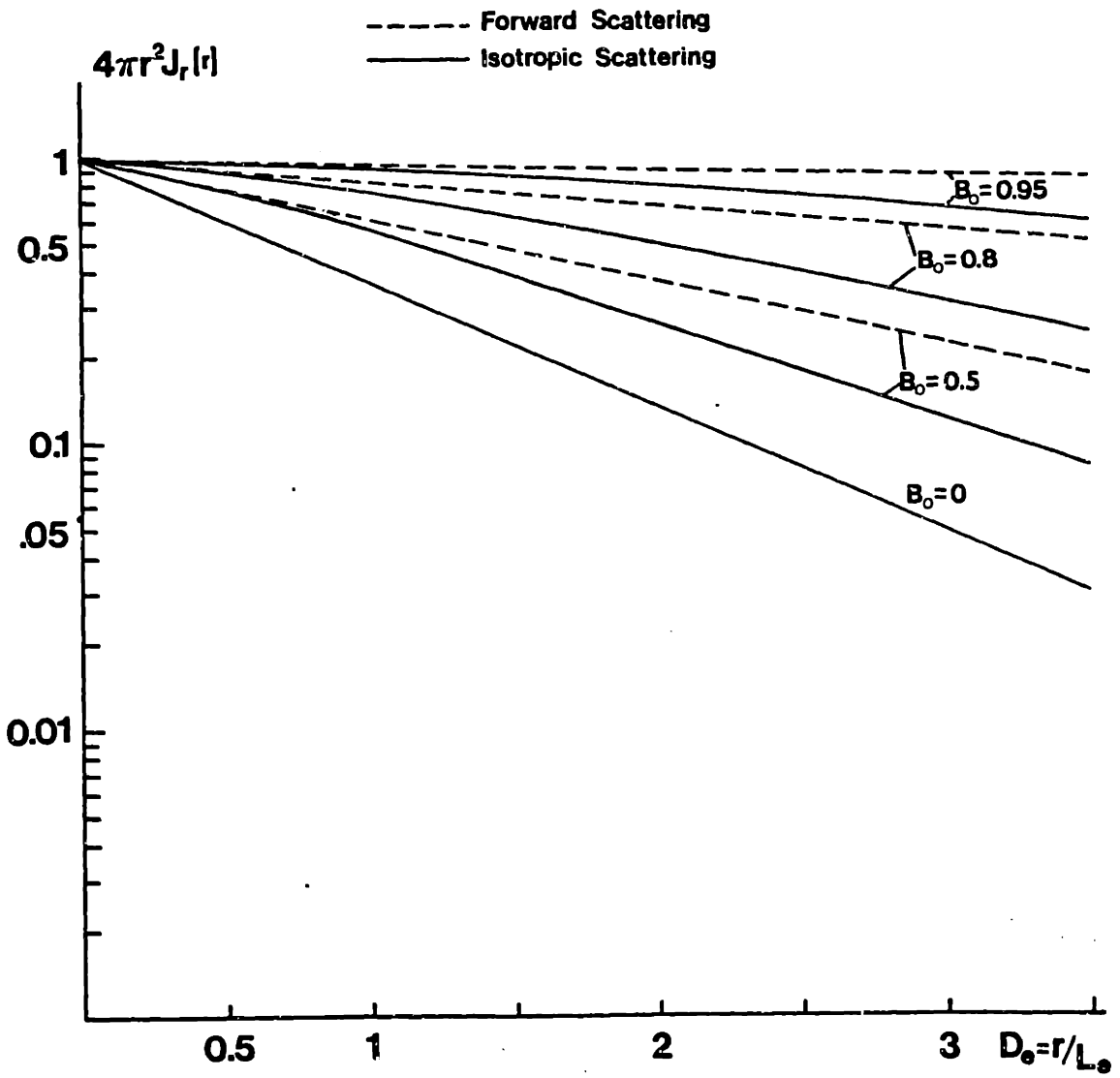

3.11 The normalized radial energy flux density $4\pi r^2 J_r(r)$ for the isotropic scatternig case and the strong forward scattering case.

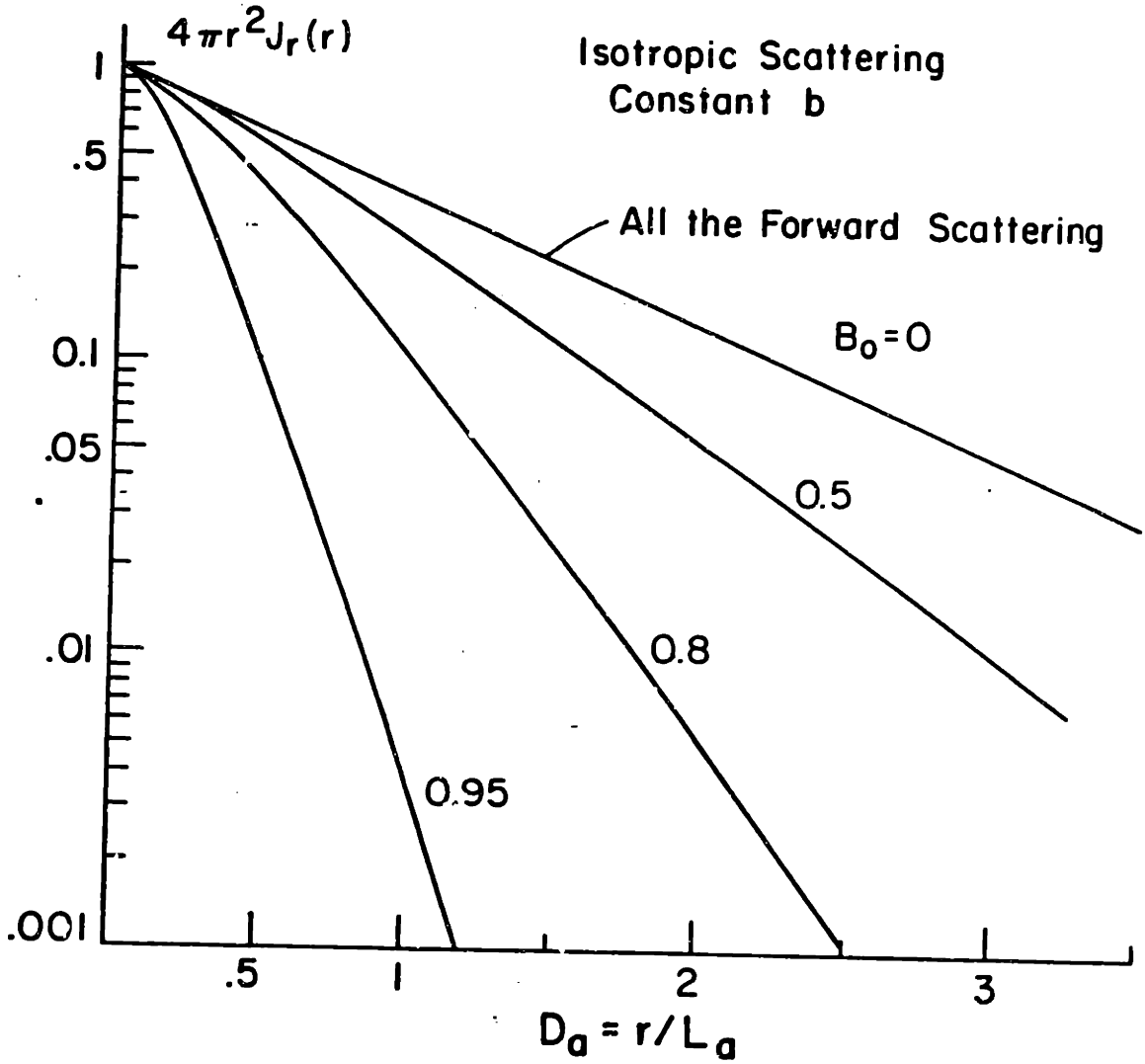

3.12 Same as 3.11. The distance is the numerical absorption distance $D_s = r/L_a$, where $L_a = 1/\eta_a$ is the absorption length of the medium.

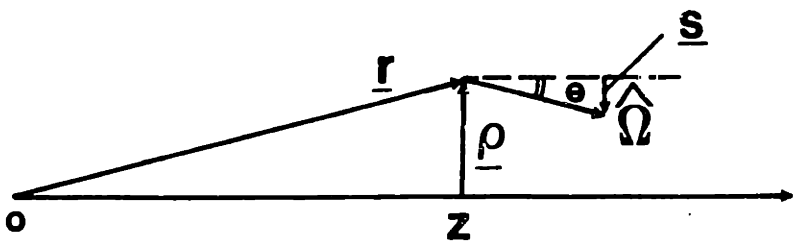

4.1 The derivation for the case of strong forward scattering approximation. z is along the forward direction. $\underline{r}$ is the position vector, $\underline{\rho}$ is the position vector in the transverse plan; $\hat{\Omega}$ is the unit vector in the scattering direction, and $\underline{s}$ is projection of $\hat{\Omega}$ in the transverse plan.

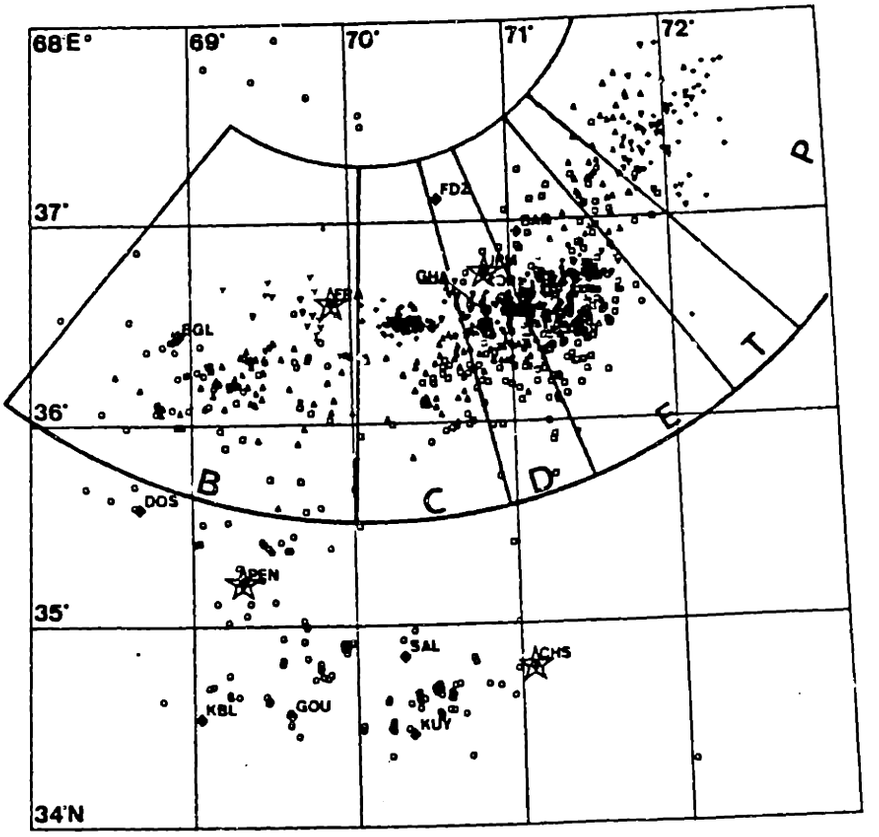

5.1 Map view of seismicity in the Hindu Kush as determined by Chatelain et al. (1980). The digital stations are indicated by open stars, and the smoked paper stations by solid diamonds.

5.2 Map view of all the Hindu Kush seismicity on smoked paper stations, divided into 50 km depth intervals. Locations of events recorded on the digital recorders are denoted by numbers used in Table 5.1 (from Roecker 1982). →

Figure (cont.)

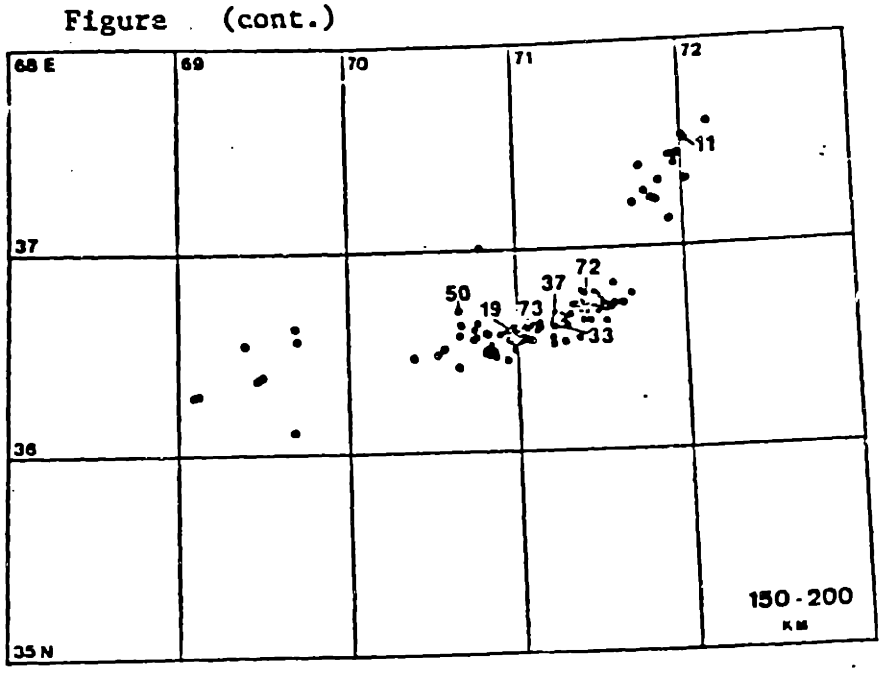
68 E
69
70
71
72
37
36
35 N
11
72
37
50
19
73
33
150 - 200
KM

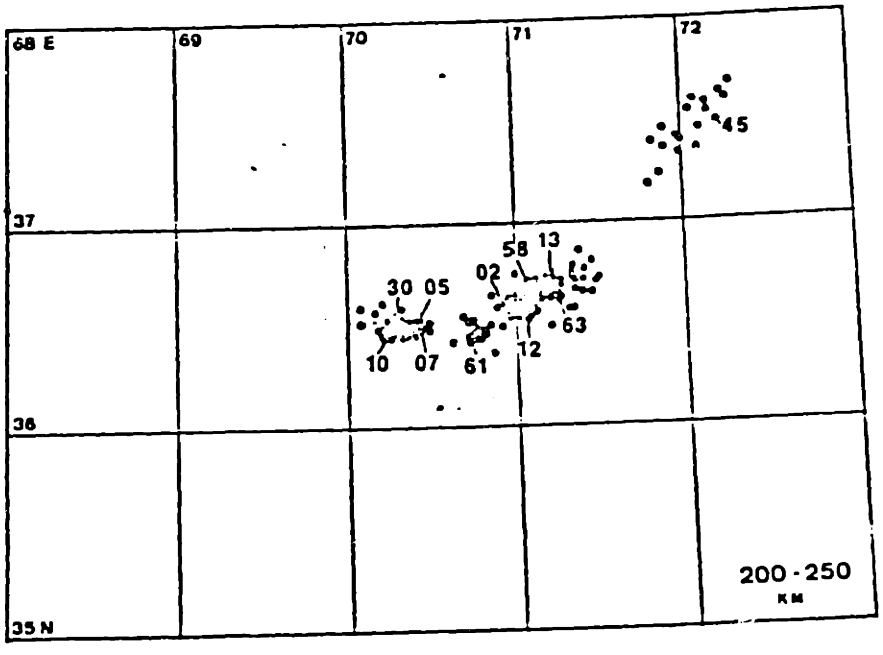
68 E
69
70
71
72
37
36
35 N
45
58
13
02
30
05
63
10
07
61
12
200 - 250
KM

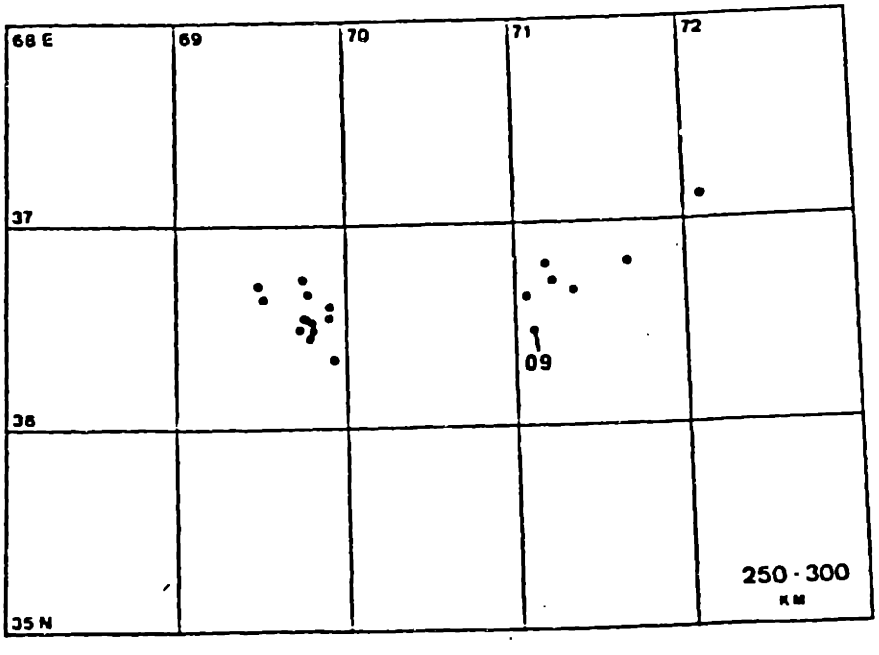
68 E
69
70
71
72
37
36
35 N
09
250 - 300
KM

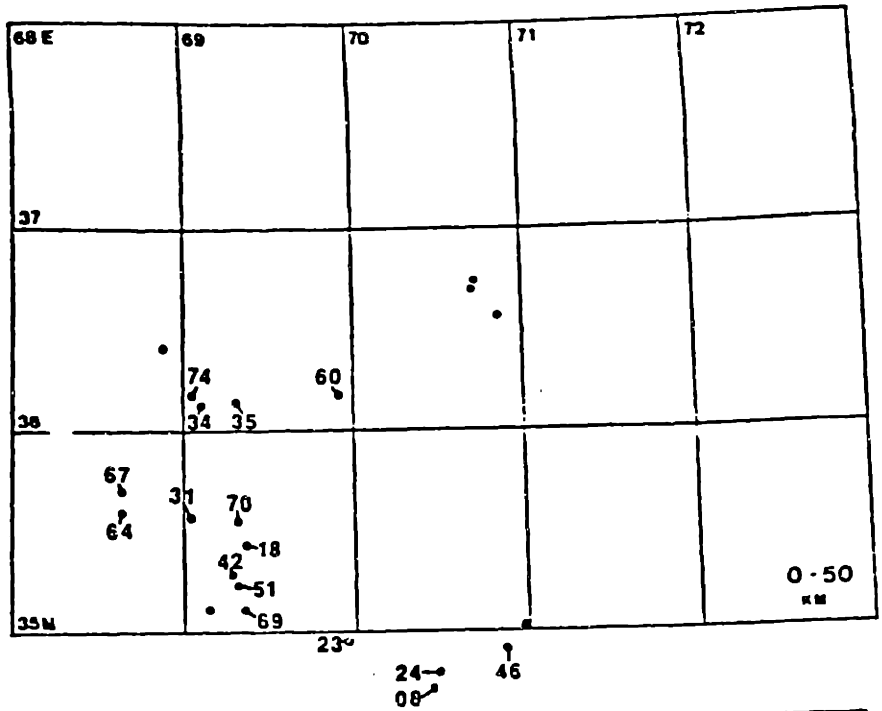
68 E
69
70
71
72
37
36
35N
74
60
34
35
67
31
70
64
18
42
51
69
23
24
08
46
0 - 50

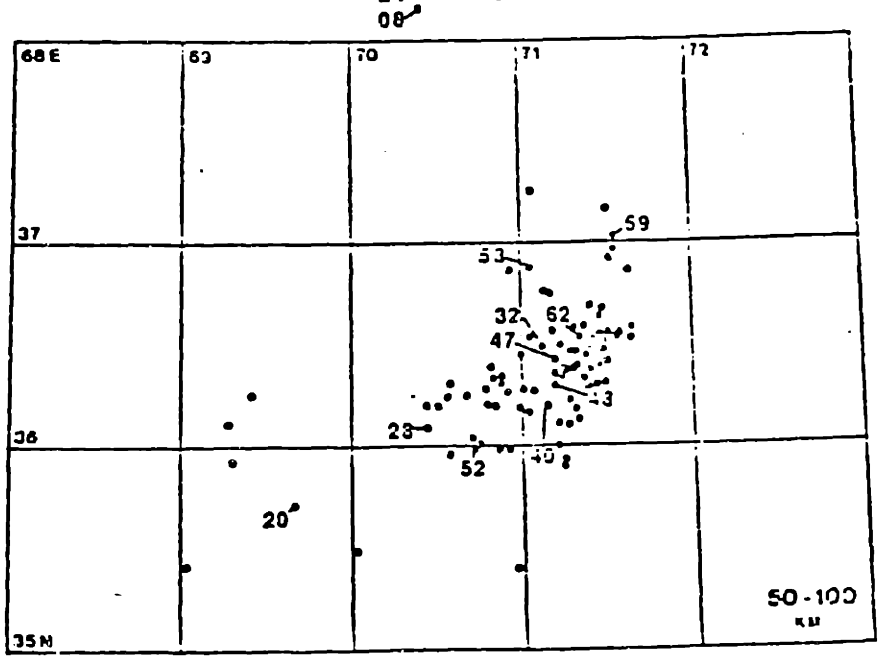
68 E
69
70
71
72
37
36
35N
59
53
32
62
47
3
23
52
20
50 - 100

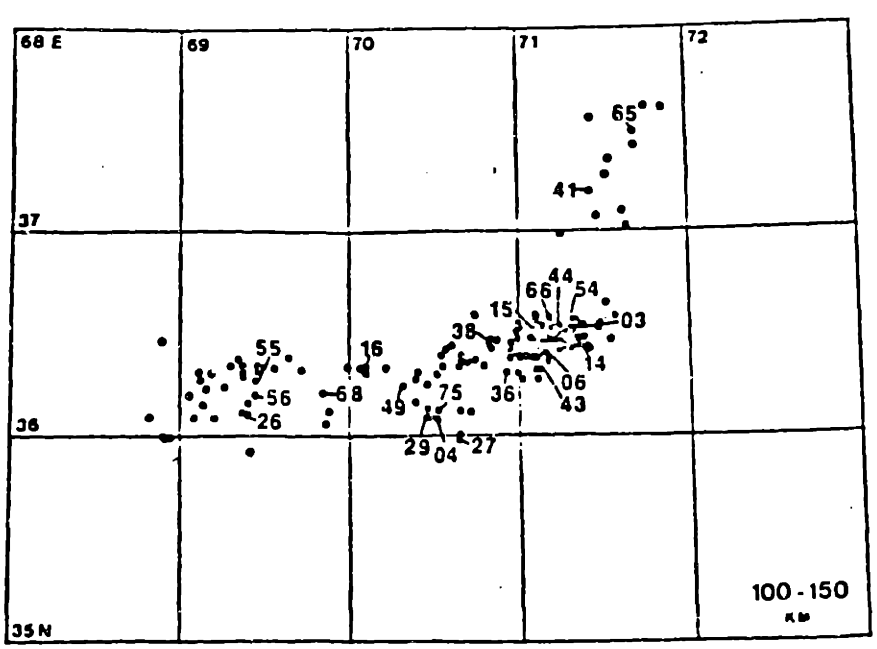
68 E
69
70
71
72
37
36
35N
65
41
44
66
54
15
03
38
14
55
16
56
68
75
36
06
43
49
26
29
04
27
100 - 150

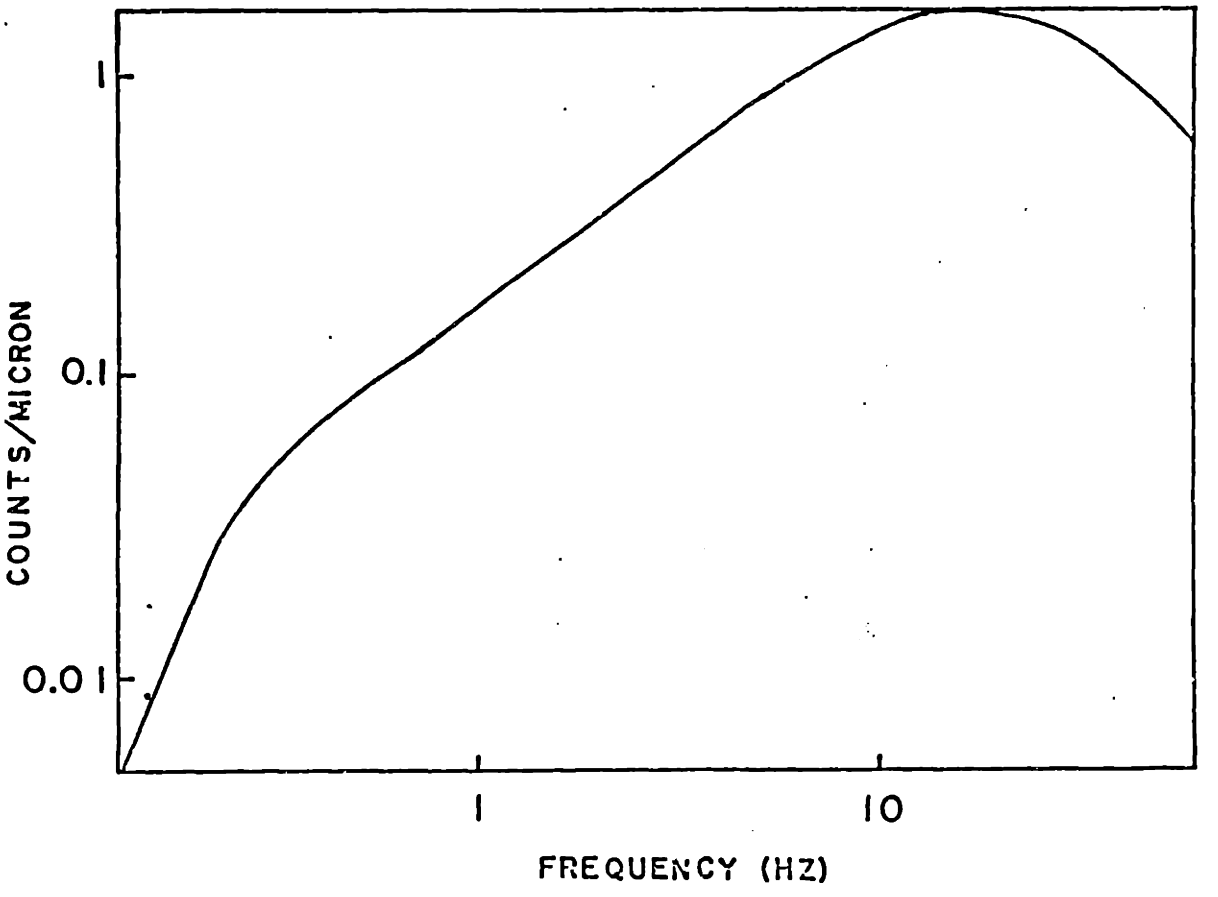

5.3 The overall response of the digital recorder (from Roecker 1981).

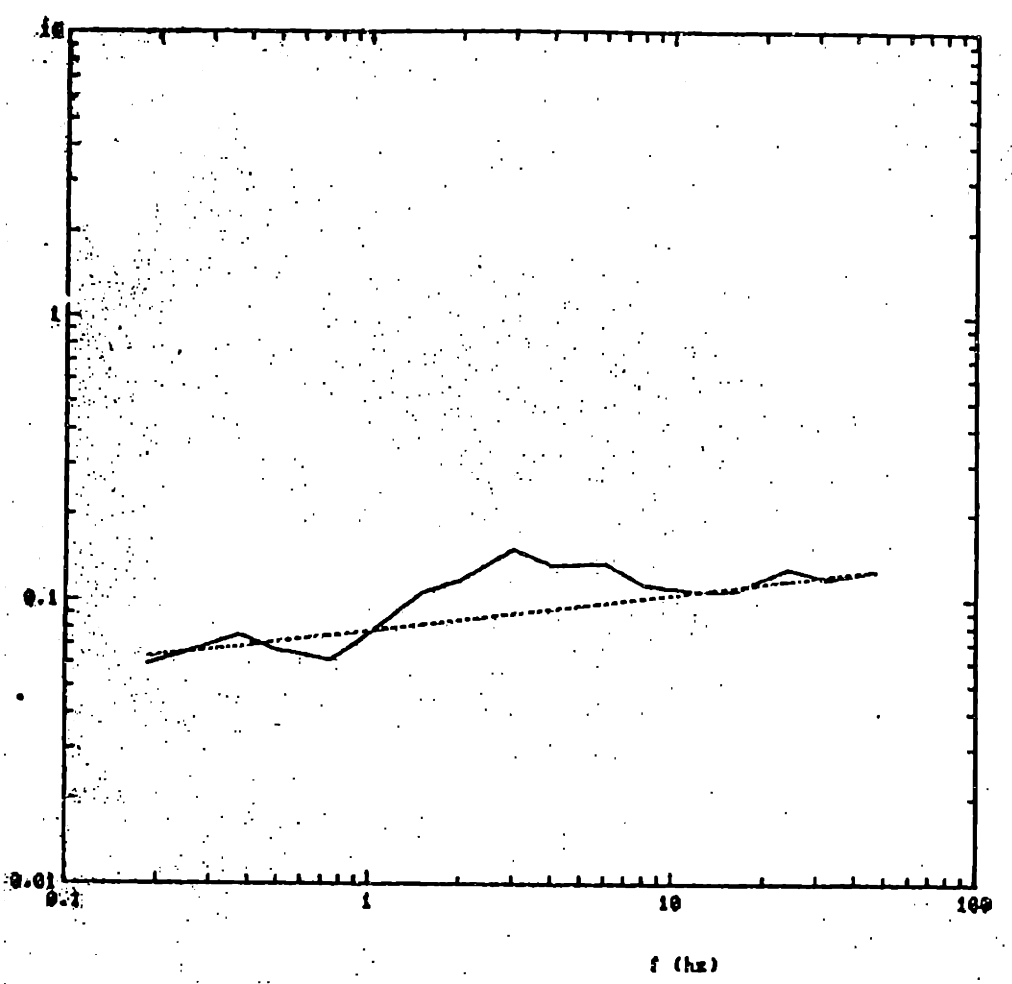

5.4 The averaged coda attenuation rate $b_t = \beta b$, where β is the shear wave velocity, b is the attenuation coefficient. The solid line is obtained by Roecker (1982) for the shallow events, and the dotted line is the smoothed curve used in this paper.

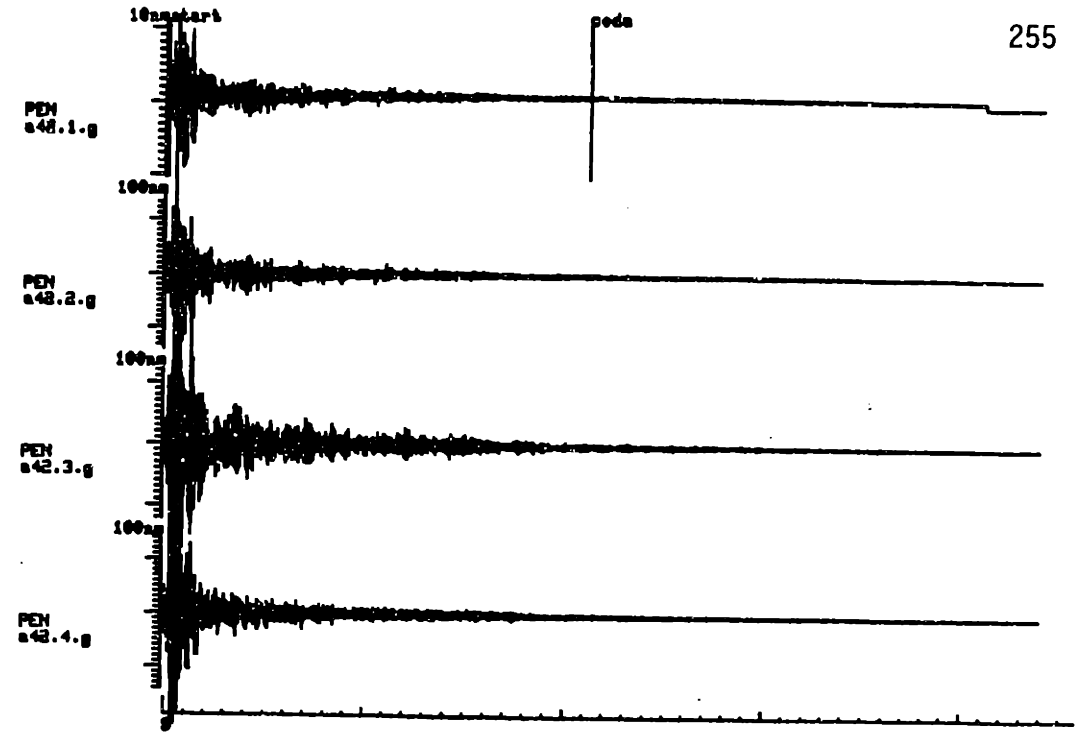

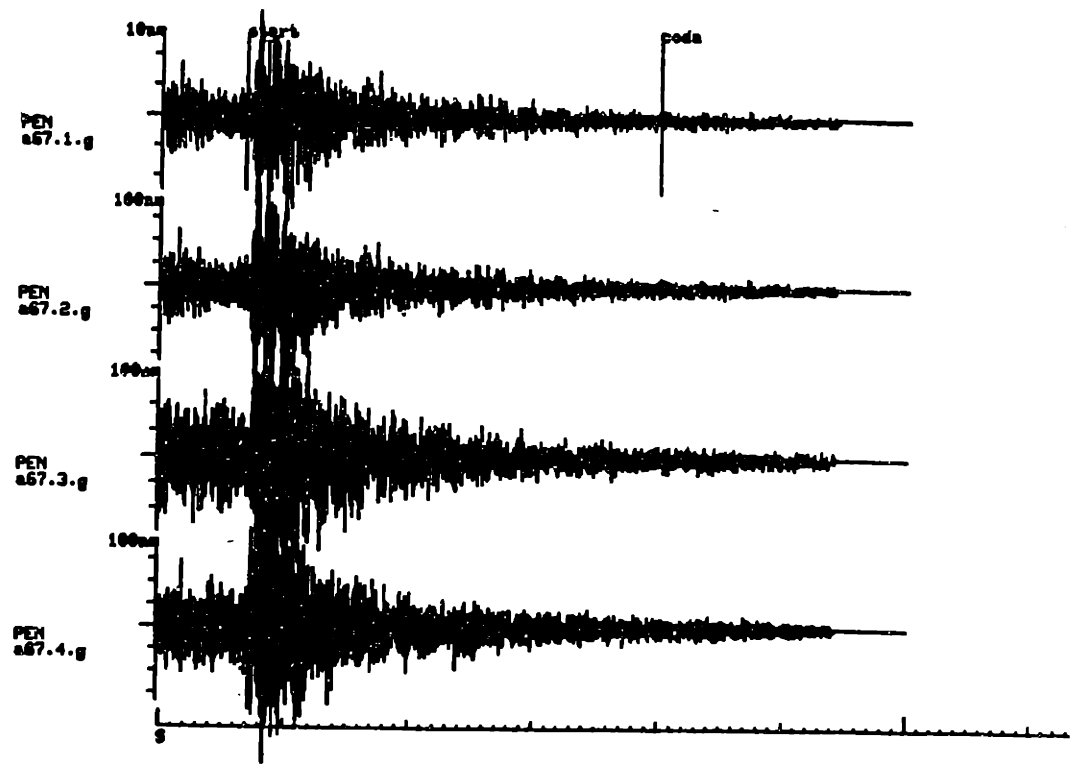

5.5 Some seismograms for different hypocenter distances at station PEN. A42, r = 11.12 km, A67, r = 8.75 km; A16, r = 196.42 km; A02, r = 310.97 km.

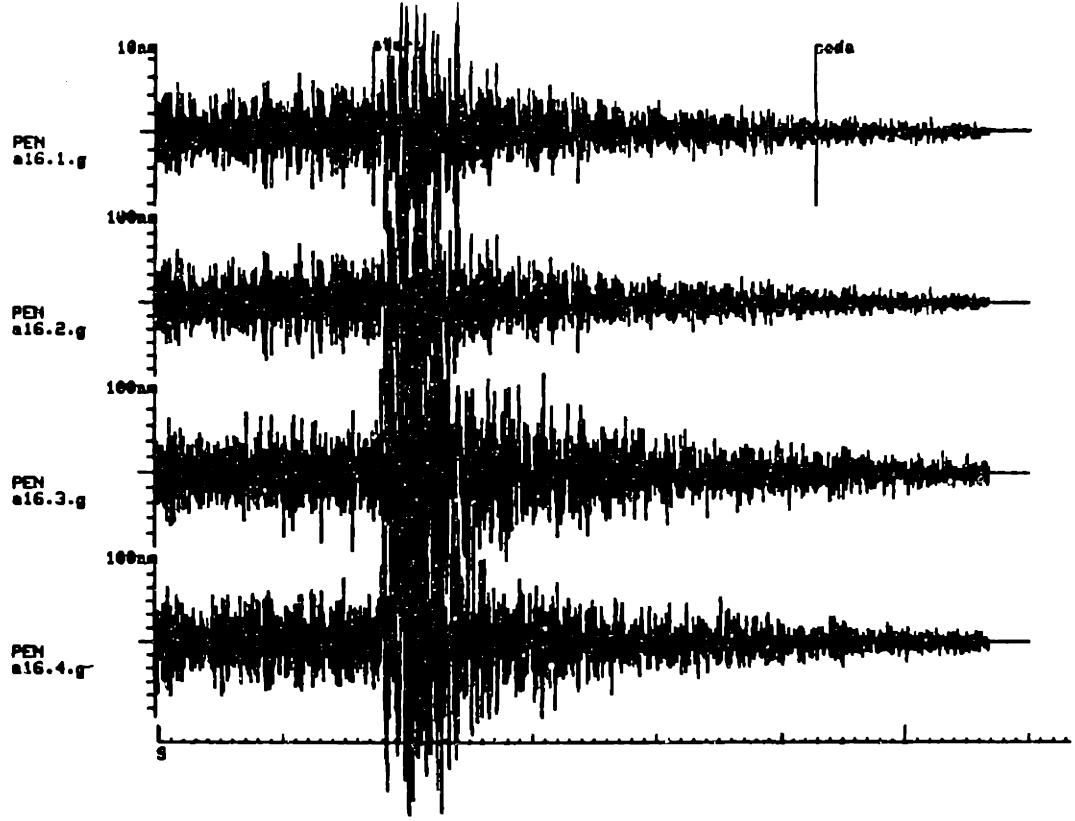
coda
PEN
a16.1.g
PEN
a16.2.g
PEN
a16.3.g
PEN
a16.4.g
S

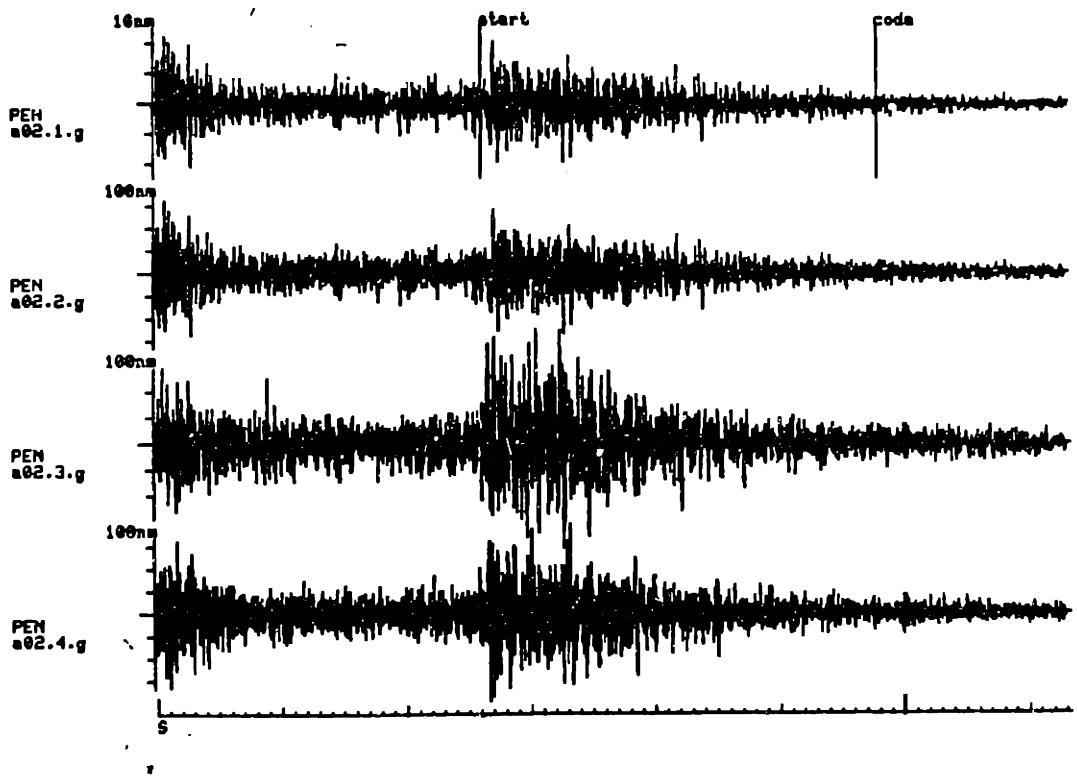
start
coda
PEN
a02.1.g
PEN
a02.2.g
PEN
a02.3.g
PEN
a02.4.g
S

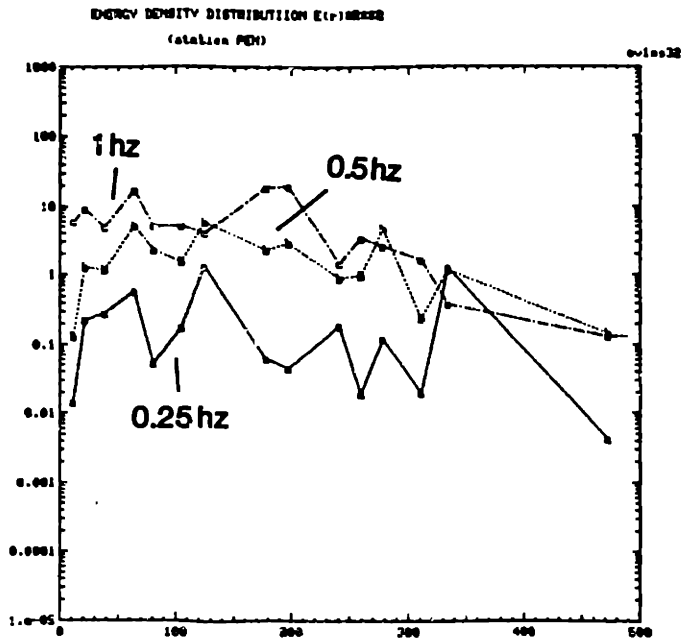
1hz
0.5hz
0.25hz

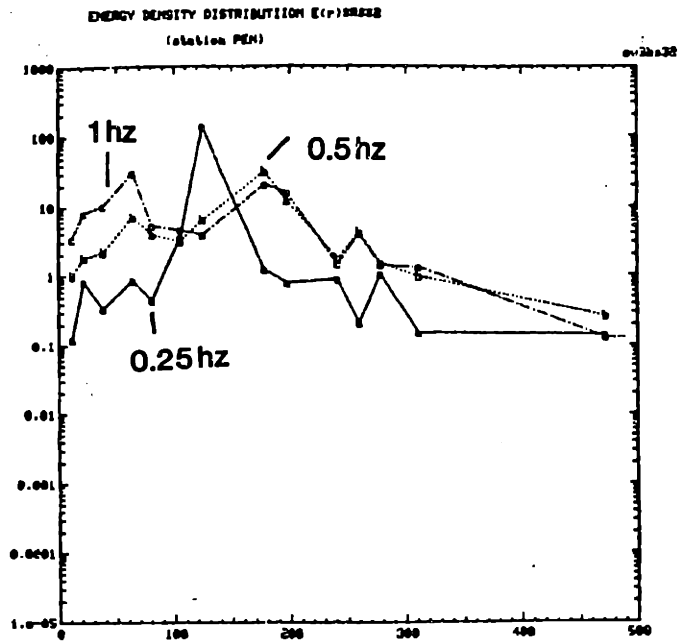
1hz
0.5hz
0.25hz

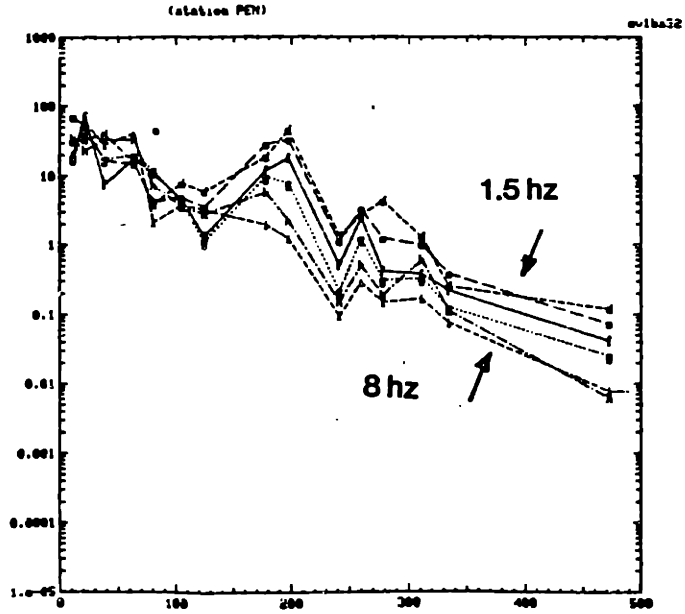
1.5hz
8hz

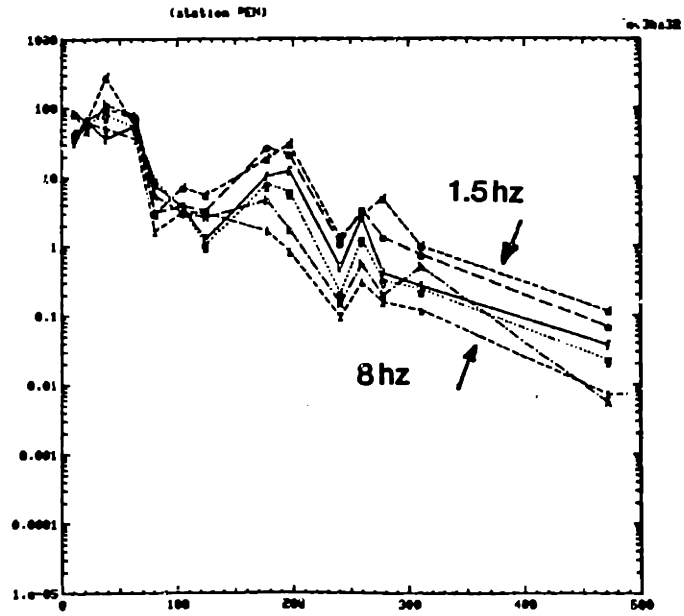
1.5hz
8hz

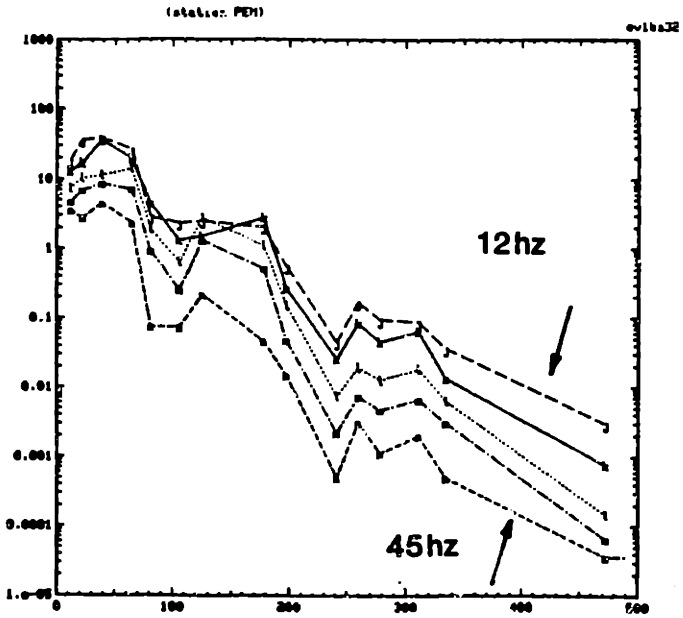
12hz
45hz

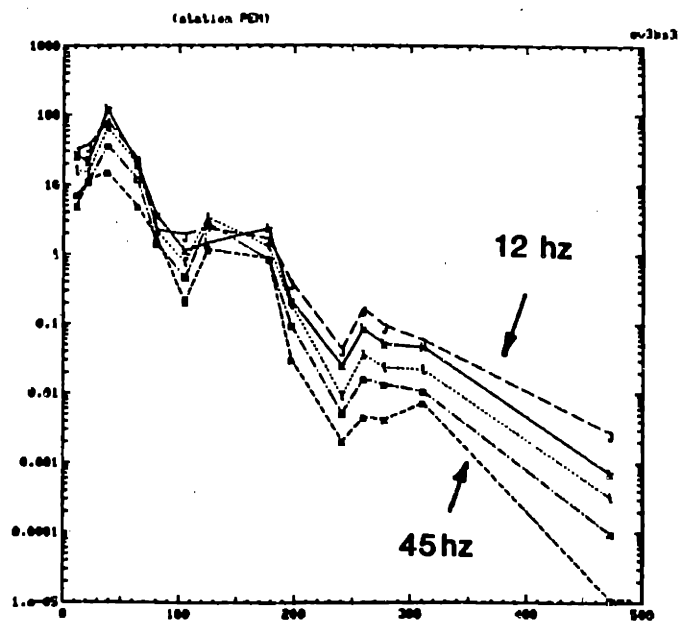
12 hz
45hz

R (km)

R (km)

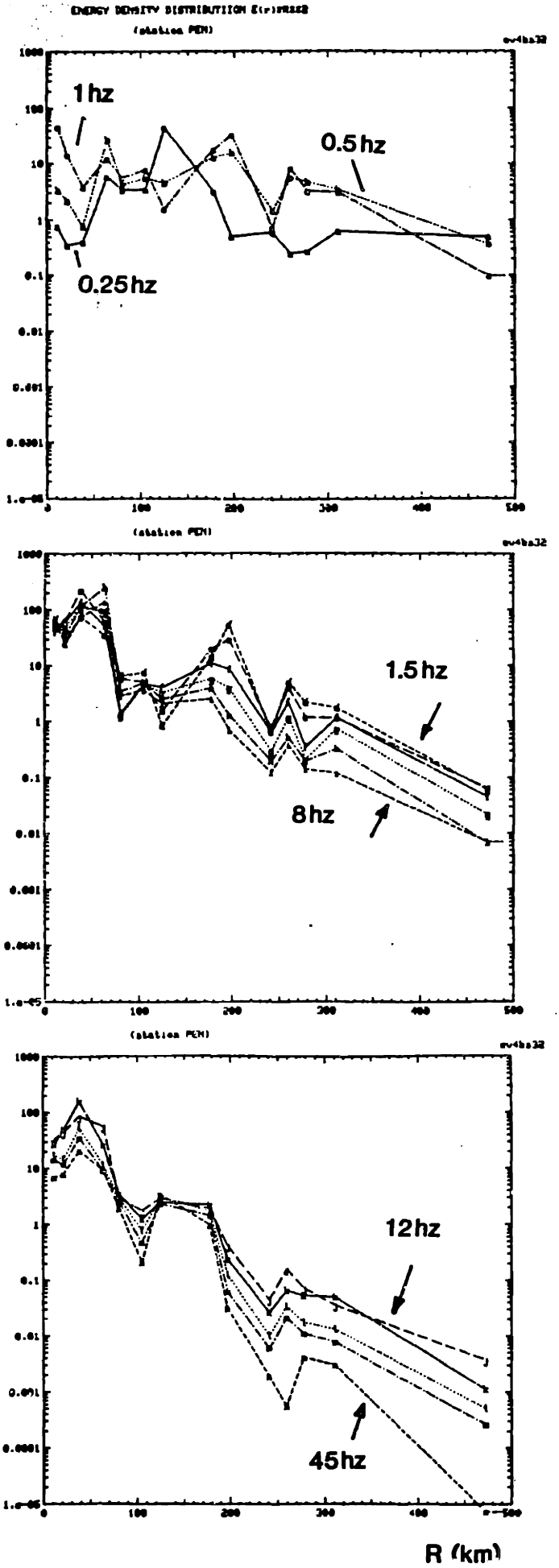

5.6 Energy distribution curves $4\pi r^2 E(r)$ obtained from the data at station PEN. From left to right: Z, EW and NS components. From top to bottom: f = 0.25-1 Hz, f = 1.5-8 Hz, and f = 12-45 Hz.

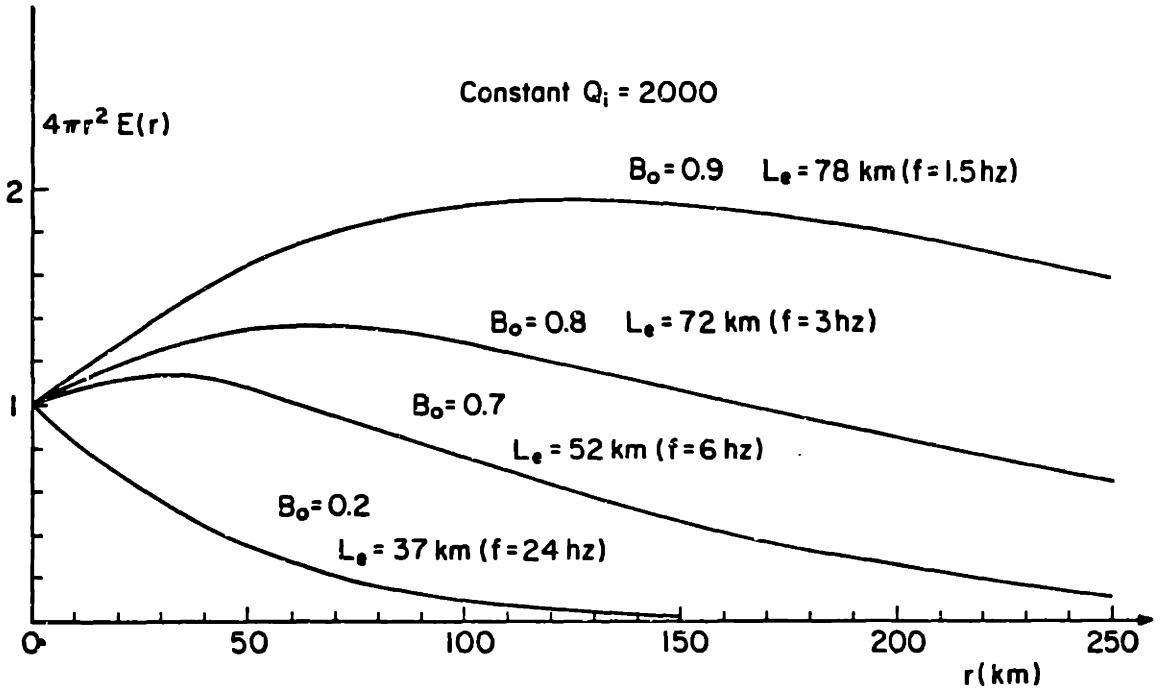

5.7 The predicted $4\pi r^2 E(r)$ curves by the constant Q (=2000) model for different frequencies, if the measured apparent attenuation in Kanto, Japan by Aki (1980a) is assumed as the sum of the absorption coefficient and the scattering coefficient (Dainty 1981).

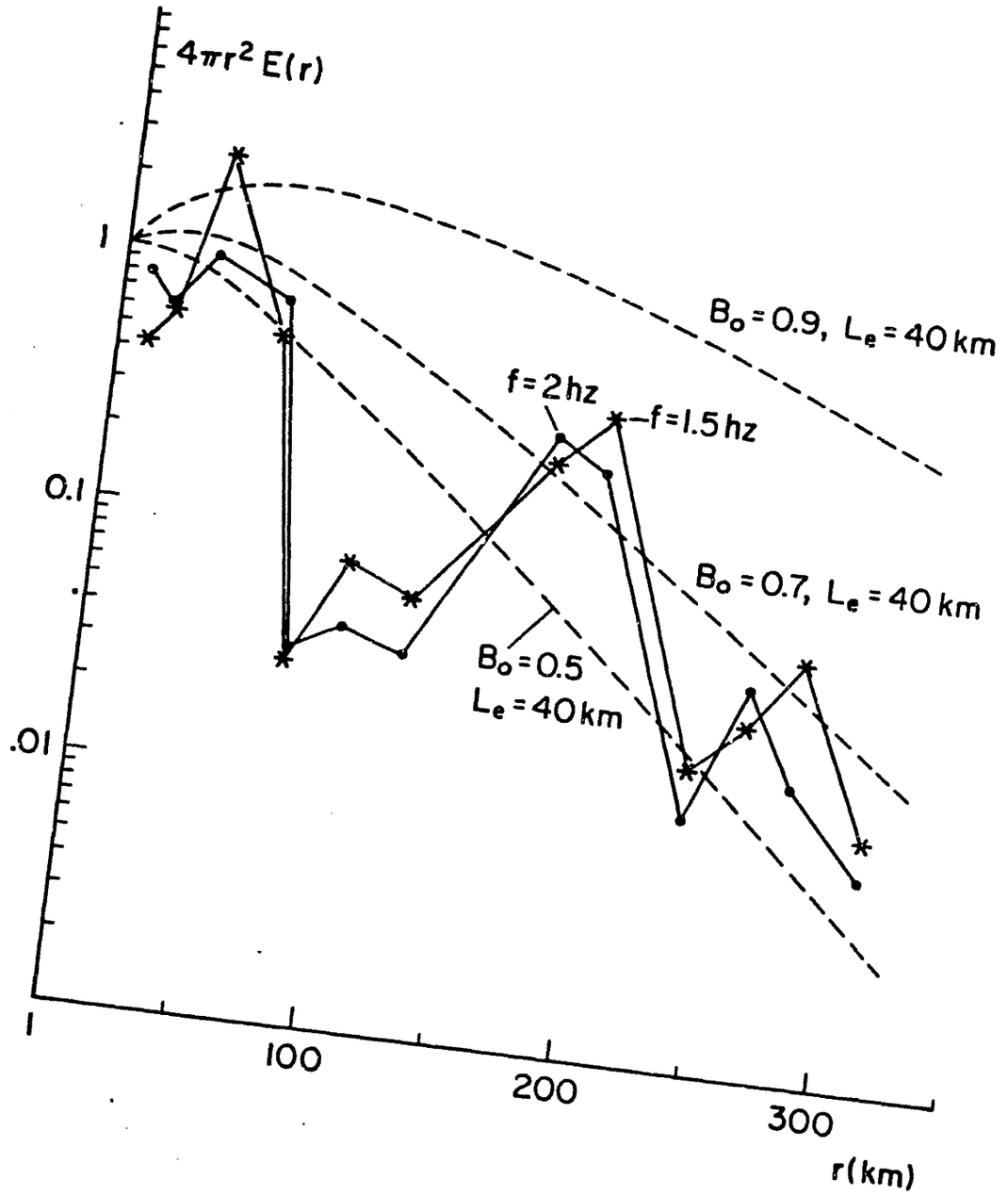

5.8 The comparison between the observed $4\pi r^2 E(r)$ for f = 1.5 and 2 hz at station PEN in Hindu Kush and the theoretical predictions for different B_o's. The curve of $B_o = 0.9$ is the prediction from the constant Q (=2500) model, which does not match with the observation.

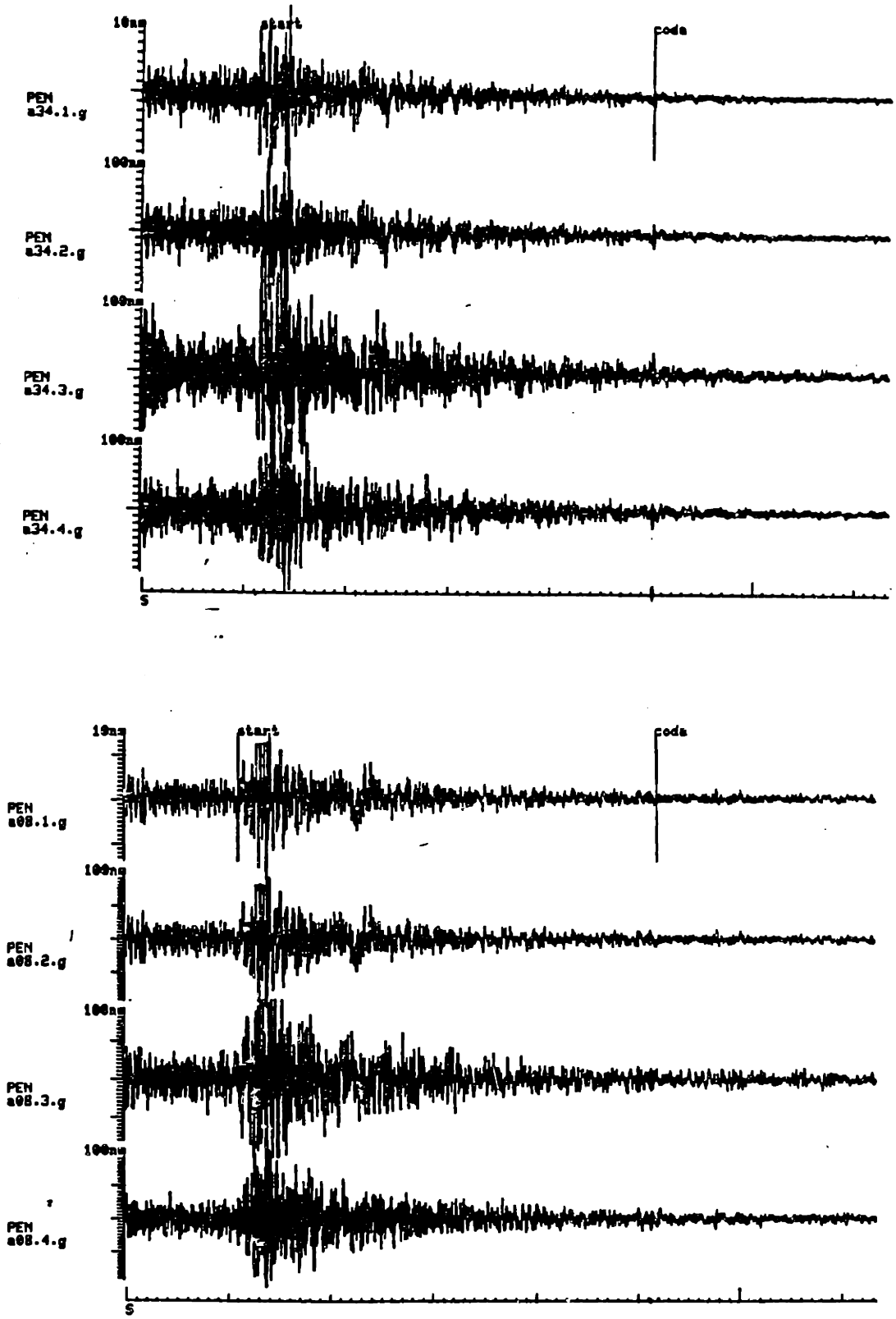

5.9 Examples of seismograms at station PEN (A34: r = 104 km, depth = 4.57 km; A08: r = 125 km, depth = 16.27 km), which show strong low frequency components immediately after the direct S).

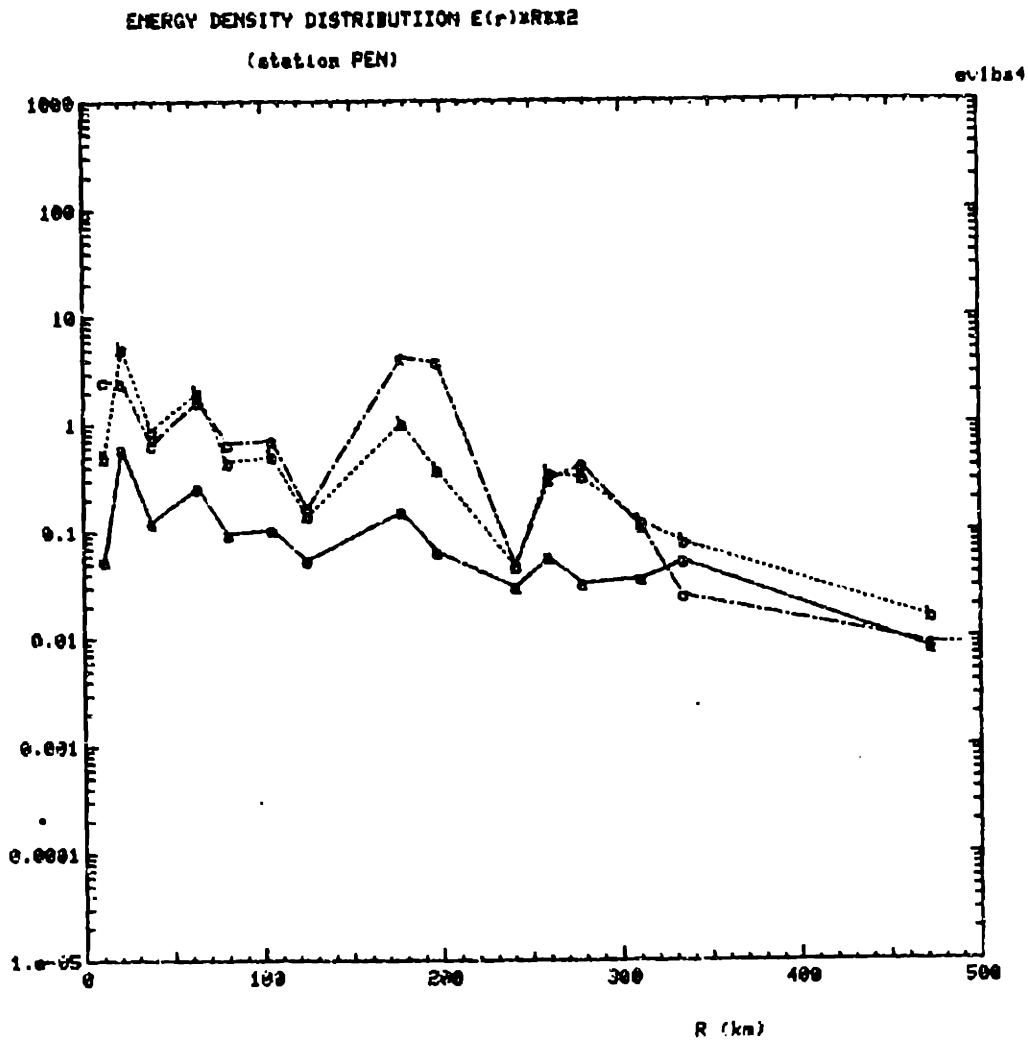

5.10 The energy density curves $4\pi r^2 E(r)$ for direct S waves at f = 0.25, 0.5 and 1 Hz for station PEN. The curves are calculated using a 4 sec Hamming window for the direct S arrivals. Compare to fig. 5.6. No arch shape appears here.

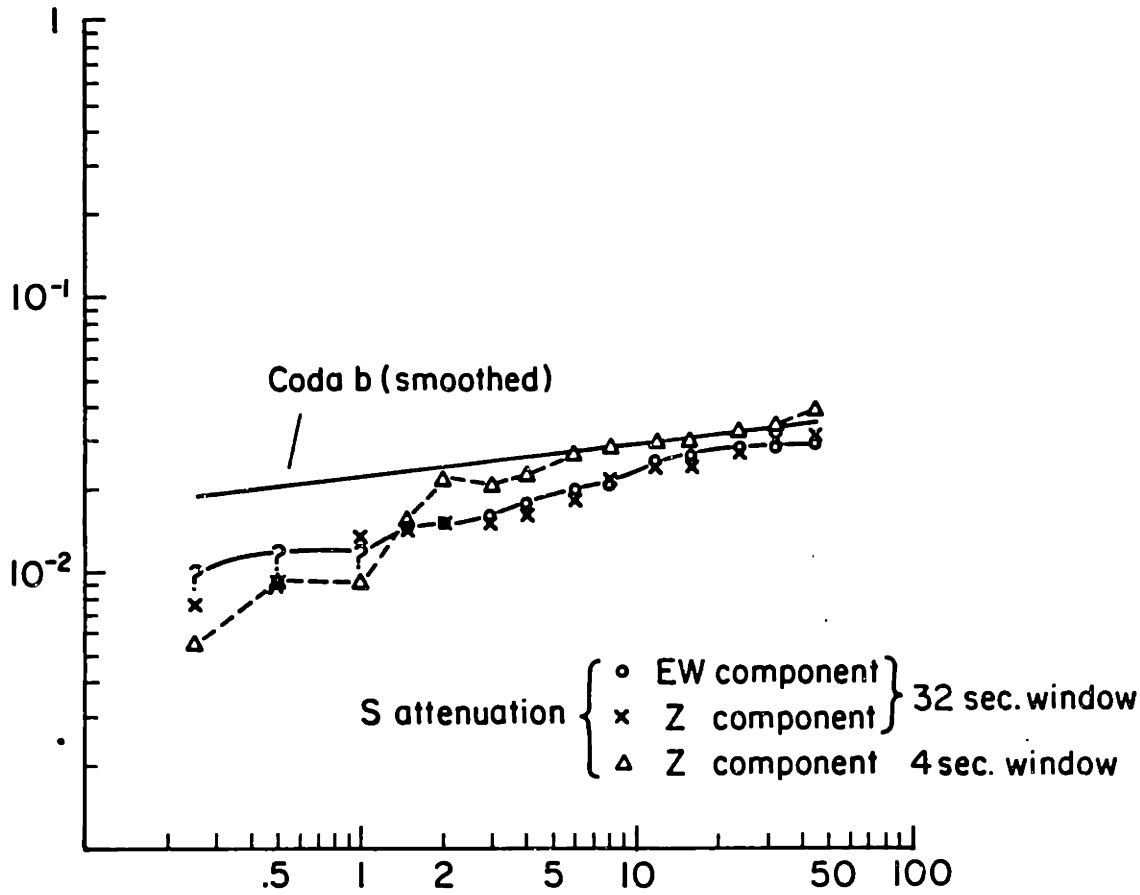

5.11 Apparent attenuations derived from the slopes of the energy density curves (Fig. 5.6) for station PEN, together with the average coda attenuations and the direct S attenuations.

O: for EW component, total S

X: for Z component, total S

Δ: Z component, direct S (4 sec. window).

Note: For f<1Hz, the apparent attenuations are calculated by using only the last part of the curves (Fig. 5.6).

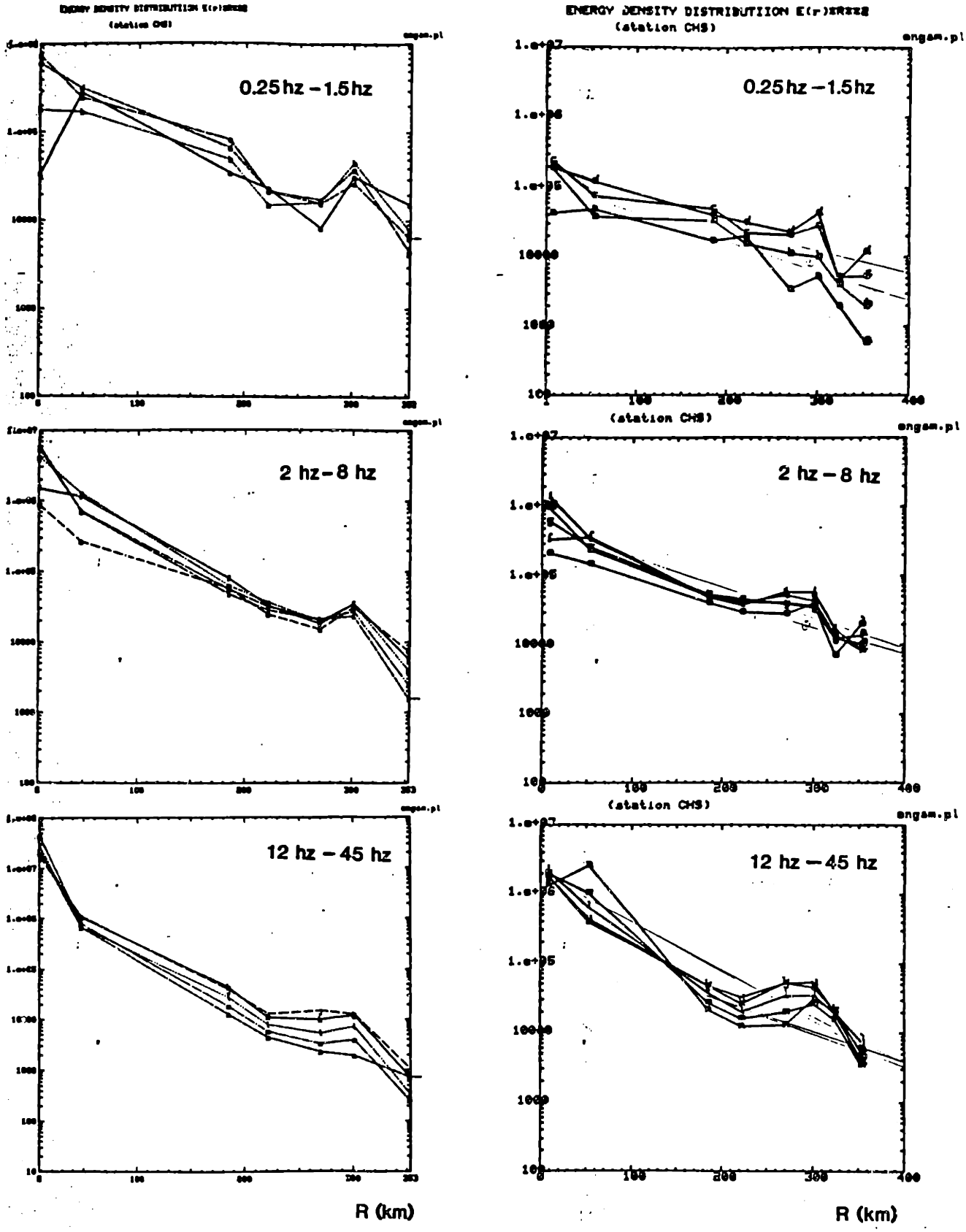

5.12 The energy density curves $4\pi r^2 E(r)$ for station CHS. From left to right: Z component and EW component. From top to bottom: f = 0.25-1 Hz, f = 1.5-8 Hz, and f = 12-45 Hz.

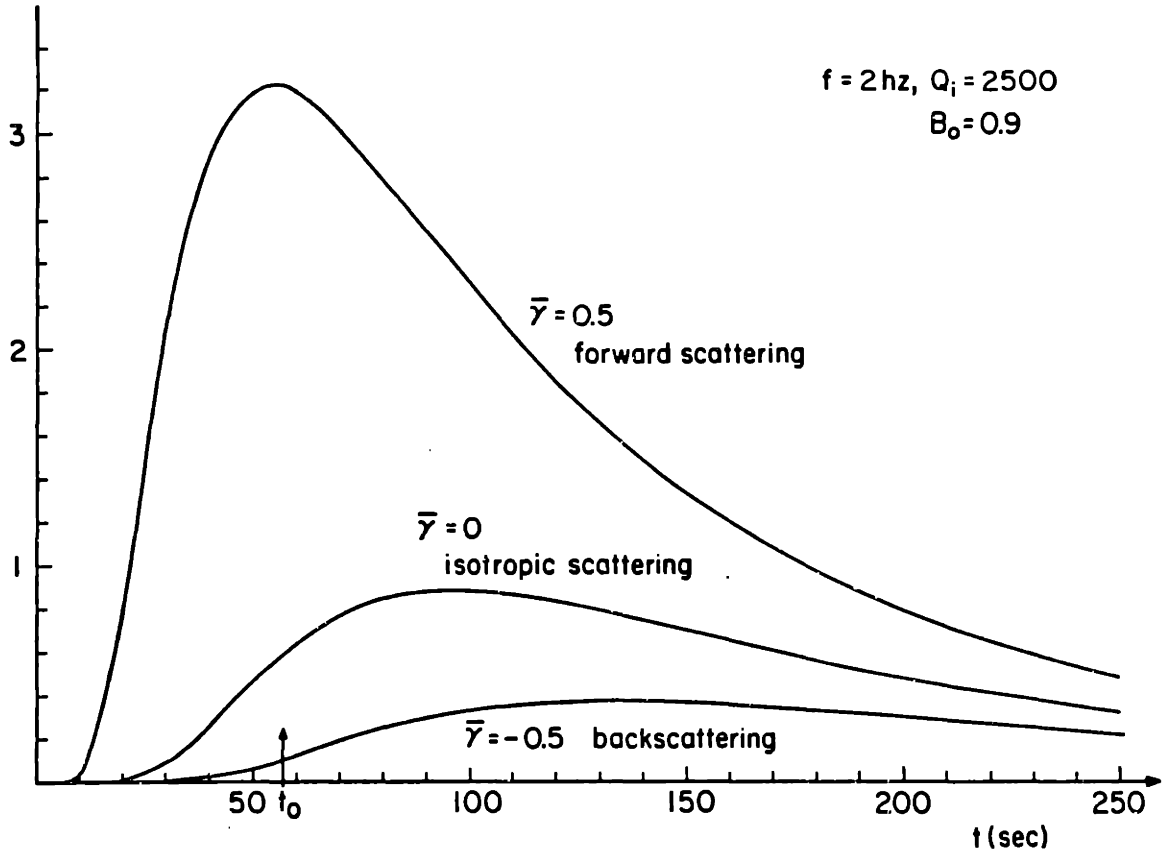

6.1 The seismogram envelopes of S waves predicted by the diffusion approximation for the case of f = 2 Hz, B_o = 0.9 (Q_i = 2500). $\bar{\gamma}$ is the mean scattering angle cosine defined by (6.10).

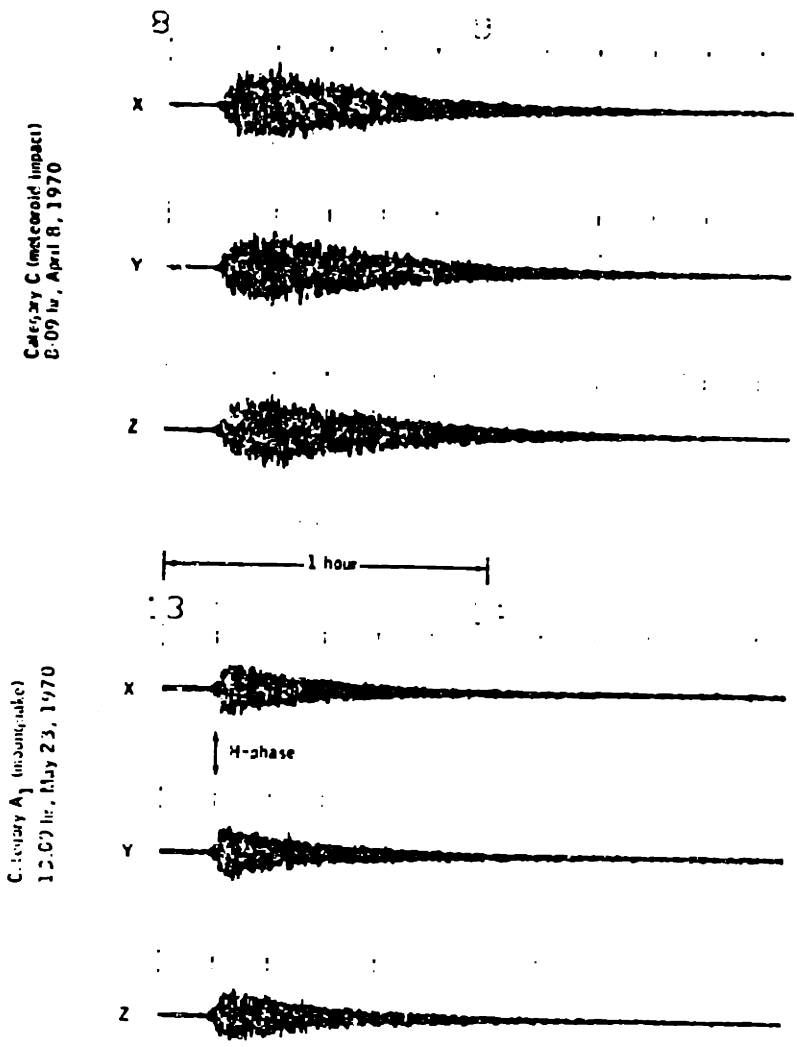

Compressed time-scale records of two of the lunar seismic events believed to be of natural origin recorded at station 12. *Z* is the vertical component seismometer; *X* and *Y* are the horizontal component seismometers. The moonquake, event of 13:09 hr., May 23, 1970, originated within the zone of greatest activity (A_1 zone). The H-phase is prominent on the seismograms from the horizontal component seismometers for category A_1 events. This phase is tentatively identified as the direct shear wave arrival. The event of 8:09 hr., April 8, 1970, is believed to be a meteoroid impact (category C event).

6.2 The seismograms of moonquakes. The event on the top is supposed to be a meteoroid impact; the bottom event is believed to be a deep moonquake (from Latham et al., 1971).

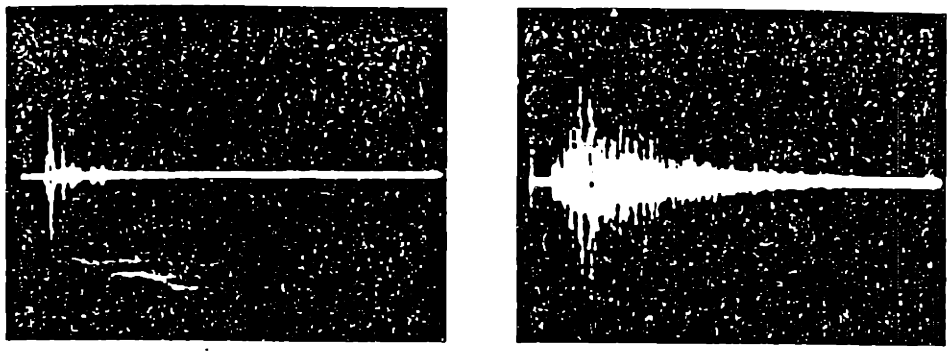

(a) (b)

6.3 The seismograms from the model experiment in laboratory (Dainty et al., 1974).

a) The seismogram with the homogeneous plate.

b) The seismogram when the plate has many grooves as scatterers.

6.4 The band-pass filtered seismograms of A06 (r = 235 km, depth = 103 km) for the stations CHS, FRA, JOR and PEN. From top to bottom: f = 0.375, 0.75, 1.5, 3, 6, 12, 24, 46 Hz. ⟶

6.5 The band-pass filtered seismograms of A15 (r = 247 km, depth = 118 km) for the stations CHS, PEN and JOR. From top to bottom: f = 0.375, 0.75, 1.5, 3, 6, 12, 24, 46 Hz. ⟶

fig. 6.4

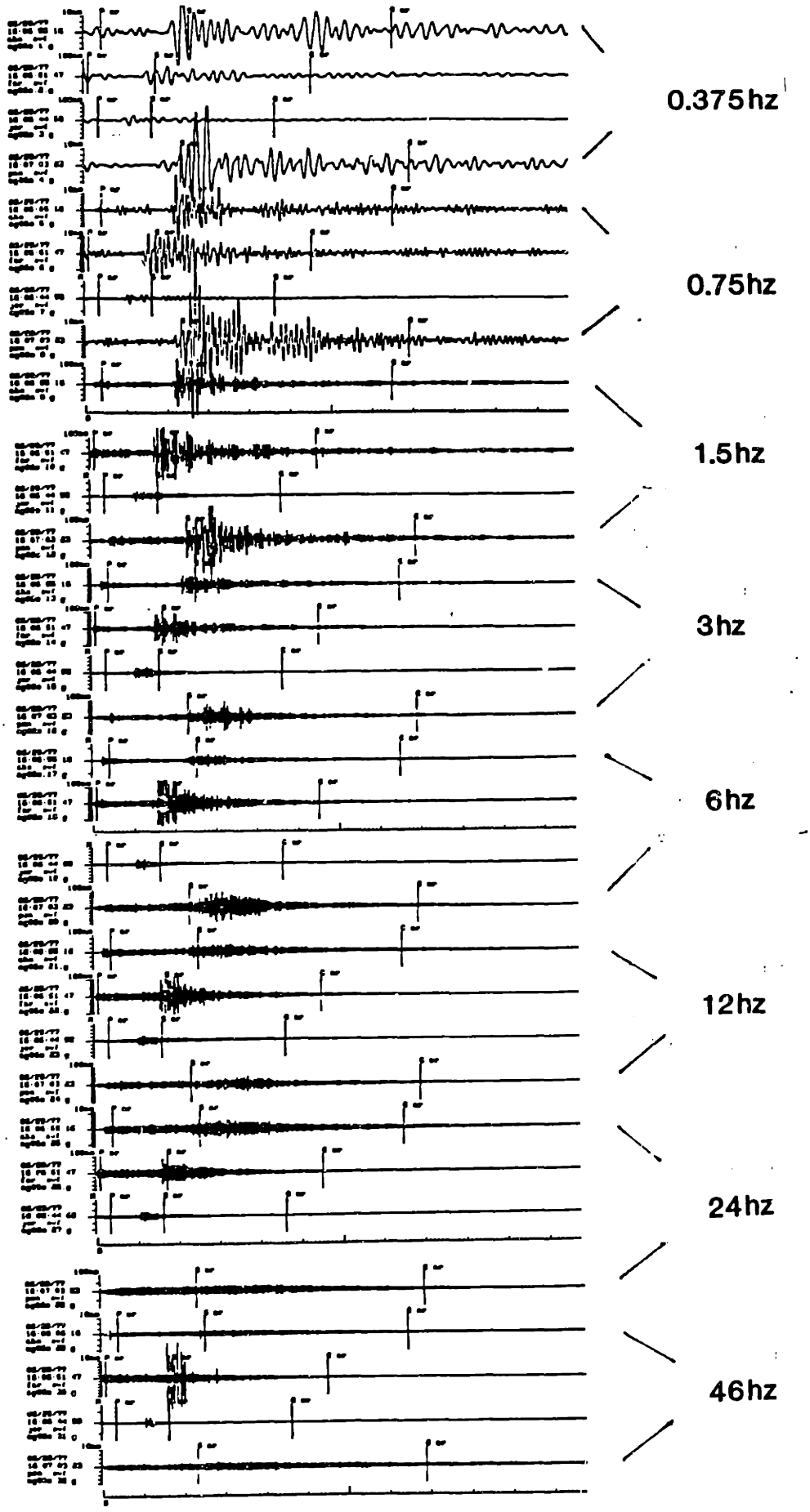

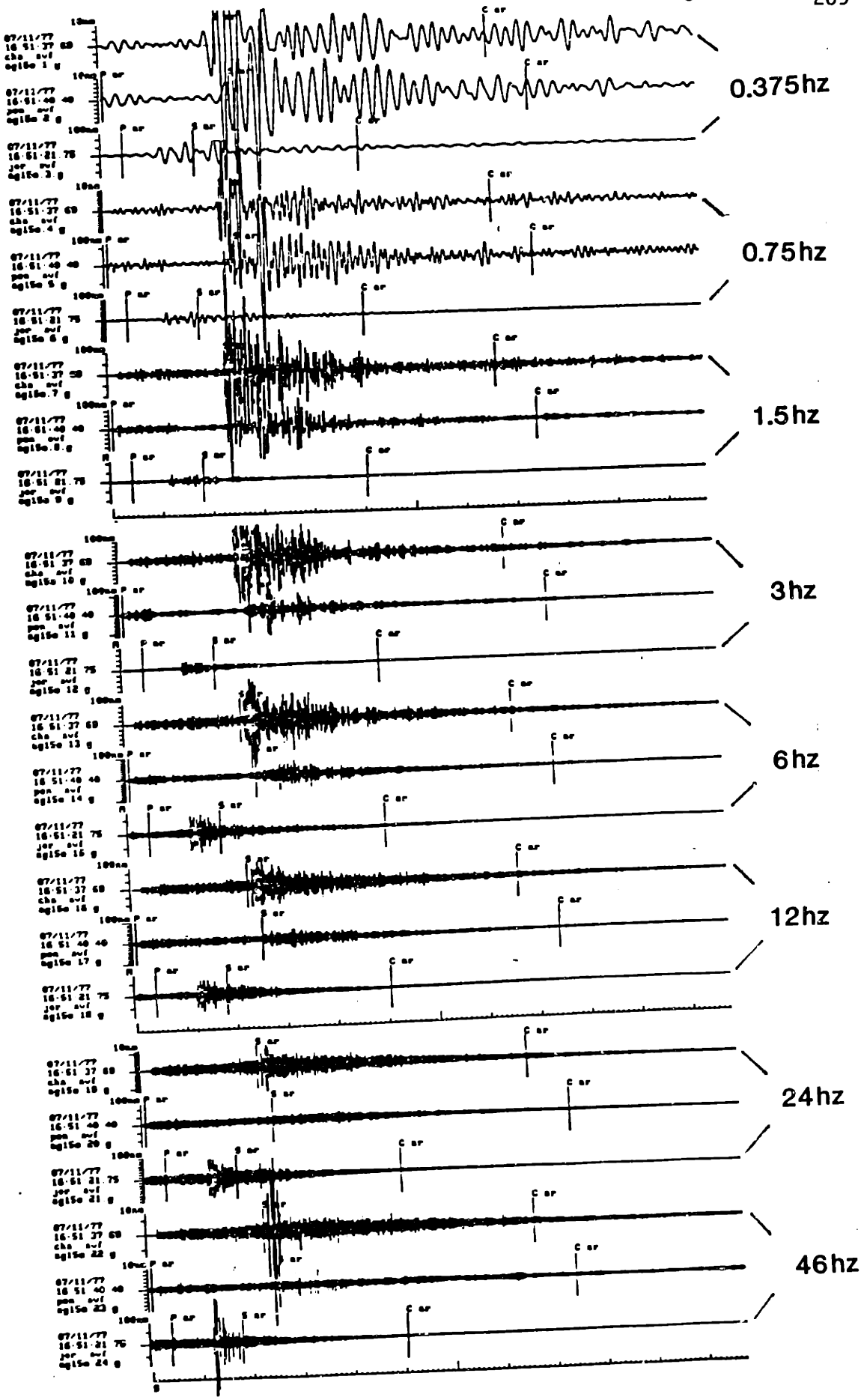
0.375hz
0.75hz
1.5hz
3hz
6hz
12hz
24hz
46hz

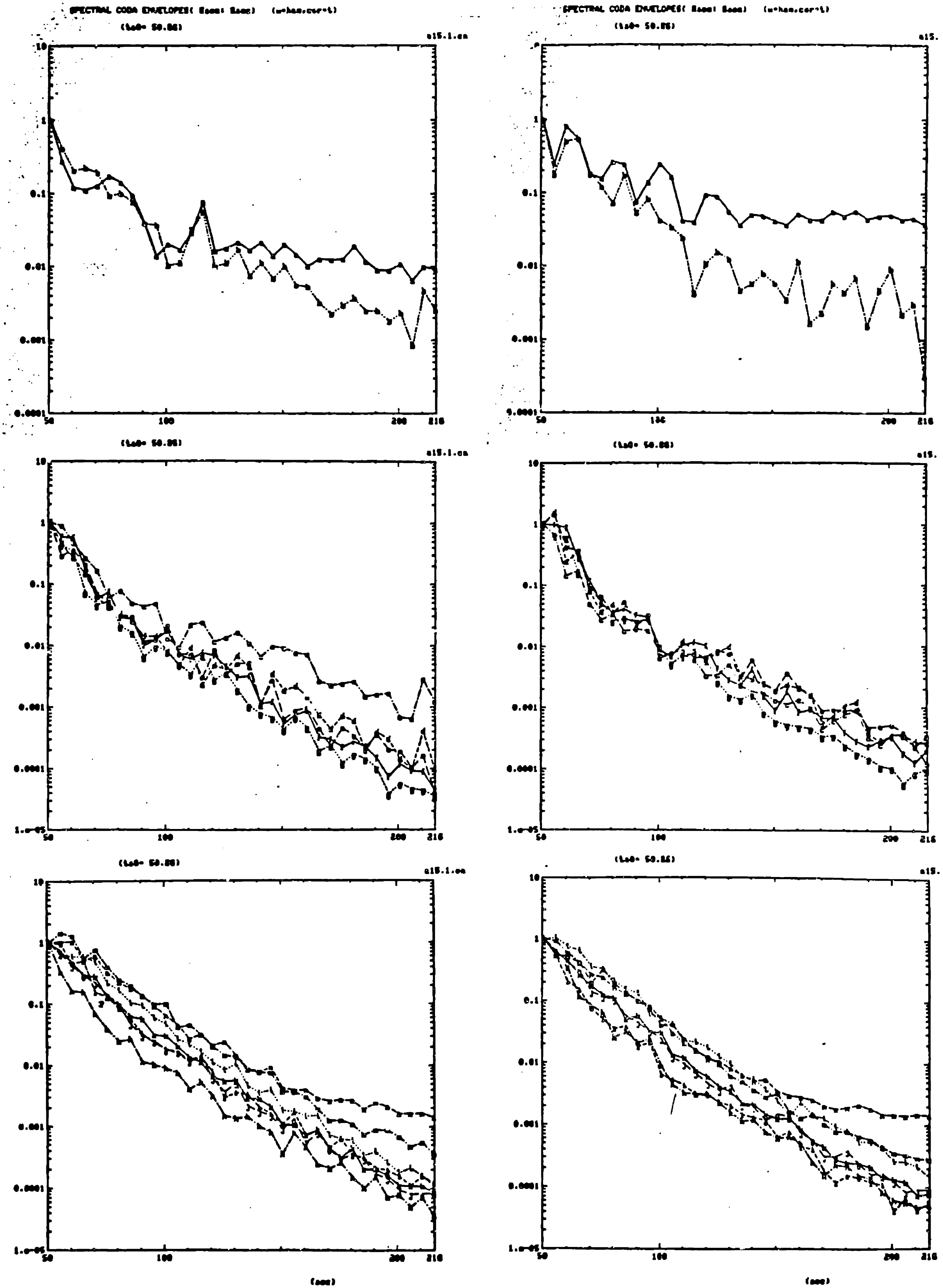

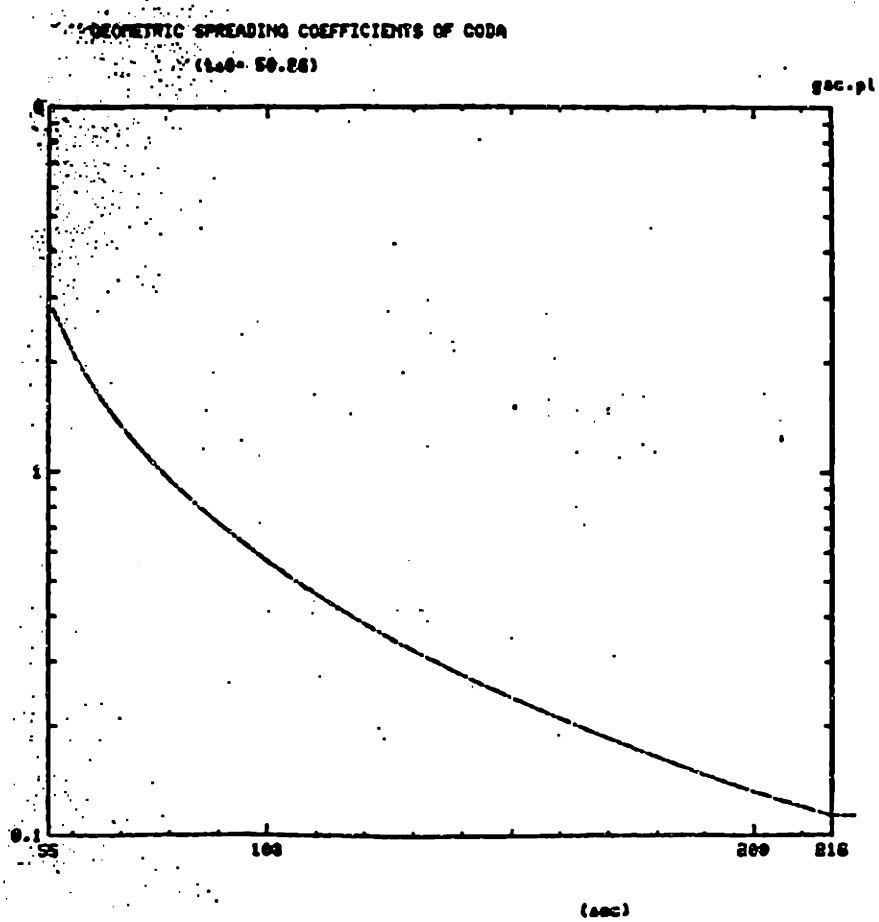

6.7 The theoretical envelope decay curve for the single isotropic scattering in a lossless medium according to Sato (1977). The envelope decay is a pure geometric spreading effect. The distance between the source and sensor is taken as 247 km (as the case of A15 to PEN).

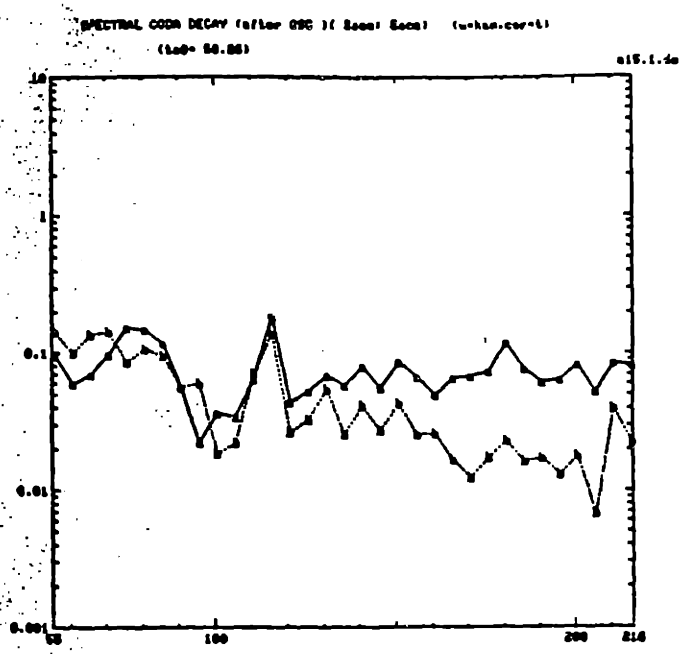

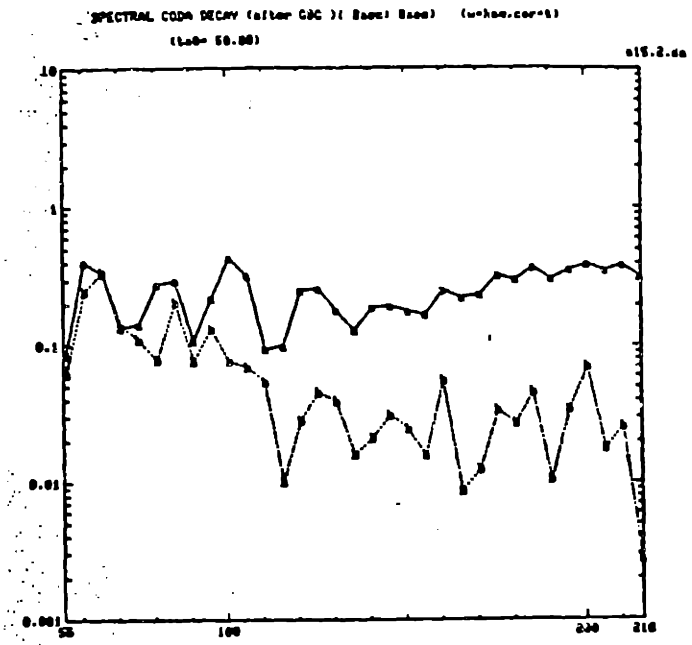

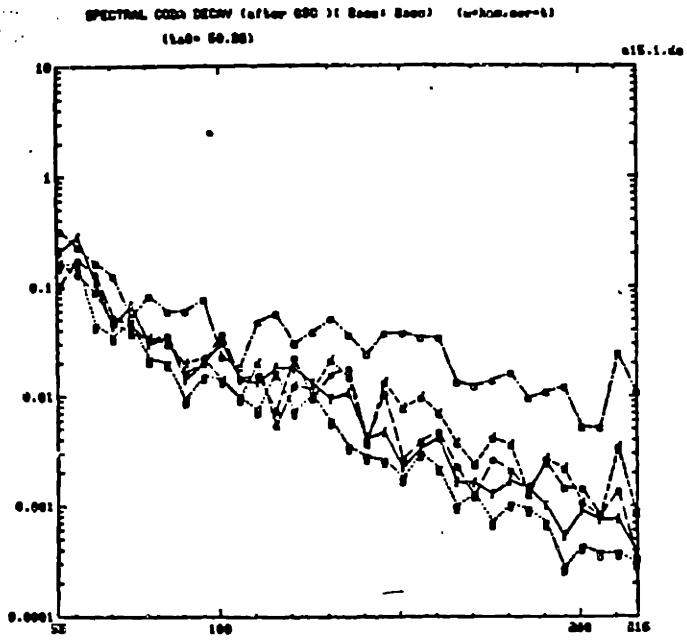

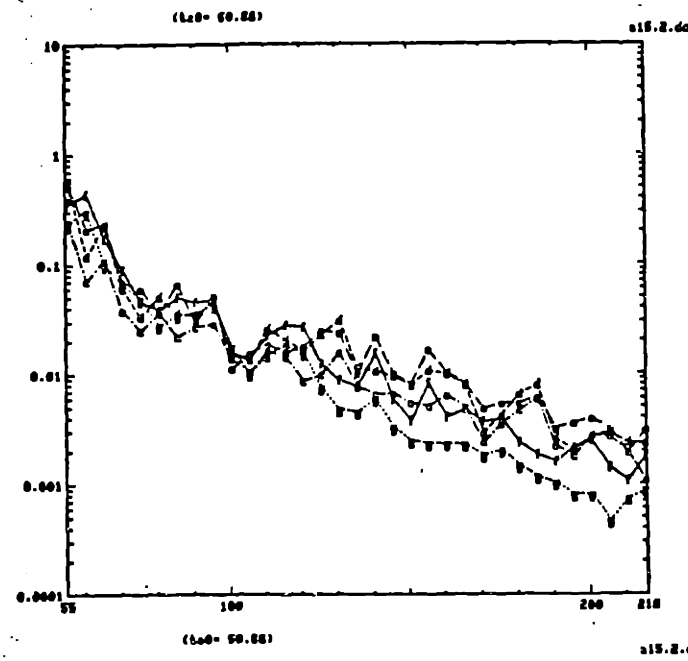

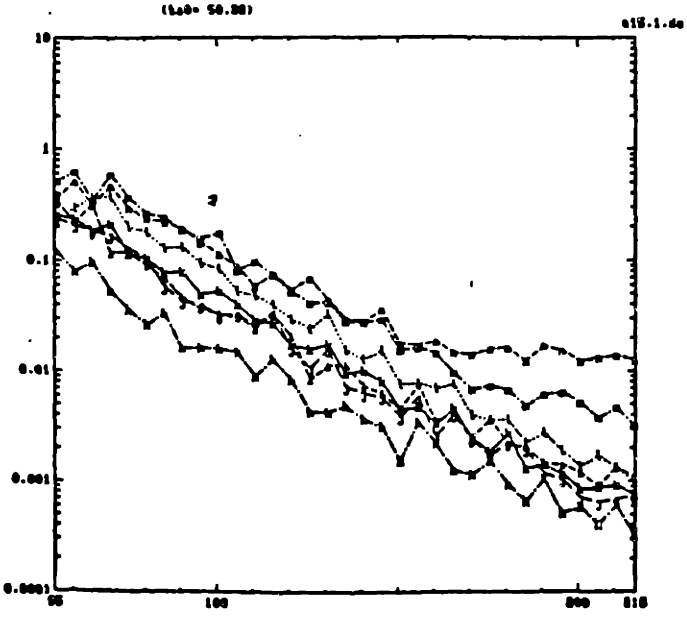

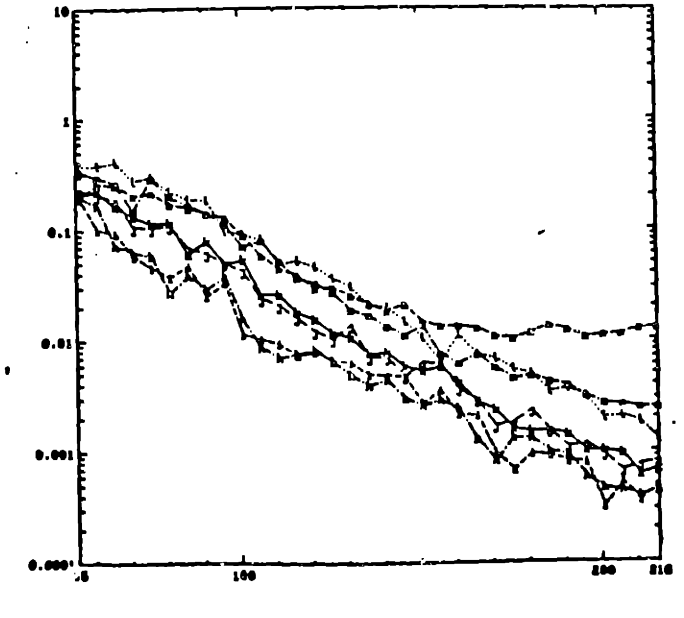

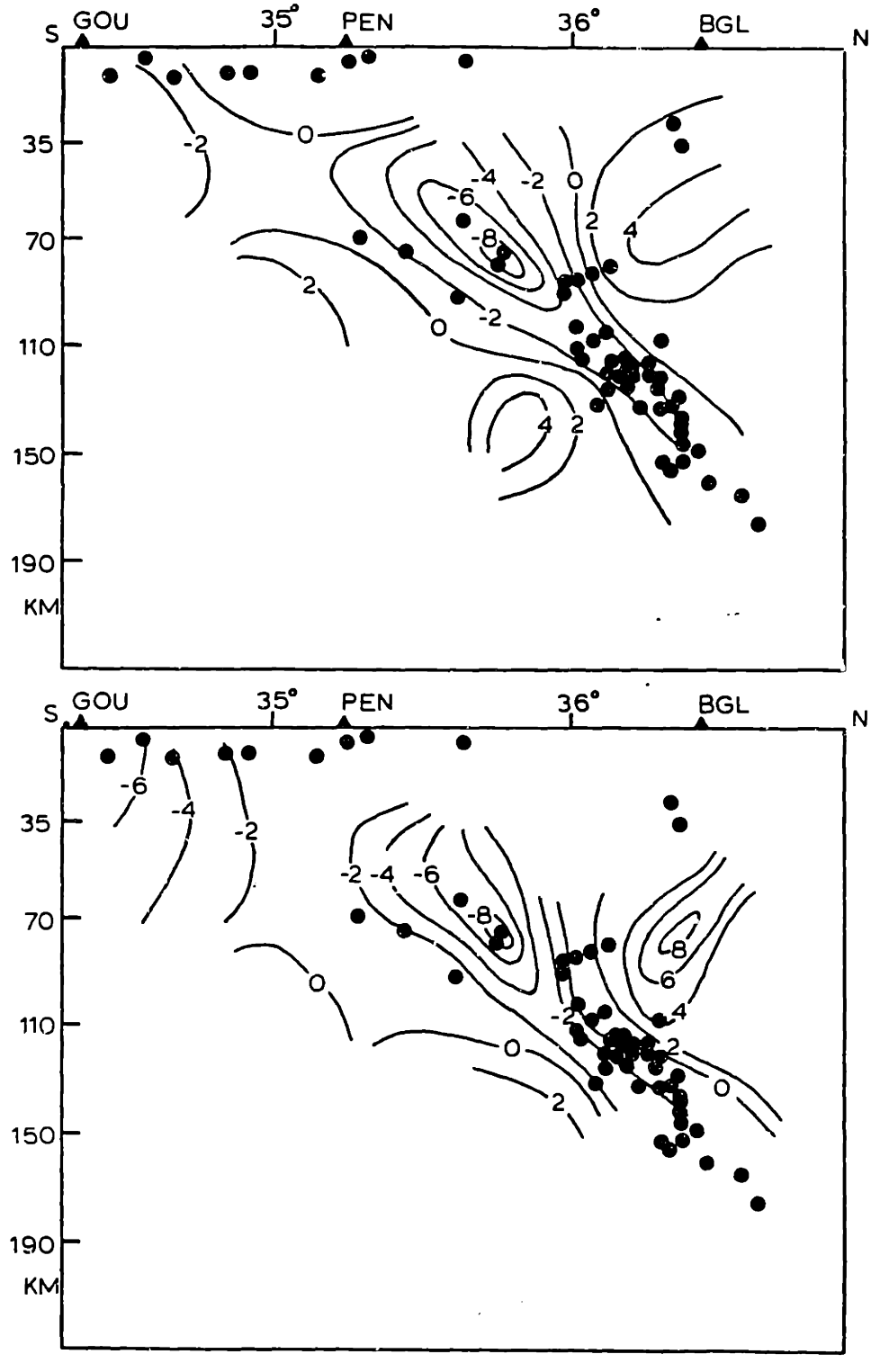

7.1 Contour plot of the vertical variations in velocity inferred from 3D inversions, along with the seismicity in the region. The North-South cross section is made along 69°E. Locations of earthquakes occuring between 68°E and 70°E are indicated by closed circles. Percent changes in P and S wave veloities are shown in the upper and lower parts of the figure, respectively (from Roecker 1981).

Chapter 5

CONCLUSIONS AND SUGGESTIONS FOR FURTHER WORK

> **If, for the study of earth physics, it becomes necessary to resort to complex theoretical devices, then the earth is to blame, not the theoreticians.**
>
> Harold Jeffrys

CONCLUSIONS AND SUGGESTIONS FOR FURTHER WORK

In the introduction I have summarized the major work done in the research related to this thesis. Here I would like to draw some conclusions from this work.

1) The elastic wave scattering theory developed in this thesis using equivalent source representation and Born approximation can be used in the case of weak heterogeneities, which includes most cases in seismology. Naturally, the Born approximation will set a high frequency limit of application, which depends on the practical problems.

The theory can serve as the basis of more advanced scattering theory, such as the multiple elastic wave scattering theory either from the analytic theory approach or from the transport equation approach.

The application of the theory to the fracture analysis by vertical seismic profiling shows that, the theory can find more applications in seismic wave exploration as well as in seismology, especially when shear wave sources and three component geophones become more and more popular.

2) From the analysis in chapter 3 based on the elastic wave scattering in random media, the use of scalar wave theory in the phase and amplitude fluctuation problem, which is a forward scattering problem, is justified. Some work based on the Born approixmation or Rytov approximation has been done to the data collected in LASA and NORSAR. However these approximations break down when the fluctuatuion is in the saturated regime, which is reached when the travel distance is so large that the average Fresnel radius of the propagation is larger than the scale length of the heterogeneities, and when the travel time fluctuation exceeds one quarter of the period of the wave.

From Aki's calculation for LASA (1973), 1 Hz wave is already in the limit of application. on the other hand, the theory about the phase and amplitude fluctuations in the saturated or partly saturated regime is available in optics, ocean acoustics and electromagnetics. Therefore the extension of the fluctuation problem to high frequencies (in the saturated regime) is possible.

3) The coda excitation problem must be treated by the elastic wave scattering theory instead of the scalar wave theory. It is also needed to use the elastic wave multiple scattering theory in strongly scattering media.

4) Transport equation approach is proved to be a very useful tool to handle the multiple scattering problem encountered in seismic wave propagation. It can help to solve the problem of separating the absorption and scattering effects. The preliminary results in this thesis are promising. It can be also helpful in solving the coda strength problem. The radiative transfer theory has been well developed over three decades in optics, neutron theory, later in acoustics and electromagnetics. Seismologists should not remain unconcerned about the treasure houses of our neighbors which are definitely open to us.

5) In the Hindu Kush region, the scattering attenuation is unlikely the major factor in the measured apparent attenuation based on the results in this thesis.

The deep extension of the high attenuation material in this region supports the concept of subducted continental crust.

6) From the analysis in Chapter 3, the lithosphere seems to have multi-scale heterogeneities. In addition to the rather large scale (>10 km) velocity inhomogeneities which have been found in many parts of the world, the sectins of lithosphere in tectonically active regions may be rich in small scale (<1 km) impedance heterogeneities. These heterogeneities may be the

faultings or fracture zones caused by earthquakes or other tectonic activities. Further study is needed to understand these heterogeneities.

SUGGESTIONS FOR FURTHER WORK

1) Applications of the energy density distribution measurement to other regions. The comparison between the results from the tectonically stable regions, such as New England area or the central U.S., and that from the tectonically active regions such as Hindu Kush and California, will benefit us both in the understanding of scattering and attenuation, and in the acquisition of information about the tectonic activities.

   The method of energy density distribution measurement proposed in this thesis is similar to Aki's method for the direct S wave attenuation measurement. The only difference is the use of whole S wave seismograms instead of the use of only direct S wave. Therefore it is advised that whenever possible, calculate both the direct S and the total S attenuation. The total S decay curve with distance is directly related to the energy density distribution curve.

2) Improvement of the theory and modeling of multiple scattering along the transport equation approach. This includes

   1. Study of the influence of the source radiation pattern.
   2. Consideration of the finite thickness of the lithosphere or modeling of the earth as a layered random medium.
   3. Derivation of the exact time domain solution of the energy transfer equation.
   4. Derivation of the elastic wave energy transfer equation and its solutions.

3) Analog and numerical experiments on seismic wave scattering. Since the real earth is very complicated and the ideal conditions for observation are very hard to find, the analog model experiments could be very good go-betweens between the theory and observation. 1D or 2D numerical experiments could be also very helpful in linking the theory and experiments.

4) Study of the statistical properties of the lithospheric inhomogeneities. The formulation of the wave scattering in random media is strongly dependent on the medium statistical properties, such as the power spectrum or correlation function of the inhomogeneities. In the atmospheric or oceanic sciences, the statistical properties of the media have been well studied and become a known factor due to the accumulation of data from the direct measuremints experiments and observations. The purpose of the study of wave propagation in random media there is to estimate the influences of the medium to communication of other measurements and observations, such as the Radar, Sonar measurements or astronomical observations. The other advantage of the atmospheric and oceanic sciences is the penetrability of their media. Some extensive direct measurements on the medium properties have been carried out using balloons or towed birds after the ships. Unfortunately, in the solid earth science we do not have the similar devices as balloon or towed bird to penetrate deeply into the lithosphere. Another dificulty is that the task of the scattering study is mostly the inverse problem in solid earth science. Therefore the interaction between the studies of the modeling and the medium properties is very important. The inverse nature of the problem and the impenetrability of the medium make the theoretical results susceptible to nonuniqueness or fallacy due to double errors in

both theory and medium properties. I guess it is inevitable for the study of seismic wave scattering in the lithosphere, to go through the painful zigzag process of self correction until a reasonable model can be established. However there are many things that can be done to accelerate this process, such as the analog model experiments, some experiments in shallow depth (e.g., VSP or sonic well-log etc.), analysis of data from geology or other geophysical measurements, etc.

5) Study the stress dependence of the seismic albedo β_0 and the scattering coefficient of the lithosphere and explore the possibility of application to earthquake prediction. From the discussion in ch. 4, we know that the weak zones (faultings and fractures) in the lithosphere are possibly the sources of absorption and scattering to seismic waves. The seismic albedo and scattering coefficient of those weak zones should be stress sensitive and therefore the monitoring of these parameters could be useful for earthquake prediction.

APPENDICES

Appendix A Summary of apparent Q_c^{-1} of coda waves and apparent Q_β^{-1} of S waves observed in different regions of the world

Appendix B Mean field attenuation and amplitude attenuation due to wave scattering

Appendix C Attenuation to short period seismic waves due to scattering

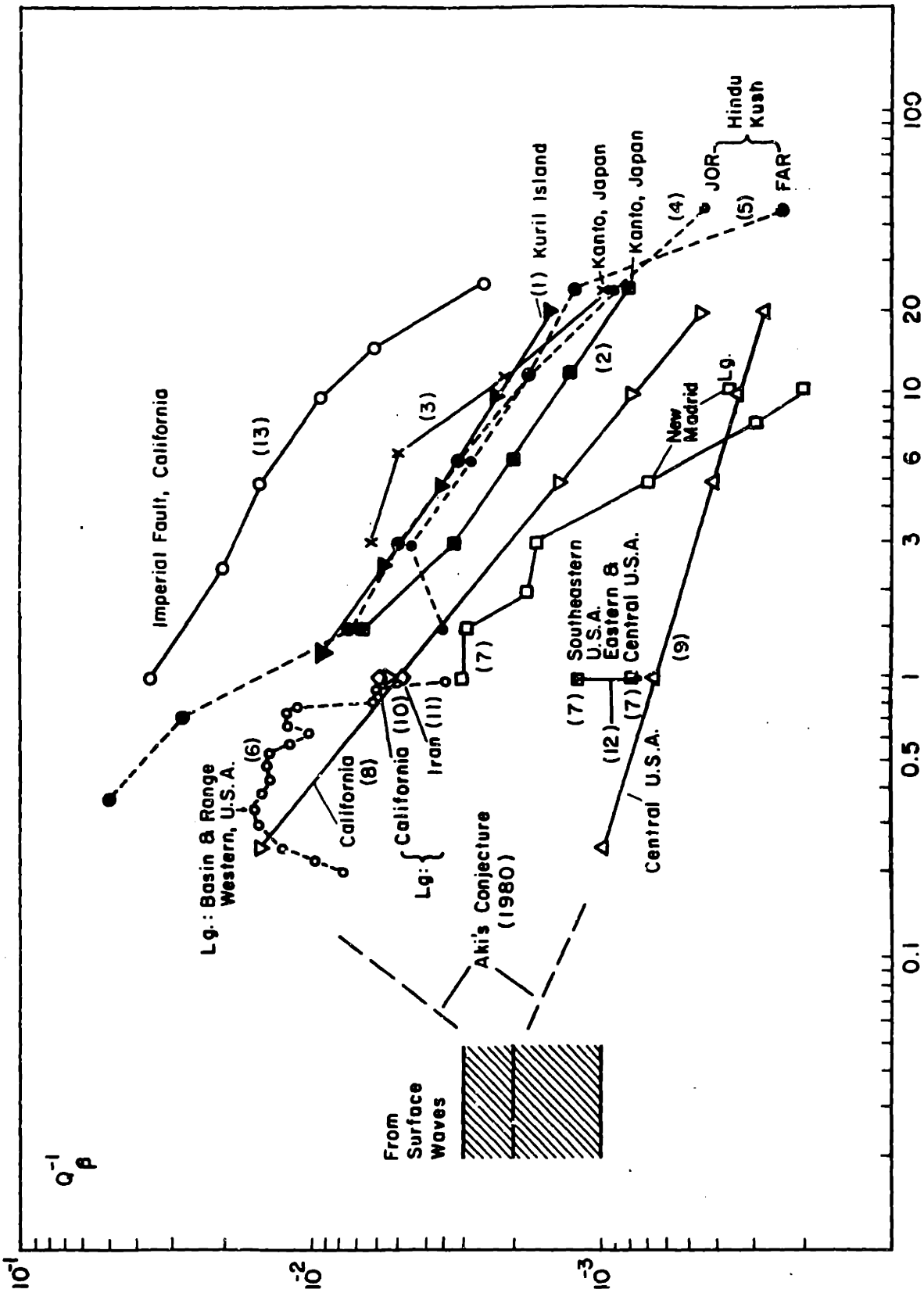
10^{-1}
10^{-2}
10^{-3}
Q_β^{-1}
0.1
0.5
1
3
6
10
20
100
Imperial Fault, California
(13)
(1) Kuril Island
Kanto, Japan
Kanto, Japan
(2)
(3)
(4)
(5)
JOR
FAR
Hindu Kush
Lg
New Madrid
(7)
Southeastern U.S.A.
Eastern & Central U.S.A.
(7)
(12)
(7)
(9)
Central U.S.A.
Lg: Basin & Range Western, U.S.A.
(6)
California (8)
California (10)
Iran (11)
Lg:
Aki's Conjecture (1980)
From Surface Waves

FIGURE CAPTIONS

Figure 1. Q_β^{-1} from S wave and Lg wave analysis.

(1) Kuril Island (Fedotov and Boldyrev, 1969)

(2) Kanto, Japan (Aki, 1980)

(3) Kanto, Japan (Sato & Matsumura, 1980)

(4) JOR
(5) FAR } Hindu Kush (Roecker et al., 1982)

(6) Basin & Range, Western USA (Patton, 1983)

(7) Central USA
New Madrid, USA
Southeastern USA } (Dwyer et al., 1983)

(8) California, USA
(9) Central USA } (Nuttli & Herrmann, 1981)

(10) California (Herrmann, 1980)

(11) Iran (Nuttli, 1980)

(12) Southeastern
Eastern
Central } USA, lg (Street, 1976; Bollinger, 1979; Nuttli, 1973)

(13) Imperial fault, California, USA (Singh et al., 1982)

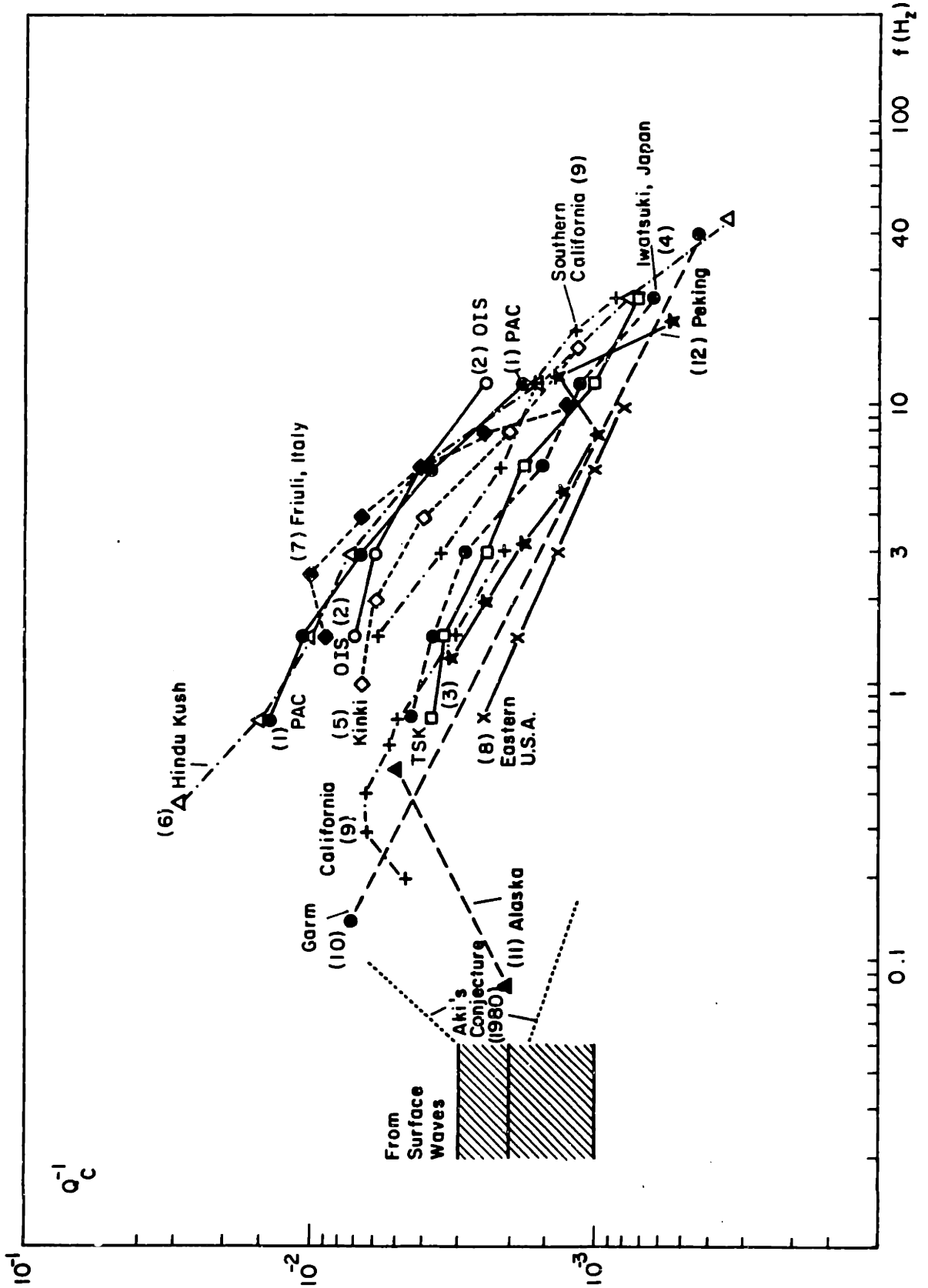
Q_c^{-1}
10^{-1}
10^{-2}
10^{-3}
0.1
1
3
10
40
100
f (Hz)
From Surface Waves
Aki's Conjecture (1980)
(11) Alaska
Garm
(10)
California (9)
(6) Hindu Kush
(1) PAC
(5) Kinki
OIS (2)
TSK
(3)
(8) X Eastern U.S.A.
(7) Friuli, Italy
(2) OIS
(1) PAC
Southern California (9)
Iwatsuki, Japan
(4)
(12) Peking

Figure 2. Q_c^{-1} from local coda analysis.

(1) PAC, Central California, USA

(2) OIS, Western Japan } (Aki & Chouet, 1975)

(3) TSK, Kanto, Japan

(4) Iwatsuki, Japan (Tsujiura, 1978)

(5) Kinki, Japan (Akamatsu, 1980)

(6) Hindu Kush, Afghanistan (Roecker et al., 1982)

(7) Friuli, Italy (Rovelli, 1982)

(8) Eastern USA (New England area) (Pulli, 1983)

(9) California, USA (Phillips, 1984)

(10) Garm, Central Asia, USSR (Rautian & Khalturin, 1978)

(11) Alaska, USA (Aki, 1982)

(12) Peking, China (Shi et al., 1980)

References

Akamatsu, J., Attenuation property of coda parts of seismic waves from local earthquakes, Bull. Disas. Prev. Res. Inst., Kyoto Univ., 30, part I, N. 268, 1-16, 1980.

Aki, K., Attenuation of shear waves in the lithosphere for frequencies from 0.05 to 25 Hz, Phys. Earth Planet. Inter., 21, 50-60, 1980.

Aki, K., personal communcation, 1982.

Aki, K. and B. Chouet, Origin of coda waves: Source, attenuation and scattering effects, J. Geophys. Res., 80, 3222-3342, 1975.

Bollinger, G.A., Attenuation of the Lg phase and the determination of m_b in the southeastern United States, Bull. Seis. Soc. Am., 69, 45-63, 1979.

Chouet, B., Source, scattering, and attenuation effects on high frequency seismic waves, Ph.D. Thesis, Mass. Inst. of Technol., Cambridge, 1976.

Console, R. and A. Rovelli, Attenuation parameters for Friuli region from strong-motion accelerogram spectra, Bull. Seis. Soc. Am., 71, 1981-1991, 1981.

Dwyer, J.J., R. Herrmann and W. Nuttli, Spatial attenuation of the Lg wave in the central United States, Bull. Seis. Soc. Am., 73, 781-796, 1983.

Fedotov, S.A. and S.A. Boldyrev, Frequency dependence of the body wave absorption in the crust and the upper mantle of the Kuril-Island chain, Izv. Earth Phys., 9, 17-33, 1969.

Herrmann, R.B., Q estimates usign the coda of local earthquakes, Bull. Seismol. Soc. Am., 70, 447-468, 1980.

Nuttli, O.W., The excitation and attenuation of seismic crustal phases in Iran, Bull. Seis. Soc. Am., 70, 469-485, 1980.

Nuttli, O.W. and R.B. Herrmann, Excitation and attenuation of strong ground motion, paper presented at IASPEI 21st General Assembly, Int. Assoc. of Seismol. and Phys. of the Earth's Inter., London, Canada, 1981.

Patton, H.J., Lg excitation and propagation in the western United States, preprint for Fifth annual DARPA/AFOSR Symposium, May, 1983.

Phillips, W.S., personal communication, 1984.

Phillips, W.S. and K. Aki, Path and site effects of high frequency S waves in central California, EOS Trans. Am. Geophys. Un., 64, 267, 1983.

Pulli, J.J., Seismicity, earthquake mechanisms, and seismic wave attenuation in the northeastern United States. Ph.D. thesis, Mass. Inst. of Tech., Cambridge, Mass., 1983.

Pulli, J.J. and K. Aki, Attenuation of seismic waves in the lithosphere: comparison of active and stable areas, Proceedings of Earthquakes and Earthquke Engineering; the eastern United States, Sept. 14-16, 1981, Knoxville, Tennessee, vol. 1, 129-142.

Rautian, T.G., and V.I. Khalturi, The use of coda for determination of the earthquake source spectrum, Bull. Seismol. Soc. Am., 68, 923-948, 1978.

Roecker, S.W., Seismicity and tectonics of the Pamir-Hindu Kush region of central Asia, Ph.D. Thesis, Mass. Inst. of Technol., Cambridge, 1981.

Roecker, S.W., B. Tucker, J. King, and D. Hatzfeld, Estimates of Q in central Asia as a function of frequency and depth using the coda of locally recorded earthquakes, Bull. Seismol. Soc. Am., 72, 129-149, 1982.

Rovelli, A., On the frequency dependence of Q in Friuli from short-period digital records, Bull. Seis. Soc. Am., 72, 2369-2372, 1982.

Rovelli, A., Frequency relationship for seismic Q of central southern Italy from accelerograms for the Irpinia earthquake (1980), Phys. Earth Planet. Int., 32, 209-217, 1983.

Sato, H., Mean free path of S waves under the Kanto district of Japan, J. Phys. Earth, 26, 185-198, 1978.

Sato, H., Attenuation of body wavs and envelope formation of 3-component seismograms of small local earthquakes in randomly inhomogeneous lithosphere, J. Geophys. Res., 89, 1221-1241, 1984.

Sato, H. and S. Matsumura, Q^{-1} value for S waves (2-32 Hz) under the Kanto district in Japan (in Japanese), Zisin, 33, 541-543, 1980.

Shi, Ru-Bin, Hen-Qi Jin, Shi-Zhong Wei and Ying-Fan Zhao, personal communication, 1980.

Singh, S., and R.B. Herrmann, Regionalization of crustal coda Q in the continental United States, J. Geophys. Res., 88, 527-538, 1983.

Singh, S.K., R.J. Apsel, J. Fried, and J.N. Brune, Spectral attenuation of SH waves along the Imperial Fault, Bull. Seismol. Soc. Am., 72, 2003-2016, 1982.

Street, R.L., Scaling northeastern United States/southeastern Canadian earthquakes by their Lg waves, Bull. Seis. Soc. Am., 66, 1525-1537, 1976.

Tsujiura, M., Spectral analysis of the coda waves from local earthquakes, Bull. Earthq. Res. Inst., Univ. of Tokyo, 53, 1-48, 1978.

WAVE MOTION 4 (1982) 305–316
NORTH-HOLLAND PUBLISHING COMPANY

MEAN FIELD ATTENUATION AND AMPLITUDE ATTENUATION DUE TO WAVE SCATTERING

Ru-Shan WU*

Department of Earth and Planetary Sciences, Massachusetts Institute of Technology, Cambridge, MA 02139, USA

Received 17 August 1981, Revised 8 February 1982

We point out the inadequacy of two widely used approaches of formulating the amplitude attenuation of seismic waves, the formulation of mean-field attenuation and that of scattering coefficient under the single scattering approximation. Using a one-dimensional layered slab, we show that the attenuation of the mean field is merely a statistical effect caused by phase interference among different realizations of the random wave ensemble, and does not represent the amplitude attenuation. We will call the attenuation coefficient of the mean field as the randomization coefficient in order to distinguish it from the amplitude attenuation coefficient.

We also show that the scattering coefficient method leads to the same result as the first order approximation to the renormalized perturbation series (or the bilocal approximation to Dyson's equation) of the mean field. Therefore these two approaches are equivalent to a certain degree. This is also shown by using the one-dimensional layered slab model as an example.

After pointing out the incorrectness of comparing experiments on amplitude attenuation with the mean field formulation, we suggest and discuss some methods of obtaining the mean field in experiments. For one-dimensional problems, the samples must be taken along the whole propagation path in order to use a spatial average to substitute for ensemble average. For a three-dimensional wave field, measurements over a large seismic array can be used to obtain the mean field. The data from Lasa measured by Aki are used to compare with theory; the agreement between them is good. Finally we compare the mean-field attenuation (randomization) and the amplitude attenuation using the back-halfspace-integration approximation introduced by Wu, and compare them with the measured data by Aki. The comparison shows further the inability of the mean-field formulation in dealing with the problem of amplitude attenuation.

Introduction

There is an increasing interest in measuring and modeling scattering and attenuation of short period seismic waves in inhomogeneous media [1–12]. Two main approaches have been used to treat theoretically the attenuation due to scattering by random inhomogeneities. One is the scattering coefficient method [2, 4, 13], which calculates the fractional energy loss using the single scattering approximation, based on Pekeris [14] and Chernov's [15] work. The other is the mean field approach, in which the statistical ensemble-mean of the wave field is taken, and the attenuation of the mean-field derived from the mean-field equation is treated as the averaged amplitude attenuation of seismic waves [16–20]. This method was borrowed from the similar approach in quantum field theory, which has a well-developed formulation and approximation methods. The formulation has been transferred first to wave propagation in random media [21–31], then to seismic waves. However, many authors failed to recognize the differences between the attenuation of the 'mean field' or the 'coherent field' and the attenuation of the actual measured field. In the practice of seismology, because of the smallness of the size of a detector compared with the wavelength, the actually measured wave amplitude is not the

* Permanent Address: Institute of Geophysical and Geochemical Prospecting of Ministry of Geology, Baiwanzhuang, Peking, China.

0165-2125/82/0000–0000/$02.75

amplitude of the mean field and there has been little work done on obtaining the 'mean field'. Therefore, the usual comparison between the measured amplitude attenuation and the calculated mean-field attenuation made by some authors cannot produce meaningful results. In fact, the attenuation of the mean field is a different physical quantity from the amplitude attenuation. It is only a statistical effect that measures the rate of randomization or the rate of losing coherence among members of a wave ensemble when passing through a random medium. Therefore, more correctly, the 'attenuation coefficient' of the mean field should be called the 'randomization coefficient'.

Interestingly, these two approaches lead to a similar result (see equation (27) in [25], comparing with Ch. 3 in [15]), even though the starting point and the condition of applicability of them are quite different. The scattering coefficient method assumes the single-scattering approximation and is thus only valid for a small-volume random medium; while the mean-field attenuation is derived under the assumption of an infinite random medium and has included the multiple-scattering effect.

In this paper we will clarify the concept and meaning of mean-field attenuation and prove the equivalence of results from the mean-field formulation and from the scattering coefficient method under certain conditions. Then we will discuss how to obtain the mean field in experiments and compare the data from a large aperture seismic array to the theoretical prediction. Finally we will compare the mean field attenuation with the recently developed formulation for average amplitude attenuation using the back-halfspace-integration approximation.

1. The randomization coefficient – the attenuation coefficient of the mean field

In order to show the meaning of the attenuation coefficient of the mean field, we shall start with a totally statistical method working on a one dimensional model. Consider a plane scalar wave of frequency ω incident on a random medium composed of n statistically independent homogeneous layers. Every layer has the same velocity mean C_0, the same velocity variance, which is small in order to have the medium weakly inhomogeneous, and the same thickness a. Thus the random medium is a family of infinite combinations of these layers.

Suppose for a given layer that the actual velocity is C (homogeneous within the layer). We define $S = C_0/C$ as refractive index or relative slowness, so the wave number k in that layer will be

$$k = \frac{\omega}{C} = \frac{\omega}{C_0} s = k_0 s = k_0(1 + \delta s), \tag{1.1}$$

where δs is the fluctuating part of s, and k_0 is the average wave number. The phase deviation resulting from the traversal of that random layer is $ka - k_0 a = k_0 a \delta s$. Therefore, the r.m.s. phase deviation, will be

$$\delta\phi_a = \langle (k_0 a \delta s)^2 \rangle^{1/2} = k_0 a \langle \delta s^2 \rangle^{1/2} = k_0 a \gamma, \tag{1.2}$$

where $\gamma = \langle \delta s^2 \rangle^{1/2}$ is the r.m.s. deviation of refractive index, which we will call fluctuation index. The phase variance resulting from the traversal of all the n layers is

$$\langle \delta\phi^2 \rangle = n(k_0 \gamma a)^2. \tag{1.3}$$

For the case $k_0 a \gg 1$, and neglecting the energy attenuation (i.e. letting the amplitude remain constant) we can write the scalar random wave after passing n layers as

$$\psi = \psi_0 e^{i\phi} = \psi_0 e^{i(\phi_0 + \delta\phi)}, \tag{1.4}$$

where ψ_0 is the incident plane wave, $\phi_0 = k_0 n a$ is the phase change of the wave passing through the n layer-medium having a uniform wave velocity C_0, and $\delta\phi$ is the phase deviation. Suppose $\delta\phi$ is a normal random variable (here $\delta\phi$ is a sum of a large number of independent identically dis-

tributed random variables), then

$$\langle\psi\rangle = \psi_0 e^{i\phi_0}\langle e^{i\delta\phi}\rangle = \psi_0 e^{i\phi_0} e^{-(\delta\phi^2)/2} \quad (1.5)$$

(see, e.g. [36], Ch. 14). Setting the propagating distance $x = na$, in (1.3) and substituting into (1.5) we get

$$\langle\psi\rangle = \psi_0 e^{i\phi_0} e^{-\gamma^2 k_0^2 ax/2} = \psi_0 e^{i\phi_0} e^{-\nu x}, \quad (1.6)$$

where

$$\nu = \frac{\langle\delta\phi^2\rangle}{2x} = \frac{\gamma^2 k_0^2 a}{2} \quad (1.7)$$

is the randomization coefficient or the attenuation coefficient of the mean field. The result (1.7) for the case of $ka \gg 1$ is the same as that obtained by other methods, such as that of Uscinski ([33], formula 4–3) by the parabolic approximation of the mean field equation, Tatarski ([27], 29a) by applying the renormalization procedure to the perturbation solutions, Howe ([29], 6.3) by binary interaction approximations (or the first order smoothing method) to the mean field equation and Keller [23], Karal and Keller [25] [1] by a second-order approximation solution to the stochastic equation. In some of these derivations the complexities of mathematics tended to obscure the physical meaning of the results. From our derivation, which did not go into the detailed physical structure or the pertinent differential equations, we can see that the attenuation of the mean field amplitude as expressed by (1.6) is a totally statistical effect, namely the result of phase interference when taking an ensemble average, since we have neglected the energy attenuation (the effect of amplitude attenuation on the decrease of the mean field is much smaller than that of phase randomizations). The amplitude of the mean field will depend on the degree of randomness of phase ϕ, which increases with distance of propagation. Therefore, we can label the 'attenuation coefficient' of the mean field as the randomization coefficient.

The randomization coefficient ν increases with the scale of inhomogeneities a (correlation length), which further proves intuitively that ν is only a measure of the rate of randomization. This is because when the scale of inhomogeneity increases (i.e. when the number of layers decreases for a given x), the energy loss due to reflections should decrease, contrary to the mean field attenuation (1.7). In the limiting case, when a grows to infinity, namely the scale of homogeneities becomes greater than the propagation distance, the medium for our model becomes homogeneous, but is still random. Because there is no reflection during propagation in the medium, there should be no amplitude attenuation; however, for randomization of phase, it reaches a maximum. Setting $a = x$ in (1.6), we get

$$\langle\psi\rangle = \psi_0 e^{i\phi_0} e^{-\gamma^2 k^2 x^2/2}, \quad (1.8)$$

the same result as obtained by the random Taylor expansion method (see [28], 3.101).

2. The randomization coefficient and the scattering coefficient

The scattering coefficient approach computes the attenuation coefficient as the fractional energy loss from the primary wave by scattering per unit distance of propagation under the single scattering approximation. This approximation implies that all the scattered energy is lost from the primary wave field. Therefore, when distance is small, it leads to the same result as the mean field attenuation approach under the bilocal approximation for the renormalized mean field equation (Dyson's equation). We will show it briefly as follows.

We adopt the smoothing method in the operator form for the derivation of Dyson's equation and

[1] See equation (27) of Karal and Keller [25], which is identical to the result obtained by the energy scattering formulation under the single-scattering approximation (e.g. Cernov [15]). We shall show that the two approaches are identical. Therefore the formula (59) of [15] for $ka \gg 1$ represents the same result for that case.

its bilocal approximation (see [28] IVC). Suppose ψ is the random field in question. It can be decomposed into a mean part $\langle\psi\rangle$ and a fluctuating part $\delta\psi$,

$$\psi = \langle\psi\rangle + \delta\psi, \tag{2.1}$$

where $\delta\psi$ has the property $\langle\delta\psi\rangle = 0$. Suppose ψ satisfies a random linear wave equation

$$L\psi = (L_0 + L_1)\psi = F, \tag{2.2}$$

where L is a linear operator, L_1 is its random part, L_0 is the operator for the corresponding non-random medium, and F is the source term. Defining G_0 as the Green function operator of L_0 (namely the inverse operator of L_0), we get from (2.2)

$$\psi = G_0F - G_0L_1\psi. \tag{2.3}$$

Now we introduce, for convenience, the averaging operator P such that

$$\langle\psi\rangle = P\psi, \qquad \delta\psi = (I - P)\psi, \tag{2.4}$$

where I is the identity operator. Knowing the rules for P operation,

$$\begin{aligned} &PL_1P = 0 \quad (\text{i.e.}\langle L_1\langle\psi\rangle\rangle = 0), \\ &PG_0 = G_0P, \\ &PF = F, \end{aligned} \tag{2.5}$$

we get a relation between the mean field $\langle\psi\rangle$ and the fluctuating field $\delta\psi$ by applying the averaging operator to (2.3)

$$\langle\psi\rangle = G_0F - G_0PL_1\delta\psi. \tag{2.6}$$

If we call G_0F the primary field ψ°, (2.6) can be written as

$$\langle\psi\rangle = \psi^\circ - G_0\langle L_1\delta\psi\rangle. \tag{2.7}$$

On the other hand, from (2.4) and (2.3) we derive

$$\delta\psi = -G_0(I - P)L_1(\langle\psi\rangle + \delta\psi). \tag{2.8}$$

By formally iterating the above equation, we get

$$\delta\psi = \sum_{n=1}^{\infty} [-G_0(I - P)L_1]^n\langle\psi\rangle. \tag{2.9}$$

Substituting (2.9) into (2.6) results in the Dyson's equation in operator form,

$$\begin{aligned} &\langle\psi\rangle = G_0F + G_0M\langle\psi\rangle, \\ &M = -\sum_{n=1}^{\infty} PL_1[-G_0(I - P)L_1]^nP, \end{aligned} \tag{2.10}$$

where M is the so-called mass operator in quantum field theory.

Notice that the Dyson's equation is an exact equation for the mean field. If we take the first order approximation to the mass operator M in (2.10), we derive the so-called bilocal approximation of Dyson's equation[2] or the first order smoothing approximation of the mean field,

$$\langle\psi\rangle = G_0F + G_0PL_1G_0L_1\langle\psi\rangle. \tag{2.11}$$

We notice that the first order approximation of the mass operator in (2.10) is equivalent to the first order approximation to the fluctuating field in (2.9)

$$\delta\psi = -G_0L_1\langle\psi\rangle, \tag{2.12}$$

which is the modified (or local) Born approximation for the fluctuating field. This can be seen by substituting the above approximation (2.12) into (2.6). Since (2.6) is an exact relation, we conclude that the modified Born approximation for the fluctuating field is equivalent to the bilocal approximations for the mean field.

Now we proceed to prove the equivalence of the scattering coefficient approach to the mean field approach under bilocal approximations. The scattered field ψ', which has a different physical meaning from the fluctuating field, is defined by

$$\psi = \psi^\circ + \psi' \tag{2.13}$$

[2] Originally Dyson's equation was derived by Dyson by using the renormalization procedure to the mean perturbation series, and the bilocal approximation was first introduced in the form of Feynman diagrams by Bourret under the name of 'one-fiction approximation' [20, 21] (also see Frisch [28] IV B). Since then similar approximations have been derived under different names, e.g. bilocal approximation [26, 27], second-order approximation to the stochastic equation [25, 24], binary interaction approximation [29, 30], etc.

where ψ is the actual random field, ψ° is the primary field, or the field when there are no inhomogeneities. The scattered field ψ' is therefore the field caused by the presence of inhomogeneities.

For a short travel distance, the scattered field ψ' can be calculated by the Born approximation,

$$\psi' = -G_0 L_1 \psi^\circ. \tag{2.14}$$

Because of the smallness of distance, the mean field $\langle\psi\rangle$ differs only slightly from the primary field ψ°. Therefore, the scattered field ψ' calculated by the Born approximation will be nearly equal to the fluctuating field $\delta\psi$ calculated by the modified Born approximation (2.12). It has been shown that, on average, energy can only flow from the mean field to the random field (in accordance with the second law of thermodynamics, [31]). Therefore, the mean field intensity will decrease continuously due to the energy loss by converting to the random field. If the total energy of the scattered field ψ' is considered to be lost, the field attenuation will have the same rate as the mean field because of the approximate equality between (2.12) and (2.14).

From what has been shown above, we know that the single-scattering approximation and the assumption of total loss of scattered energy lead to the equivalence of the energy scattering coefficient and the mean field attenuation. In fact, unlike the fluctuating field $\delta\psi$, the energy of the scattered field can be transferred back to the total field. The scattered energy is not necessarily lost totally. Suppose the primary wave is travelling along the x-direction through an n layered medium. For the second layer there is a loss of energy due to single-scattering in the layer but it also gains some energy from the waves scattered by the first layer. For the third layer, the wave will gain scattered energy from single-scattering by the second layer and from double scattering by the first layer. Generally, the nth layer will gain scattered energy from layers 1 through $n-1$. In the case of large scale inhomogeneities ($ka \gg 1$), when forward scattering is dominant, the energy loss by scattering can be quite different from the result obtained by the Born approximation, especially in the forward direction. Even when the criterion for the Born approximation is satisfied, namely that the fractional energy loss calculated by single-scattering formula is much smaller than 1, the frequency dependence of the total field attenuation obtained by considering multiple scattering will be different from the single scattering approximation. This can be seen from the frequency dependence of the directivity pattern of the scattered energy. The directivity of the mean intensity of the scattered field for the correlation functions $e^{-r/a}$ is [15]

$$f(\theta) = \frac{1}{(1+4k_0^2a^2\sin^2\frac{1}{2}\theta)^2}, \tag{2.15}$$

where θ is the angle between incident wave and scattered wave, k_0 is the wave number and a is the correlation length. For greater k_0, more scattered energy will be concentrated in the forward direction so that scattered energy loss will deviate more seriously from the calculation of the single-scattering approximation.

To make the physical meaning clearer, we will use again the one-dimensional wave propagation model over the sliced random slab. Suppose that the primary wave is

$$\psi^\circ = A\, e^{ik_0 x}, \tag{2.16}$$

and there is no energy loss during propagation (neglecting reflections). In spite of this, as shown below, we will find that there is a scattering loss equal to the mean field attenuation, if we follow the scattering coefficient approach.

The one-dimensional scalar wave equation is

$$\begin{aligned}&(\nabla^2 + k^2)\psi = 0,\\ &[\nabla^2 + k_0^2(1+\delta s)^2]\psi\\ &\quad = [\nabla^2 + k_0^2(1+2\delta s+\delta s^2)]\psi\\ &\quad = 0,\end{aligned} \tag{2.17}$$

where δs is the fluctuating part of the refractive index (see (1.1)). Neglecting the δs^2 term and using

(2.13), we get

$$(\nabla_0^2 + k_0^2)\psi' = -k_0^2 2\delta s \psi. \tag{2.18}$$

Now we solve the equation for the scattering field by the first slice. Since $a\delta s$ is small, we can use the Born approximation

$$(\nabla^2 + k_0^2)\psi' = -2k_0^2\delta s\psi^\circ. \tag{2.19}$$

Knowing the 1-D wave Green function ([34],

$$g(x, x') = \frac{-\mathrm{i}}{2k_0} \mathrm{e}^{\mathrm{i}k_0|x-x'|}, \tag{2.20}$$

and recognizing that

$$L_1 = 2k_0^2\delta s, \tag{2.21}$$

we obtain the scattered field under the Born approximation

$$\begin{aligned}\psi'(x) &= -\int g(x, x')L_1\psi^\circ(x')\,\mathrm{d}x' \\ &= \int \frac{\mathrm{i}}{2k_0}\mathrm{e}^{\mathrm{i}k_0|x-x'|}(2k_0^2\delta s)A\,\mathrm{e}^{\mathrm{i}k_0x'}\,\mathrm{d}x' \\ &= \int_0^a A\frac{\mathrm{i}}{2k_0}(2k_0^2\delta s)\,\mathrm{e}^{\mathrm{i}k_0x}\,\mathrm{d}x \\ &= A\,\mathrm{e}^{\mathrm{i}k_0x}\mathrm{i}k_0\delta s a \\ &= \psi^\circ \mathrm{i}k_0\delta s a. \end{aligned} \tag{2.22}$$

In obtaining (2.22) we use the fact that $x \geq a \geq x'$, where a is the thickness of the layer, in view of the assumption that all the scattered energy goes to the positive x-direction.

For our special model we can, in fact, use a simpler derivation for scattered waves (2.22). We know that the phase deviation for the wave after passing through a layer is $k_0a\delta s$, then the resultant field will be

$$\begin{aligned}\psi &= A\,\mathrm{e}^{\mathrm{i}k_0x + \mathrm{i}k_0a\delta s} \\ &= \psi^\circ + \psi'. \end{aligned} \tag{2.23}$$

Therefore, we have

$$\begin{aligned}\psi' &= \psi - \psi^\circ \\ &= \psi^\circ(\mathrm{e}^{\mathrm{i}k_0a\delta s} - 1). \end{aligned} \tag{2.24}$$

When $k_0a\delta s$ is small,

$$\psi' \simeq \psi^\circ \mathrm{i}k_0a\delta s. \tag{2.25}$$

The mean intensity of the scattered field is

$$\begin{aligned}\langle|\psi'|^2\rangle &= \langle\psi'\psi'^*\rangle \\ &= \langle|\psi^\circ|^2(k_0^2a^2\delta s^2)\rangle \\ &= |\psi^\circ|k_0^2a^2\gamma^2 \end{aligned} \tag{2.26}$$

where γ is the r.m.s. deviation of refractive index (see 1.2). If we assume that the total energy scattered by single-scattering is lost, the energy loss by scattering of the whole n-layer slab will be proportional to $n\langle|\psi'|^2\rangle$, because of the independence between different layers. Therefore the scattering coefficient defined as the fractional energy loss per unit distance by passing through the random slab will be

$$\begin{aligned}\frac{1}{na}\frac{n\langle|\psi'|^2\rangle}{|\psi^\circ|^2} &= \frac{nk_0^2a^2\gamma^2}{na} \\ &= k_0^2a\gamma^2 \\ &= 2\nu, \end{aligned} \tag{2.27}$$

where ν is the field randomization coefficient, i.e. the attenuation coefficient of the mean field defined by (1.6) and (1.7). We know that the intensity of the mean field will decrease as

$$|\langle\psi\rangle|^2 = |\psi^\circ|^2\,\mathrm{e}^{-2\nu x}, \tag{2.28}$$

so we can see how the premise of the total loss of single-scattered energy leads to an identity between the scattering coefficient and the attenuation coefficient of the mean field energy.

3. On acquiring experimental data of the mean field with an example from Lasa

A random medium by mathematical definition is an ensemble or a family of innumerable inhomogeneous components. Each component, with a certain probability of existence, differs from others in its detailed structure, but there are some statistical similarities among all components. When we consider wave propagation in a random

medium, we are dealing therefore with a random wave, namely an infinitely large family of waves, each propagating in an inhomogeneous medium with a certain probability. The mean of a random wave field is the ensemble average over the whole wave family. Therefore, statistically, the average should be taken over a great many experiments for different members of the considered random medium under the same condition. For seismic wave propagation in the earth, the ensemble average may be approximated by a spatial average in certain cases in view of the ergodicity, or as considered within the framework of a 'pseudo-random medium' [35, 28]. However, when taking spatial averages, the non-random phase relation between waves at different points must be taken into account. In the case of $ka \gg 1$ (i.e. wavelength much smaller than the scale of inhomogeneity), the spatial averaging, which of course should cover an area spanning many correlation lengths, will be taken over many wavelengths. The average of the waves will diminish due to non-random term phase interference, if no phase corrections for waves at different points have been implemented. Therefore, as we take the spatial average, a phase correction, which corresponds to the phase change caused by propagation from the reference point to the point considered with the average velocity, must be performed.

First we consider the 1-D problem. A scalar monochromatic wave $A\,e^{ik_0x}$ is incident on and propagates in a random medium along the x-direction. Each member of the random medium family is a weakly inhomogeneous medium with a scale of inhomogeneity a (correlation length). We know that the phase deviation of the random wave after passing through a distance a is $k_0a\delta s$, where δs is the fluctuation of the refractive index; then the wave becomes

$$\psi(a) = A(a)\,e^{i(k_0a + k_0a\delta s)}.$$

When the wave travels within the second layer, since δs in this layer is uncorrelated with the first layer and is arbitrary, we can consider the two layer medium as being from another member of the random medium family, and so on. Thus for a wave which has traveled a distance na,

$$\psi(na) = A(na)\exp\Big(ik_0na + i\sum_{j=1}^{n} k_0a\delta s_j\Big). \quad (3.1)$$

For a sufficiently large n, assuming the condition for ergodicity is nearly satisfied, we can take the average of these n waves as the approximation of the ensemble average. However, the phase term e^{ik_0na}, which has nothing to do with the randomness of the medium, will interfere with the result. Therefore we must perform a phase correction e^{-ik_0x} to eliminate the phase interference. From the above arguments, we conclude that for one-dimensional problems, the mean field at point x can be approximated by

$$\langle\psi(x)\rangle = \frac{1}{x}\int_0^x \psi(x')\,e^{-ik_0x'}\,dx'. \quad (3.2)$$

Here $\psi(x') = A(x')\,e^{i\phi(x')}$ is the measured field at point x' ($\leq x$). Therefore

$$\psi(x')\,e^{-ik_0x'} = A(x')\,e^{i\delta\phi(x')},$$

where $\delta\phi(x')$ is the phase deviation from the field of the homogeneous medium.

If the family of n waves for $x = na$ is taken as a random function or a random process, the $\psi(x)$ is a non-stationary process. The decrease of the mean of the process will approximate the 'attenuation' of the mean field, i.e. the randomization of the field. In the simplified model, in which the phase deviation by passing one layer of thickness a can be with equal probability either $\Delta\phi_a$ or $-\Delta\phi_a$, where $\Delta\phi_a$ is a fixed small quantity, the total phase deviation then is a Wiener–Levy process with zero mean and a variance equal to

$$n(\Delta\phi_a)^2 = (x/a)\,(\Delta\phi_a)^2$$

([36], Ch. 9). We know from (1.5) that the mean of $\psi(x)$ will decrease exponentially with increasing variance of phase deviation, which explains the decrease of mean field with distance x.

The averaging formula for a stationary process

$$\langle\psi(x_0)\rangle = \frac{1}{2x}\int_{x_0-x}^{x_0+x} \psi(x')\, e^{-ik_0x'}\, dx'$$

would not have any use here. If the process is stationary, its mean should remain unchanged, and the decreasing nature of the mean field can not be obtained.

For three dimensional isotropic problems, in the case of $ka \gg 1$, the measurements on the transverse section (or ones that can be reduced to the transverse section), such as the measurements in a seismic array over many correlation lengths, can be used for the calculation of the mean field. Different ray paths with separations larger than the correlation length can be thought of as different realizations of the random medium. However, no attempt has been made, to my knowledge, in obtaining the experimental value of the mean field of seismic waves and comparing them with theoretical calculations. Some authors simply compare those measurements on amplitude attenuation with the theoretical results for the mean field, or equivalently, with scattering coefficient calculations under the single-scattering approximation. Nevertheless, the coherency measurements using the beam forming method conducted by Mereu and Ojo [37] are closely related to the mean field measurement, though no comparison was made to the mean field formulation.

The records of Lasa, Norsa or any large aperture seismic array can be used to obtain the mean field. Some authors have used these array data in studying the statistical properties of the under-array media [2, 6, 7]. We will use Aki's data on phase fluctuation across Lasa to infer the mean field attenuation. From the amplitude fluctuation and phase delay fluctuation measurements over the large seismic array, Lasa, consisting of 21×25 vertical seismographs and covering an area of diameter 200 km, Aki derived a 10 km correlation length for the inhomogeneities, and the velocity fluctuation index

$$\gamma = \langle(\delta c/C_0)^2\rangle^{1/2} = 4\%.$$

From these parameters, we can calculate the randomization coefficient ν. To compare the calculated values of ν with the experiments, we use the phase fluctuation data given by Aki ([2], table 1). In the table he listed the rms (root mean square) phase fluctuations over the seismic array measured in the frequency range 0.5 Hz–1.5 Hz for 17 events. As we pointed out, when the area of the seismic array is large enough to cover many correlation lengths, the spatial average over the array can approximate the ensemble average. We use only the data for frequencies from 0.5 Hz to 1 Hz. Above 1 Hz there are few events to be averaged. The frequencies used and the corresponding average rms phase fluctuations (over all events), as well as the numbers of events over which the averages were taken, are listed in Table 1.

Table 1

Randomization coefficients in the frequency range 0.5 Hz to 1 Hz for the medium under Lasa

f(Hz)	$\sigma\phi = \frac{\sum_{i=1}^{N}\langle\delta\phi_i^2\rangle^{1/2}}{N}$ (rad.)	N	$\nu_\phi = \frac{\sigma\phi^2}{2X_0}$ (10^{-3}/km)	$\nu = \frac{\gamma^2 k_0^2 a}{2}$ (10^{-3}/km)
0.5	0.57	11	3.2	2.19
0.6	0.52	1	2.7	3.16
0.7	0.59	5	3.5	4.30
0.8	0.74	4	5.5	5.61
1.0	0.94	13	8.8	8.77

$\langle\delta\phi_i^2\rangle^{1/2}$ is the rms phase fluctuation for the ith event. N is the number of events over which the average is taken.

For $ka \gg 1$, forward scattering is dominant. If we neglect the amplitude attenuation in calculating the decrease of the mean field, the randomization coefficient ν has a simple relation with the rms phase fluctuation $\sigma\phi = \langle\delta\phi^2\rangle^{1/2}$. From (1.5) and (1.6), the amplitude of the mean field $\langle\psi\rangle$ is obtained as

$$|\langle\psi\rangle| = |\psi_0| e^{-\langle\delta\phi^2\rangle/2}$$

$$= |\psi_0|\, e^{-\nu x}. \qquad (3.3)$$

Therefore, if the average propagation distance X_0 in the random medium is known, we can relate the randomization coefficient with the phase variance $\langle \delta\phi^2 \rangle$ as

$$\nu = \frac{\langle \delta\phi^2 \rangle}{2X_0} = \frac{\sigma\phi^2}{2X_0}. \tag{3.4}$$

On the other hand we can calculate ν from the medium parameter γ and a using

$$\nu = \frac{\gamma^2 k_0^2 a}{2}. \tag{1.7}$$

The ν value calculated from the measured σ_ϕ (assuming $X_0 = 50$ km) and that from the medium parameters are given in Table 1 and are shown in Fig. 1. The square frequency dependence of ν agrees fairly well with the measured phase fluctuations, though the data are not sufficient for a decisive test.

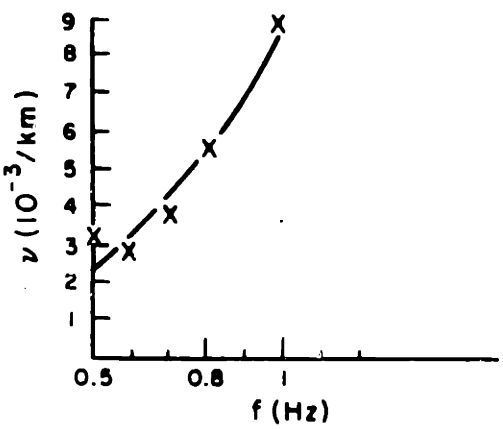

Fig. 1. Comparison of (×) randomization coefficient ν_ϕ (attenuation coefficient of mean field) calculated from measured phase fluctuations by Aki at Lasa, Montana and (—) ν, calculated by the mean-field formulation from the medium parameters.

4. Amplitude attenuation and mean-field attenuation

We have shown that the mean-field attenuation is mainly a statistical effect due to phase 'interference' among members of a random wave ensemble when the ensemble mean is taken. It has very little connection with amplitude attenuation. A random wave field is a random complex function of position

$$\psi(r) = A(r)\, e^{i\phi(r)} = A(r)\, e^{i[\langle\phi(r)\rangle + \delta\phi(r)]}, \tag{4.1}$$

where $\psi(r)$ is the random wave, $A(r)$ is its amplitude, and $\phi(r)$ is its phase. Both amplitude A and phase ϕ are random variables. Also, $\langle\phi\rangle$ is the ensemble average of ϕ, and $\delta\phi$ is the fluctuating part. Since phase ϕ usually changes much faster than A, we can consider A and ϕ as linearly independent random variables. Therefore

$$\langle\psi\rangle = \langle A\rangle\langle e^{i\phi}\rangle = \langle A\rangle\, e^{i\langle\phi\rangle}\, e^{-\langle\delta\phi^2\rangle/2}. \tag{4.2}$$

The attenuation of the average amplitude $\langle A\rangle$ is usually much slower than the term $e^{-\langle\delta\phi^2\rangle/2}$, so that the mean-field attenuation is determined mainly by the phase-interfering term $e^{-\langle\delta\phi^2\rangle/2}$. If we neglect the attenuation of the average amplitude $\langle A\rangle$, we get

$$\langle\psi\rangle = A_0\, e^{-\langle\delta\phi^2\rangle/2}\, e^{i\langle\phi\rangle}. \tag{4.3}$$

This is the result we obtained in (1.6). Therefore the mean-field attenuation derived from the parabolic approximation or other approximation methods is merely accounted for by the statistical effect due to phase randomization, and has nothing to do with the average amplitude attenuation.

From the above analysis, we know that the information concerning amplitude attenuation cannot be extracted or recovered from the mean field formulation.

In order to derive the average amplitude attenuation, we need to remove the phase influence before taking the ensemble average. The best way is to multiply its complex conjugate to the wave field, which corresponds to performing a phase

correction for every realization of the ensemble before averaging. Thus we get

$$\langle \psi \psi^* \rangle = \langle A\, e^{i\phi} A\, e^{-i\phi} \rangle = \langle A^2 \rangle. \tag{4.4}$$

We must solve the equation for the second moment $\langle \psi \psi^* \rangle$, not for the first moment $\langle \psi \rangle$, in order to describe the average amplitude attenuation of a random wave field.

Recently, Wu [32] has derived the amplitude attenuation from the energy transfer relations within a random slab. The basic idea is the following. The random slab is sliced into layers of thickness a (correlation length) and the Born approximation is used for each slice to calculate the scattered field. To include the multiple scattering effect, only the energy scattered to the back-half-space is considered lost (for the case that the wavelength is much smaller than the correlation length), and the energy correction is done for each successive slice.

The derived amplitude attenuation has a quite different behavior from the mean-field attenuation in the high frequency range. Contrary to the mean-field attenuation, which has a unique frequency-dependence regardless of the form of the correlation function of the inhomogeneities, the frequency dependences of the amplitude attenuation have different forms for different correlation functions. For exponential correlation function, the equivalent inverse quality factor of scattering attenuation Q_S^{-1} equals ((22) in [32])

$$Q_S^{-1} = \frac{2b}{k_0} = \frac{4\gamma^2 k_0^3 a^3}{1 + 6k_0^2 a^2 + 8k_0^4 a^4}, \tag{4.5}$$

where b is the attenuation coefficient of amplitude due to scattering, k_0 is the wavenumber for the unperturbed medium, and a is the correlation length. The Q_S^{-1} curve has a peak at $k_0 a \approx 1$. In the high frequency range, when $k_0 a \gg 1$,

$$Q_S^{-1} = \frac{\gamma^2}{2k_0 a}. \tag{4.6}$$

Therefore the apparent amplitude attenuation b, in the high frequency range can be approximated by

$$b \approx \frac{\gamma^2}{4a}. \tag{4.7}$$

In the case of Lasa data, taking $\gamma = 0.04$, $a = 10$ km, $v_p = 6$ km/sec, we have $b \approx 4 \times 10^{-5}$/km for frequencies from 0.5 to 1 Hz. Comparing to Fig. 1, we can see that not only is b much smaller than ν, but the frequency dependence of b is also quite different from that of ν. In addition, from (4.7) the attenuation b is nearly inversely proportional to correlation a when $k_0 a$ is large. This property is expected for attenuation. In the case when the scale of inhomogeneities is larger than the wavelength, a decrease in the size of inhomogeneities will increase the number of scatterers and therefore increase the scattering energy loss. This is contrary to the mean field attenuation, which decreases with decreasing correlation length a (cf. (1.7) and the related comments).

Fig. 2 shows the comparison between the attenuation measurements and the theoretical prediction by mean field attenuation and by amplitude attenuation. The measurements were made by Aki in Kanto, Japan, using a single-station S-coda-ratio method [3]. In the calculation we took the intrinsic attenuation as 4×10^{-4}, based on the observation that most of the Q^{-1} curves converge at high frequencies to a certain value, which is assumed to be the intrinsic Q^{-1} [4]. In general the theoretical curve of amplitude attenuation agrees well with the measurements. The discrepancy between the measured data and the prediction by mean-field attenuation further attest to the inadequacy of the mean field formulation for the problem of amplitude attenuation.

Acknowledgement

I am grateful to Professor Keiiti Aki for his encouragement, criticism and valuable discussions. He pointed out first to me the incon-

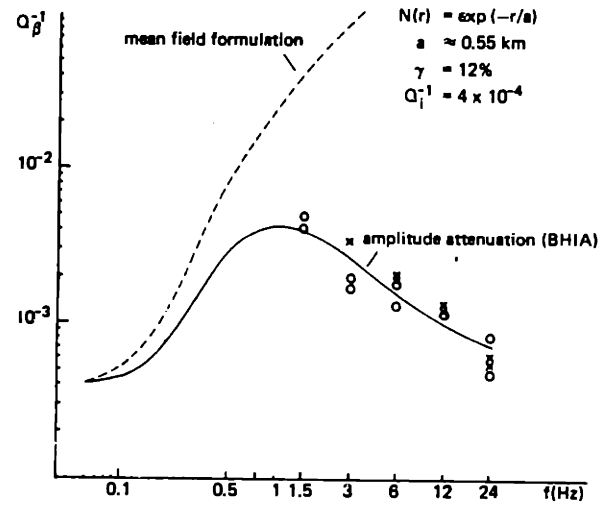

Fig. 2. Comparison between measurements of amplitude attenuation and theoretical predictions by the mean field formulation and by the amplitude attenuation formula (4.5).
∘ is Q^{-1} of S-wave from measured data at area A, Kanto, Japan;
× is Q^{-1} of S-wave from measured data at area B+C, Kanto, Japan (from Aki, 1980);
— is $Q_\beta^{-1} = Q_S^{-1} + Q_i^{-1}$, calculated Q^{-1} of S-wave, where Q_S^{-1} is the equivalent Q^{-1} of scattering attenuation, and Q_i^{-1} is the intrinsic Q^{-1}, here taken as 4×10^{-4}.

sistency of the mean field concept with actual measurements of seismic waves and has suggested many improvements to this work. This work was done during my stay in the Department of Earth and Planetary Sciences of MIT as a visiting scientist sponsored by Professor Aki. I wish to thank the Department and MIT for offering me this opportunity. I have also benefitted from the discussions with Prof. T. Madden, Prof. N. Toksöz, Dr. D. Morgan and Dr. H. Sato. Support for this research was provided in part by Department of Energy contract # DE-AC02-76ER02534.

References

[1] K. Aki, "Analysis of the seismic coda of local earthquakes as scattered waves", *J. Geophys. Res. 74*, 615–631 (1969).
[2] K. Aki, "Scattering of P waves under the Montana Lasa", *J. Geophys. Res. 78*, 1334–1346 (1973).
[3] K. Aki, "Attenuation of shear waves in the lithosphere for frequencies from 0.05 to 25 Hz", *Phys. Earth Planet. Int. 21*, 50–60 (1980).
[4] K. Aki, "Scattering and attenuation of shear waves in the lithosphere", *J. Geophys. Res. 85*, 6496–6504 (1980).
[5] S.A. Fedotov and S.A. Boldyrev, "Frequency dependence of the body-wave absorption in the crust and the upper mantle of the Kuril-Island chain", *Izv. Earth Physics 9*, 17–33 (1969).
[6] J. Capon, "Characterization of crust and upper mantle structure under Lasa as a random medium", *Bull. Seis. Soc. Amer. 64*, 235–266 (1974).
[7] K.A. Berteussen, A. Christoffersson, E.S. Husebye, and A. Dahle, "Wave scattering theory in analysis of P wave anomalies at NORSAR and LASA", *Geophys. J. Roy. Astr. Soc. 42*, 403–417 (1975).
[8] K. Aki and B. Chouet, "Origin of coda waves: source, attenuation and scattering effects", *J. Geophys. Res. 80*, 3322–3342 (1975).
[9] B. Chouet, Source, Scattering and attenuation effects on high frequency seismic waves, Ph.D. Thesis, Massachusetts Institute of Technology, Cambridge, MA (1976).
[10] M. Tsujiura, "Spectral analysis of the coda waves from local earthquakes", *Bull. Earthquake Res. Inst. Tokyo Univ. 53*, 1–48 (1978).
[11] T.G. Rautian and V.I. Khalturin, "The use of coda for determination of the earthquake source spectrum", *Bull. Seis. Soc. Amer. 68*, 923–948 (1978).
[12] S.W. Roecker, Seismicity and tectonics of the Pamir-Hindu Kush Region of Central Asia, Ph.D. Thesis, Massachusetts Institute of Technology, Cambridge, MA, Ch. 5 (1981).
[13] H. Sato, "Energy propagation including scattering effects, single isotropic scattering approximation", *J. Phy. Earth 25*, 27–41 (1977).
[14] C.L. Pekeris, "Note on the scattering of radiation in an inhomogeneous medium", *Phys. Rev. 71*, 268–269 (1947).
[15] L.A. Chernov, *Wave Propagation in a Random Medium*, McGraw-Hill, New York (1960).
[16] P.R. Beaudet, "Elastic wave propagation in heterogeneous media", *Bull. Seismol. Soc. Amer. 60*, 769–784 (1970).
[17] V.K. Varadan, V.V. Varadan, and Y.H. Pao, "Multiple scattering of elastic waves by cylinders of arbitrary cross section. I. SH waves", *J. Acoust. Soc. Amer. 63* (5), 1310–1319 (1978).
[18] V.K. Varadan and V.V. Varadan, "Frequency dependence of elastic (SH-) wave velocity and attenuation in anisotropic two phase media", *Wave Motion 1*, 53–63 (1979).
[19] H. Sato, "Wave propagation in one-dimensional inhomogeneous elastic media", *J. Phys. Earth 27*, 455–466 (1979).
[20] R.C. Bourret, "Seismic waves in a randomly stratified earth model", preprint (1980).

[21] R.C. Bourret, "Stochastically perturbated fields, with application to wave propagation in random media", *Nuovo Cimento 26*, 1–31 (1962).

[22] R.C. Bourret, "Propagation of randomly perturbated fields", *Canad. J. Phys. 40*, 782–790 (1962).

[23] J.B. Keller, "Wave propagation in random media", *Proc. Symp. Appl. Math. 13*, 227–246 (1962).

[24] J.B. Keller, "Stochastic equations and wave propagation in random media", *Proc. Symp. Appl. Math. 16*, 145–170 (1964).

[25] F.C. Karal and J.B. Keller, "Elastic, electromagnetic and other waves in a random medium", *J. Math. Phys.* 5 (4), 537–549 (1964).

[26] V.I. Tartaski and M.E. Gertsenshtein, "Propagation of waves in a medium with strong fiuctuation of the refractive index", *Soviet Physics JETP 17* (2), 458–463 (1963).

[27] V.I. Tatarski, "Propagation of electromagnetic waves in a medium with strong dielectric-constant fluctuations", Soviet Physics JETP 19 (4) 946–953 (1964).

[28] V. Frisch, *Wave Propagation in Random Media*, Probabilistic Methods in Applied Mathematics, Vol. 1, Academic Press, New York (1968) 76–198.

[29] M.S. Howe, "Wave propagation in random media", *J. Fluid Mech. 45*, 769–783 (1971).

[30] M.S. Howe, "On wave scattering by random inhomogeneities with application to the theory of weak bores", *J. Fluid Mech. 45*, 785–804 (1971).

[31] M.S. Howe, "Conservation of energy in random media, with application to the theory of sound absorption by an inhomogeneous flexible plate", *Proc. Roy. Soc. London A 331*, 479–496 (1973).

[32] R.S. Wu, "Attenuation of short period seismic waves due to scattering", *Geophys. Res. Lett. 9* (1), 9–12 (1982).

[33] B.J. Usinski, *The Elements of Wave Propagation in Random Media*, McGraw-Hill, New York (1977).

[34] P.M. Morse and H. Feshbach, *Methods of Theoretical Physics*, McGraw-Hill, New York (1953).

[35] J. Bass, *Les Fonctions Pseudo-Aleatoires*, Gauthier-Villars (1962).

[36] A. Papoulis, *Probability, Random Variables and Stochastic Process*, McGraw-Hill, New York (1965).

[37] R.F. Mereu, and S. Ojo, "Seismic wave propagation through a crust with random lateral and vertical inhomogeneities", *AGU 1980 Spring Meeting*, Abstract 593 (1980).

GEOPHYSICAL RESEARCH LETTERS, VOL. 9, NO. 1, PAGES 9-12, JANUARY 1982

ATTENUATION OF SHORT PERIOD SEISMIC WAVES DUE TO SCATTERING

Wu Ru-Shan

Department of Earth and Planetary Sciences, Massachusetts Institute of Technology
Cambridge, Massachusetts 02139

Abstract. We point out first the inadequacy of the two widely used approaches in calculating the amplitude attenuation of seismic waves in a random medium, the formulation of mean field attenuation and that of the scattering coefficient under the single-scattering approximation. Then we calculate the average amplitude attenuation due to scattering in an infinite random slab. We slice the random slab into layers of thickness a correlation length and use the Born approximation for each slice to calculate the scattered field. To include the effect of multiple scattering, we take the back-halfspace integration of the scattered energy as the energy loss and do energy correction for each successive slice. Taking scalar wave approximation for seismic waves, we get a formula for average amplitude attenuation essentially valid for high frequency range (ka>>1). The attenuation depends strongly on the form of correlation function of the random inhomogeneities. We derive the formulas for Gaussian, exponential and Von Karman correlation functions. The frequency dependence of attenuation by our formulation agrees well with experiments.

There have been two main approaches in treating the attenuation of seismic waves due to scattering. One is the use of mean field attenuation in a random medium (e.g., Beaudet 1970, Varadan et al. 1978, Varadan and Varadan 1979, Sato 1980). Many authors, however, failed to recognize the differences between the attenuation of "mean field" and the attenuation of the actual field. It can be shown (Wu 1981) that the attenuation of mean field in fact is only a statistical effect that measured the rate of randomization for waves passing through a random medium. In practice, what is actually measured is not the amplitude of mean field, and there is little work done on observing the "mean field." Therefore, the usual comparison between the measured attenuation of amplitude and the calculated mean field attenuations cannot produce meaningful results.

The other approach to studying the attenuation due to scattering is to use the energy scattering coefficient under the single-scattering approximation, based on Chernov's work (Chernov 1960). However, it can be shown (Wu 1981) that when the travel distance is short, this leads to the same result as that obtained by the mean field formulation under bilocal approximation for Dysons's equation. Since the single-scattering approximation neglects the multiple-scattering, which is important for attenuation calculation, this equivalence is not totally unexpected.

We will find the average amplitude attenuation for short period seismic waves passing through a random medium using a simple model. First let us derive the general solution for a scalar wave.

Consider a scalar plane wave

$$\psi^\circ = Ae^{ik_0 x} \qquad (1)$$

incident normally on an infinite slab of thickness X_0 made of random medium with correlation length a. We divide the random medium into slices of thickness a (Figure 1). Consider a thin plate with side-length ℓ in the first slice. Let the total field be

$$\psi = \psi^\circ + \psi' ,$$

where ψ' is the scattered field, which satisfies the following equation under the Born approximation,

$$L_0\psi' = -L_1\psi^\circ , \qquad (2)$$

where L_0 is the linear operator of wave equation for the homogeneoue case and L_1 is the random operator (or scattering operator). Therefore

$$\psi' = -G_0L_1\psi^\circ , \qquad (3)$$

where $G_0 = L_0^{-1}$ is the homogeneous unbounded Green function operator. Multiplying (3) by the conjugate scattered wave and taking the average, we get the mean intensity

$$\begin{aligned}\langle|\psi'|^2\rangle &= \langle G_0G_0^*\, L_1L_1^*\, \psi^\circ\psi^{\circ *}\rangle \\ &= [G_0G_0^*\,\langle L_1L_1^*\rangle\, e^{ik_0(x_1-x_2)}]\,|\psi^\circ|^2 \\ &= B|\psi^\circ|^2 ,\end{aligned} \qquad (4)$$

where the stars stand for the complex conjugate, and B is the directional scattering ratio.

The scattered energy is proportional to the integral of $\langle|\psi'|^2\rangle$ over all directions. Under the single-scattering approximation, the total scattered energy is considered to be lost, and all the thin plates within the random medium scatter the same amount of energy, while the primary wave remains unchanged after passing the random medium. Therefore, the energy conservation law is violated and the net scattered energy wil be overestimated. When X_0>>a and the forward scattering is dominant (ka>>1), the single scattering assumption becomes intolerable for the attenuation calculation based on scattered energy loss. The multiple scattering must be taken into account and the energy correction has to be done. For the infinite slab, the forward scattered energy will hit upon other inhomogeneities (multiple-scattering), so the related energy can be assumed as not lost for the first-order correction. The back-scattered energy can be considered totally lost, because there are no inhomogeneities in the back space. Thus the energy loss ΔI will be proportional to the integral of back-scattered energy,

$$\Delta I = D\int_b \langle|\psi'|^2\rangle\, dS = D|\psi^\circ|^2\int_b B\,dS , \qquad (5)$$

Paper number 1L1399

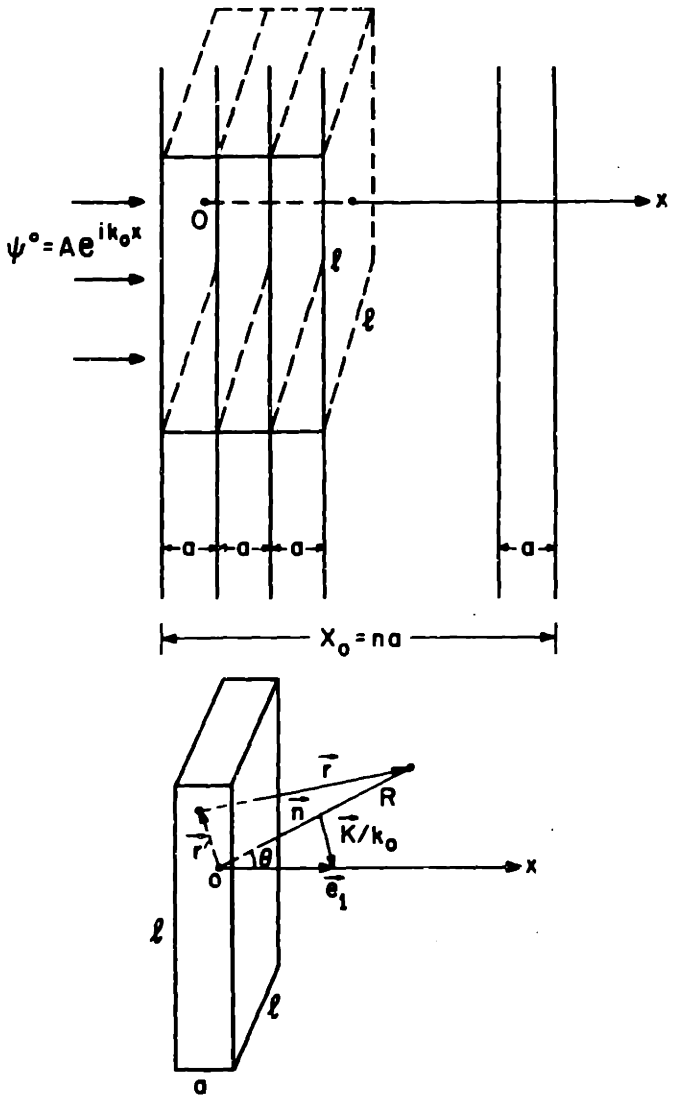

Fig. 1. The coordinate system of the random slab.

where $\int_b$ indicates the integration is over the back half-space, D is constant, and dS is the surface element of integration.

The incident energy flow upon the thin plate is

$$I_0 = D\ell^2|\psi^o|^2 , \tag{6}$$

then

$$\frac{\Delta I}{I_0} = \frac{\int_b B\, dS}{\ell^2} = \xi a , \tag{7}$$

where

$$\xi = \frac{\Delta I}{I_0 a} = \frac{\int_b B\, dS}{a\ell^2} . \tag{8}$$

When the wave falls upon the next slice, the energy correction will be done for the incident energy flow

$$I_1 = I_0 - \Delta I = I_0(1-\xi a) . \tag{9}$$

Under local Born approximations, we can calculate the scattered energy loss by the second slice and so forth. Here we will neglect the second back-scattering by the first slice toward the second slice. In the case of ka>>1, the back scattering is small, the second back-scattering wil be a second order small quantity. Suppose $X_0 = na$. When n is large, it can be approximated by

$$I = \lim_{\substack{n\to\infty \\ a\to 0}} I_n = I_0 \lim_{a\to 0} (1-\xi a)^{x_0/a} = I_0 e^{-\xi x_0} . \tag{10}$$

We recognize ξ to be the energy attenuation coefficient.

Now we calculate ξ for a linear elastic isotropic weakly random medium. When the wave conversion between P and S waves as well as the coupling between different polarizations can be neglected, for example in the case of ka>>1 (Knopoff and Hudson, 1967), we need only solve a scalar equation for scattering of the corresponding wave component. That is the scalar wave approximation. We know the pertinent scalar equation is

$$\left(\frac{1}{C_0^2}\frac{\partial^2}{\partial t^2} - \nabla^2\right)\psi' = f(\vec{F}) , \tag{11}$$

where C_0 is the unperturbed wave velocity and $f(\vec{F})$ is a scalar function of $\vec{F}$, which is the equivalent body force for the secondary source due to inhomogeneities. When the scattering effects of the space gradients of the velocity and elastic constants can be neglected, for instance in the case ka>>1 (see Aki and Richards, 1980 or Haddon and Husebye, 1978), for harmonic plane wave incidence, we get

$$f(\vec{F}) = -\frac{2\omega^2}{C_0^2}\frac{\delta C}{C_0}\psi^0 = -2k_0^2\frac{\delta C}{C_0}\psi^0 , \tag{12}$$

where δC is the fluctuating part of velocity. Introduce

$$N(|\vec{r}_1' - \vec{r}_2'|) = \frac{\left\langle \frac{\delta C(\vec{r}_1')}{C_0}\cdot\frac{\delta C(\vec{r}_2')}{C_0}\right\rangle}{\gamma^2} \tag{13}$$

where

$$\gamma = \left\langle\left(\frac{\delta C}{C_0}\right)^2\right\rangle^{1/2} \tag{14}$$

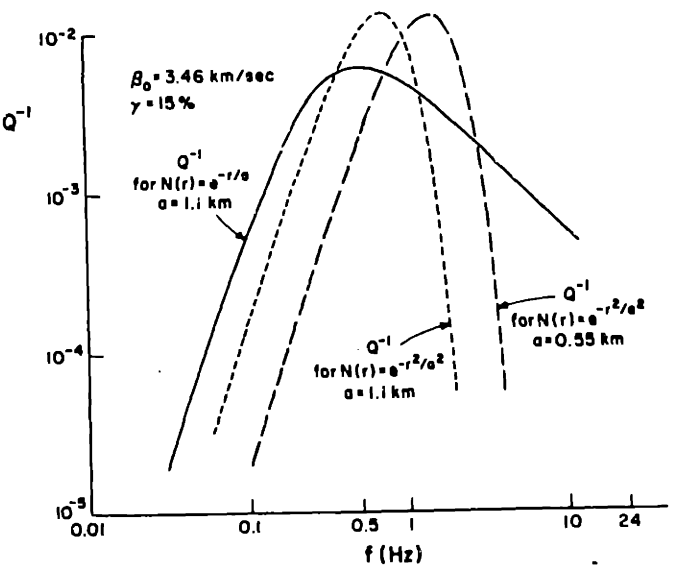

Fig. 2. The frequency dependencies of Q^{-1} due to scattering for exponential correlation function and for Gaussian correlation function.

is the r.m.s. relative velocity variation for the statistically homogeneous random medium. We can calculate B from (4) by Fraunhoffer approximation (the reader is referred to Chernov 1960, Ch. 3 of Aki and Richards 1980, 13.3.1),

$$B = \frac{k_0^4 \gamma^2 V}{\pi R^2} \int_0^{\ell} N(r') \frac{\sin(2k_0 \sin\theta/2)}{2k_0 \sin\theta/2} r'dr' \quad (15)$$

where θ is the angle between the incident direction and the scattering direction. Thus from (8), by integrating over back hemisphere, we can derive the equivalent quality factor Q of the scattering attenuation,

$$Q^{-1} = \frac{\xi}{k_0} = \frac{1}{k_0 a \ell^2} \int_b B.R^2 \sin\theta d\theta d\phi$$

$$= 2\gamma^2 k_0 \int_0^{\infty} [\cos(\sqrt{2}\, k_0 r') - \cos(2k_0 r')]\, N(r')dr'$$

$$= \gamma^2 k_0 [P(\sqrt{2}\, k_0) - P(2k_0)] , \quad (16)$$

where P (k) is the one dimensional power spectral density of the random medium. Since correlation function N(r) is very small beyond correlation length a, the limit of integration has been extended to infinity. It can be seen from (16) that both magnitude and frequency dependence of Q^{-1} are strongly affected by the spectral density of the random medium, that is the feature of amplitude attenuation different from the mean field attenuation. The frequency dependence of mean field attenuation is independent of the spectral density function (or the correlation function) of the random medium.

In the following, we will derive Q^{-1} expressions for several correlation functions.

For exponential correlation function N(r) = exp[-r/a], substituting into (16) leads to

$$Q^{-1} = 2\gamma^2 k_0 \left[\frac{a}{1+2k_0^2a^2} - \frac{a}{1+4k_0^2a^2}\right] = \frac{4\gamma^2 k_0^3 a^3}{1+6k_0^2a^2+8k_0^4a^4} \quad (17)$$

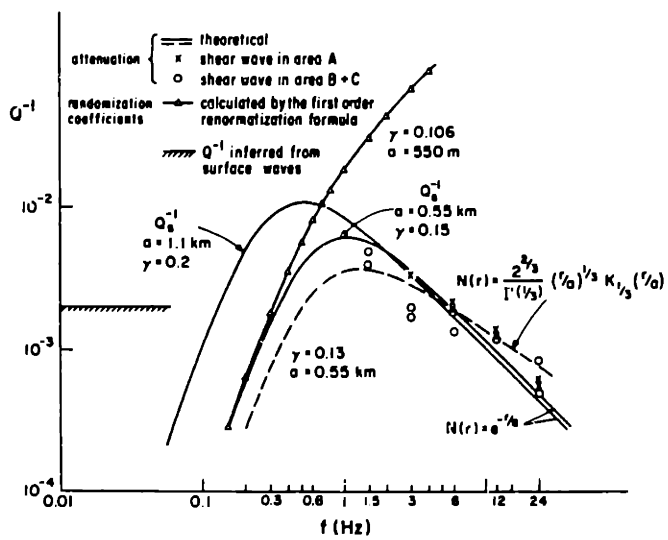

Fig. 3. Comparison of theoretical correlation functions with the experimental data obtained by Aki in Kanto, Japan.

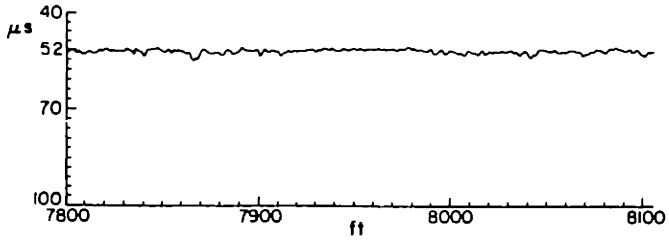

Fig. 4. Acoustic velocity log at Fenton Hill (7800 ft - 8100 ft), Sandoval, New Mexico, from Los Alamos Scientific Laboratories.

When $k_0 a \ll 1$,

$$Q^{-1} = 4\gamma^2 k_0^3 a^3 \quad (18)$$

When $k_0 a \gg 1$,

$$Q^{-1} = \frac{\gamma^2}{2k_0 a} \quad (19)$$

For Gaussian correlation function $N(r)=\exp[-r^2/a^2]$ we get

$$Q^{-1} = \sqrt{\pi}\, \gamma^2 k_0 a \,(e^{-1/2\, k_0^2 a^2} - e^{-k_0^2 a^2}) . \quad (20)$$

When $k_0 a \ll 1$,

$$Q^{-1} = \frac{\sqrt{\pi}}{2} \gamma^2 k_0^3 a^3 \quad (21)$$

If we use the Von Kármán correlation function, which is widely used in fluid turbulence theory (e.g., Tatarski, 1961),

$$N(r) = \frac{1}{2^{m-1}\Gamma(m)} \left(\frac{r}{a}\right)^m K_m\left(\frac{r}{a}\right) , \quad (22)$$

where $\Gamma(m)$ is a gamma function, $K_m(x)$ is m order modified Bessel function (m is not necessarily an integer), we get by substituting into (16)

$$Q^{-1} = 2\sqrt{\pi}\, \gamma^2 k_0 a \frac{\Gamma(m+1/2)}{\Gamma(m)} \cdot \frac{(1+4a^2k_0^2)^{m+1/2} - (1+2a^2k_0^2)^{m+1/2}}{(1+6a^2k_0^2+8a^4k_0^4)^{m+1/2}}$$

When $k_0 a \ll 1$,

$$Q^{-1} = 4(m+1/2)\sqrt{\pi}\, \gamma^2 \frac{\Gamma(m+1/2)}{\Gamma(m)} k_0^3 a^3 \quad (23)$$

When $k_0 a \gg 1$,

$$Q^{-1} = 2\sqrt{\pi}\, \gamma^2 \frac{(2^{m+1/2}-1)}{2^{2m+1}} \frac{\Gamma(m+1/2)}{\Gamma(m)} (k_0 a)^{-2m} \quad (24)$$

For m = 1/3, that is, when the structure function of the random medium observes the Kolmogorov's "two thirds law" (see Tatarski 1961), it results in

$$Q^{-1} = 1.49\, \gamma^2 k_0 a \frac{(1+4k_0^2a^2)^{5/6} - (1+2k_0^2a^2)^{5/6}}{(1+6k_0^2a^2+8k_0^4a^4)^{5/6}} \quad (25)$$

For $k_0 a \ll 1$,

$$Q^{-1} = 2.49\, \gamma^2 (k_0 a)^3 \quad (26)$$

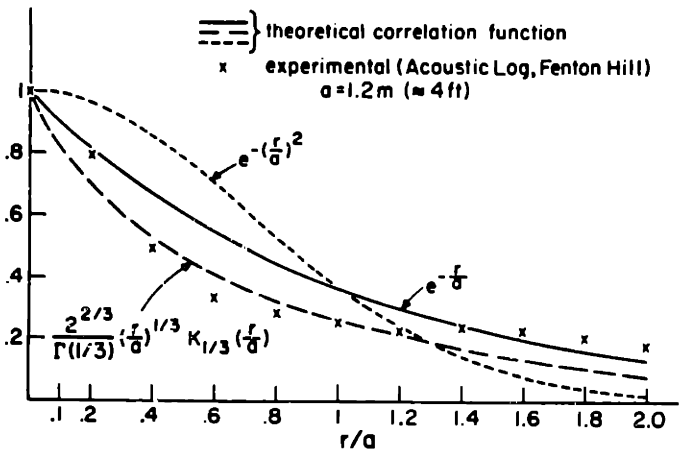

Fig. 5. The comparison of theoretical correlation functions with the experimental values calculated from the velocity log in the granite at Fenton Hill.

For $k_0a \gg 1$,

$$Q^{-1} \approx 0.35\ \gamma^2(k_0a)^{-2/3} \qquad (27)$$

From (18), (21) and (23), it can be seen that for small scale inhomogeneities, namely $k_0a \ll 1$, the attenuation is proportional to the fourth power of frequency, that is Rayleigh scattering, and is independent of the form of correlation function. However, for large scale inhomogeneities, namely $ka \gg 1$, the frequency dependence of attenuation or equivalently of Q^{-1} differs from each other distinctly (see fig. 2).

Fig. 3 shows the comparison between the calculation and the measured S-wave attenuation by Aki in the Kanto region of Japan (Aki, 1980). Because the attenuation peak has not atually been measured, there is some uncertainty in the medium parameters. There is little knowledge about the forms of correlation function of the random velocity inhomogeneities in the lithosphere of the earth. For shallow depths, we can use the data of velocity log. Fig. 4 shows the acoustic log at Fenton Hill, New Mexico at depths of 7800-8100 ft. The comparison between theoretical and measured correlation functions for small distances are shown in Fig. 5. The measured data fit the Von Kárman type or exponential type correlation function better. Therefore the calculations have been carried out for a = 1.1 km, γ = 20% and a = 0.55 km, γ = 15% for the exponential correlation function and for a = 0.55 km, γ = 13% for the Von Kárman correlation function. The scattering attenuation behavior predicted by mean field formulation or by single-scattering approximation is also shown in the figure. For our model, if we consider the pulse envelope spreading effect (we will discuss it in future publications), the attenuation coefficients can have a correction term up to 1/3 or 1/2. Therefore the inferred fluctuation index γ could be reduced to 15% or 10%.

Although there is no data on correlation length a and velocity fluctuation γ available in this region, the value of γ predicted by our formula is somewhat larger than expected. Other corrections must be made before the predicted values can fit the experimental one. However, the general trend of frequency dependence of scattering attenuations in the high frequency range agrees well with the experimental data, assuming that the observed attenuation is due to scattering. We know that the equivalent Q^{-1} of the measured attenuations has the form f^{-n}, n equal 0.6-0.8 for the Kanto region of Japan (Aki 1980), 0.6 for the Kurile Islands (Fedotov and Baldyrev 1969), 0.5 for Garm (Rautian and Khalturin 1978). This agreement shows the importance of considering multiple scattering in calculating scattering attenuation.

Acknowledgements. I wish to thank Prof. Aki for his suggestions and discussions. This work was partially supported by Department of Energy contract DE-AC02-76ER-2534.

References

Aki, K., Attenuation of shear waves in the lithosphere for frequencies from 0.05 to 25 Hz, Phys. Earth Planet. Int., 21, 50-60, 1980.

Aki, K., and P. G. Richards, Quantitative seismology, theory and methods, V. II (W.H. Freeman and Co., 1980).

Beaudet, P. R., Elastic wave propagation in heterogeneous media, Bull. Seismol. Soc. Amer., 60, 769-784, 1970.

Chernov, L. A., Wave propagation in a Random Medium (New York: McGraw Hill, 1960).

Fedotov, S. A. and S. A. Boldyrev, Frequency dependence of the body-wave absorption in the crust and upper mantle of the Kuril-Island chain, Izv., Earth Physics, No. 9, 17-33, 1969.

Hadden, R. A. W. and E. S. Husebye, Joint interpretation of P-wave time and amplitude anomalies in terms of lithosphere heterogeneities, Geophys. J. R. Astron. Soc., 55, 19-43, 1978.

Knopff, L. and J. A. Hudson, Frequency dependence of amplitudes of scattered elastic waves, J. Acoust. Soc. Amer., 42, 18-20, 1967.

Rautian, T. G. and V. I. Khalturin, The use of coda for determination of the earthquake source spectrum, Bull. Seis. Soc. Am., 68, 923-948, 1978.

Sato, H., Wave propagation in one dimensional inhomogeneous elastic media, J. Phys. Earth, 28, in press.

Tatarski, V. I., Wave propagation in a turbulent medium (Dover, 1961).

Varadan, V. K., Varadan, V. V. and Y. H. Pao, Multiple scattering of elastic waves by cylinders of arbitrary cross section. I. SH waves, J. Acoust. Soc. Am., 63, 1310-1319, 1978.

Varadan, V. K., and V. V. Varadan, Frequency dependence of elastic (SH-) wave velocity and attenuation in anisotropic two phase media, Wave motion, 1, 53,63, 1979.

Wu, R. S., The mean field attenuation and amplitude due to wave scattering, submitted to Wave motion, 1981.

(Received August 18, 1981;
accepted August 31, 1981.)

BIOGRAPHICAL NOTE

WU, RU-SHAN

Birth date: Dec. 1938.
Birth place: Xiao-Zhai vilage, Xing-Yang, Henan province, China.

Education and professional experiences:

1957. graduated from Xing-Yang high school.
1962. 10. graduated from Department of physics, North-Western University, Sian, China
1962-1965 research assistant, working on the underground electromagnetic wave exploration, in the Institute of Geophysical prospecting of Ministry of Geology of China,
1966-1972 reseach scientist, on geological radar exploration, in the same institute,
1973-1978 research scientist and a group leader, on the applications of holography and information theory to geophysical exploration, including
multi-frequency holography,
computer reconstruction of holography,
applications of digital holography of underground electromagnitic wave exploration,
applications of digital algebraic and geometric reconstruction to underground electromagnetic wave exploration,
1979-1980 visiting scientist in Dep. Earth and Planetary Sci., MIT, USA,
1981.2. graguate student in geophysics, MIT,
1981.4. candidate for ph.d. program in geophysics,MIT,
1984.8. gradiated from the dept. earth, atmosphere & planet. sci. of M.I.T.
1984.9. research associate in the Dept. earth, atmosphere & planet. sci. of M.I.T.

Activities:

1977 attended " exploration 77 ", a international symposium on geophysical exploration for minerals, in Ottawa, Canada, as a member of chinese delegation .

received a certificate of merit from the National Conference of Science and Technology.

1978. dec. came to U.S. among the first group of chinese visiting scholars.

1965-1977 participated in several field experimints in different regions of China.

Publications:

1976,The research graoup of holography, Chinese Academy of Ceological Sci.: A multifrequency synthetic detecting holography with a high depth resolution, Peking, China.
1977,Wu Ru-Shan, Wu Yu-Lin,Liu Cai-Rong, Peng Chun-Yi and Wang Mao-Ji: Multi-frequency synthetic detecting holography, Acta geophysica sinica, 20, 1.

1978,Wu Ru-Shan and Xu Shao-Hui: A fast algorithm for near region in holographic reconstruction, Acta geophyseca sinica, 21,3.
1979,Wu Ru-Shan and Xu Shao-Hui: The applications of digital holography to borehole electromagnetic wave exploration, Acta seismologica sinica, 1, 2.
1980,Wu Ru-Shan and Xu Shao-Hui: Determination of underground profile of electromagnetic absorption --a method of geometrical digital imaging, Geophysical and geochemical prospecting, 6.
1981,Wu,R.S.: The attenuation of seismic waves due to scattering in a random medium,(abstract), AGU fall meeting, 1980, EOS, 61, 46, 1049.
1982,Wu,R.S.:Attenuation of short period seismic waves due to scattering, Geophys. Res. Lett.,9,9-12.
1982,Wu,R.S.: Mean field attenuation and amplitude attenuation due to wave scattering,Wave motion,4,305-316.
1983,Wu,R.S.: Scattering characteristics of elastic waves by an elastic inclusion, I. Rayleigh scattering of elastic waves,
II. Elastic wave scattering beyond Rayleigh scattering, presented at 53rd annual meeting og SEG,sept. 12,1983. See extended abstracts of the technical program with authors' biographies, SEG annual meeting 1983.
1984, Wu,R.S. and K. Aki: Scattering characteristics of elastic waves by an elastic heterogeneity, Geophysics, in press.
1984, Wu,R.S. and K.Aki: Elastic wave scattering by a random medium and the scale inhomogeneities in the lithosphere, presented at the annual meeting of the Seis. soc. of Amer., May 2,1983, J. Geophys. Res., in press.
1984, Wu,R.S. and A.Ben-Menahem: Elastodynamic near field, Submitted to Geophys. J.R.astr. Soc..
1984, Wu,R.S: Analytic extension of Green's function, complex rays and Gaussian beams in smoothly inhomogeneous midia,submitted to Geophys. J.R.astr. Soc..